Photochemical Modeling of the Earth's Stratosphere

Thesis by

Lucien Froidevaux

In Partial Fulfillment of the Requirements

for the Degree of

Doctor of Philosophy

California Institute of Technology

Pasadena, California

1984

(Submitted 26 July 1983)

A mes parents

ACKNOWLEDGMENTS

I first thank my parents, who started me on the track to education by teaching me French and English at an early stage. At the time, I did not always enjoy translating part of the book "Tarzan the ape-man" from French to English, but I can now appreciate the lessons of my mother, who probably was never aiming at helping me write a thesis in English. At present, my family teases me about occasional hints of an American accent when I speak French...They also guided me to and through the "Lycée d'Orsay," near Paris, which provided a good stepping stone before my college years in the United States.

After three enjoyable years at U.C.L.A. as an undergraduate in physics, the experience and knowledge I gained as a first year graduate student in the Space Science Department there were quite enriching. In particular, the guidance and kindness of my advisor, M. Kivelson, are deeply appreciated. I also acknowledge the support and teachings of I. Shapiro, my advisor at M.I.T., where I was introduced to VLBI (Very Long Baseline Interferometry) and some of the jargon used in radio astronomy.

After these two years, it was time to "settle down" (getting married was part of that), and I am very grateful for the continued education provided by the various faculty members at Caltech. Thanks to them, I have learned, learned how to learn, criticized and self-criticized. The opportunities for research in planetary and atmospheric science were numerous. Before my work in the area of stratospheric photochemistry, I was able to pursue a variety of publishable research projects. I extend my thanks to G. Siscoe of U.C.L.A. for discussions related to charged particle diffusion

in Io's torus, as well as the JPL researchers involved in the Pioneer Venus infrared radiometer data analysis (D. Mc Cleese and C. B. Farmer in particular) for their assistance in some of the work pertinent to water vapor. I also had the opportunity to pursue various research projects related to the infrared behavior of Saturn's rings. In this respect, I acknowledge the help (and writing lessons) of P. Goldreich, A. Ingersoll, K. Matthews, G. Neugebauer, and P. Nicholson, as well as comments by H. Aumann, J. Cuzzi, C. B. Farmer, B. Jakosky, H. Kieffer, D. Muhleman, A. Tokunaga, and Y. Yung.

More directly, the stratospheric research described here has been stimulated and encouraged by my thesis advisor, Y. Yung, who introduced me to this fascinating subject in his class on atmospheric chemistry. His enthusiasm and support (scientific and financial) are greatly appreciated. I also confess to feeding on M. Allen's brains, where essentially all source of knowledge related to the basic KINETICS computer program resides. The completion of this thesis is in large part due to his patience, encouragement, and assistance, whether it had to do with a chemistry question, or the dreadful appearance of an "OC4" error message in the computer output. His love for detail and thoroughness has hopefully rubbed off on me to some extent. Since atmospheric photochemistry is tied to many disciplines, I have benefited from discussions with many experimentalists (involved in laboratory and atmospheric work) and modelers alike. The proximity of JPL has allowed for a fruitful interaction with the laboratory kinetics group of W. DeMore , who was always available for comments. I followed their work with interest and benefited from discussions with L. Keyser, M. T. Leu, J. Margitan, M. Molina, and--more often than not--S. Sander. I also thank

R. de Zafra, D. Ehhalt, P. Fabian, C. B. Farmer, S. Epstein, J. Frederick, J. Herman, D. Hunten, G. Kattawar, B. Menzies, S. Prasad,O. Raper, N. D. Sze, P. Solomon, J. Waters, and R. Zurek for their comments, communications,or preliminary results (or any combination of the above). I am grateful to M. Nicolet for sending me a copy of his book on photochemistry.

My stay at Caltech was also enriched by the friendship and scientific advice of past and present fellow students. In addition, I wish to acknowledge the (non-scientific) teachings of japanese karate master T. Ohshima, that Caltech is fortunate to have had for over 25 years. He provided a welcome--although sometimes grueling--distraction from work. Concentration, mental strength, and the focusing of energy are needed in karate and other sports, as well as in the successful completion of a graduate degree, although I do not think that I will defend my thesis in a gi.

I cannot forget the expert typing of this thesis by R. Stratton, who was simply excellent. I also thank D. Lathrop and K. Campbell for their assistance in typing and administrative matters over the years at Caltech. The drafting of figures for this thesis was efficiently performed by W. All; I can sympathize with her urge to draw something a little different (like a dead fish), after some 70 scientific graphs...

Last, but certainly not least, much of this work was made easier by the emotional support and comforting presence of my wife Marty and her family, who treated me so kindly. This last year was somewhat of an experience, due to the birth of our daughter Natalie, and the tiring schedule of her mother as an intern in internal medicine. The patient assistance and sacrifices of my sister-in-law, Diane Preciado, and her family, as loving babysitters to our little "bolà" are deeply appreciated. Gracias a todos!

ABSTRACT

We have helped develop a one-dimensional photochemical model of the Earth's stratosphere, in order to provide an up-to-date comparison with mid-latitude observations. This work focuses on the present state of the stratosphere, and includes studies of the radiation field (absorption and scattering), the important partitioning and vertical distribution of halocarbons and their products, as well as certain intriguing discrepancies related to light and heavy ozone.

We briefly comment on the detection by J. R. Herman and J. E. Mentall of a 10% ratio of total scattered flux to direct solar flux at a wavelength of about 200 nm and an altitude of 40 km. This ratio is over a factor of two higher than our theoretical results and cannot be explained without the existence of a scattering component not included in the model. We also explicitly demonstrate the first-order effects of the inclusion of sphericity (spherical shell atmosphere) on the stratospheric photochemistry at solar zenith angles close to 90°. The resulting changes in model concentrations for short-lived radicals such as O, OH, ClO, and NO are largest in the lower stratosphere, but relatively small compared to current observational uncertainties.

We propose that a significant overestimate of the molecular oxygen absorption cross sections in the important spectral window from about 200 to 220 nm is in large part responsible for the discrepancy between observed and modeled vertical profiles of some halocarbons ($CFCl_3$ in particular), as well as for the long-standing problem of simultaneously fitting N_2O, CH_4, CF_2Cl_2, and $CFCl_3$ profiles with a single eddy diffusion model. Recent

measurements of atmospheric transmission by J. R. Herman and coworkers seem to support this idea. The use of their proposed reduction in O_2 cross sections leads to significant decreases in the $CFCl_3$ concentration above about 20 km, with smaller reductions in N_2O, CF_2Cl_2 and HNO_3. The concentrations of CH_4, H_2, and CO are not significantly altered. Changes in other gases (including ozone) are also discussed, as well as the effect on eddy diffusion coefficients obtained from measurements of N_2O or CH_4 profiles in the stratosphere. Accurate determinations of these small O_2 absorption cross sections are needed, since they affect the vertical distribution of halocarbons in the stratosphere, and the lifetime of these species has an impact on ozone depletion estimates.

In terms of the halocarbon decomposition products in the stratosphere, our model vertical distribution of ClO is shown to provide a reasonably good fit to the mean of available observations. As discussed by others, changes in certain rate constants affecting HO_x in the lower stratosphere have led to decreases in model ClO concentrations by over a factor of three in the lower stratosphere, thus improving the shape of the vertical profile. In addition, the amount of upper stratospheric ClO has increased due to recent changes in the kinetics (reactions $O + HO_2$, $O + ClO$, and possibly $OH + HCl$). The diurnal variation of ClO observed from the ground (microwave emission) by P. Solomon and coworkers is consistent with our model results in terms of the maximum day-to-night decrease in column abundance above about 30 km. However, the observed mid-morning increase is slower than theoretical values, while the predicted afternoon decrease might be too slow, even if one considers the uncertainties in photochemical data. This could indicate the existence of missing chemistry in the models, although

the different observations show somewhat contradictory results. Other observations (balloon-borne microwave spectroscopy and infrared laser radiometry) are also discussed in relation to our model. To first-order, indirect evidence for the breathing cycle between ClO and $ClONO_2$ seems to have been established. The mean observed HCl mixing ratio profile decreases somewhat faster towards the lower stratosphere than model profiles, a discrepancy which has previously been noted, particularly at high latitudes. Measurements of ethane in the lower stratosphere seemed to indicate that the atomic chlorine concentration was three to five times lower than predicted, but more recent data do not show such a discrepancy.

The fluorine products consist mostly of HF and COF_2. We show that the main uncertainty for this system is the value of the quantum yield (as a function of wavelength) for COF_2 photodissociation, which translates into a factor of three or more uncertainty in the ratio of HF to COF_2 concentrations in the upper stratosphere. If this quantum yield has an average value close to 0.25, a better model fit to observations of HF and [HF]/[HCl] is obtained than if the value is close to unity. Simultaneous stratospheric measurements of COF_2 and HF, as well as ClO and HCl, would greatly enhance our ability to test photochemical models of these halocarbon products.

Finally, we stress that, although generally good agreement is found between our model and observations of HO_x, NO_x, and ClO_x species (involved in catalytic cycles destroying ozone), the mean observed mid-latitude ozone abundance from about 35 to 50 km is up to 50 or 60% greater than current model results. Certain observations of a 10 to 15% daytime increase in ozone concentration in the 30 to 40 km region are

also puzzling, if real. We explore the model sensitivity to various input parameters and point out that, given the present uncertainties in photochemical laboratory data, no reasonable change in one or even three or four of these parameters can eliminate the ozone discrepancy. There might well be some missing chemistry in relation to the effectiveness of the loss processes for odd oxygen, or a (less likely) unknown significant O_3 source. We have to understand the present upper stratospheric ozone distribution, before estimates of possible future ozone depletion can be made with confidence. We also discuss our understanding of heavy ozone photochemistry, which might be related to a light ozone photochemical source. Fast isotopic exchange processes between O and O_2 will dominate the heavy odd oxygen chemistry, and we do not find any significant heavy ozone enhancement possibilities in the stratosphere, unless unusually large fractionation processes exist. The in situ mass spectrometer observations of a 40% enhancement in $^{18}O^{32}O_2$ near 30 km by K. Mauersberger remain a mystery, and further data collection--possibly via infrared or microwave spectroscopy as well--should be undertaken if this potentially significant discrepancy is to be understood.

TABLE OF CONTENTS

I'm sick and tired of hearing things
From uptight short sighted narrow minded hypocritics
All I want is the truth
Just gimme some truth

I've had enough of reading things
By neurotic psychotic pig headed politicians
All I want is the truth
Just gimme some truth

No short haired yellow bellied son of tricky dicky
Is gonna mother hubbard soft soap me
With just a pocketful of hope
Money for dope
Money for rope

I'm sick to death of seeing things
From tight lipped condescending mommies little
Chauvinists
All I want is the truth
Just gimme some truth

I've had enough of watching scenes
Of schizophrenic egocentric paranoic prima donnas
All I want is the truth
Just gimme some truth

Gimme some truth

(John Lennon, Imagine Album, 1971)

... In a somewhat more relevant context for scientists ...

I'm not after a "nice" paper

I want the truth!

(D.O.Muhleman,during a seminar, 1982)

INTRODUCTION

The relatively thin atmospheric layer above us is the scene of many different dynamical and photochemical processes. These processes can be global or local, and they occur on a wide range of time scales. Solar radiation provides the most important driving force, via absorption and photodissociation processes that release energy and heat up the atmosphere; temperature gradients lead to pressure gradients which can accelerate air masses on a global scale. Temperature also affects chemical reaction rates and changes the relative amounts of trace gases, some of which can catalytically modify the ozone distribution, which in turn influences temperature, dynamics and photochemistry. The coupling between radiation, dynamics and chemistry, the three-dimensional and nonlinear aspects of the atmosphere, as well as the interactions at the upper and lower boundaries and the wide range of temporal and spatial scales have made it very difficult to model the exact behavior of the atmosphere. Progress is being made in developing General Circulation Models which include some chemistry, but there are limitations in terms of computer size and speed (cost) of calculations. One-dimensional photochemical models describe the vertical distribution of chemical species in the atmosphere, with a crude parametrization of transport processes. Two-dimensional models provide a compromise by using the important photochemistry and zonally-averaged dynamics to compute latitudinal and vertical distributions of gases. The fact that a model is two- or three-dimensional does not in itself qualify it to more accurately describe the behavior of gases in the atmosphere. For example, eddy coefficients corresponding to horizontal transport are subject to uncertainties, just as the vertical component of a 1-D model

is. The dynamical aspects of the atmosphere are not yet as satisfactorily understood as the purely photochemical processes, which are in some sense more predictable, thanks to the large amount of laboratory data obtained in the last two decades. Although we seem to have a good first-order understanding of the distribution of minor and trace gases in the atmosphere, discrepancies remain between models and observations. Our research addresses various problems related to photochemistry in the stratosphere (from about 10 to 50 km altitude), with the help of a 1-D model. In the words of Massie and Hunten [1981] "one-dimensional models are still the workhorses of stratospheric chemistry." Photochemical sensitivity tests are most easily performed on a 1-D model and processes that occur on time scales short compared to horizontal transport--e.g., diurnal variations--do not require multi-dimensional modeling (if the long-lived species are correctly defined).

Since one cannot be expected to "solve the stratosphere" in a few years, our more modest goals are to focus on some of the current discrepancies and interesting problems in photochemistry. A better understanding of the chemical composition will eliminate some of the uncertainties in dynamical studies, since tracer gases can be affected by air motions as well as by photochemistry. Ozone is of primary importance in the stratosphere, where it is produced by photolysis of oxygen and subsequent reaction of oxygen atoms and molecules. It is responsible for the temperature increase in the stratosphere, which leads to relative stability against convection (and smoother flights for airline passengers). The strong ozone absorption below 300 nm prevents hazardous ultraviolet radiation from reaching the ground. The original formulation of ozone

photochemistry is due to Chapman [1930], who considered pure oxygen species only. Such basic reactions produced an ozone concentration peak in the lower stratosphere, as observed, but overestimated the absolute amounts. More recent studies have demonstrated the importance of hydrogen oxides [Bates and Nicolet, 1950], nitrogen oxides [Crutzen, 1970], and chlorine compounds [Wofsy and McElroy, 1974; Stolarski and Cicerone, 1974] for the destruction of ozone. The potential impact of human activities on the steady-state concentration of ozone through anthropogenic perturbations of the above compounds has generated a large amount of theoretical and experimental research during the past decade. The possible impact of a steady increase in stratospheric nitrogen oxides due to aircraft emissions was initially discussed by Johnston [1971] and further investigated by McElroy et al. [1974]. The apparent lack of significant tropospheric sinks for anthropogenically-produced halocarbons and the potentially important catalytic destruction of ozone by chlorine radicals produced by stratospheric photolysis of these source species were problems pointed out by Molina and Rowland [1974] and Rowland and Molina [1975]. The importance of trace amounts (typically parts per billion) of man-made nitrogen or chlorine compounds on the stratospheric ozone balance arises from the catalytic nature of the destruction processes, whereby these rapidly reacting radicals can interact many times with ozone (and atomic oxygen) before being lost from the system. The ultimate steady-state ozone concentration will be determined by the source strengths and lifetimes of stratospheric pollutants. The concern is over irreversible transformations of the environment, although the exact effects of a small decrease in total column ozone on animals and humans (sunburn, effects on DNA and immune system response, skin cancer) as well as plants are not yet

well defined [NRC, 1982]. The predictions of ozone decrease over the next century have varied in recent years, not only in magnitude, but also in sign. This is due to our incomplete understanding of the present stratospheric photochemistry. Clearly, in order to accurately predict small changes in steady-state ozone amounts, we have to accurately know the chemical processes affecting ozone, as well as the possible radiative-dynamical coupling mechanisms. Considering past experience, it is probably safe to say that predictions will continue to change somewhat, although one hopes that we are converging towards the truth. A recent paper by Cicerone et al. [1983] demonstrates some of the nonlinearities involved in the photochemistry alone and suggests that total column ozone could be increasing slightly for a few decades before a sharper decrease sets in. The problem with a fast (10-20 years) detection of an ozone decrease is due to the smallness of the effect over such a time scale and the required accuracy and repeatability of global observations, as well as the interference from diurnal, seasonal and solar cycle effects. Long-term satellite observations of global ozone, in particular in the upper stratosphere where chlorine-catalyzed destruction is predicted to peak, should help elucidate this question. In the meantime, however, vigorous research concerning the present state of the atmosphere is being pursued and regular reports are published almost every year by various workshops and agencies. Excellent collections of papers can be found, for example, in Hudson and Reed [1979], Nicolet and Aikin [1980], Hudson et al. [1982], NRC [1982] and other references therein. A concise review of the physical and chemical processes involved in planetary atmospheres can be found in the textbook by Chamberlain [1978]. For those with some French reading ability, a good reference to stratospheric photochemical reactions and

laboratory work is provided in the book by Nicolet [1978]. Some of the above references are already somewhat out of date, but that is a healthy indication that progress is being made in this field.

The present work focuses on a refinement of our understanding of the present atmosphere in terms of photochemical modeling and comparisons with observations. Chapter 1 presents the basic Caltech one-dimensional photochemical model. This includes a discussion of the model input parameters and laboratory data relevant to the stratosphere, as well as a description of the basic schemes related to absorption and scattering of solar radiation. In Chapter 2, we present further analyses of the diffuse flux in the stratosphere: part 1 is a comment on observations by Herman and Mentall [1982], while part 2 explicitly demonstrates the effects of Rayleigh scattering on the photochemistry at large solar zenith angles, where the influence of sphericity is largest. Chapter 3 is a somewhat expanded version of the work presented by Froidevaux and Yung [1982] on the sensitivity of the vertical profiles of certain gases (halocarbons in particular) to changes in the molecular oxygen absorption cross sections near 200 nm. Lower cross sections would help resolve the discrepancies that have been found between halocarbon observations and models. The vertical distribution of other chlorine and fluorine compounds and their partitioning is analyzed in Chapter 4. Special emphasis is placed on the chlorine monoxide diurnal variation (section 4.2), in light of recent observations. Can we understand the various observations in terms of the present chemistry or are there some missing factors? The same questions are raised in Chapter 5 with respect to ozone in the upper stratosphere, where photochemistry--rather than transport--should dominate, but where the model underestimates the ozone concentration by a non-negligible

amount. The latest WMO/NASA report [Hudson et al., 1982] lacked such a comparison between observed and theoretical upper stratospheric ozone profiles, but this problem could have significant implications for the present and future stratosphere. Relevant comparisons are presented in terms of observed and modeled radical profiles, and the sensitivity of ozone to photochemical parameters is discussed. The small, but interesting diurnal variations of ozone are discussed in section 5.2 and compared to observations. In view of the controversial observations of an enhancement in isotopic ozone ($^{18}O^{32}O_2$) near 30 km by Mauersberger [1981], we present our current understanding of heavy ozone photochemistry in section 5.3.

References

Bates, D. R., and M. Nicolet, The photochemistry of water vapor, J. Geophys. Res., 55, 301, 1950.

Chamberlain, J. W., Theory of Planetary Atmospheres, An Introduction to Their Physics and Chemistry, International Geophysics Series, Vol. 22, Academic Press, 1978.

Chapman, S., A theory of upper-atmospheric ozone, Mem. R. Meteorol. Soc., 3, 103, 1930.

Cicerone, R. J., S. Walters, and S. C. Liu, Nonlinear response of stratospheric ozone column to chlorine injections, J. Geophys. Res., 88, 3647, 1983.

Crutzen, P. J., The influence of nitrogen oxides on the atmospheric ozone content, Quart. J. Roy. Meteorol. Soc., 96, 320, 1970.

Froidevaux, L., and Y. L. Yung, Radiation and chemistry in the stratosphere: Sensitivity to O_2 absorption cross sections in the Herzberg continuum, Geophys. Res. Lett., 9, 854, 1982.

Herman, J. R., and J. E. Mentall, The direct and scattered solar flux within the stratosphere, J. Geophys. Res., 87, 1319, 1982.

Hudson, R. D., and E. I. Reed (editors), The Stratosphere: Present and Future, NASA RP 1049, 1979.

Hudson, R. D. (editor-in-chief) et al. (16 editors), The Stratosphere 1981: Theory and Measurements. WMO Global Ozone Research and Monitoring Project Report No. 11, 1982.

Johnston, H. S., Reduction of stratospheric ozone by nitrogen oxide catalysts from supersonic transport exhausts, Science, 173, 517, 1971.

Massie, S. T., and D. M. Hunten, Stratospheric eddy diffusion coefficients from tracer data, J. Geophys. Res., 86, 9859, 1981.

Mauersberger, K., Measurement of heavy ozone in the stratosphere. Geophys. Res. Lett., 8, 935, 1981.

McElroy, M. B., S. C. Wofsy, J. E. Penner, and J. C. McConnell, Atmospheric ozone: Possible impact of stratospheric aviation, J. Atmos. Sci., 31, 287, 1974

Molina, M. J., and F. S. Rowland, Stratospheric sink for chlorofluoromethanes: Chlorine atom catalyzed destruction of ozone, Nature, 249, 810, 1974.

Nicolet, M., Etude des réactions chimiques de l'ozone dans la stratosphere, Comite d'etudes sur les consequences des vols stratospheriques, Institut Royal Météorologique de Belgique, 1978.

Nicolet, M., and A. C. Aikin (editors), Proceedings of the NATO Advanced Study Institute on Atmospheric Ozone: Its Variation and Human Influences, Report No. FAA-EE-80-20, U. S. Department of Transportation, 1980.

NRC, Causes and Effects of Stratospheric Ozone Reduction: An Update, National Academy Press, Washington, D.C., 1982.

Rowland, F. S., and M. J. Molina, Chlorofluoromethanes in the environment, Rev. Geophys. Space Phys., 13, 1, 1975.

Stolarski, R. S., and R. J. Cicerone, Stratospheric chlorine: A possible sink for ozone, Canad. J. Chem., 52, 1610, 1974.

Wofsy, S. C., and M. B. McElroy, HO_x, NO_x, and ClO_x: Their role in atmospheric photochemistry, Canad. J. Chem., 52, 1582, 1974.

Chapter 1

THE CALTECH 1-D PHOTOCHEMICAL MODEL

1.1 Basic Concepts

The basic Caltech photochemical model is intended for a wide variety of possible atmospheric studies, ranging from the Earth to Jupiter and planetary satellites, as well as cometary comae. It originated with the work of Y. Yung and J. Pinto and was subsequently improved into a convenient general package by M. Allen. Specialized subroutines are introduced for problems that are specific to a particular atmosphere or atmospheric region. Earlier applications of the basic model include studies of the primitive Earth's photochemistry and evolution [Pinto et al., 1980], modeling of the Earth's mesosphere and thermosphere [Allen et al., 1981, 1983] and photochemistry of the atmospheres of Venus [DeMore and Yung, 1982; Yung and DeMore, 1983], Jupiter [Gladstone and Yung, 1983], and Titan [Allen et al., 1980]. In terms of the Earth's stratosphere, we have been continually updating the input parameters, as well as refining certain features of the model, which--as most modelers know--can often occupy a significant fraction of the time spent towards obtaining a particular scientific result.

The continuity equation lies at the center of all photochemical models. In the vertical (z) dimension, we write this equation for the i^{th} constituent at each altitude as follows:

$$\frac{\partial n_i}{\partial t} = P_i(n_j,n_k) - L_i(n_i,n_k) - \frac{\partial \Phi_i}{\partial z} \qquad (1)$$

where n_i is number density (cm^{-3}), $P_i(n_j,n_k) = \sum_{j,k} k_{jk} n_j n_k$ is the photochemical production rate ($cm^{-3} s^{-1}$) which includes two-body and three-body reactions (effective rate constant k_{jk} in $cm^3 s^{-1}$) as well as photodissociations. $L_i(n_i,n_k)$ is similar in form to $P_i(n_j,n_k)$ except that it expresses the photochemical loss rate ($cm^{-3} s^{-1}$), and Φ_i is a vertical flux ($cm^{-2} s^{-1}$), positive upwards. The transport contribution resides in the last term of equation (1) and is parametrized in the standard eddy diffusion formulation:

$$\Phi_i(z) = -K(z)\, n_a(z)\, \frac{\partial f_i(z)}{\partial z} \qquad (2)$$

where K is the eddy diffusion coefficient ($cm^2 s^{-1}$), n_a is the total atmospheric density (cm^{-3}) also written as [M] in later sections, and $f_i = n_i/n_a$ is the volume mixing ratio of the i^{th} constituent. Making use of the ideal gas law for n_a and the equation of hydrostatic balance, relation (2) can be written as:

$$\Phi_i = -K\left\{\frac{\partial n_i}{\partial z} + \left(\frac{1}{T}\frac{\partial T}{\partial z} + \frac{m_a g}{kT}\right) n_i\right\} \qquad (3)$$

where T is temperature (degrees K), m_a is mean molecular weight (g) of the atmosphere, g is gravity ($cm^2 s^{-1}$), and $k = 1.38 \times 10^{-16}$ (erg/K) is Boltzmann's constant. The terms $m_a g/kT$ and $[(1/T)(\partial T/\partial z) + m_a g/kT]$ are the inverse of the pressure and density scale heights of the atmosphere [see Colegrove et al., 1965; Hunten, 1975]. In applications such as the Earth's thermosphere or Jupiter's upper atmosphere, a molecular diffusion term is added to the flux expression. We present in section 1.2

the various input parameters, such as reactions, rate constants, absorption and scattering cross sections, model atmospheres, eddy diffusion coefficients, and boundary conditions needed to solve equation (1). Substituting for Φ_i into equation (1) yields a second order partial differential equation for n_i with respect to z. Two boundary conditions are needed and the system is nonlinear due to the production and loss terms P_i and L_i. An iterative method with finite differences (implicit scheme) is used [See for example Shimazaki, 1972; Stewart and Hoffert, 1975; Ashby, 1976]. Boundary conditions can be expressed as fixed concentration, mixing ratio, flux or velocity. The convergence parameter used to check the variation in concentrations between successive iterations is typically set to 10^{-3} for diurnal average (steady-state) runs and 10^{-4} for diurnal runs. Species can be separated into groups of coupled constituents that are solved for independently before the total solution is checked for convergence; this allows a reduction in program size, although a large single group usually converges faster. A group can also be chosen for species that are short-lived and in local photochemical equilibrium at any time (transport unimportant). Once a steady-state solution has been found, source species that are long-lived with respect to transport processes can be fixed and a diurnal calculation performed for other species, with no transport involved. Such decoupling of transport and photochemistry allows for a more economical solution to be reached in the diurnal mode. Another feature of the model involves the choice of spherical versus plane parallel geometry. Sphericity is accounted for in the flux divergence term, in the varying daylight period as a function of altitude, as well as in the calculation of slant optical depths (see section 1.3).

1.2 Input Parameters

For stratospheric calculations, close to 50 species (including N_2 and O_2 as fixed major gases) are typically coupled by 130 to 150 photodissociation and chemical reactions. Table I lists the set of reactions used and the associated rate constants (two-body, three-body or equilibrium values). Since our model spans the 0 to 80 km range (16 to 60 km for diurnal runs), some of the reactions in Table I are more important in the troposphere or mesosphere than in the stratosphere directly, but are included in order to minimize uncertainties in fluxes to the stratosphere or in boundary effects. The ethane, propane and acetylene reactions (#130 to 134) are usually not included in diurnal runs due to their limited effect on other species in the stratosphere; fluorine reactions (#135 to 145) were included only in the particular study of Chapter 4. The set of reaction rate constants is essentially taken from the recent JPL 82-57 Report [DeMore et al., 1982], which is a recommendation based on a selective average of laboratory kinetics data accumulated over the past two decades with increasing frequency and sophistication. Regular reports such as this one or the CODATA references [latest version, see Baulch et al., 1982] are an important part of atmospheric chemistry. It might be that most of the large (> 50%) changes in rate constants have occurred by now, given that most reactions have been studied by more than one person or group with often different techniques, but unexpected surprises (or missing chemistry) may still lurk ahead. The uncertainties in most of the important reaction rate constants are of order 10 to 30% at room temperature as well as at colder stratospheric temperatures. Some of the more recent changes are discussed in Chapter 4 in relation to

Table I. Input Data for Photochemical Reactions

	Reaction	Rate Constant[1] or Cross Section Data	Reference[2]
(1)	$O_2 + h\nu \rightarrow 2O$	$180 < \lambda < 255$	Allen et al. (1981), Allen and Frederick (1982)
(2)	$O_2 + h\nu \rightarrow O + O(^1D)$	$\lambda < 175$	As in (1)
(3)	$O_3 + h\nu \rightarrow O_2 + O$	$200 < \lambda < 800$	Allen et al. (1981), Nicolet (1978)
(4)	$O_3 + h\nu \rightarrow O_2 + O(^1D)$	$170 < \lambda < 317.5$	Allen et al. (1981), DeMore et al. (1982)
(5)	$H_2O + h\nu \rightarrow H + OH$	$\lambda < 200$	Allen et al. (1981)
(6)	$H_2O_2 + h\nu \rightarrow 2OH$	$\lambda < 352.5$	DeMore et al. (1982), Hudson and Kieffer (1975)
(7)	$H_2CO + h\nu \rightarrow HCO + H$	$240 < \lambda < 332.5$	
(8)	$N_2O + h\nu \rightarrow N_2 + O(^1D)$	$\lambda < 240$	
(9)	$NO + h\nu \rightarrow N + O$	$\lambda < 200$	Allen and Frederick (1982)
(10)	$NO_2 + h\nu \rightarrow NO + O$	$\lambda < 420$	DeMore et al. (1982), Nicolet (1978)
(11)	$NO_3 + h\nu \rightarrow NO_2 + O$	$470 < \lambda < 630$	Magnotta and Johnston (1980)
(12)	$N_2O_5 + h\nu \rightarrow 2NO_2 + O$	$205 < \lambda < 382.5$	
(13)	$HNO_3 + h\nu \rightarrow NO_2 + OH$	$190 < \lambda < 327.5$	
(14)	$CFCl_3 + h\nu \rightarrow 3Cl + products$	$175 < \lambda < 257.5$	
(15)	$CF_2Cl_2 + h\nu \rightarrow 2Cl + products$	$175 < \lambda < 240$	
(16)	$ClONO_2 + h\nu \rightarrow Cl + NO_3$	$185 < \lambda < 450$	
(17)	$CCl_4 + h\nu \rightarrow 4Cl + products$	$175 < \lambda < 272.5$	
(18)	$CO_2 + h\nu \rightarrow CO + O$	$\lambda < 205$	Allen et al. (1981)

Table I (continued)

	Reaction	Rate Constant[1] or Cross Section Data	Reference[2]
(19)	$ClO + h\nu \rightarrow Cl + O$	$200 < \lambda < 337.5$	Nicolet (1978), Langhoff et al. (1977)
(20)	$H_2CO + h\nu \rightarrow H_2 + CO$	$240 < \lambda < 362.5$	
(21)	$CH_3OOH + h\nu \rightarrow CH_3O + OH$	$205 < \lambda < 352.5$	
(22)	$NO_3 + h\nu \rightarrow NO + O_2$	$590 < \lambda < 630$	Magnotta and Johnston (1980)
(23)	$HOCl + h\nu \rightarrow OH + Cl$	$195 < \lambda < 420$	
(24)	$O(^1D) + O_2 \rightarrow O + O_2$	$3.2(-11)\ e^{67/T}$	
(25)	$O(^1D) + N_2 \rightarrow O + N_2$	$1.8(-11)\ e^{107/T}$	
(26)	$O(^1D) + H_2O \rightarrow 2OH$	$2.2(-10)$	
(27)	$O(^1D) + H_2 \rightarrow H + OH$	$1.0(-10)$	
(28)	$O(^1D) + CH_4 \rightarrow CH_3 + OH$	$1.4(-10)$	
(29)	$O(^1D) + N_2O \rightarrow 2NO$	$6.7(-11)$	
(30)	$O(^1D) + N_2O \rightarrow N_2 + O_2$	$4.9(-11)$	
(31)	$O + O_2 + M \rightarrow O_3 + M$	$(3.0(-28)\ T^{-2.3};\ 2.8(-12);\ 0.85)$	Baulch et al. (1982)
(32)	$O_3 + O \rightarrow 2O_2$	$1.5(-11)\ e^{-2218/T}$	
(33)	$2O + M \rightarrow O_2 + M$	$4.3(-28)\ T^{-2.0}$	Hampson (1980)
(34)	$O_3 + NO \rightarrow NO_2 + O_2$	$2.2(-12)\ e^{-1430/T}$	
(35)	$O + NO_2 \rightarrow NO + O_2$	$9.3(-12)$	
(36)	$N + O_3 \rightarrow NO + O_2$	$1.0(-15)$	
(37)	$OH + O_3 \rightarrow HO_2 + O_2$	$1.6(-12)\ e^{-940/T}$	

Table I (continued)

	Reaction	Rate Constant[1] or Cross Section Data	Reference[2]
(38)	$HO_2 + O_3 \rightarrow OH + 2O_2$	$1.4(-14)\ e^{-580/T}$	
(39)	$O + OH \rightarrow O_2 + H$	$2.2(-11)\ e^{117/T}$	
(40)	$O + HO_2 \rightarrow OH + O_2$	$3.0(-11)\ e^{200/T}$	
(41)	$H + O_3 \rightarrow OH + O_2$	$1.4(-10)\ e^{-470/T}$	
(42)	$H + O_2 + M \rightarrow HO_2 + M$	$1.6(-28)\ T^{-1.4}$	
(43)	$N + O_2 \rightarrow NO + O$	$4.4(-12)\ e^{-3220/T}$	
(44)	$N + NO \rightarrow N_2 + O$	$3.4(-11)$	
(45)	$OH + NO_2 + M \rightarrow HNO_3 + M$	$(4.0(-23)\ T^{-2.9};\ 4.0(-8)\ T^{-1.3};\ 0.6)$	
(46)	$OH + HNO_3 \rightarrow NO_3 + H_2O$	$9.4(-15)\ e^{778/T}$	
(47)	$OH + HO_2 \rightarrow H_2O + O_2$	$2.2(-12)\ (7 + 4\ P_{atm})\ e^{450/T}$	See text
(48)	$H + HO_2 \rightarrow H_2 + O_2$	$3.8(-12)$	See text
(49)	$H + HO_2 \rightarrow 2OH$	$6.8(-11)$	See text
(50)	$H + HO_2 \rightarrow H_2O + O$	$3.2(-12)$	See text
(51)	$HO_2 + HO_2 \rightarrow H_2O_2 + O_2$		See text
(52)	$H_2O_2 + OH \rightarrow H_2O + HO_2$	$3.1(-12)\ e^{-187/T}$	
(53)	$OH + CH_4 \rightarrow CH_3 + H_2O$	$2.4(-12)\ e^{-1710/T}$	
(54)	$HO_2 + NO \rightarrow NO_2 + OH$	$3.7(-12)\ e^{240/T}$	
(55)	$NO_3 + NO \rightarrow 2NO_2$	$2.0(-11)$	
(56)	$NO_2 + O_3 \rightarrow NO_3 + O_2$	$1.2(-13)\ e^{-2450/T}$	

Table I (continued)

	Reaction	Rate Constant[1] or Cross Section Data	Reference[2]
(57)	$NO_3 + NO_2 + M \rightarrow N_2O_5 + M$	$(1.9(-23)\ T^{-2.8};\ 1.0(-12);\ 0.6)$	
(58)	$OH + HCl \rightarrow Cl + H_2O$	$2.8(-12)\ e^{-425/T}$	See text
(59)	$Cl + CH_4 \rightarrow CH_3 + HCl$	$9.6(-12)\ e^{-1350/T}$	
(60)	$Cl + O_3 \rightarrow ClO + O_2$	$2.8(-11)\ e^{-257/T}$	
(61)	$O + ClO \rightarrow Cl + O_2$	$7.7(-11)\ e^{-130/T}$	See text
(62)	$ClO + NO \rightarrow Cl + NO_2$	$6.2(-12)\ e^{294/T}$	
(63)	$Cl + HO_2 \rightarrow HCl + O_2$	$1.8(-11)e^{170/T}$	
(64)	$ClO + NO_2 + M \rightarrow ClONO_2 + M$	$(4.8(-23)\ T^{-3.4};\ 7.6(-7)\ T^{-1.9};\ 0.6)$	See text
(65)	$CO + OH \rightarrow CO_2 + H$	$1.35(-13)[1 + P_{atm}]$	
(66)	$H_2 + OH \rightarrow H_2O + H$	$6.1(-12)\ e^{-2030/T}$	
(67)	$NO + O + M \rightarrow NO_2 + M$	$(3.5(-27)\ T^{-1.8};\ 3.0(-11);\ 0.6)$	
(68)	$N_2O_5 + M \rightarrow NO_3 + NO_2 + M$	$k_{57}/(1.77(-27)\ e^{11001/T})$	
(69)	$ClONO_2 + O \rightarrow ClO + NO_3$	$3.0(-12)\ e^{-808/T}$	
(70)	$Cl + H_2 \rightarrow HCl + H$	$3.7(-11)\ e^{-2300/T}$	
(71)	$Cl + O_2 + M \rightarrow ClOO + M$	$3.3(-30)\ T^{-1.3}$	
(72)	$ClOO + M \rightarrow Cl + O_2 + M$	$k_{71}/(2.43(-25)\ e^{2979/T})$	
(73)	$CH_3O_2 + NO \rightarrow CH_3O + NO_2$	$4.2(-12)\ e^{180/T}$	
(74)	$CH_3O_2 + NO_2 + M \rightarrow CH_3O_2NO_2 + M$	$(1.2(-20)\ T^{-4.0};\ 5.8(-7)\ T^{-2.0};\ 0.4)$	F_c from Baulch et al. (1982)
(75)	$CH_3O + O_2 \rightarrow H_2CO + HO_2$	$1.2(-13)\ e^{-1350/T}$	

Table I (continued)

	Reaction	Rate Constant[1] or Cross Section Data	Reference[2]
(76)	$2CH_3O_2 \rightarrow 2CH_3O + O_2$	$1.6(-13)\ e^{220/T}$	
(77)	$H_2CO + OH \rightarrow HCO + H_2O$	$1.0(-11)$	
(78)	$HCO + O_2 \rightarrow CO + HO_2$	$3.5(-12)\ e^{140/T}$	
(79)	$CH_3O_2 + HO_2 \rightarrow CH_3OOH + O_2$	$7.7(-14)\ e^{1300/T}$	
(80)	$CH_3OOH + OH \rightarrow CH_3O_2 + H_2O$	$2.6(-12)\ e^{-190/T}$	
(81)	$CH_3 + O_2 + M \rightarrow CH_3O_2 + M$	$(6.2(-26)\ T^{-2.2};\ 3.3(-8)\ T^{-1.7};\ 0.6)$	
(82)	$CH_3 + O_2 \rightarrow H_2CO + OH$	$5.0(-17)$	Baulch et al. (1982)
(83)	$NO_2 + O + M \rightarrow NO_3 + M$	$(8.1(-27)\ T^{-2.0};\ 2.2(-11);\ 0.6)$	
(84)	$CH_3Cl + OH \rightarrow Cl + H_2O + products$	$1.8(-12)\ e^{-1112/T}$	
(85)	$Cl + H_2CO \rightarrow HCl + HCO$	$8.2(-11)\ e^{-34/T}$	
(86)	$ClO + HO_2 \rightarrow HOCl + O_2$	$4.6(-13)\ e^{710/T}$	
(87)	$HNO_3 \xrightarrow{rainout}$ products		Logan et al. (1981)
(88)	$HCl \xrightarrow{rainout}$ products		As in (87)
(89)	$H_2CO \xrightarrow{rainout}$ products		As in (87)
(90)	$H_2O_2 \xrightarrow{rainout}$ products		As in (87)
(91)	$CH_3OOH \xrightarrow{rainout}$ products		As in (87)
(92)	$HO_2NO_2 \xrightarrow{rainout}$ products		As in (87)
(93)	$HNO_2 \xrightarrow{rainout}$ products		As in (87)
(94)	$HO_2 + NO_2 + M \rightarrow HO_2NO_2 + M$	$(5.7(-20)\ T^{-4.6};\ 4.2(-12);\ 0.6)$	

Table I (continued)

	Reaction	Rate Constant[1] or Cross Section Data	Reference[2]
(95)	$O(^1D) + CH_4 \rightarrow H_2 + H_2CO$	1.4(-11)	
(96)	$O(^1D) + CFCl_3 \rightarrow 3Cl + products$	2.3(-10)	
(97)	$O(^1D) + CF_2Cl_2 \rightarrow 2Cl + products$	1.4(-10)	
(98)	$O + NO_3 \rightarrow O_2 + NO_2$	1.0(-11)	
(99)	$2OH \rightarrow H_2O + O$	$4.2(-12)\ e^{-242/T}$	
(100)	$OH + HOCl \rightarrow H_2O + ClO$	$3.0(-12)\ e^{-150/T}$	
(101)	$2OH + M \rightarrow H_2O_2 + M$	$(2.1(-28)\ T^{-1.0};\ 3.0(-9)\ T^{-1.0};\ 0.6)$	
(102)	$Cl + H_2O_2 \rightarrow HCl + HO_2$	$1.1(-11)\ e^{-980/T}$	
(103)	$ClO + OH \rightarrow HO_2 + Cl$	$5.1(-12)\ e^{180/T}$	
(104)	$CH_3 + O \rightarrow H_2CO + H$	1.4(-10)	
(105)	$H_2CO + O \rightarrow OH + HCO$	$3.0(-11)\ e^{-1550/T}$	
(106)	cosmic ray source $\rightarrow$ NO	see text	Nicolet (1975)
(107)	$HO_2NO_2 + h\nu \rightarrow HO_2 + NO_2$	$190 < \lambda < 327.5$	
(108)	$CH_3Cl + h\nu \rightarrow Cl + CH_3$	$175 < \lambda < 220$	DeMore et al. (1981)
(109)	$HNO_2 + h\nu \rightarrow OH + NO$	$312.5 < \lambda < 392.5$	
(110)	$OH + NO + M \rightarrow HNO_2 + M$	$(1.0(-24)\ T^{-2.5};\ 2.6(-10)\ T^{-0.5};\ 0.6)$	
(111)	$NO + CH_3O_2 \rightarrow H_2CO + HNO_2$	7.4(-13) (~10% of k_{73})	
(112)	$HO_2 + NO_2 \rightarrow HNO_2 + O_2$	3.0(-15)	Hampson and Garvin (1977)
(113)	$OH + HNO_2 \rightarrow H_2O + NO_2$	6.6(-12)	

Table I (continued)

	Reaction	Rate Constant[1] or Cross Section Data	Reference[2]
(114)	$NO_2 + h\nu \rightarrow NO_2$ (extinction)	$\lambda < 710$	Gelinas (1974), DeMore et al. (1982)
(115)	$M + h\nu \rightarrow$ Rayleigh scattering	$292.5 < \lambda < 800$	See text
(116)	$HO_2NO_2 + OH \rightarrow H_2O + NO_2 + O_2$	$1.3(-12)\ e^{380/T}$	
(117)	$HO_2NO_2 + M \rightarrow HO_2 + NO_2 + M$	$k_{94}/(2.33(-27)\ e^{10870/T})$	
(118)	tropospheric source $\rightarrow NO_2$	See text	Logan et al. (1981)
(119)	$C_2H_3Cl_3 + h\nu \rightarrow 3Cl$ + products	$180 < \lambda < 240$	
(120)	$C_2F_3Cl_3 + h\nu \rightarrow 3Cl$ + products	$180 < \lambda < 220$	
(121)	$C_2F_4Cl_2 + h\nu \rightarrow 2Cl$ + products	$175 < \lambda < 220$	Nicolet (1978)
(122)	$C_2H_3Cl_3 + OH \rightarrow 3Cl$ + products	$5.4(-12)\ e^{-1820/T}$	
(123)	$CHF_2Cl + OH \rightarrow Cl$ + products	$7.8(-13)\ e^{-1530/T}$	
(124)	$CHF_2Cl + O(^1D) \rightarrow HCl$ + products	1.9(-10)	Pitts et al. (1974)
(125)	$C_2F_3Cl_3 + O(^1D) \rightarrow 3Cl$ + products	2.9(-10)	Pitts et al. (1974)
(126)	$C_2F_4Cl_2 + O(^1D) \rightarrow 2Cl$ + products	1.8(-10)	Pitts et al. (1974)
(127)	$CH_3O_2NO_2 + M \rightarrow CH_3O_2 + NO_2 + M$	$k_{74}/(1.2(-28)\ e^{11320/T})$	See text
(128)	$CH_3O_2NO_2 + h\nu \rightarrow CH_3O_2 + NO_2$	$200 < \lambda < 312.5$	Baulch et al. (1982)
(129)	$HCl + h\nu \rightarrow H + Cl$	$\lambda < 230$	Inn (1975), Myer and Samson (1970)
(130)	$C_2H_2 + OH \rightarrow H_2$ + products	$6.5(-12)\ e^{-650/T}$	See text
(131)	$C_2H_6 + OH \rightarrow H_2O$ + products	$1.9(-11)\ e^{-1260/T}$	
(132)	$C_2H_6 + Cl \rightarrow HCl$ + products	$7.7(-11)\ e^{-90/T}$	

Table 1 (continued)

	Reaction	Rate Constant[1] or Cross Section Data	Reference[2]
(133)	$C_3H_8 + OH \rightarrow H_2O$ + products	$1.6(-11)\ e^{-800/T}$	
(134)	$C_3H_8 + Cl \rightarrow HCl$ + products	$1.4(-10)\ e^{40/T}$	
(135)	$F + O_3 \rightarrow FO + O_2$	$2.8(-11)\ e^{-226/T}$	
(136)	$F + H_2 \rightarrow HF + H$	$1.9(-10)\ e^{-570/T}$	
(137)	$F + CH_4 \rightarrow HF + CH_3$	$3.0(-10)\ e^{-400/T}$	
(138)	$F + H_2O \rightarrow HF + OH$	$2.2(-11)\ e^{-200/T}$	
(139)	$FO + NO \rightarrow F + NO_2$	2.6(-11)	
(140)	$2FO \rightarrow 2F + O_2$	1.5(-11)	
(141)	$FO + O \rightarrow F + O_2$	5.0(-11)	
(142)	$HF + O(^1D) \rightarrow F + OH$	2.0(-10)	See text
(143)	HF $\xrightarrow{\text{rainout}}$ products		As in (87)
(144)	$COF_2 + h\nu \rightarrow 2F + CO$	$185 < \lambda < 225$	
(145)	$COFCl + h\nu \rightarrow F + Cl + CO$	$185 < \lambda < 225$	

[1] Read a(-b) as a x 10^{-b}. Units are $cm^3\ s^{-1}$ for two-body reactions, $cm^6\ s^{-1}$ for three-body reactions, and nm for photodissociation wavelength range. For three-body reactions, values are usually listed as (k_o; k_∞; F_c) where k_o ($cm^6\ s^{-1}$) and k_∞ ($cm^3\ s^{-1}$) are low and high pressure limits and the rate constant is expressed as:

$$k(M,T) = \frac{k_o\,[M]}{1 + (k_o[M]/k_\infty)}\ F_c^{\left\{1 + [\log(k_o[M]/k_\infty)]^2\right\}^{-1}}$$

[2] Unless otherwise stated, reference is DeMore et al. (Report JPL 82-57, 1982).

chlorine chemistry. The expression used for H_2O_2 formation (reaction #51) is based on the work of Kircher and Sander [1983] (S. Sander, private communication, 1982), without their recently determined temperature dependence (whose main effect is to lower the H_2O_2 abundance in the stratosphere, see Chapter 4):

$$k_{51} = \frac{k_o + 5.2 \times 10^{-11} C_{H_2O} + 1.2 \times 10^{-14} C_{H_2O}^2}{(1 + C_{H_2O})^2} \times (1 + 5.4 \times 10^{-32}[M]/k_o)$$

where $k_o = 4.5 \times 10^{-14} e^{1200/T}$ and $C_{H_2O} = 1.25 \times 10^{-25} e^{4100/T} [H_2O]$. The bracketed term includes a water vapor-dependent effect (useful only in the troposphere) and its associated temperature dependence, whereas the second term expresses the pressure-dependent effect. In the stratosphere (low pressure, low $[H_2O]$), k_{51} becomes equal to k_o. The value for k_{51} recommended in DeMore et al. (1982) is about 40% lower than the above value. A lower value yet is indicated by the pressure and temperature-dependent studies of Kircher and Sander [1983]; a lower temperature dependence has also been determined by Patrick and Pilling [1982] and Thrush and Tyndall [1982]. The $OH + HO_2$ reaction rate constant (k_{47}) follows the pressure dependence recommended in DeMore et al. [1982], but includes a temperature-dependent factor consistent with the--somewhat preliminary--results of F. Kaufman's group (paper presented at the 7th International Symposium on Gas Kinetics, Göttingen, 1982), which increases the total HO_x ($OH + HO_2$) destruction rate by 10 to 40% in the stratosphere. The rate constants for the various channels of the $H + HO_2$

reaction (#48, 49, and 50) are consistent with the experimental results of Sridharan et al. [1982], although their final published values are slightly different from the results that we used here. Recent possible changes in k_{58} and k_{61} for the OH + HCl (M. Molina, private communication, 1983) and O + ClO [M. T. Leu, 1983; J. Birks, private communication, 1983] reactions are discussed in later chapters. The rate constant k_{64} used for $ClONO_2$ formation follows the "fast" recommended value in DeMore et al. [1982] and is consistent with chlorine nitrate being "the sole product of the $ClO + NO_2 + M$ recombination," as demonstrated by Margitan [1983]. The HO_2NO_2 formation reaction rate constant k_{94} is slightly modified to account for tropospheric water vapor dependence [Sander and Peterson, 1983], which introduces a multiplicative factor of $(1 + 1.07 \times 10^{-18} [H_2O])$ (S.Sander, private communication, 1982). The equilibrium rate constant used in the expression for k_{127} was obtained by S. Sander (private communication, 1982) from data on the thermal decomposition of $CH_3O_2NO_2$ [Bahta et al., 1982], coupled with the forward rate constant data of Sander and Watson [1980]. The rate constant for $HF + O(^1D)$ is estimated to be close to the gas-kinetic limit [Stolarski and Rundel, 1977], but is uncertain by over a factor of three [see DeMore et al., 1982, who recommended $k_{142} = 1 \times 10^{-10}$ $cm^3 s^{-1}$]. This uncertainty is not critical, however, since transport time scales are many times faster than this chemical loss time scale and HF will be lost mostly by downward transport to the troposphere and subsequent rainout. Reactions (87) through (93), as well as (143) are an attempt to describe average rainout losses for water soluble gases in the troposphere, as discussed in Logan et al. [1981]. Reaction (130) between hydroxyl radicals and acetelyne should probably be modified

at low pressures (DeMore, private communication, 1982); we note that it is a significantly faster rate than the expression used in Chameides and Cicerone [1978], which produced a much better fit to the C_2H_2 data of Rudolph et al. [1981]. Reaction 106 schematically represents a latitude-dependent average production of NO by cosmic ray ionization of nitrogen mostly in the lower stratosphere [see Dalgarno, 1967; Nicolet, 1975]. This source varies with solar activity (deflecting action) and latitude (magnetic focusing at high latitudes) and we have used average production rates based on Nicolet [1975] for six latitude bins (four 10° bins between 15° and 55°, one bin below 15°, and one above 55°). This produces a non-negligible natural source of NO mostly at high latitudes and at night [see also Ashby, 1976]. Reaction (118) represents a tropospheric source of odd nitrogen apparently required (in simple one-dimensional models) to match observations of NO_x, HNO_3, and O_3 in the clean troposphere [see Logan et al., 1981]. Lightning and oxidation of ammonia have been proposed as significant global odd nitrogen sources, but the relative role of in-situ sources versus downward transport from the stratosphere is not yet well determined in terms of NO_x and O_3 production in the troposphere [see e.g., Fishman and Crutzen, 1977; Fishman, 1981; Callis et al., 1983].

For the photodissociation reactions in Table I, reference is made to the source of the cross section data (mostly from the complication in DeMore et al. [1982] as well as the wavelength region used in the model. Our total coverage in wavelength extends from 96 to 800 nm, although strong O_2 absorption as well as the wavelength variation in solar flux at the top of the atmosphere limit the radiation in the stratosphere to

wavelengths above 175 nm. The model wavelength bins are typically 5 nm wide below 402.5 nm and 10 nm wide from 410 to 800 nm. Cross sections sometimes depend on temperature, and quantum yields for various channels can also depend on temperature and wavelength. An example of the effect of temperature and wavelength dependences on photodissociation rates is shown in Figure 1 for reaction (4), the major source of $O(^1D)$ radicals in the stratosphere. The photodissociation rate constant ("j value") for this process can be written as:

$$j(z) = \sum_{\lambda} F_{\infty}(\lambda)\ \sigma(\lambda)\ \phi(\lambda,T)\ e^{-\tau_s(z)} \qquad (4)$$

where $F_{\infty}(\lambda)$ is the solar flux ($cm^{-2}\ s^{-1}$) at the top of the atmosphere, $\sigma(\lambda)$ is the absorption cross section (cm^2) for ozone (in cases such as O_2, CF_2Cl_2, N_2O_5, or N_2O, $\sigma(\lambda) = \sigma(\lambda,T)$), $\phi(\lambda,T)$ is the temperature (and wavelength) dependent quantum yield for $O(^1D)$ formation near 310 nm [DeMore et al., 1982], and $\tau_s(z)$ is the slant optical depth from height z to ∞.

Figure 1 shows the effect of neglecting the temperature (altitude) variation of $\phi(\lambda,T)$ on j_4 and j_3; the temperature-independent case (solid line) follows the recommendation of DeMore et al. [1981] for 263 K, whereas the dashed line represents the temperature-dependent values [DeMore et al., 1982]. In both cases, $\phi = 0.90$ below 300 nm. These calculations are diurnally-averaged for 45°N latitude at 23° solar declination (summer), with U. S. Standard Atmosphere 1976 profiles for O_2, N_2, O_3, P and T. While the total photodissociation rate ($j_3 + j_4$) of O_3 is essentially unchanged due to the limited contribution from j_3 and the decreasing importance of the 310 nm wavelength range as z increases, there is a decrease

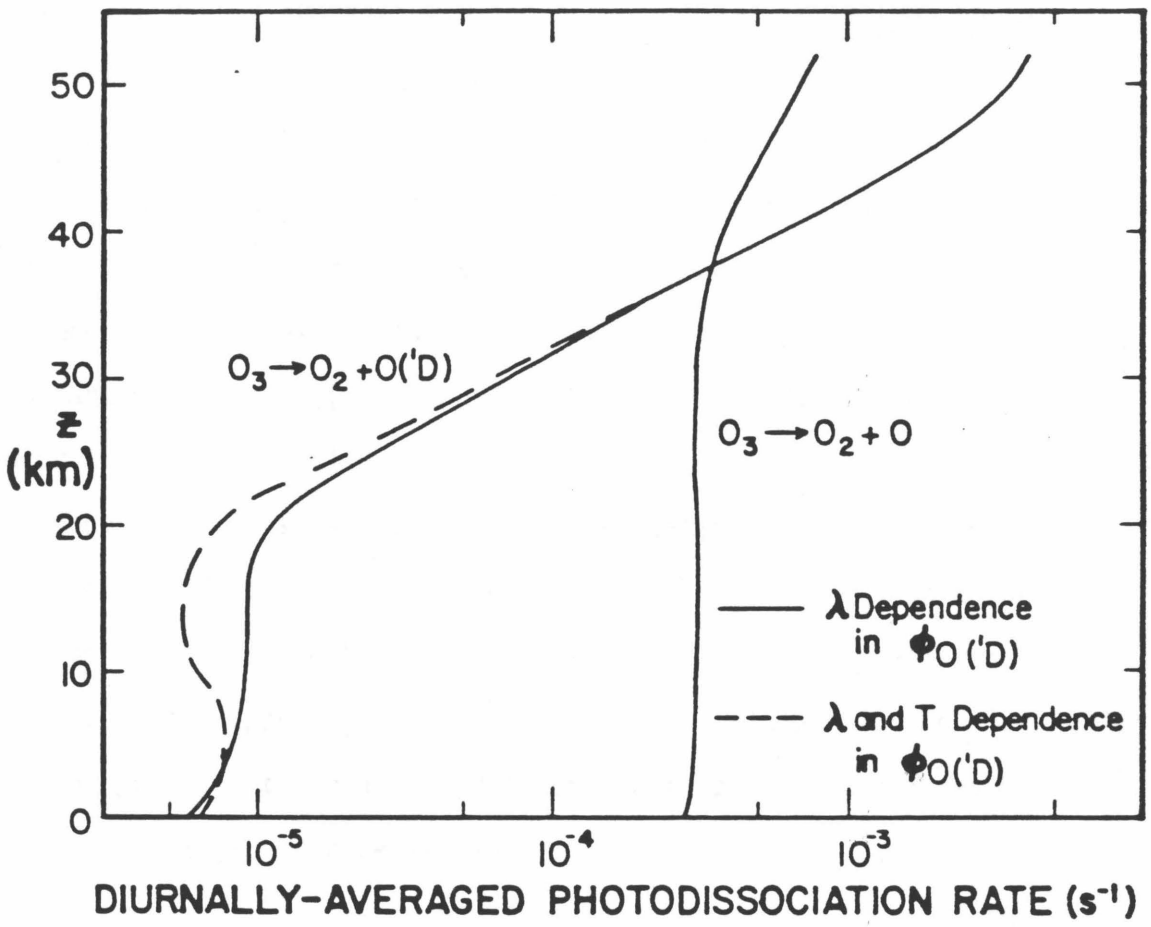

Figure 1. Effect of the temperature dependence of the quantum yield for $O(^1D)$ production on the ozone photodissociation rate constants versus altitude.

in j_3 of up to 30% in the lower stratosphere. This leads to fewer $O(^1D)$ radicals, which will imply less production of OH and NO via reactions (26) and (29). Reactions (1) through (4), (114), and (115) constitute the important extinction reactions that contribute to the calculation of optical depths (see section 1.3). NO_2 extinction, reaction (114), represents absorption without photodissociation (NO_2 photolysis is reaction (10)) and is everywhere quite small compared to absorption by O_2 or O_3. Reaction (115) refers to the Rayleigh scattering cross sections discussed in the next section. Most photodissociation reactions occur at wavelengths less than 400 nm and an earlier version of our model did not explicitly include the range beyond 400 nm. Instead, constant values for $j(NO_3)$ and $j(O_3$, Chappuis band) were used. We have added the range from 410 to 800 nm in order to more accurately describe the above reactions as well as Rayleigh scattering in the atmosphere. For example, Figure 2 illustrates the variation of $j(O_3)$ as a function of time of day for 30°N latitude, equinox conditions, scattering included. The Chappuis band (410 nm $< \lambda <$ 800 nm) contribution is a major part of $j(O_3)$ in the middle and lower stratosphere and becomes more important at large solar zenith angles (χ). The oxygen atom production from ozone photolysis is correctly calculated at all times if the Chappuis band is explicitly included in the model. At the shorter wavelengths, from 175 to 200 nm, we have to deal with the very fine structure of the O_2 Schumann-Runge bands [see e.g., Frederick and Hudson, 1979, 1980; Yoshino et al., 1983]. The bands comprise hundreds of lines which become rapidly opaque as the height decreases; as z decreases, or as χ increases, photons become more sensitive to the regions between lines and

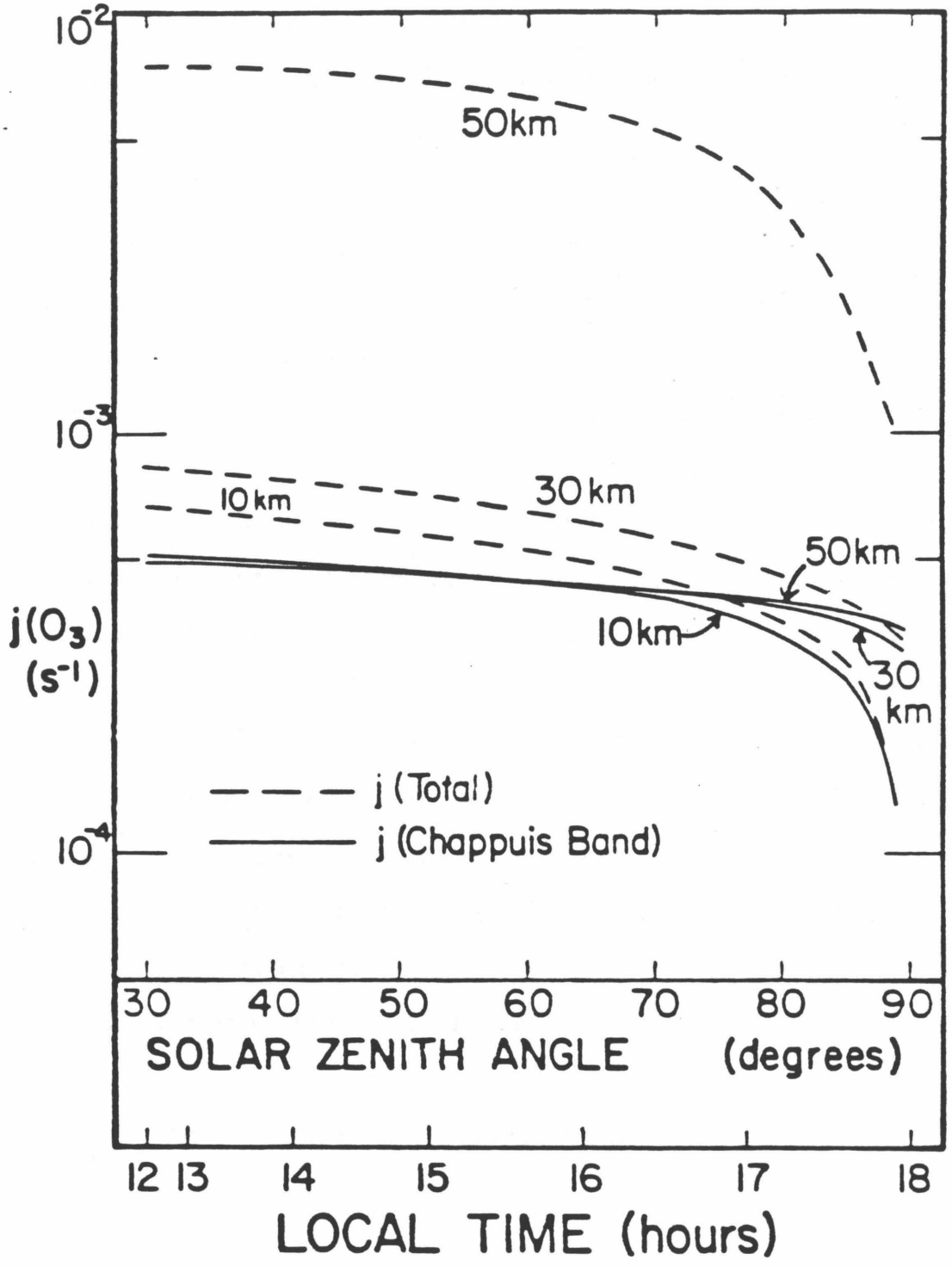

Figure 2. Ozone photodissociation rate constant versus solar zenith angle, at various heights. The Chappuis band (410 to 800 nm) contribution is compared to the total value.

the effective cross section in a 5 nm bin decreases. The computationally accurate (compared to line-by-line calculations) and efficient parametrization of altitude- and zenith-dependent O_2 cross sections by Allen and Frederick [1982] is used in this work. This also affects photolysis of H_2O and NO. The O_2 absorption cross sections in the 200 to 230 nm region (Herzberg continuum) have been measured by various groups with a wide range of results (almost a factor of two); this uncertainty leads to a large uncertainty in the absolute amount of solar radiation reaching the lower stratosphere, where species such as N_2O, HNO_3, and the halocarbons photodissociate near 200 nm. If one adopts cross section values significantly lower (by about 0.6) than the average laboratory data, significant improvement between the model chlorofluorocarbon vertical profiles and observations is obtained [Froidevaux and Yung, 1982], as discussed in Chapter 3. Recent in situ observations of solar fluxes transmitted down to the 30-40 km region [Frederick and Mentall, 1982; Herman and Mentall, 1982] have led to a determination of the O_2 absorption cross sections in the Herzberg continuum and the results are lower than the lowest laboratory data. We have adopted the values from Herman and Mentall [1982] in the 196 to 250 nm region (similar to data of Shardanand and Prasad Rao, 1977, beyond 215 nm) for model results described in Chapters 2, 4, and 5. Above 196 nm in the Schumann-Runge band region (spectral intervals 1 through 5 in Allen and Frederick, 1982), we have reduced the effective cross section by a factor of 0.55.

The input for solar flux at the top of the atmosphere comes from various sources. The accuracy of measurements made from rocket and, more recently, from satellites has improved to the point that the

uncertainty in fluxes is about 10% or less. There is, however, some natural variability in the solar output, mostly below 200 nm, in relation to the 27-day solar rotation period as well as the 11-year solar cycle [Rottman et al., 1982; Mount et al., 1980; Mount and Rottman, 1981; Rottman, 1981; Lean et al., 1982]. The reference solar flux generally used below 315 nm corresponds to the observations near solar maximum of Mount and Rottman [1981], while above that wavelength, the tables of Hudson et al. [1982] are used. Our models of the ClO diurnal variation for the most recent observations of ClO by Solomon et al. [1983] used the solar minimum flux observations of Mount and Rottman [1983]. The model atmospheres for the mid-latitude work described here involve pressure and temperature values for every level, total number density (from ideal gas law), and number densities for N_2 (78.08% x [M]) and O_2 (20.95% x [M]). Summer, winter and spring/fall models are taken from the CIRA 1972 tabulations for 30°N latitude and altitudes above 25 km. Below 25 km, we refer to the tables in Houghton [1977] for 40°N latitude, June, December, and March. Another model often used near 45°N is the U. S. Standard Atmosphere 1976. Water vapor amounts vary significantly from season to season, particularly in the troposphere. We fix the H_2O concentrations in our model calculations from 0 to 80 km, but generally solve for [H_2O] along with other species when 16-80 km or 16-60 km runs are involved. The fixed tropospheric profile is taken from an average of the northern mid-latitude data shown in Logan et al. [1981]. Our fixed profile from 16 to 40 km is taken from an average of 4 profiles obtained from mass spectrometer balloon measurements in the stratosphere (Mauersberger, private communication, 1982); these data

show remarkable consistency (spread of ±20%), given that they were taken at various seasons from 1979 to 1981. Above 40 km, the fixed profile is extrapolated using model results. The resulting profile is constant at 3.6 ppm from 16 to 34 km and increases to 4.5 - 5 ppm between 40 and 50 km with a slow decrease above the stratopause. When we solve for water vapor above the tropopause, we typically find about 7 ppm between 40 and 50 km, a value close to the average of a large number of past observations (J. Frederick, private communication. 1983). We agree with Frederick that any individual observed profile can vary significantly from model predictions due to variations in the release rate at the cold tropopause as well as horizontal transport, but that the increase in the average of many measurements seems to fit model results in terms of the methane oxidation sequence producing H_2O in the stratosphere. Nevertheless, such variations in H_2O are a source of uncertainty in hydroxyl radical concentrations throughout the atmosphere.

Northern mid-latitude model boundary conditions for the longer-lived species and upward diffusing source species of biologic or anthropogenic ground origin (such as H_2, N_2O, CH_4, CO_2, CO, chlorofluorocarbons) are listed in Table II. All other species are relatively short-lived with respect to transport and assumed in local photochemical equilibrium with $\Phi = 0$ at both boundaries. After experimenting with various types of boundary conditions, we have found that the list in Table II is probably as valid as any other reasonable choice of boundary conditions. This is particularly true for model results at altitudes sufficiently removed (5 to 10 km) from the boundaries so that their sensitivity to the boundary condition types or values is small. For example, reasonable velocity or flux boundary conditions at 80 km will produce negligible differences

Table II. Boundary Conditions[1] for Northern Mid-latitudes

Species[2]	0 km	16 km[3]	80 km	Fixed Profile in Diurnal Run
O_3	v = -0.2	Fixed f	ǎ = 0	No
H_2	f = 5.30(-7)	Fixed f	ǎ = -5.0(8)	Yes
H_2O	Fixed in troposphere	f = 3.60(-6)	ǎ = 0 (or fixed profile)	Yes
H_2O_2	v = -0.2	Fixed f	ǎ = 0	No
N_2O	f = 3.10(-7)	Fixed f	ǎ = 0	Yes
HNO_3	v = -0.2	Fixed f	ǎ = 0	No
HO_2NO_2	v = -0.2	ǎ = 0	ǎ = 0	No
CH_4	f = 1.65(-6)	Fixed f	ǎ = 0	Yes
$CH_3O_2NO_2$	v = -0.2	ǎ = 0	ǎ = 0	No
CO	f = 1.10(-7)	Fixed f	ǎ = -3.0(9)	Yes
CO_2	f = 3.20(-4)	Fixed f	ǎ = +3.0(9)	Yes
CH_3OOH	v = -0.2	Fixed f	ǎ = 0	No
$ClONO_2$	v = -0.2	ǎ = 0	ǎ = 0	No
HCl	f = 8.00(-10)	Fixed f	ǎ = 0	No
CH_3Cl	f = 6.10(-10)	Fixed f	ǎ = 0	Yes
CF_2Cl_2 (FC12)	f = 2.40(-10)	Fixed f	ǎ = 0	Yes
$CFCl_3$ (FC11)	f = 1.40(-10)	Fixed f	ǎ = 0	Yes
CCl_4	f = 1.30(-10)	Fixed f	ǎ = 0	Yes
$C_2H_3Cl_3$	f = 1.10(-10)	Fixed f	ǎ = 0	Yes
CHF_2Cl (FC22)	f = 6.00(-11)	Fixed f	ǎ = 0	Yes
$C_2F_3Cl_3$ (FC113)	f = 1.90(-11)	Fixed f	ǎ = 0	Yes

Table II (continued)

Species[2]	0 km	16 km[3]	80 km	Fixed Profile in Diurnal Run
$C_2F_4Cl_2$ (FC114)	f = 1.20(-11)	Fixed f	$\bar{s}$ = 0	Yes
C_2H_2	f = 4.00(-10)		$\bar{s}$ = 0	
C_2H_6	f = 2.00(-9)		$\bar{s}$ = 0	
C_3H_8	f = 4.00(-10)		$\bar{s}$ = 0	
COF_2	v = -0.2		$\bar{s}$ = 0	
COFCl	v = -0.2		$\bar{s}$ = 0	
HF	v = -0.2		$\bar{s}$ = 0	

[1]Read a(-b) as a x 10^{-b}. Symbols are v for vertical velocity (cm s^{-1}), f for volume mixing ratio, and $\bar{s}$ for vertical flux (cm^{-2} s^{-1}). $\bar{s}$ and v are positive upwards and negative downwards.

[2]All other species are assumed in local photochemical equilibrium with $\bar{s}$ = 0. The last six species were not included in models other than diurnal average calculations from 0 to 80 km.

[3]In model calculations above 16 km, the "Fixed f" lower boundary condition is obtained from 0 to 80 km model results.

in model concentrations obtained with boundary conditions described in Table II. The main exceptions involve H_2 and CO, for which downward flux conditions are used at 80 km; the latter flux values were obtained from model results for mesosphere/thermosphere photochemistry at mid-latitudes (Allen, private communication, 1982), in the 40 to 130 km range. The downward fluxes of H_2 and CO are due to photodissociation of H_2O and CO_2 above 80 km. Our 0 to 80 km ("stratospheric") and 40 to 130 km ("mesospheric") models have been compared in detail for similar latitudes and solar flux conditions and were found to be in very good agreement in the overlapping region (40 to 80 km), taking into account the small differences produced by the lack of chlorine and nitrogen chemistry in the mesospheric version. The odd nitrogen ($NO_x = NO + NO_2$) fluxes in the mesosphere consist of an upward stratospheric contribution and a downward thermospheric contribution which probably cancel to a large extent [Jackman, et al., 1980]; hence, our choice of zero flux at 80 km should be reasonable in terms of the effect on stratospheric NO_x amounts (at mid-latitudes). The limited sensitivity to the upper boundary condition comes from the fact that the concentrations drop fairly rapidly with altitude for most gases, so that even a significant change in flux (or concentration) at 80 km will produce little change in the stratosphere. We are therefore justified in using somewhat crude estimates for all mid-latitudes and seasons, although this might not hold for polar latitudes. Similarly, the lower boundary deposition velocities ($v = -0.2$ cm/s) that are applied to certain species (mostly of stratospheric origin, diffusing downwards) are rough average values. Aldaz [1969] estimated the deposition rates of ozone over land and ocean surfaces and

found the land sink to be largest by an order of magnitude. However, changes in v by a factor of three produce little variation in important chemical species above the tropopause. The most important boundary conditions involve the source species that diffuse upwards into the stratosphere and directly affect the photochemistry in that region; these are H_2O (see previous discussion), H_2, N_2O, CH_4, CO_2, CO, and the halocarbons. A review of their source origins and strengths can be found in Hudson and Reed [1979] and Hudson et al. [1982]. Mixing ratios are generally used as lower boundary conditions, although some modelers choose average fluxes, particularly in the case of chlorofluorocarbons; while fluxes might be more physically realistic, they are not measured directly like mixing ratios. The halocarbon mixing ratios used here correspond to average 1978 values for the four major anthropogenic sources (CF_2Cl_2, $CFCl_3$, CCl_4, and $C_2H_3Cl_3$). Since it takes about two years to thoroughly transport and mix these source gases into the stratosphere, there will be a certain time lag before steady state is reached (or approached) in the upper atmosphere, given that the total amount at ground level increases by about 10% per year [Hudson et al., 1982]. Our stratospheric results are probably best compared to 1979-80 data, in terms of chlorine chemistry. Boundary conditions for FC113 and FC114 are taken from the review by Cicerone [1981] and the FC22 value is consistent with measurements of Rasmussen et al. [1980] and Leifer et al. [1981], which indicate about 50 ppt (slightly less than our adopted value of 60 ppt) near the ground at northern mid-latitudes. These three gases are less abundant than the 5 main chlorine source species in the troposphere, but they are not destroyed as fast in the stratosphere and can contribute a

non-negligible source of chlorine in the middle and upper stratosphere (see Chapter 4). The HCl mixing ratio of 8×10^{-10} at ground level is consistent with the results of Farmer et al. [1976], although their estimate of tropospheric HCl was rather crude; their profile implies that about two-thirds of the total HCl column resides in the troposphere. The HCl amount in the troposphere might be influenced by ocean proximity. More recent infrared ground spectra taken from Los Angeles (by Farmer's group) and Kitt Peak (by R. Zander) show much less tropospheric HCl contribution (Farmer, private communication, 1983). A varying tropospheric HCl amount should not, however, influence the stratospheric abundance by more than 5-10% due to the tropospheric rainout rate which acts as a loss of HCl before transport can bring it into the stratosphere, where it is produced from halocarbons.

The eddy diffusion coefficients used in this work are plotted as a function of altitude in Figure 3 and discussed further in Chapter 3 in terms of CF_2Cl_2 and $CFCl_3$ stratospheric profiles [see also Froidevaux and Yung, 1982]. We have varied the eddy diffusion profile in various ways and checked the sensitivity of N_2O, CH_4, and halocarbon mid-latitude profiles to transport. Given the range of observed profiles, there is no unique solution for an acceptable eddy diffusion profile, although it is clear that a sharp decrease in the lower stratosphere ($\sim$18 km), followed by a relatively smooth increase to higher altitudes, is needed. If the increase is too abrupt, values of N_2O, CH_4, and chlorofluorocarbon mixing ratios become too large compared to observations. As discussed further in Chapter 3, the sharp decrease in halocarbons (FCl1 in particular) in the stratosphere probably requires more than a vertical

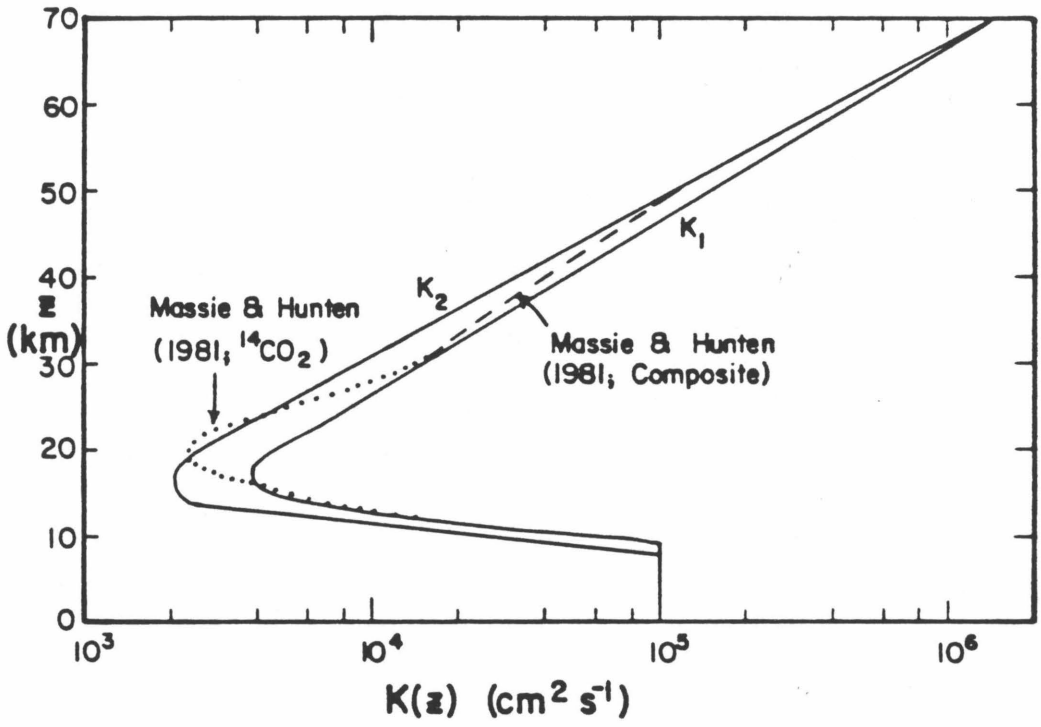

Figure 3. Model eddy diffusion coefficients versus height. Profile K_1 is very similar to the composite profile deduced by Massie and Hunten (1981) and is used for latitudes near 30° N. Profile K_2 is preferred for latitudes near 45°N (see text) and is closer to the values derived from $^{14}CO_2$ tracer data by Massie and Hunten.

transport adjustment (in order to still fit N_2O and CH_4 observations) and the radiation field near 200 nm should also be known accurately. Massie and Hunten [1981] have made a more systematic study of N_2O and CH_4 vertical profiles as a function of latitude and solved for K(z) using equations (1) and (2) in steady-state:

$$K(z) = n_a(z) \frac{\partial f_i(z)}{\partial z}^{-1} \int_z^\infty [P_i(z) - L_i(z)]\, dz \qquad (5)$$

where $\partial f_i/\partial z$ represents a weighted global average of observations. $P_i(z)$ is zero for species such as N_2O and CH_4 and $L_i(z)$ is calculated from a photochemical model--photodissociation is the main loss for N_2O, attack by OH, $O(^1D)$ and Cl destroys CH_4--and observations (extrapolated above 40 km). Massie and Hunten also used downward ozone flux estimates in the lower stratosphere to obtain limited information on K(z) in the region below 20 km. Diffusion of $^{14}CO_2$ left over from a large series of nuclear tests in the 1960's provided another constraint with time information as well [see also Johnston et al., 1976]. The resulting "best fit" composite eddy diffusion profile of Massie and Hunten [1981], along with their $^{14}CO_2$ profile, is shown in Figure 3 (0 to 50 km). Our profile $K_1(z)$ is very similar to the composite profile and is continued upward to 70 km, where it matches the K(z) value obtained by Allen et al. [1981] in a study of O, O_2, CO_2, Ar, and CO observations in relation to thermospheric and mesospheric transport. This profile is used (in conjunction with the values above 70 km from Allen et al. [1981]) for our standard models near 30°N. For observations of N_2O, CF_2Cl_2, and $CFCl_3$ near 45°N [see Hudson et al., 1982], we prefer to use a somewhat slower rate of mixing, namely profile

$K_2(z)$ in Figure 3, as discussed further in Chapter 3. It is generally agreed that vertical transport decreases from the equatorial regions (upwelling part of Hadley cell) to mid-latitudes. This idea seems to be supported by observations of the mixing ratio vertical gradients for CH_4 [Ehhalt and Tönnissen, 1980] as a function of latitude, as well as for N_2O, CF_2Cl_2, $CFCl_3$, and CCl_4 [Vedder et al., 1978, 1981; Goldan et al., 1980; Gallagher et al., 1983]. Two-dimensional models typically use a latitudinally-varying K(z) [e.g., Miller et al., 1981]. The eddy diffusion vertical profiles used here can be described semi-analytically as shown in Table III. Values in the troposphere are difficult to determine from observations of vertical concentration profiles since fast convection and small photochemical losses yield small $\partial f_i/\partial z$ values for observable species. The adopted value of $1 \times 10^5 cm^2/s$ translates into a transport (mixing) time scale (H_a^2/K) of about 3 months, where H_a is the atmospheric scale height. The large uncertainty below the tropopause is not very crucial since the "bottleneck" for vertical transport occurs in the lower stratosphere.

1.3 Absorption and Scattering of Solar Radiation

Since the photodissociation of various molecules plays an important role in stratospheric photochemical processes, it is necessary to model the absorption and scattering of the solar flux as accurately as possible. We thus define a mean state of the radiation field, determined by molecular absorption by O_2, O_3, and NO_2, as well as Rayleigh scattering (by O_2 and N_2) and ground Lambert reflection. Our standard model and the results in later chapters combine the absorbed fluxes in a

Table III. Mid-latitude Model Eddy Diffusion Coefficients*

Altitude z (km)	Model K_1	Model K_2
$z \leq 8$	As in Massie and Hunten (1981)	As in Massie and Hunten (1981)
$8 \leq z \leq 14$	As in Massie and Hunten (1981)	$K(z) = 1.0 \times 10^5 \exp\{-(z-8)/1.59\}$
$z = 16$; $z = 18$	As in Massie and Hunten (1981)	$K(z) = 2.1 \times 10^3$
$20 \leq z \leq 70$	$K(z) = 4.6 \times 10^3 \exp\{(z-20)/8.64\}$	$K(z) = 2.5 \times 10^3 \exp\{(z-20)/7.82\}$
$z \geq 70$	As in Allen et al. (1981)	As in Allen et al. (1981)

*Units are $cm^2 s^{-1}$; only 2 significant digits are used in model values.

spherical shell atmosphere with the diffuse component calculated in a plane parallel geometry. We take a closer look at the effects of spherical geometry on the diffuse flux and photochemistry in Chapter 2.

In the case of absorption (or extinction) in a spherical shell atmosphere, many modelers use the Chapman function formulation to calculate slant optical depths. We have replaced this approach (used in our earlier models) by a more exact geometrical ray path length calculation. Although the Chapman function is quite accurate for the Earth's atmospheric applications, our general model is applicable to other systems (such as Titan) where the differences between approaches can become larger; moreover, the exact calculation is implemented in a clearer fashion in our program and, although it requires integration along the ray path for each level, we have saved a little computing time. Figure 4 depicts the geometry--not to scale--for absorption without refraction along a ray path $\overline{SA_o}$ in the Earth's atmosphere. The flux along this path has been exponentially attenuated by the slant optical depth τ_s, which is merely the sum of each layer's incremental opacity along the path: $\Delta\tau_s = s \sum_k \bar{n}_k \bar{\sigma}_k$, where s is the incremental distance through the layer and $\bar{n}_k$ and $\bar{\sigma}_k$ represent average densities and absorption cross sections for each absorbing gas. For point A_o at latitude ϕ_o, height z_{a_o}, hour angle $L_o(t) = (\pi/12)(t - 12)$, with t in hours, and a solar declination δ, the local zenith angle $\chi_{a_o}(t)$ is given by

$$\cos \chi_{a_o}(t) = \sin\delta \sin \phi_o + \cos\delta \cos \phi_o \cos L_o(t) \qquad (6)$$

The general procedure is then to calculate the path length (and opacity) from A_o to the tangent point M, given χ_{a_o} and $h_{a_o} = R + z_{a_o}$, where R is

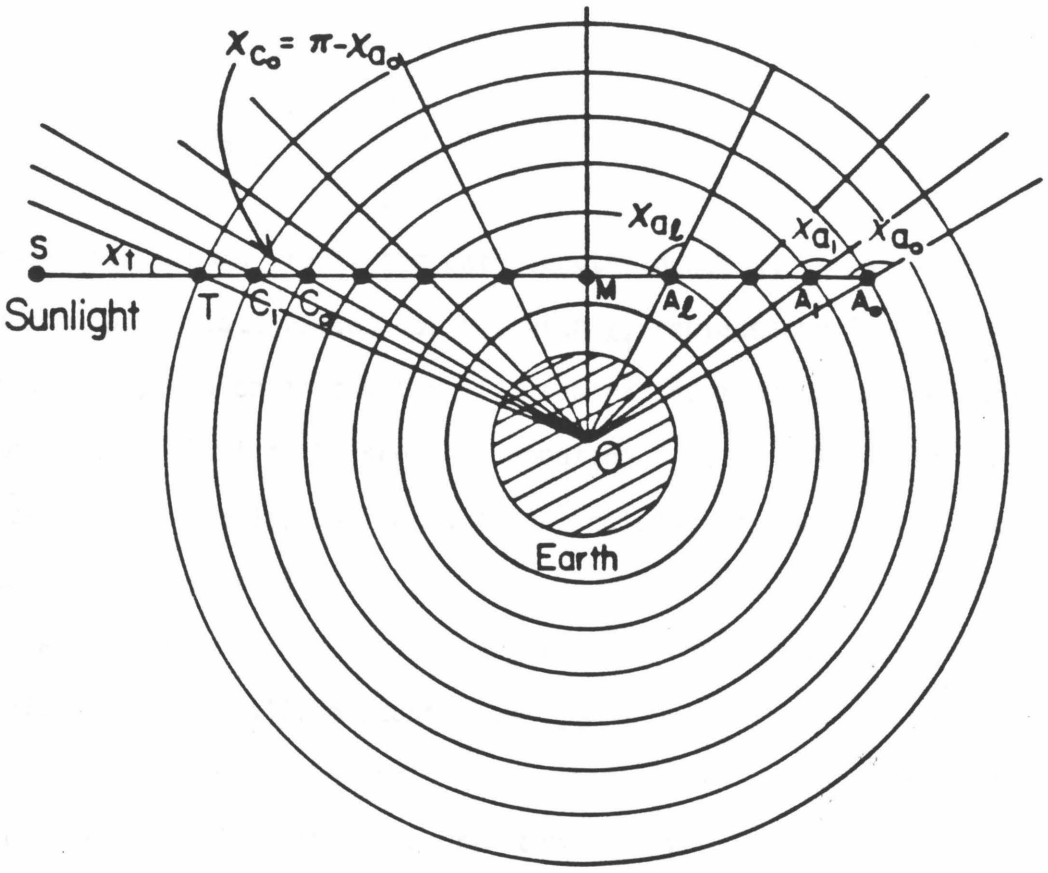

Figure 4. Geometry (not to scale) for calculation of geometric ray path length through the Earth's atmosphere (see text).

the Earth's mean radius (6372 km), and add $\overline{C_oT} + 2\overline{A_oM}$ to obtain $\overline{A_oT}$ (since $\overline{A_oM} = \overline{MC_o}$). Details are given in Appendix A, but simple trigonometry is used to compute values for χ_{a_i} and h_{a_i} at point A_i between A_o and A_ℓ (lowest level before tangent point):

$$\chi_{a_i} = \pi/2 + \arccos[(h_{a_o}/h_{a_i}) \cos(\chi_{a_o} - \pi/2)] \tag{7}$$

and

$$s_{a_i} = (h_{a_{i-1}}^2 - h_{a_i}^2 \sin^2\chi_{a_i})^{1/2} + h_{a_i} \cos \chi_{a_i} \tag{8}$$

In the range from C_o to T, the path length increment is as given in (8) with the appropriate values for h_i, with χ_i replaced by $(\pi - \chi_i)$, and the arccosine expression in equation (7) subtracted from $\pi/2$ rather than being added. Extrapolation is used for computing $\overline{A_\ell M}$, as well as if the ray passes through low layers that are not included in the model altitude range (see Appendix A).

We can compare the above geometrical approach to the Chapman function formulation, originally discussed by Chapman [1931] and reviewed in Appendix B. For a point at height z and zenith angle χ, the total slant optical depth τ_s is related to the normal τ by

$$\tau_s = \tau \, Ch(X,\chi) \tag{9}$$

where $X = (R + z)/H$ and H is the density scale height for the absorbing gas at height z. The Chapman function $Ch(X,\chi)$, which is well represented by $\sec\chi$ for $\chi < 75°$ in the Earth's atmosphere, is defined as follows:

$$Ch(X,\chi) = X \sin\chi \int_0^{\chi} \exp[X(1 - \sin\chi/\sin\chi')] \operatorname{cosec}^2\chi' \, d\chi' \tag{10}$$

$$\text{for } \chi \leq \pi/2$$

and

$$Ch(X,\chi) = 2\exp[X(1-\sin\chi)]\,Ch(X\sin\chi,\pi/2) - Ch(X-\chi) \qquad (11)$$

$$\text{for } \chi > \pi/2$$

Numerical evaluation of these integrals can be performed accurately by using the erf function, as described by Fitzmaurice [1964]. The Chapman function is strictly valid only for exponentially varying density distributions $n = n_0 \exp(-(z - z_0)/H)$, and it takes into account the variation of χ' along the ray path. Moreover, it assumes a constant H (or isothermal atmosphere) and constant absorption cross section σ along the ray path. In an earlier version of our model, we were using the Chapman function in an incremental sense: $\Delta\tau_s = \Delta\tau\ Ch(X,\chi)$, which allows one to vary H and σ along the ray path. However, this is good only if $Ch(X,\chi)$ does not vary much between layers. The total optical depth calculation consists of three main terms (NO_2 is quite insignificant at most wavelengths): O_2 absorption, O_3 absorption and Rayleigh scattering (extinction). The radiation that is removed from the direct flux via Rayleigh scattering is then multiply scattered and returned as a diffuse flux contribution, as discussed later; in terms of the extinction at a given wavelength, the density of interest is [M], which varies in a way similar to O_2. Let us compare the Chapman functions for O_2 and O_3 in the Earth's atmosphere. Figure 5 displays the variation in X(z) for O_2 and O_3 vertical profiles (and inferred scale heights) from the U. S. Standard Atmosphere 1976. H(z) is obtained by inverting the equation $n(z+\Delta z) = n(z)\exp[-(\Delta z/H(z)]$, where $\Delta z = 2$ km. Since $[O_3]$ increases up to about 20 km, the scale height is negative in the lower atmosphere and we have used its absolute

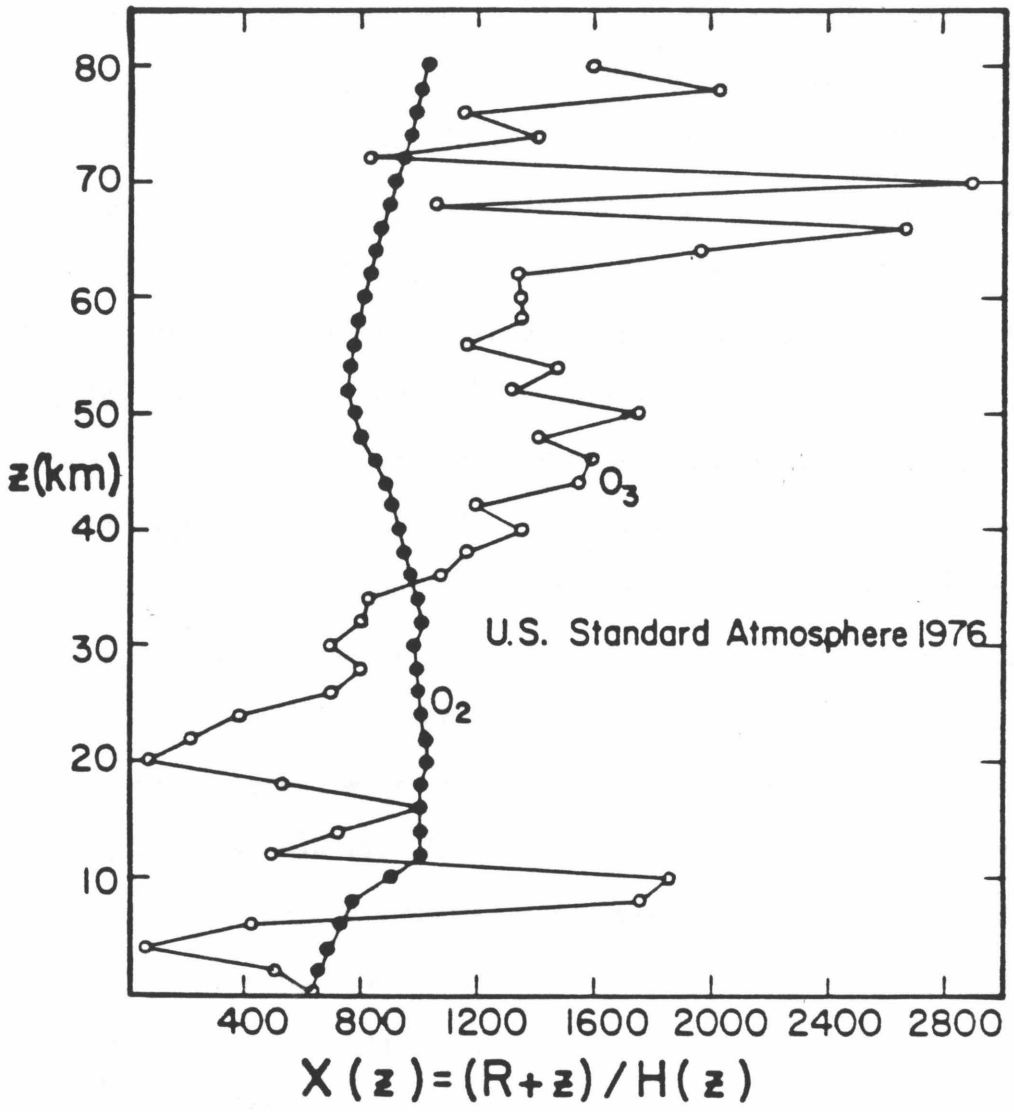

Figure 5. Altitude variation of the variable X that enters in the Chapman function. Differences between O_2 and O_3 profiles are due to scale height variations versus height.

value. This is part of the problem with the Chapman function, which assumes monotonically, as well as exponentially varying densities with height. X_{O_3} also varies significantly with height as compared to X_{O_2}. However, $Ch(X,\chi)$ does not vary much as a function of X for χ less than about 85°, as expected. As shown in Figure 6, the variation with X occurs mainly at the large zenith angles, particularly for $\chi \geq 90°$. The height variation of $Ch(X,\chi)$ is plotted in Figure 7 for 87°, 90°, and 93° zenith angles and U. S. Standard Atmosphere 1976 O_2 and O_3 profiles. The profile for O_2 is rather smooth from level to level, whereas the O_3 curve is much more variable with height, due to the O_3 scale height variations (mostly below 25 km). The total slant optical depth will be affected by both Chapman functions with weighting factors depending on the wavelength. Photodissociation rates are usually a sum over a large number of wavelengths, which dilutes the sensitivity to any particular wavelength. These j-values are, however, the ultimate test of interest, in a comparison of Chapman versus geometric approach to the absorption of solar radiation. For $\chi < 75°$, as expected, we find that both approaches yield j-values equal to within less than 1%. For a zenith angle of 90°, differences of up to 30% can occur for the lower stratosphere and j near $10^{-10}s^{-1}$; however, such low photodissociation rates will not affect the gas abundances, given that little time is usually available for photodissociation near sunset or sunrise. In the optically thinner regions (in altitude and wavelength), the Chapman formulation still yields j-values within 5-10% of the exact calculations at zenith angles near 90°. However, our use of the Chapman function in incremental opacity calculations is not as accurate as in a total slant optical depth determination

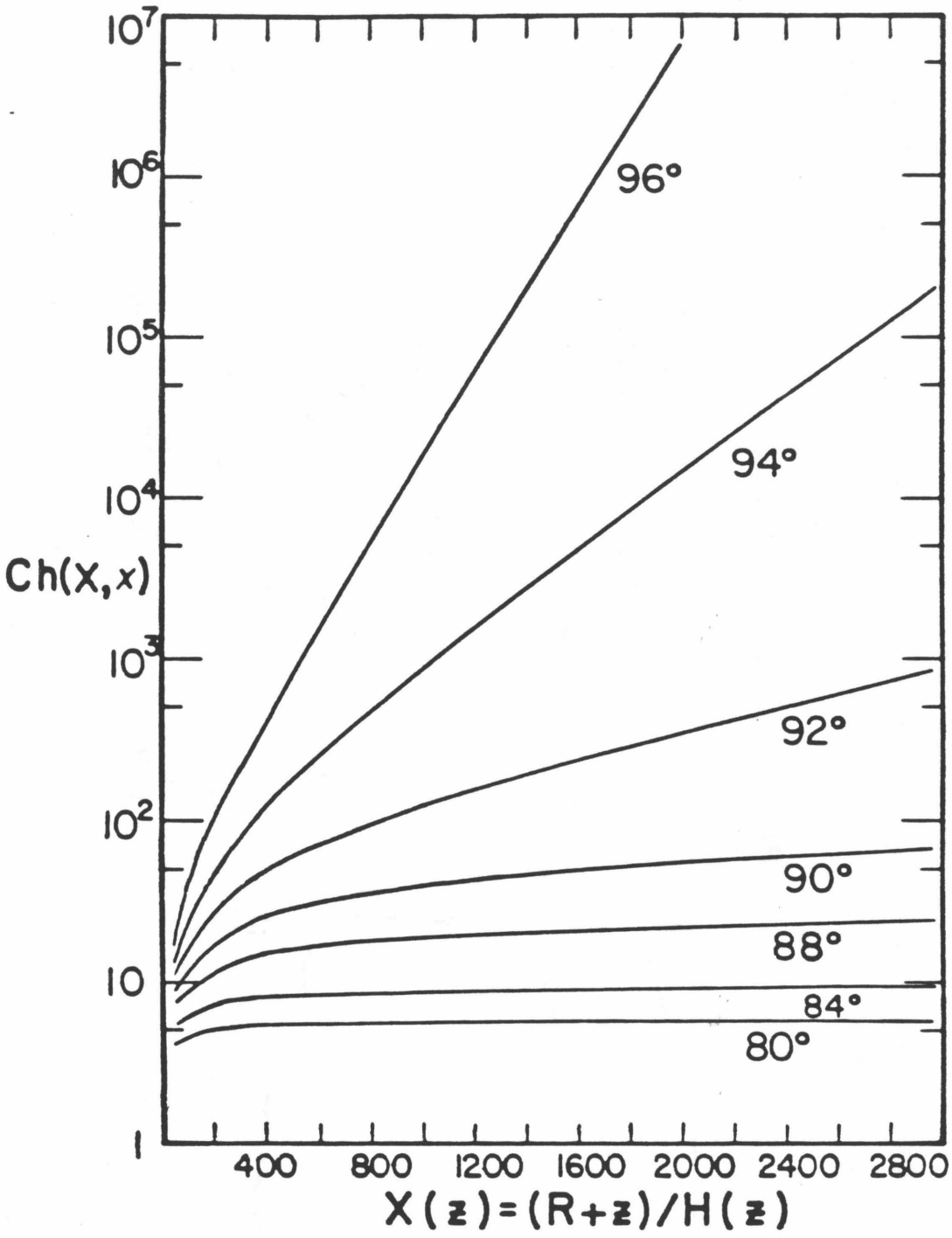

Figure 6. Plot of Chapman function versus X, for various zenith angles. Variation is most pronounced for angles larger than 90°. X varies mostly between 800 and 1600 for the Earth's mid-latitude stratosphere (see Figure 5).

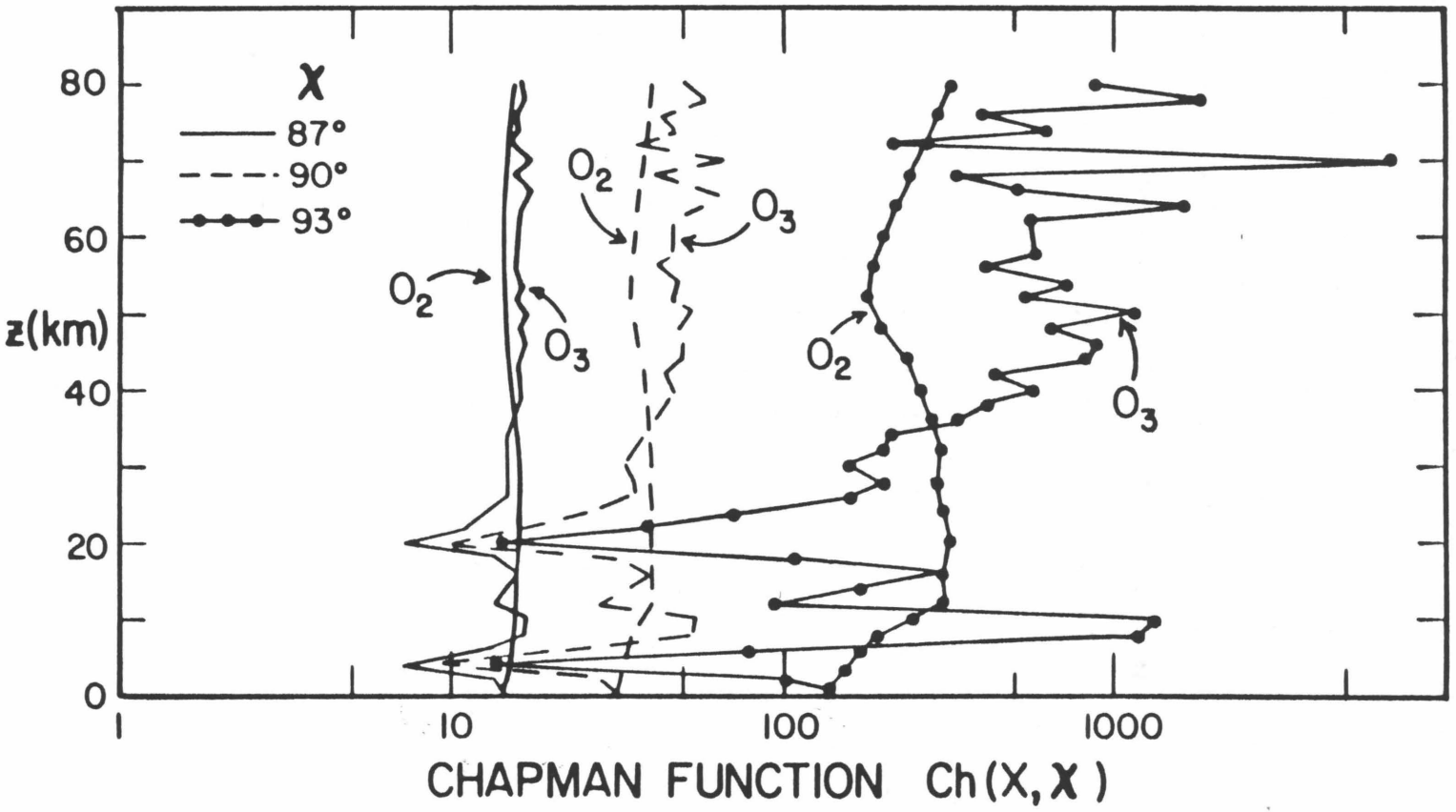

Figure 7. Altitude variation of Chapman function at solar zenith angles of 87, 90, and 93 degrees. O_2 and O_3 abundances are taken from the U.S. Standard Atmosphere 1976 .

(equation (9)), due to the sometimes large height variations in $Ch(X_{O_3},\chi)$ and the non-monotonic O_3 vertical profile. An example of the calculated slant extinction optical depths (τ_s) at various altitudes and as a function of wavelength (λ) between 210 and 800 nm is presented in Figure 8. Strong ozone absorption is evident below 300 nm, as is the weaker O_3 Chappuis band between 500 and 700 nm. The underlying slope between 350 and 800 nm is due to Rayleigh scattering out of the direct solar beam (λ^{-4} dependence of the cross section). The crossing of curves for 20 km and 30 km below 300 nm is due to the ozone peak density region just above 20 km, through which a ray from the sun to 30 km passes twice (for $\chi = 93°$), as opposed to the single passage for a ray terminating at 20 km (beyond its tangent point). The Chapman function approach will not produce such a behavior. Molecular oxygen starts absorbing below about 250 nm and mostly below the 200 nm window region, in the Schumann-Runge bands. As mentioned in section 1.2, the effects of temperature and O_2 column amount are folded into the parametrization of the effective Schumann-Runge band cross sections (σ_{SRB}) versus height and zenith angle [Allen and Frederick, 1982]. The zenith angle dependence for σ_{SRB} in each of the 17 spectral intervals is written as:

$$\sigma_{SRB}(z,\chi) = \sigma_{SRB}(z,0)/(\sec\chi)^{c(z)} \qquad (12)$$

$$\text{for } \chi \leq 60°$$

and

$$\sigma_{SRB}(z,\chi) = \sigma_{SRB}(z,0)/[Ch(z,\chi)]^{c(z)} \qquad (13)$$

$$\text{for } 60° < \chi \leq 90°$$

Values for $\sigma_{SRB}(z,0)$ and $c(z)$ are obtained from Allen and Frederick [1982]

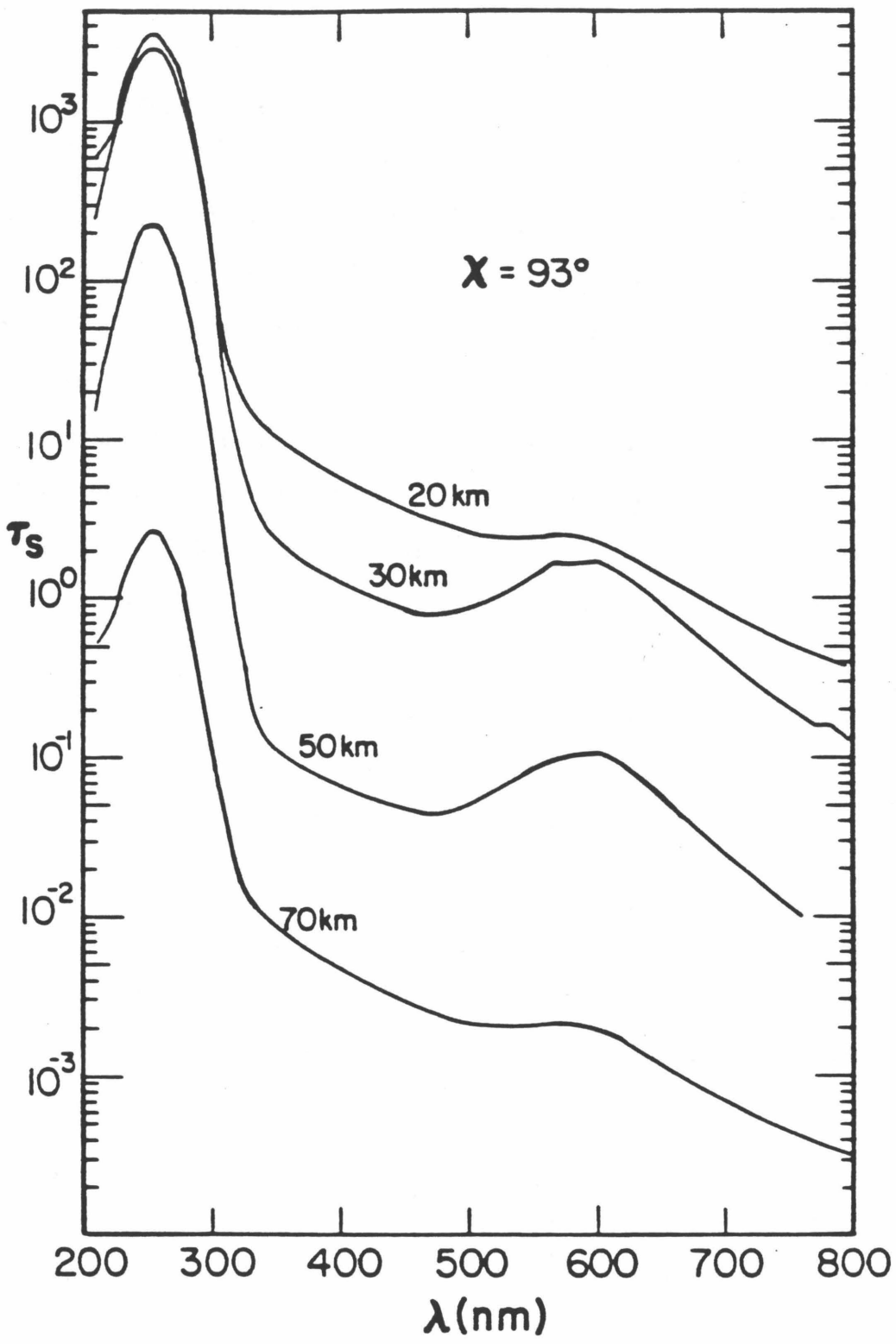

Figure 8. Variation of total slant optical depth versus wavelength, for various altitudes and a solar zenith angle of 93°. Model atmosphere is same as in Figure 7.

as implemented by M. Allen in our program. The Chapman function is retained in the above equations; for $\chi > 90°$, we use $Ch(z,90°)$ in equation (13), since the tangent point should provide the largest weighting for the effective cross section along the ray path. Furthermore, we set a lower limit on $\sigma_{SRB}(z,\chi)$ in each band, as determined by the continuum limit results of Allen and Frederick [1982]. Refraction effects will introduce some errors in the flux calculations at large zenith angles. Figure 9 illustrates the ratio of air mass (column density) for the Chapman function (u_{Ch}) versus an exact ray tracing calculation (u_{Re}), using the results of Snider and Goldman [1975]. The main effect is an overestimate of the absorption in the non-refracted case. While this effect can be non-negligible if one wants to model intensities received at a given altitude, the net effect on the photochemistry should be qualitatively similar to the effect due to the inclusion of diffuse flux in a spherical shell (versus plane parallel) atmosphere discussed in Chapter 2. The cost and difficulties involved in treating refraction in a photochemical model, the probable smallness of the resulting effect on photochemistry and the importance of other uncertainties (cross section values, scattering by air molecules or aerosols and clouds) do not warrant an attempt at including this effect in photochemical models for $\chi \gtrsim \pi/2$.

Multiple scattering has been shown to have a significant effect on photodissociation rates and photochemistry in the stratosphere [Callis et al., 1975; Sundararaman, 1975; Luther and Gelinas, 1976; Isaksen et al., 1977; Luther et al., 1978; Pitari and Visconti, 1979; Fiocco, 1980; Meier et al, 1982; Nicolet et al., 1982]. We have therefore incorporated a

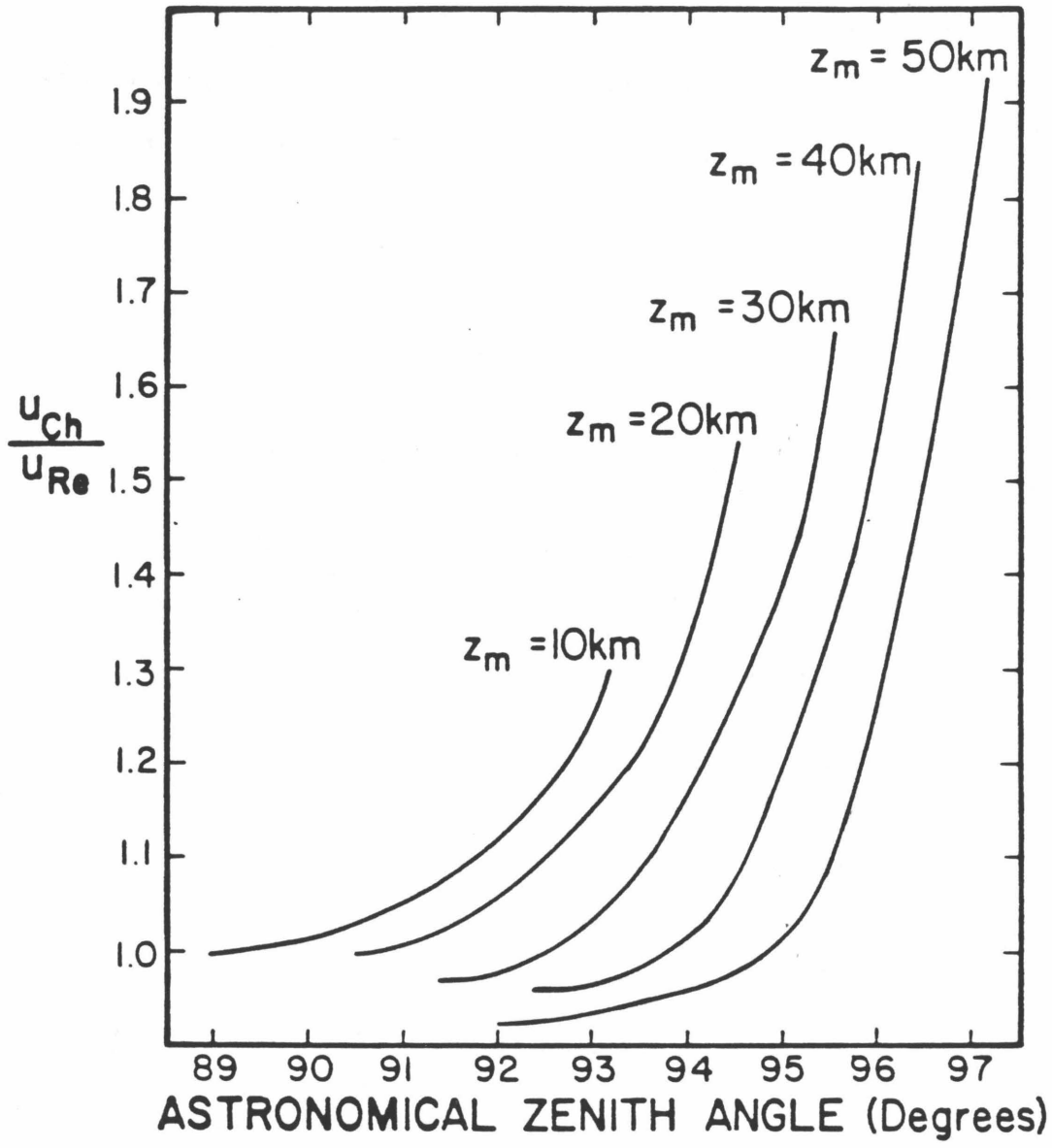

Figure 9. Ratio of air masses from Chapman function calculation to exact, refracted ray tracing results (Snider and Goldman, 1975), as a function of solar zenith angle. Height z_m is the tangent point altitude (refracted ray).

calculation of the diffuse flux in our photochemical model. Without intending to repeat all the results from the above references, we briefly describe our approach and the validation with earlier work on this subject. The total flux F^T affecting molecular photodissociation rates in equation (4) has to be modified to include the diffuse intensity I integrated over solid angle [see e.g., Luther and Gelinas, 1976]. At any wavelength λ, we can write:

$$F^T(z) = F^A(z) + \int_{4\pi} I(z,\omega)\, d\omega \tag{14}$$

where

$$F^A(z) = F_\infty \exp\{-\tau_s(z)\}$$

and τ_s has been defined previously and includes absorption by O_2, O_3, NO_2, as well as extinction due to Rayleigh scattering. According to the classical theory of Rayleigh scattering [see e.g., Liou, 1980] an incident wave (field E_o, intensity I_o) induces an oscillating dipole moment (αE_o, where α is polarizability) in the scattering molecules--O_2 and N_2 in our case--whose acceleration in turn leads to a scattered wave describable at a distance r far from the dipole by an intensity

$$I(\Theta) = \frac{I_o}{r^2}\,\alpha^2\,\frac{128\,\pi^5}{3\lambda^4}\,\frac{p(\Theta)}{4\pi} \tag{15}$$

where the normalized phase function for unpolarized sunlight is

$$p(\Theta) = \frac{3}{4}\,(1+\cos^2\Theta) \tag{16}$$

and Θ is the scattering angle. The familiar dependence on the fourth

power of the frequency comes from the second time derivative of the oscillating field (dipole acceleration), coupled with the proportionality of the intensity on the square of the electric field. The Rayleigh scattering cross section is defined from (15) by:

$$\sigma_R = \frac{128\,\pi^5}{3\lambda^4}\,\alpha^2 \tag{17}$$

The polarizability is related to the index of refraction m of air at density n by the Lorentz-Lorenz formula [see Liou, 1980]:

$$\alpha = \frac{3}{4\pi n}\,\frac{m^2 - 1}{m^2 + 2} \tag{18}$$

Since m is very close to unity for air, we can simplify (18) and use

$$\alpha = \frac{m - 1}{2\pi n} \tag{19}$$

which is not density or height dependent [(m - 1)/n is constant]. For $P_o = 101325\ N/m^2$ and $T_o = 288.16\ K$, such that $n_o = 2.548 \times 10^{19} cm^{-3}$, dispersion measurements by Edlen [1966] have led to the wavelength-dependent formula:

$$m_o - 1 = 10^{-6}[64.328 + 29498.1(146 - 1/\lambda^2)^{-1} + 255.4(41 - 1/\lambda^2)^{-1}] \tag{20}$$

where λ is in μm. This wavelength dependence of the index of refraction leads to a 20% decrease in α between 0.2 and 0.6 μm, implying about 40% variation in σ_R, in addition to the much larger λ^{-4} dependence (factor of 80 effect on σ_R). Combining equations (17), (19), and (20) and including a multiplicative anisotropy factor (King factor) of 1.048 [see Young,

1980], the Rayleigh cross section becomes:

$$\sigma_R(\lambda) = 3.466 \times 10^{-32} \left(\frac{25.25}{\lambda^2} + \frac{11577.0}{(146\,\lambda^2 - 1)} + \frac{100.24}{(41\,\lambda^2 - 1)} \right)^2 \qquad (21)$$

with σ_R in cm^2 and λ in μm. This leads to values very similar to those tabulated by Penndorf [1957].

The diffuse radiation field has been shown to significantly affect photochemistry and photodissociation rates mostly above 290 nm, beyond the strong absorption region due to O_3 and O_2 [e.g., Luther and Gelinas, 1976; Luther et al., 1978], although large changes in flux can occur in the lower stratosphere and troposphere below 290 nm. We have included the diffuse flux in our model for wavelengths above 290 nm. The calculation is based on the solution of the radiative transfer equation [Chandrasekhar, 1960] for an inhomogeneous, plane parallel atmosphere:

$$\mu \frac{dI}{d\tau}(\tau,\mu,\phi) = I(\tau,\mu,\phi) - \frac{\tilde{\omega}_o}{4\pi} \int_{-1}^{1} \int_{0}^{2\pi} p(\mu,\phi;\mu',\phi')\, I(\tau,\mu',\phi')\, d\phi'\, d\mu'$$

$$- \frac{\tilde{\omega}_o}{4} F\, e^{-\tau/\mu_o}\, p(\mu,\phi;-\mu_o,\phi_o) \qquad (22)$$

where $\mu = \cos\theta$ (θ is zenith angle) and ϕ is azimuth; $\mu_o = \cos\theta_o$ and ϕ_o refer to the solar coordinates, and ϕ_o is usually set equal to zero. Also, τ is normal total optical depth, $\pi F = F_\infty$ and $\tilde{\omega}_o$ is the single-scattering albedo:

$$\tilde{\omega}_o = \frac{\sigma_R n_a}{\sigma_R n_a + (\sigma_{O_3} n_{O_3} + \sigma_{NO_2} n_{NO_2})} \qquad (23)$$

and n_a, n_{O_3}, n_{NO_2} represent the air, ozone, and nitrogen dioxide densities, and σ_R, σ_{O_3}, and σ_{NO_2} are cross sections. If shorter wavelengths

were included, $\sigma_{0_2} n_{0_2}$ would have to be added to the denominator. We note that

$$\cos\Theta = \mu\mu' + (1-\mu^2)^{1/2}\,(1-\mu'^2)^{1/2}\cos(\phi-\phi') \tag{24}$$

which allows us to write the phase function (16) as:

$$p(\mu,\phi;\mu',\phi') = p^{(0)}(\mu,\mu') + p^{(1)}(\mu,\mu')\cos(\phi-\phi') + p^{(2)}(\mu,\mu')\cos[2(\phi-\phi')] \tag{25}$$

with

$$p^{(0)}(\mu,\mu') = p^{(0)}(-\mu,\mu') = \frac{3}{8}\left[3-\mu^2+(3\mu^2-1)\,\mu'^2\right] \tag{26}$$

$$p^{(1)}(\mu,\mu') = -p^{(1)}(-\mu,\mu') = \frac{3}{2}(1-\mu^2)^{1/2}\,(1-\mu'^2)^{1/2}\,\mu\mu' \tag{27}$$

$$p^{(2)}(\mu,\mu') = p^{(2)}(-\mu,\mu') = \frac{3}{8}(1-\mu^2)\,(1-\mu'^2) \tag{28}$$

We use the Feautrier method [Feautrier, 1964] to solve the integro-differential equation (22). This procedure has been described by Gladstone [1982] in a somewhat different application for radiative transfer in the Jovian upper atmosphere and we have used the basic subroutines developed by R. Gladstone for calculating $I(\tau,\mu,\phi)$ and the diffuse flux of interest. Prather [1974] has also described this method of solution for a Rayleigh scattering atmosphere, including polarization. Briefly, one can expand the intensity to the same order as the phase function:

$$I(\tau,\mu,\phi) = I^{(0)}(\tau,\mu) + I^{(1)}(\tau,\mu)\cos(\phi-\phi_o) + I^{(2)}(\tau,\mu)\cos[2(\phi-\phi_o)] \tag{29}$$

which then yields three separate equations for $I^{(0)}$, $I^{(1)}$, and $I^{(2)}$, similar to (22). For each component i, upwards and downwards intensities are defined

$$I^{+(i)}(\tau,\mu) = I^{(i)}(\tau,\mu) ; \qquad \mu > 0 \tag{30a}$$

$$I^{-(i)}(\tau,\mu) = I^{(i)}(\tau,\mu) ; \qquad \mu < 0 \tag{30b}$$

for which the radiative transfer equation is written. Combining these upwards and downwards equations (sum and difference) yields two equations in terms of mean and net intensities $j^{(i)}(\tau,\mu)$ and $h^{(i)}(\tau,\mu)$

$$j^{(i)}(\tau,\mu) = \frac{1}{2} \left(I^{+(i)}(\tau,\mu) + I^{-(i)}(\tau,\mu)\right) \tag{31}$$

$$h^{(i)}(\tau,\mu) = \frac{1}{2} \left(I^{+(i)}(\tau,\mu) - I^{-(i)}(\tau,\mu)\right) \tag{32}$$

For components $j^{(0)}(\tau,\mu)$ and $h^{(0)}(\tau,\mu)$, for example, we get:

$$\mu^2 \frac{d^2 j^{(0)}}{d\tau^2}(\tau,\mu) = j^{(0)}(\tau,\mu) - \frac{3}{8} \tilde{\omega}_o \int_0^1 \left[3 - \mu^2 + (3\mu^2 - 1)\mu'^2\right] j^{(0)}(\tau,\mu')\, d\mu' - \frac{3}{32} \tilde{\omega}_o F e^{-\tau/\mu_o} \left[3 - \mu^2 + (3\mu^2 - 1)\mu_o^2\right] \tag{33a}$$

and

$$\mu \frac{dj^{(0)}(\tau,\mu)}{d\tau^2} = h^{(0)}(\tau,\mu) \tag{33b}$$

A Gaussian quadrature can accurately replace the integrals over μ' by discrete equivalents over several (typically 6) streams, upwards and

downwards. Finite differences are used and a tridiagonal system of equations in $j(\tau,\mu)$ for components 0 and 2, or in $h(\tau,\mu)$ for component 1 is then solved, subject to upper and lower boundary conditions [see also Mihalas, 1978]. At the top, zero downward intensity is imposed (no scattering at low densities), while the ground boundary condition is Lambert reflection (isotropic upwards intensity) with albedo A. For mid-latitudes, we use an albedo of 0.25 which is representative of a combination of ground and cloud effects. Atmospheric cloud variability will introduce an uncertainty not taken into account by a model which represents average conditions, since clouds can significantly increase the diffuse flux in the lower stratosphere [Callis et al., 1975]. To compute the additional flux due to multiple scattering (second term in (14)), we only need to calculate the isotropic component $I^{(0)}(\tau,\mu)$ since the integration over solid angle of the last two terms in equation (29) is identically zero. Therefore, the diffuse component

$$F^D(\tau) = 2\pi \int_0^1 I^{(0)}(\tau,\mu')\, d\mu' \qquad (34)$$

is added to the direct flux $F^A(\tau)$ to obtain $F^T(\tau)$.

The U. S. Standard Atmosphere 1976 is used for air and ozone densities in our radiative transfer program with an arbitrary model profile for NO_2. The model covers the 0 to 60 km range, but densities are interpolated to a finer grid so that the total opacity in each level is always about 0.1 or less; 76 levels are used above 315 nm, and 355 below this wavelength. Values for F^D are stored on disk in an array that is subsequently read into the photochemical model; 26 altitude levels in the 0 to 50 km range are saved (this corresponds to our 2 km model grid

for photochemistry) and the flux above 50 km is set equal to its value at 50 km. The latter statement holds true to better than 1% and the diffuse flux in the upper stratosphere and mesosphere is essentially all upwards radiation due to scattering and reflection from the lower atmosphere and ground. Moreover, only 19 wavelengths are stored and calculations are saved for 13 values of solar zenith angle (μ_o = 0.0125, 0.025, 0.05, and 0.1 to 1.0 in steps of 0.1). Linear interpolation in μ_o and λ is used in our photochemical model to calculate intermediate values with accuracy of a few percent in most regions, owing to the relatively smooth variation in F^D. We have tested our radiation results by using the input model atmosphere of Luther and Gelinas [1976] and comparing their results to our model. These authors show plots of the ratio of total flux to pure absorption flux as a function of height, wavelength and ground albedo, for $\chi = 60°$. Our results are essentially identical in the 290-800 nm range, for various albedos, and we will not duplicate their graphs. Photodissociation rates from the above authors and others are also in good agreement with our results, although there have been some changes in cross sections. The effect of multiple scattering on the photodissociation of O_3 ($\rightarrow O_2 + O$), NO_2, and $ClONO_2$, three species that are affected by the diffuse radiation, is illustrated in Figures 10 and 11 for small and large solar zenith angles. For $\chi = 30°$, multiple scattering and ground reflection (A = 0.25) enhance these photodissociation rates at all altitudes. For $\chi = 85°$, however, a small enhancement is seen in the stratosphere, but a reduction in fluxes occurs below $\sim$20 km due to the scattering out of the direct beam which is not compensated for by multiple scattering from below or ground reflection. In our photochemical

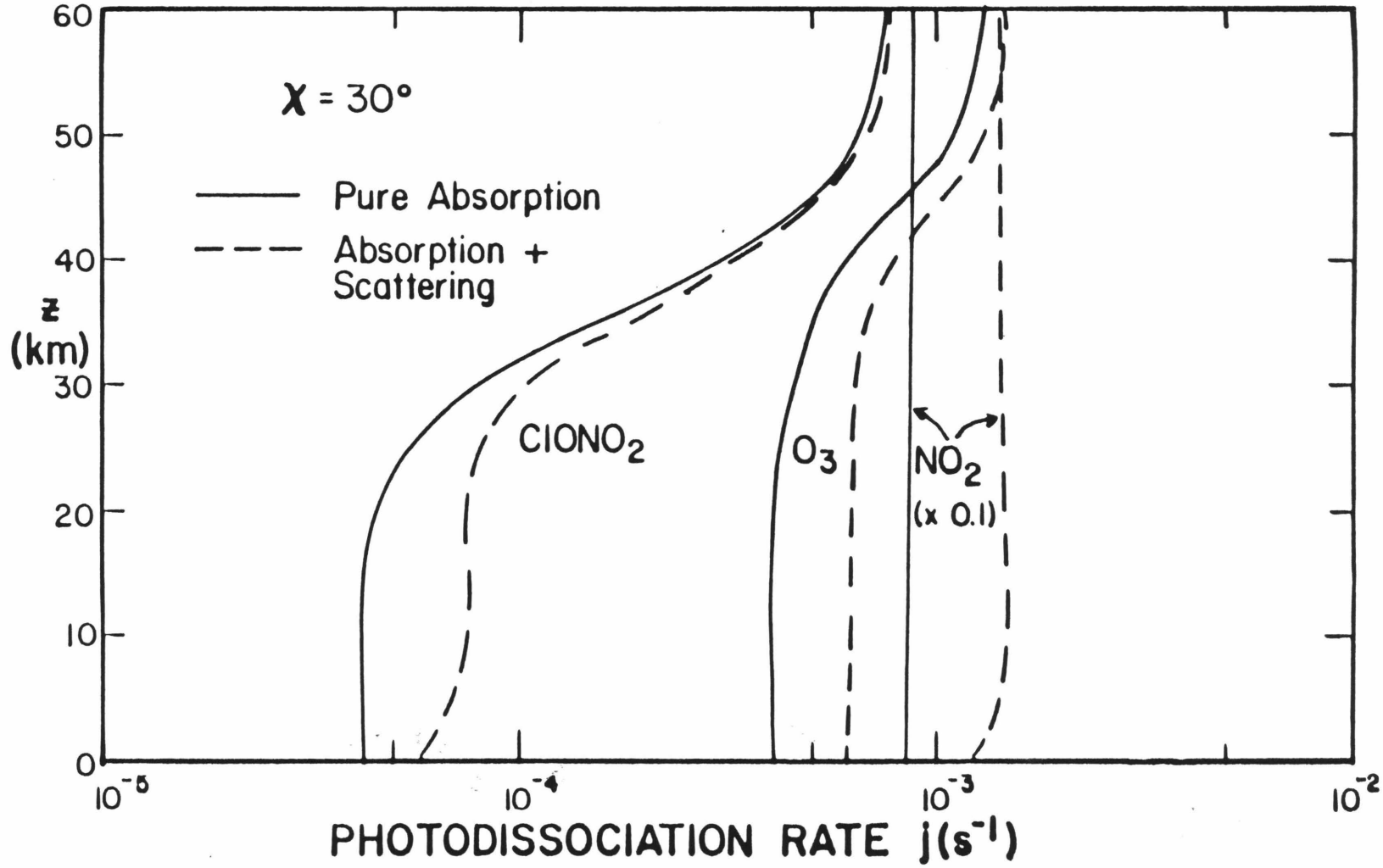

Figure 10. Effect of Rayleigh scattering on photodissociation rate constants for $ClONO_2$, O_3, and NO_2, below 60 km. Ground albedo is equal to 0.25, and solar zenith angle equals 30°.

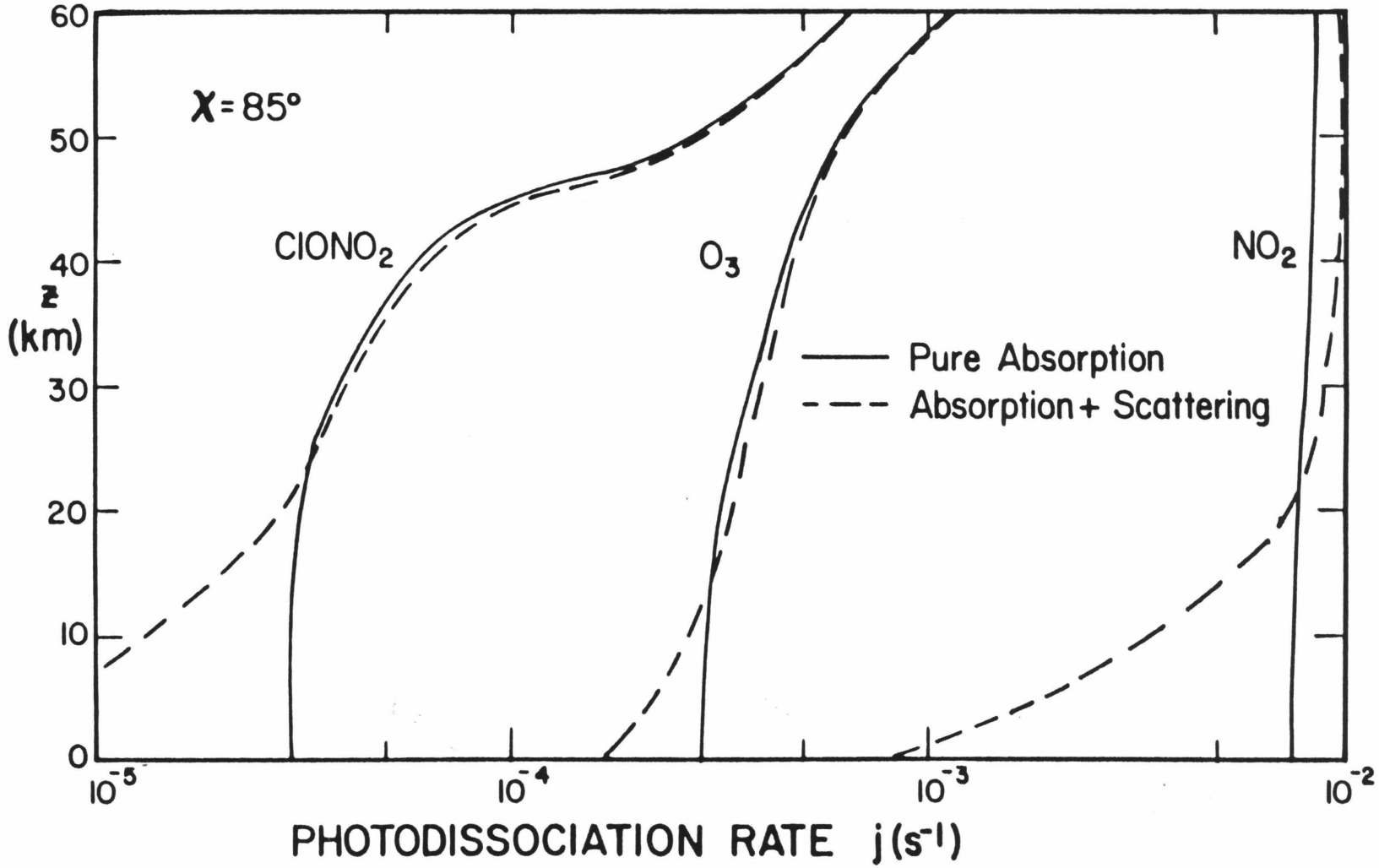

Figure 11. Same as Figure 10, but for solar zenith angle of 85°.

model, the diffuse flux is calculated (by interpolation from the stored coefficients) at every time step in a diurnal run, whereas an average zenith angle ($\bar{\mu}_{av}$) is used for diurnal average runs, as defined by the diurnally-averaged direct flux at any height and wavelength: $F^A(z,\lambda) = F_\infty(\lambda)\ \exp\{-\tau/\bar{\mu}_{av}\}$. We now discuss some of the aspects of diurnal averaging, as treated in our model.

1.4 Diurnal Average and Diurnal Calculations

The diurnal average model represents the basic state from which diurnal runs are started. The concentration of species whose lifetimes are short compared to a day often varies significantly during the day, as well as at night, when photolysis no longer drives the chemical cycles. This applies to radicals such as OH, HO_2, NO, NO_2, NO_3, Cl, ClO, O and $O(^1D)$. Combinations of some of these radicals lead to temporary reservoir species, whose photochemical lifetimes vary between about one day and several weeks, depending on the altitude. Examples include H_2O_2, HNO_3, HO_2NO_2, N_2O_5, HCl, and $ClONO_2$, trace gases showing slow diurnal variations, if any. The radicals themselves are derived from source species with long lifetimes (about a year or more in lower stratosphere), for which transport is an important factor. These source species show no diurnal variations and their concentrations are fixed to diurnal average values, when the model is stepped in time for diurnal calculations: N_2O, H_2O, H_2, CH_4, CO, CO_2 and the halocarbons comprise this group. The diurnal average model computes photodissociation rates averaged over 24 hours as input to the continuity equation (1) for each species. Various approaches to diurnally-averaged calculations have been given by Whitten and Turco [1974],

Kurzeja [1975, 1977], Martin [1976], Cogley and Borucki [1976], Rundel [1977], Kramer and Widhopf [1978], Turco and Whitten [1978], and Boughner [1980]. The use of a fixed sun at an average zenith angle has been shown to be less accurate than a 12 hr or 24 hr average of photodissociation rates. We define a 24 hr average for the fluxes at each height and wavelength in terms of an average transmission

$$\overline{tr}(z,\lambda) = \frac{1}{12}\int_{12}^{t_{ss}} \exp\{-\tau_s(z,\lambda,t)\}dt \qquad (35)$$

where t is the local time in hours and t_{ss} is the time at sunset for altitude z. In a plane parallel atmosphere, the slant opacity τ_s is related to the normal optical depth τ and $\cos\chi(t) = A + B\cos L(t)$, with $A = \sin\delta\sin\phi$ and $B = \cos\delta\cos\phi$, as defined in (6). A good approximation to the integrated transmission in (35) is given by the transmission at noon ($tr(12) = \exp\{-\tau/(A+B)\}$) multiplied by $(t^* - 12)$, where t^* is defined by $tr(t^*) = 0.5\ tr(12)$, which leads to

$$\overline{tr}(\tau) = \frac{1}{\pi} e^{-\tau/A+B} \arccos \frac{\tau/(A+B) - (A/B)\ln 2}{\tau/(A+B) + \ln 2} \qquad (36)$$

This analytic formulation can well reproduce the exact numerical evaluation of the integral in (35), as demonstrated by the fit to the results of Rundel [1977] in Figure 12, for $\phi = 30°$ and $\delta = 0°$. At low optical depths, the daytime transmission is close to unity during the day and drops sharply to zero at sunset and sunrise, so that $\overline{tr} \simeq 0.5$. If one were to represent $\overline{tr}(z,\lambda)$ by $\exp(-\tau(z,\lambda)/\cos\bar{\chi})$, where $\bar{\chi}$ is an average solar zenith angle, the value of $\bar{\chi}$ would be close to 90° for the low

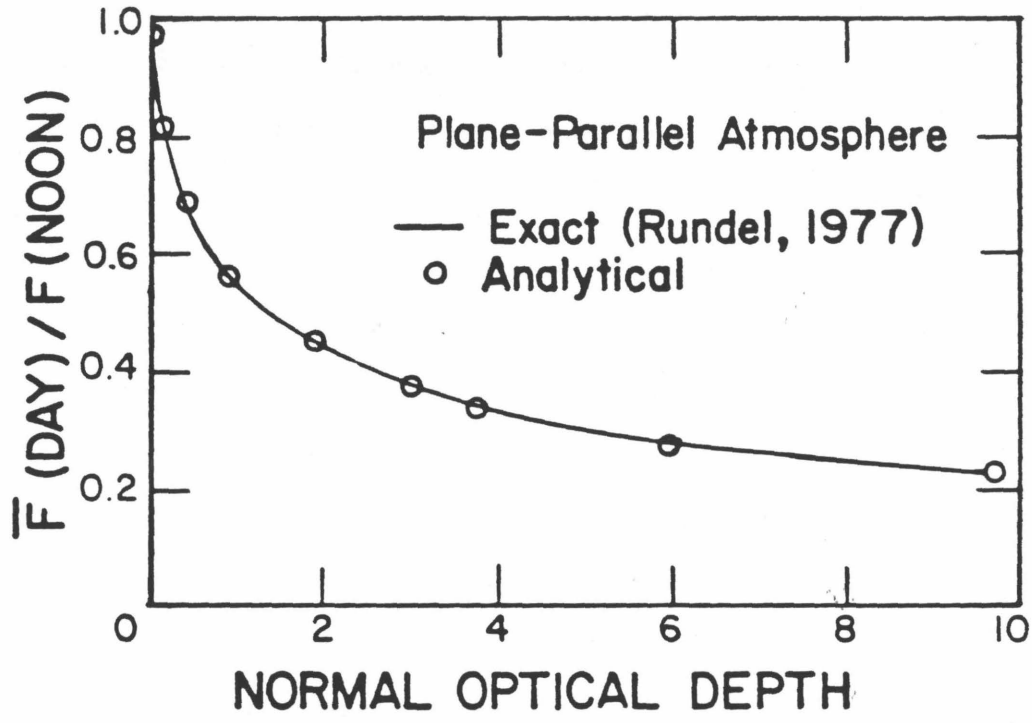

Figure 12. Ratio of average daytime to noon flux (or transmission) as a function of total normal optical depth. The exact integration results of Rundel (1977) are closely matched by the plane parallel analytical representation described in the text. Calculations are for a latitude of 30° and a solar declination of 0°.

opacity limit, but near 30 or 40° for large optical depths ($\tau \geq 10$) in the lower stratosphere. Figure 13 illustrates this variation of $\overline{\chi}$ as a function of altitude and wavelength, demonstrating that a poor approximation would result if one used a fixed $\overline{\chi}$ for all z and λ values. In general, the spherical nature of the Earth's atmosphere, as well as the varying daylight period as a function of height is taken into consideration, and $\overline{tr}(\tau)$ is evaluated numerically using $\tau_s = \tau\, Ch(X,\chi)$ at each altitude and zenith angle. Since a large number of calculations would have to be done in the photochemical model (for each z and λ), a polynomial series of the form $\sum_{j=1}^{9} a_{ij}\, \tau_i^{j-1}$ is fit to the function $\overline{tr}(\tau_i)$ over a wide range of normal optical depths and the coefficients a_{ij} are stored for fast evaluation of the diurnal transmissions (and fluxes) during a model calculation. Care has to be taken to ensure accuracy of the fit (5% or less for most cases) at all relevant optical depths.

Use of diurnally-averaged photodissociation rates in the continuity equation is necessary to evaluate the concentrations of long-lived species such as N_2O or the halocarbons, whose chemical destruction is essentially all due to photolysis. However, there is no exact method for diurnally-averaged chemical reaction rates, which involve products of concentrations. The diurnal average model calculates a rate $k[\overline{X}][\overline{Y}]$, as opposed to the average rate $\overline{k[X][Y]}$. Similarly for photodissociation, $\overline{j}[\overline{X}] \neq \overline{j[X]}$; for the halocarbons, N_2O or diurnally-invariant species in general, one can use $\overline{j}[\overline{X}]$ for an accurate description of the loss process, but this will not hold for constituents which vary during the day. Moreover, nighttime chemistry is important for certain species such as NO_3, $ClONO_2$, and N_2O_5, which build up after sunset. The concentrations of these species

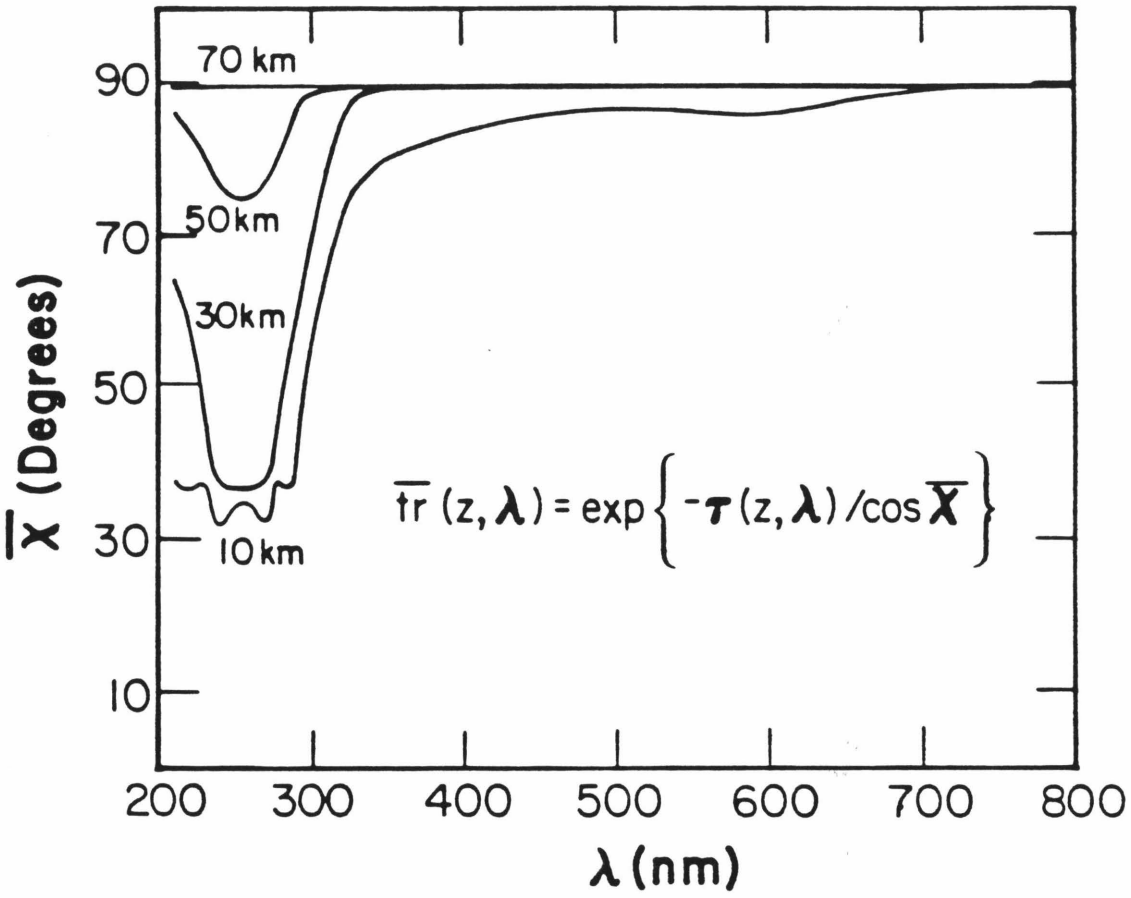

Figure 13. Altitude and wavelength variation of average solar zenith angle $\overline{\chi}$, defined from equation above, where $\overline{tr}(z,\lambda)$ is the (24 hour) diurnally-averaged transmission. Calculations are for 30°N latitude, 0° solar declination. $\overline{\chi}$ varies between 30 and 90 degrees, depending on the optical depth (wavelength and altitude dependence).

will be underestimated by a diurnal average model which assumes that daytime processes (photolysis) are most important. The above factors and nonlinearities are responsible for differences between the true diurnally-averaged concentrations of certain species and the concentrations obtained via our diurnal average model. Turco and Whitten [1978] describe a procedure that takes into account nighttime averages and daytime averages to yield more accurate diurnal (24 hr) averages. They note that erroneous diurnal average concentrations for short-lived species can also affect longer-lived species. No method is perfect in terms of diurnal averaging and each modeler should be aware of his or her own model limitations. We have compared the true diurnal averages versus the diurnal averages, where a true diurnal average represents the average of a quantity over 24 hours, as computed from a full diurnal calculation. The largest differences occur for NO_3 and N_2O_5 for reasons of nighttime build-up mentioned before. In terms of the long-lived source species mentioned above, many are mostly affected by photolysis, so that the 24 hr average photodissociation rate calculations are sufficiently accurate. Short-lived species will not dominate over transport effects in determining the abundances of the source species. Even if 20-30% differences occur in the calculated concentrations of some source species due to inexact values for the radical concentrations, we are conscious of the fact that one-dimensional models suffer from inaccuracies in the transport processes affecting the source species. In terms of ozone, our diurnal average calculations are within about 10% of the true diurnal average concentrations; further discussion is given in Chapter 5. Temporary reservoir species are generally strongly coupled to short-lived radicals,

and even though their concentrations might not vary significantly over the course of a day, the true diurnal average values can be quite different than the simple diurnal average model results, as illustrated in Figure 14 for HNO_3, HO_2NO_2, and H_2O_2 in particular. This can be traced to the differences in production rates, which involve products of radicals, averaged over the day. The diurnal run used for this test is from the fifth day and night of a model used in Chapter 4 for comparison to ClO observations (32°N latitude, -11° solar declination). True diurnal average and diurnal average HNO_3 volume mixing ratios are compared to a compilation of mid-latitude observations [see references in Hudson et al., 1982] in Figure 15. The true diurnal average results are about a factor of two lower than the diurnal average values in the upper stratosphere, and show better agreement with the observed decrease above 25 km.

Long-lived source species will be sensitive to both transport and photochemistry, and multi-dimensional models will lend themselves best towards producing a simultaneous fit to such gases, when a good set of global observations becomes available. One-dimensional models could then use a fixed series of vertical profiles corresponding to such observations in order to study processes, such as diurnal variations of short-lived species (ideally measured at the same time as well), which depend much less on vertical or horizontal transport. In this work, we compare our model results with average mid-latitude data, often obtained by a variety of techniques at different times, and look for a reasonable model fit to long-lived species, even though the transport processes are parametrized in a fairly simplistic fashion. Water vapor was discussed earlier and our model profile is within the range of observed mid-

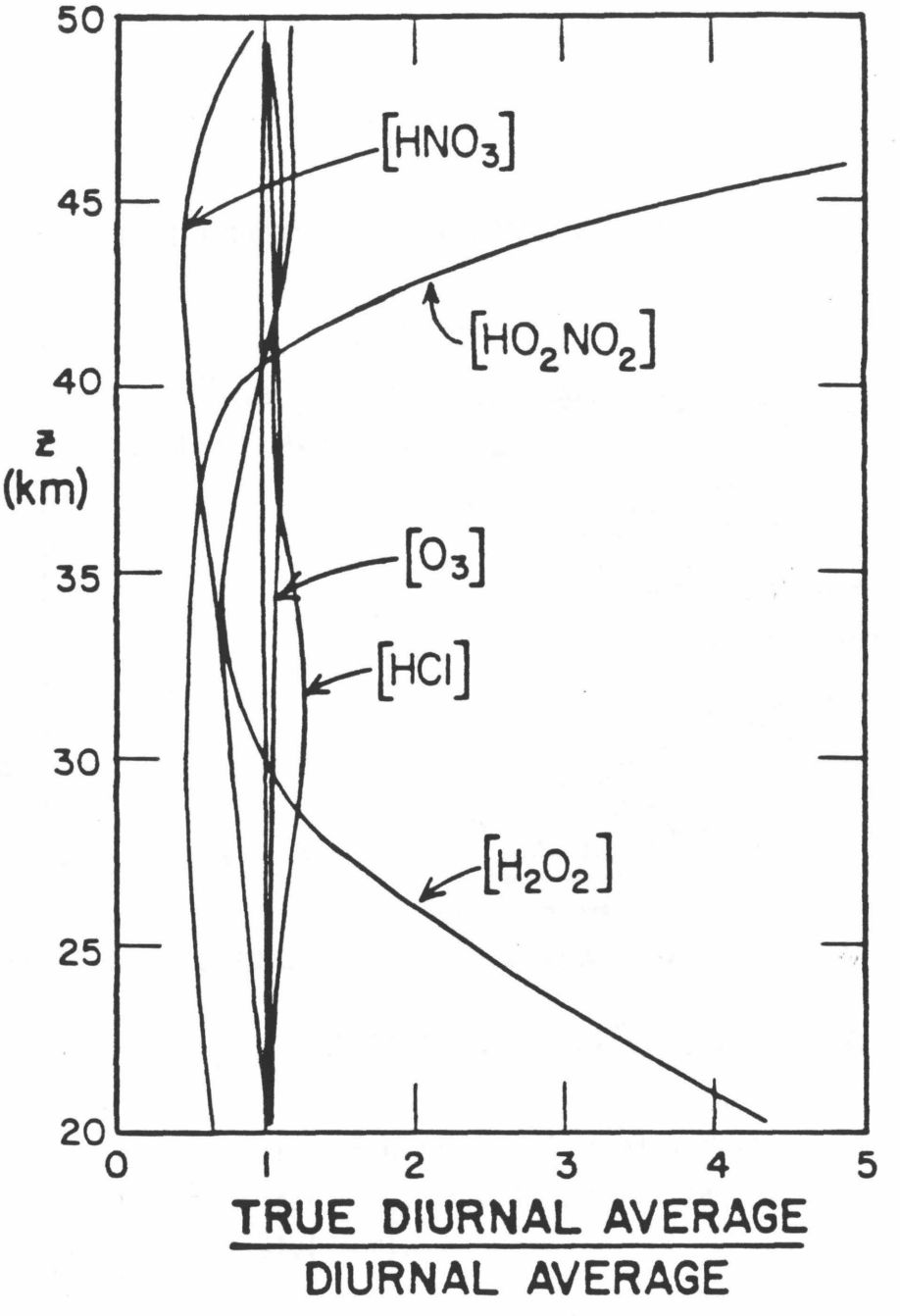

Figure 14. Ratio of true diurnal average concentrations (obtained from a 24 hour integration of diurnal run results) to our model diurnal average concentrations (see text).

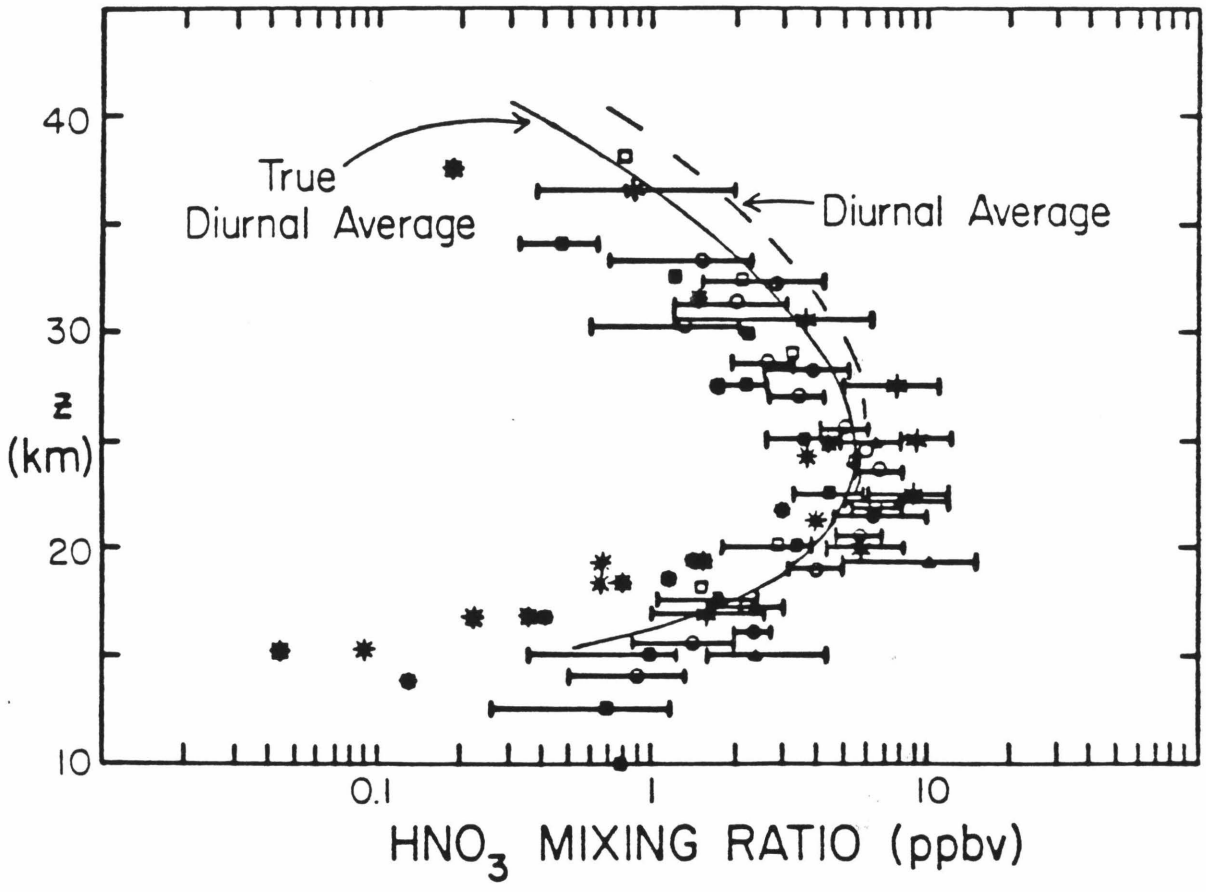

Figure 15. Comparison of true diurnal average and diurnal average model results for HNO_3. Mid-latitude data are taken from summary in Hudson et al.(1982).

latitude data, given the uncertainties and variability in these data. Typical H_2 and CO vertical profiles are compared to mid-latitude observations in Figures 16 and 17. The H_2 data for 25-35°N are taken from the summary in Hudson et al. [1982]; individual observed profiles show some decrease, particularly at somewhat higher latitudes (45°N), although maybe not quite as strong as in the model. H_2 is sensitive both to transport and production by CH_4 oxidation [Ehhalt and Tönnissen, 1980]. The CO data shown here extend to 80 km for completeness and are mostly taken from the recent review of Louisnard and Lado-Bordowsky [1983]. Above 60 km, the microwave data of Clancy et al. [1982] and some later (unpublished) data provided by R. T. Clancy (private communication, 1983) are used to delineate an acceptable range of CO mixing ratios. The microwave results of Waters et al. [1976] and Goldsmith et al. [1979] also fall within this range, and the uncertainty limits shown in the figure are typical of ground-based observations; below ∿60 km, the CO profile (particularly the lower limit) is not well constrained by these observations and the range shown is merely indicative of the expected trend. The general shape of the observed CO profile from 0 to 80 km is reproduced by mid-latitude models, although the minimum occurs at somewhat higher altitudes in our model. Stratospheric CO is sensitive to the CH_4 profile and the CH_4 oxidation sequence producing H_2CO, HCO, and eventually CO [see Calvert, 1980; Logan, 1980; Ehhalt and Tönnissen, 1980], while CO_2 photolysis becomes a dominant source above ∿60 km. Destruction in the atmosphere occurs via the CO + OH reaction, which shows some not clearly understood pressure dependence [DeMore et al., 1982]. Further studies of this molecule in relation to CO_2, CH_4, H_2O,

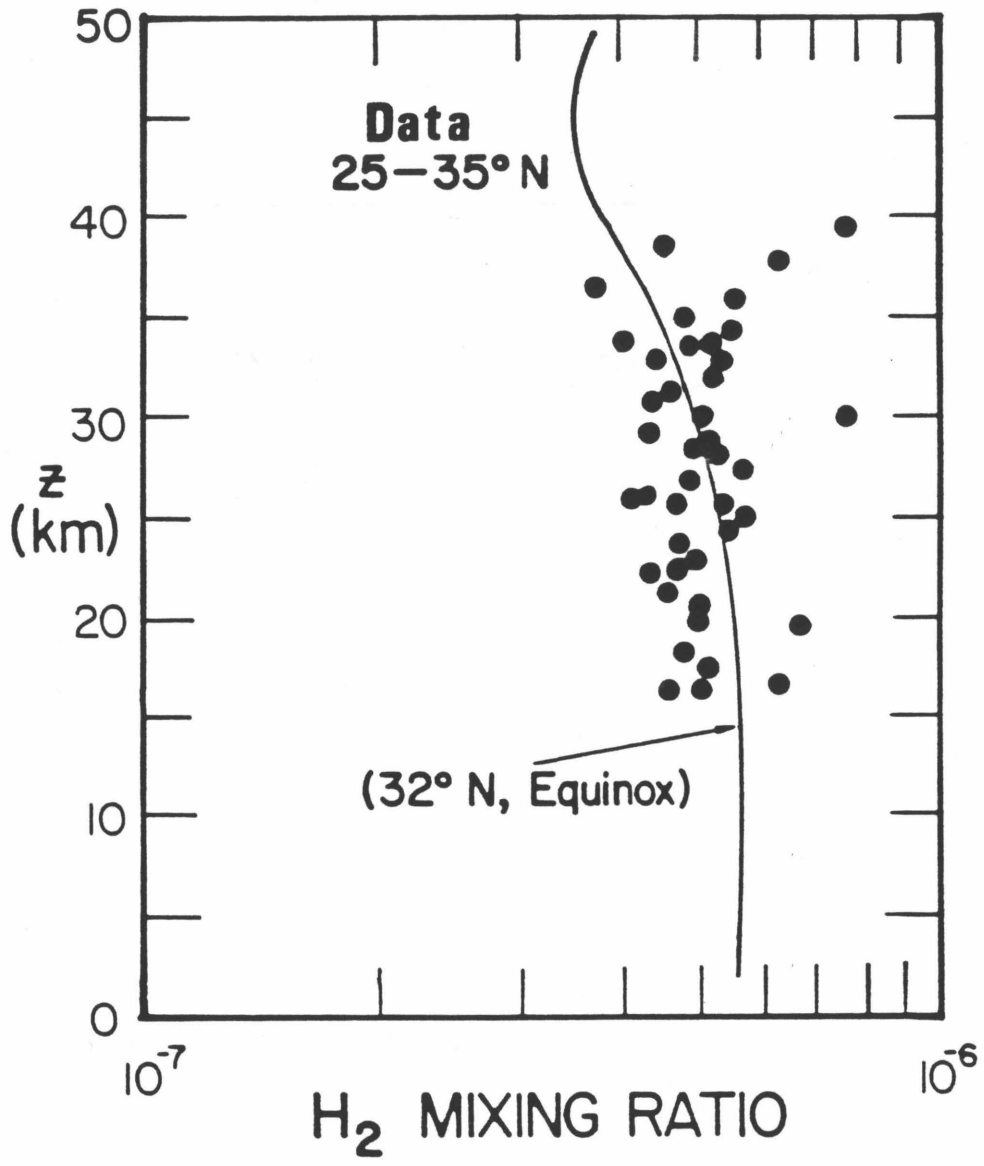

Figure 16. H_2 model for 32°N, equinox (and K_1 eddy diffusion profile). See Hudson et al. (1982) for data references.

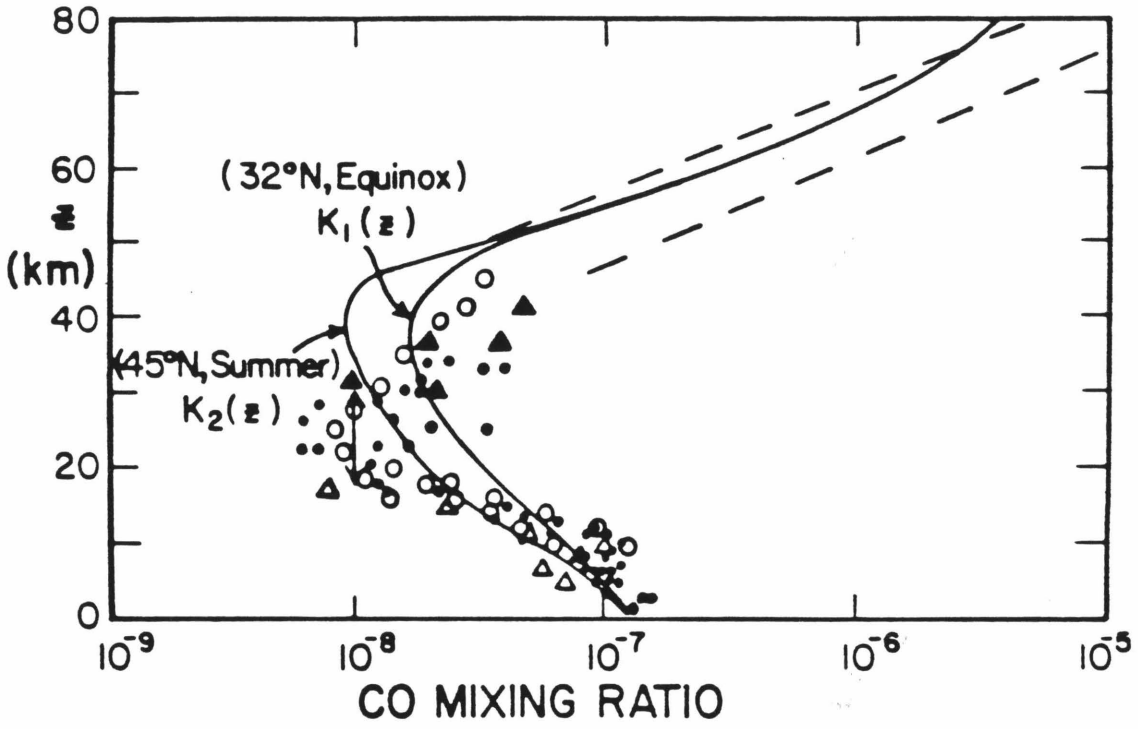

Figure 17. Mid-latitude models of CO abundance between 0 and 80 km. Stratospheric data are taken from compilation by Louisnard and Lado-Bordowsky (1983), and mesospheric data range comes from ground-based microwave observations (see text).

and possibly H_2CO on a more global scale should soon be possible with the use of infrared spectroscopy measurements from the Space Shuttle (ATMOS project). CO_2 in our model has a constant mixing ratio throughout the atmosphere due to its very long lifetime and upward diffusion from the ground. A small, but persistent increase of less than 0.5% per year, presumably related to fossil fuel burning, has been recorded [Keeling et al., 1976a,b]. Long-lived natural and man-made source species for chlorine and fluorine products in the stratosphere, as well as N_2O and CH_4, are discussed in Chapter 3, in relation to transport and to molecular oxygen absorption cross sections (radiation field).

References

Aldaz, L., Flux measurements of atmospheric ozone over land and water, J. Geophys. Res., 74, 6943, 1969.

Allen, M., and J. E. Frederick, Effective photodissociation cross sections for molecular oxygen and nitric oxide in the Schumann-Runge bands, J. Atmos. Sci., 39, 2066, 1982

Allen, M., J. P. Pinto, and Y. L. Yung, Titan: Aerosol photochemistry and variations related to the sunspot cycle, Astrophys. J., 242, L125, 1980.

Allen, M., Y. L. Yung, and J. W. Waters, Vertical transport and photochemistry in the terrestrial mesosphere and lower thermosphere (50-120 km), J. Geophys. Res., 86, 3617, 1981.

Allen, M., J. I. Lunine, and Y. L. Yung, The vertical distribution of ozone in the mesosphere and lower thermosphere, submitted to J. Geophys. Res., 1983.

Ashby, R. W., A numerical study of the chemical composition of the stratosphere, Ph.D. Thesis, University of Wisconsin--Madison, 1976.

Bahta, A., R. Simonaitis, and J. Heicklen, Thermal decomposition kinetics of $CH_3O_2NO_2$, J. Phys. Chem., 86, 1849, 1982.

Baulch, D. L., R. A. Cox, P. J. Crutzen, R. F. Hampson, Jr., J. A. Kerr, J. Troe, and R. T. Watson, Evaluated kinetic and photochemical data for atmospheric chemistry: supplement 1. CODATA task group on chemical kinetics, J. Phys. Chem. Ref. Data, 11, 327, 1982.

Boughner, R. E., A simplified method for the calculation of diurnally averaged photodissociation rates, J. Atmos. Sci., 37, 1308, 1980.

Callis, L. B., V. Ramanathan, R. E. Boughner, and B. R. Barkstrom, The stratosphere: scattering effects, a coupled 1-D model, and thermal balance effects, Fourth Conference on CIAP, U. S. Dept. of Transportation, pp. 224-233, 1975.

Callis, L. B., M. Natarajan, and R. E. Boughner, On the relationship between the greenhouse effect, atmospheric photochemistry, and species distribution, J. Geophys. Res., 88, 1401, 1983.

Calvert, J. G., The homogeneous chemistry of formaldehyde generation and destruction within the atmosphere, Proceedings of the NATO Advanced Study Institute on Atmospheric Ozone: Its Variation and Human Influences, Report No. FAA-EE-80-20, U. S. Dept. of Transportation, pp. 153-190, 1980.

Chameides, W. L., and R. J. Cicerone, Effects of non-methane hydrocarbons in the atmosphere, J. Geophys. Res., 83, 947, 1978.

Chandrasekhar, S., Radiative Transfer, Dover Publications Inc., New York, 1960.

Chapman, S., The absorption and dissociative or ionizing effect of monochromatic radiation in an atmosphere on a rotating Earth, Part II. Grazing incidence, Proc. Phys. Soc., 43, 483, 1931.

Cicerone, R. J., Halogens in the atmosphere, Rev. Geophys. Space Phys., 19, 123, 1981.

CIRA 1972, Cospar international reference atmosphere, Berlin: Akademie-Verlag, 1972.

Clancy, R. T., D. O. Muhleman, and G. L. Berge, Microwave spectra of terrestrial mesospheric CO, J. Geophys. Res., 87, 5009, 1982.

Cogley, A. C., and W. J. Borucki, Exponential approximation for daily

average solar heating or photolysis, J. Atmos. Sci., 33, 1347, 1976.

Colegrove, F. D., W. B. Hanson, and F. S. Johnson, Eddy diffusion and oxygen transport in the lower thermosphere, J. Geophys. Res, 70, 4931, 1965.

Dalgarno, A., Atmospheric reactions with energetic particles, Space Res., 7, 849, 1967.

DeMore, W. B., and Y. L. Yung, Catalytic processes in the atmospheres of Earth and Venus, Science, 217, 1209, 1982.

DeMore, W. B., L. J. Stief, F. Kaufman, D. M. Golden, R. F. Hampson, M. J. Kurylo, J. J. Margitan, M. J. Molina, and R. T. Watson, Chemical Kinetics and Photochemical Data for Use in Stratospheric Modeling, JPL Publication 79-27, Jet Propulsion Laboratory, Pasadena, California, 1979.

DeMore, W. B., R. T. Watson, D. M. Golden, R. F. Hampson, M. J. Kurylo, C. J. Howard, M. J. Molina, and A. R. Ravishankara, Chemical Kinetics and Photochemical Data for Use in Stratospheric Modeling, JPL Publication 82-57, Jet Propulsion Laboratory, Pasadena, California, 1982.

Edlen, B., The refractive index of air, Metrologia, 2, 71, 1966.

Ehhalt, D. H., and A. Tönnissen, Hydrogen and carbon compounds in the stratosphere, Proceedings of the NATO Advanced Study Institute on Atmospheric Ozone: Its Variation and Human Influences, Report No. FAA-EE-80-20, U. S. Dept. of Transportation, pp. 129-152, 1980.

Farmer, C. B., O. F. Raper, and R. H. Norton, Spectroscopic detection and vertical distribution of HCl in the troposphere and stratosphere, Geophys. Res. Lett., 3, 13, 1976.

Feautrier, P., Sur la résolution numérique de l'équation de transfert, C. R. Acad. Sc. Paris, 258, 3189, 1964.

Fiocco, G., Influence of diffuse solar radiation on stratospheric chemistry, Proceedings of the NATO Advanced Study Institute on Atmospheric Ozone: Its Variation and Human Influences, Report No. FAA-EE-80-20, U. S. Dept. of Transportation, pp. 555-587, 1980.

Fishman, J., The distribution of NO_x and the production of ozone: Comments on 'On the origin of tropospheric ozone, by S. C. Liu et al.,' J. Geophys. Res., 86, 161, 1981.

Fishman, J., and P. J. Crutzen, A numerical study of tropospheric photochemistry using a one-dimensional model, J. Geophys. Res., 82, 5897, 1977.

Fitzmaurice, J. A., Simplification of the Chapman function for atmospheric attenuation, Appl. Opt., 3, 640, 1964.

Frederick, J. E., and R. D. Hudson, Predissociation linewidths and oscillator strengths for the (2-0) to (13-0) Schumann-Runge bands of O_2 J. Mol. Spectrosc., 74, 247, 1979.

Frederick, J. E., and R. D. Hudson, Dissociation of molecular oxygen in the Schumann-Runge bands, J. Atmos. Sci., 37, 1099, 1980.

Frederick, J. E., and J. E. Mentall, Solar irradiance in the stratosphere: implications for the Herzberg continuum absorption of O_2, Geophys. Res. Lett., 9, 461, 1982.

Froidevaux, L., and Y. L. Yung, Radiation and chemistry in the stratosphere: sensitivity to O_2 absorption cross sections in the Herzberg continuum, Geophys. Res. Lett., 9, 854, 1982.

Gallagher, C. C., C. A. Forsberg, and R. V. Pieri, Stratospheric N_2O, CF_2Cl_2, and $CFCl_3$ composition studies utilizing in situ cryogenic, whole air sampling methods, J. Geophys. Res., 88, 3798, 1983.

Gelinas, R. J., Summary of radiative data used in LLL atmospheric physics codes, UCRL-74944 (Change 4), 1974.

Gladstone, G. R., Radiative transfer with partial frequency redistribution in inhomogeneous atmospheres: application to the Jovian aurora, J. Quant. Spectrosc. Radiat. Transfer, 27, 545, 1982.

Gladstone, G. R., and Y. L. Yung, An analysis of the reflection spectrum of Jupiter from 1500 Å to 1740 Å, Astrophys. J., 266, 415, 1983.

Goldan, P. D., W. C. Kuster, D. L. Albritton, and A. L. Schmeltokopf, Stratospheric $CFCl_3$, CF_2Cl_2, and N_2O height profile measurements at several latitudes, J. Geophys. Res., 85, 413, 1980.

Goldsmith, P. F., M. M. Litvak, R. L. Plambeck, and D.R.W. Williams, Carbon monoxide mixing ratio in the mesosphere derived from ground-based microwave measurements, J. Geophys. Res., 84, 416, 1979.

Hampson, R. F., Chemical Kinetic and Photochemical Data Sheets for Atmospheric Reactions, FAA Report No. EE-80-17, 1980.

Hampson, R. F., and D. Garvin (Eds.), Reaction Rate and Photochemical Data for Atmospheric Chemistry--1977, NBS SP-513, National Bureau of Standards, Gaithersburg, Maryland, 1978

Herman, J. R., and J. E. Mentall, O_2 absorption cross sections (187-225 nm) from stratospheric solar flux measurements, J. Geophys. Res., 87, 8967, 1982.

Hudson, R. D., and L. J. Kieffer, Absorption Cross Sections of Stratospheric Molecules, The Natural Stratosphere of 1974, CIAP Monograph 1, 1975.

Hudson, R. D., and E. I. Reed (Eds.), The Stratosphere: Present and Future, NASA Reference Publication 1049, 1979.

Hudson, R. D. (editor-in-chief) et al. (16 editors), The Stratosphere 1981: Theory and Measurements, WMO Global Ozone Research and Monitoring Project Report No. 11, 1982.

Hunten, D. M., Vertical transport in atmospheres, in Atmospheres of Earth and the Planets, edited by B. M. McCormac, pp. 59-72, D. Reidel, Hingham, Massachusetts, 1975.

Inn, E. C., Absorption coefficient of HCl in the region 1400 to 2200 Å, J. Atmos. Sci., 32, 2375, 1975.

Isaksen, I.S.A., K. H. Midtbo, J. Sunde, and P. J. Crutzen, A simplified method to include molecular scattering and reflection in calculations of photon fluxes and photodissociation rates, Geophys. Norv., 31, 11, 1977.

Jackman, C. H., J. E. Frederick, and R. S. Stolarski, Production of odd nitrogen in the stratosphere and mesosphere: an intercomparison of source strengths, J. Geophys. Res., 85, 7495, 1980.

Johnston, H. S., D. Kattenhorn, and G. Whitten, Use of excess carbon-14 data to calibrate models of stratospheric ozone depletion by supersonic transports, J. Geophys. Res., 81, 368, 1976.

Keeling, C. D., R. B. Bacastow, A. E. Bainbridge, C. A. Ekdahl, Jr., P. R. Guenther, L. S. Waterman, and J. F-S. Chin, Atmospheric carbon dioxide variations at Mauna Loa Observatory, Hawaii, Tellus, 28, 538, 1976a.

Keeling, C. D., J. A. Adams, Jr., C. A. Ekdahl, Jr., and P. R. Guenther, Atmospheric carbon dioxide variations at the south pole, Tellus, 28 552, 1976b.

Kircher, C. C., and S. P. Sander, Kinetics and mechanism of HO_2 and DO_2 disproportionations, submitted to J. Phys. Chem., 1983.

Kramer, R. F., and G. F. Widhopf, Evaluation of daylight or diurnally averaged photolytic rate coefficients in atmospheric photochemical models, J. Atmos. Sci., 35, 1726, 1978.

Kurzeja, R. J., The diurnal variation of minor constituents in the stratosphere and its effect on the ozone concentration, J. Atmos. Sci., 32, 899, 1975.

Kurzeja, R. J., Effects of diurnal variations and scattering on ozone in the stratosphere for present-day and predicted future chlorine concentrations, J. Atmos. Sci., 34, 1120, 1977.

Langhoff, S. R., L. Jaffe, and J. O. Arnold, Effective cross sections and rate constants for predissociation of ClO in the earth's atmosphere, J. Quant. Spectrosc. Rad. Transfer, 18, 227, 1977.

Lean, J. L., O. R. White, W. C. Livingston, D. F. Heath, R. F. Donnelly, and A. Skumanich, A three-component model of the variability of the solar ultraviolet flux: 145-200 nm, J. Geophys. Res., 87, 10307, 1982.

Leifer, R., K. Sommers, and S. F. Guggenheim, Atmospheric trace gas measurements with a new clean air sampling system, Geophys. Res. Lett., 8, 1079, 1981.

Leu, M. T., Kinetics of the reaction $O + ClO \rightarrow Cl + O_2$, submitted to J. Phys. Chem., 1983.

Liou, K-N., An Introduction to Atmospheric Radiation, International Geophysics Series, Vol. 26, Academic Press, 1980.

Logan, J. A., Sources and sinks for carbon monoxide, Proceedings of the NATO Advanced Study Institute on Atmospheric Ozone: Its Variation

and Human Influences, Report No. FAA-EE-80-20, U. S. Dept. of Transportation, pp. 323-344, 1980.

Logan, J. A., M. J. Prather, S. C. Wofsy, and M. B. McElroy, Tropospheric chemistry: a global perspective, J. Geophys. Res., 86, 7210, 1981.

Louisnard, N., and O. Lado-Bordowsky, Spectroscopic measurements of carbon monoxide in the stratosphere, J. Geophys. Res., 88, 3789, 1983.

Luther, F. M., and R. J. Gelinas, Effect of molecular multiple scattering and surface albedo on atmospheric photodissociation rates, J. Geophys. Res., 81, 1125, 1976.

Luther, F. M., D. J. Wuebbles, W. H. Duewer, and J. S. Chang, Effect of multiple scattering on species concentrations and model sensitivity, J. Geophys. Res., 83, 3563, 1978.

Magnotta, F., and H. S. Johnston,Photodissociation quantum yields for the NO_3 free radical, Geophys. Res. Lett., 10, 769, 1980.

Margitan, J. J., Chlorine nitrate: the sole product of the $ClO + NO_2 + M$ recombination, J. Geophys. Res., 88, 5416, 1983.

Martin, B., Accuracy of some methods for determining photodissociation rates in the modeling of stratospheric ozone, J. Atmos. Sci., 33 131, 1976.

Massie, S. T., and D. M. Hunten, Stratospheric eddy diffusion coefficients from tracer data, J. Geophys. Res., 86, 9859, 1981.

Meier, R. R., D. E. Anderson, Jr., and M. Nicolet, Radiation field in the troposphere and stratosphere from 240-1000 nm--I. General Analysis, Planet. Space Sci., 30, 923, 1982.

Mihalas, D., Stellar Atmospheres, W. H. Freeman and Co., San Francisco, 1978.

Miller, C., D. L. Filkin, A. J. Owens, J. M. Steed, and J. P. Jesson, A two-dimensional model of stratospheric chemistry and transport, J. Geophys. Res., 86, 12039, 1981.

Mount, G. N., and G. J. Rottman, The solar spectral irradiance 1200-3184 Å near solar maximum: July 15, 1980, J. Geophys. Res., 86, 9193, 1981.

Mount, G. N., and G. J. Rottman, The solar absolute spectral irradiance 1150-3173 Å: 17 May 1982, J. Geophys. Res., in press, 1983.

Mount, G. N., G. J. Rottman, and J. G. Timothy, The solar spectral irradiance 1200-2550 Å at solar maximum, J. Geophys. Res., 85, 4271, 1980.

Myer, J. A., and J.A.R. Samson, Vacuum-ultraviolet absorption cross sections of CO, HCl, and ICN between 1050 and 2100 Å, J. Chem. Phys., 52, 266, 1970.

Nicolet, M., On the production of nitric oxide by cosmic rays in the mesosphere and stratosphere, Planet. Space Sci., 23, 637, 1975.

Nicolet, M., R. R. Meier, and D. E. Anderson, Jr., Radiation field in the troposphere and stratosphere--II. Numerical analysis, Planet. Space Sci., 30, 935, 1982.

Nicolet, M., Etude des réactions chimiques de l'ozone dans la stratosphère, Comité, d'études sur les consequences des vols stratosphériques, Institut Royal Météorologique de Belgique, 1978.

Patrick, R., and M. J. Pilling, The temperature dependence of the $HO_2 + HO_2$ reaction, Chem. Phys. Lett., 91, 343, 1982.

Penndorf, R., Tables of the refractive index for standard air and the Rayleigh scattering coefficient for the spectral region between 0.2 and 20.0 μ and their application to atmospheric optics, J. Opt. Soc. Am., 47, 176, 1957.

Pinto, J. P., G. R. Gladstone, and Y. L. Yung, Photochemical production of formaldehyde in Earth's primitive atmosphere, Science, 210, 183 1980.

Pitari, G., and G. Visconti, A simple method to account for Rayleigh scattering effects on photodissociation rates, J. Atmos. Sci., 36, 1803 1979.

Pitts, Jr., J. N., H. L. Sandoval, and R. Atkinson, Relative rate constants for the reaction of $O(^1D)$ atoms with fluorocarbons and N_2O, Chem. Phys. Lett., 29, 31, 1974.

Prather, M. J., Solution of the inhomogeneous Rayleigh scattering atmosphere, Astrophys. J., 192, 787, 1974.

Rasmussen, R. A., M.A.K. Khalil, and A. J. Crawford, Natural and anthropogenic trace gases in the southern hemisphere, Geophys. Res. Lett., 9, 704, 1982.

Rottman, G. J., Rocket measurements of the solar spectral irradiance during solar minimum, 1972-1977, J. Geophys. Res., 86, 6697, 1981.

Rottman, G. J., C. A. Barth, R. J. Thomas, G. H. Mount, G. M. Lawrence, D. W. Rusch, R. W. Sanders, G. E. Thomas, and J. London, Solar spectral irradiance, 120 to 190 nm, October 13, 1981 - January 3, 1982, Geophys. Res. Lett., 9, 587, 1982.

Rudolph, J., D. H. Ehhalt, and A. Tönnissen, Vertical profiles of ethane and propane in the stratosphere, J. Geophys. Res., 86, 7267, 1981.

Rundel, R. D., Determination of diurnal average photodissociation rates, J. Atmos. Sci., 34, 639, 1976.

Sander, S. P., and M. E. Peterson, Kinetics of the reaction $HO_2 + NO_2 + M \rightarrow HO_2NO_2 + M$, submitted to J. Phys. Chem., 1983.

Sander, S. P., and R. T. Watson, Kinetics studies of the reactions of CH_3O_2 with NO, NO_2, and CH_3O_2 at 298 K, J. Phys. Chem., 84, 1664 1980.

Shardanand, and A. D. Prasad Rao, Collision-induced absorption of O_2 in the Herzberg continuum, J. Quant. Spectrosc. Radiat. Transfer, 17 433, 1977.

Shimazaki, T., On the boundary conditions in the theoretical model calculations of the distribution of minor neutral constituents in the upper atmosphere, Radio Science, 7, 695, 1972.

Snider, D. E., and A. Goldman, Refractive effects in remote sensing of the atmosphere with infrared transmission spectroscopy, BRL Report No. 1790, USA Ballistic Research Laboratories, Aberdeen Proving Ground, Maryland, 1975.

Solomon, P. M., R. L. de Zafra, A. Parrish, and J. W. Barrett, manuscript in preparation, 1983.

Sridharan, U. C., L. X. Qiu, and F. Kaufman, Kinetics and product channels of the reactions of HO_2 with O and H atoms at 296 K, J. Phys. Chem., 86, 4569, 1982.

Stewart, R. W., and M. I. Hoffert, A chemical model of the troposphere and stratosphere, J. Atmos, Sci., 32, 195, 1975.

Stolarski, R. S., and R. D. Rundel, Fluorine photochemistry in the stratosphere, Geophys. Res. Lett., 2, 443, 1975.

Sundararaman, N., The UV radiation field in the stratosphere, Fourth Conference on CIAP, U. S. Dept. of Transportation, pp. 234-241, 1975.

Thrush, B. A., and G. S. Tyndall, The rate of reaction between HO_2 radicals at low pressures, Chem. Phys. Lett., 92, 232, 1982.

Turco, R. P., and R. C. Whitten, A note on the diurnal averaging of aeronomical models, J. Atmos. Sci., 40, 13, 1978.

U. S. Standard Atmosphere 1976, U. S. Government Printing Office, Washington, D. C., 1976.

Vedder, J. R., B. J. Tyson, R. B. Brewer, C. A. Boitnott, and E.C.Y. Inn, Lower stratosphere measurements of variation with latitude of CF_2Cl_2, $CFCl_3$, CCl_4, and N_2O profiles in the northern hemisphere, Geophys. Res. Lett., 5, 33, 1978.

Vedder, J. F., E.C.Y. Inn, B. J. Tyson, C. A. Boitnott, and D. O'Hara, Measurements of CF_2Cl_2, $CFCl_3$, and N_2O in the lower stratosphere between 2°S and 73°N latitude, J. Geophys. Res., 86, 7363, 1981.

Waters, J. W., W. J. Wilson, and F. I. Shimabukruo, Microwave measurements of mesospheric carbon monoxide, Science, 191, 1174, 1976.

Whitten, R. C., and R. P. Turco, Diurnal variations of HO_x and NO_x in the stratosphere, J. Geophys. Res., 79, 1302, 1974.

Yoshino, K., D. E. Freedman, J. R. Esmond, and W. H. Parkinson, High resolution absorption cross section measurements and band oscillator strengths of the (1,0)-(12,0) Schumann-Runge bands of O_2, Planet. Space Sci., 31, 339, 1983.

Young, A. T., Revised depolarization corrections for atmospheric extinction, Appl. Opt., 19, 3427, 1980.

Yung, Y. L., and W. B. DeMore, Photochemistry of the stratosphere of Venus: Implications for atmospheric evolution, Icarus, 51, 199, 1982.

Chapter 2

FURTHER STUDIES OF THE DIFFUSE FLUX IN THE STRATOSPHERE

2.1 Comment on Ultraviolet Solar Flux Measurements

We wish to comment on a feature of the observations of "direct and scattered solar flux within the stratosphere," by Herman and Mentall [1982a]. These authors conducted an interesting study of the ultraviolet flux from 190 to 320 nm, as measured from a balloon-borne gondola at 40 km and a rocket payload during parachute descent (60 to 38 km) with nearly identical spectrometers. In addition to direct flux measurements, with the instrument pointing at the sun, the balloon platform carried another spectrometer, successively pointed at different directions away from the sun for measurements of the scattered (diffuse) flux. The observations of direct flux, coupled with Nimbus 7 observations of the solar flux $F_{\infty}(\lambda)$ above the atmosphere, led to a wavelength-independent result for the ozone column amount above 40 km. The above measurements thus indicated consistency with the laboratory measurements of ozone absorption in the Hartley band [Inn and Tanaka, 1959]. Ackerman [1971] and Nicolet [1978] have compared the existing laboratory data in that spectral range and the ozone absorption cross sections are seen to be in very good agreement (within a few percent of the mean at most wavelengths); high resolution measurements not fully published [Bass and Paur, 1981] show no indication of significant changes. The scattered flux observations of Herman and Mentall [1982a] were shown to match theoretical calculations at wavelengths longer than about 215 nm. Our multiple scattering model

results also agree quite well with their measured ratios of diffuse to direct flux longward of 210 nm, as shown in Figure 18, where the O_3 profile deduced by Herman and Mentall and an appropriate solar zenith angle (41°) were used. A ratio of 10% at 200 nm, however, is larger than calculated [see also Luther and Gelinas, 1976] by more than a factor of two. We disagree with the suggestion that this discrepancy is simply the result of an inaccurate treatment of the solar radiation penetration in the Schumann-Runge band region. The bands themselves are weak and the underlying continuum is important near 200 nm [Hudson and Mahle, 1972]. Using average O_2 cross sections at 200 nm of $1.45 \times 10^{-23} cm^2$ for the older accepted value and $8.0 \times 10^{-24} cm^2$ (reduction by a factor of 0.55) for the more recent value used in our model [see Chapter 3; Herman and Mentall, 1982b], we obtain the different ratios of scattered to direct flux shown in Figure 18, below 210 nm. The change in $\sigma(O_2)$ affects this ratio only below 215 nm, because O_3 absorption dominates O_2 absorption beyond that wavelength. Nevertheless, the resulting ratios of 3.9% and 4.7% are more than a factor of two less than the observations at 200 nm. Even if only O_3 absorption was considered at that wavelength (i.e., $\sigma(O_2) = 0.0$), in order to allow for greater penetration of the solar flux to lower levels where multiple scattering is more important, the ratio of diffuse to direct solar flux at 40 km would be only 6.7%. Moreover, such a change in $\sigma(O_2)$ would make the direct flux too high compared to the observations.

A required change in total (O_2 and O_3) opacity of a factor of three at 200 nm is very large and unrealistic. The diffuse to direct flux ratio is also quite insensitive to reasonable uncertainties or changes in ground albedo, solar zenith angle, or total atmospheric density. Herman and

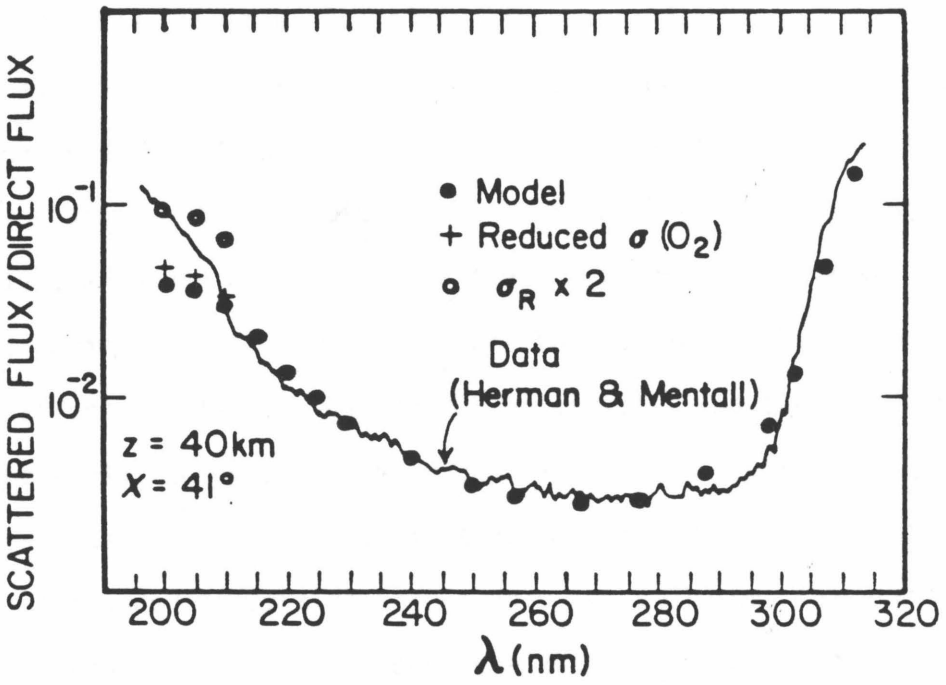

Figure 18. Comparison of our model ratio of total scattered flux to direct solar flux with the in situ spectrometer data of Herman and Mentall (1982a). Note discrepancy below about 210 nm, not explainable by a reduction in O_2 cross sections (see text).

Mentall [1982a] also point out that, although the total scattered flux is obtained by integrating over a finite number of viewing angles, the pattern of intensities is not far from isotropic in the short wavelength region, and that the anisotropy should not be a source of much uncertainty. The authors quote an experimental uncertainty of ±10% in the ratio of diffuse to direct solar flux and note that "successive spectral scans at balloon float altitude differ by less than ±10%." It would seem that the discrepancy noted below 210 nm is real, barring an unexpected systematic instrumental effect at those wavelengths, and that uncertainties in O_2 or O_3 absorption cannot account for most of the problem. The scattered flux is enhanced in absolute value, compared to theoretical expectations. A change in the Rayleigh cross section by a factor of two seems prohibitive, although we do not know the exact uncertainty associated with that parameter. As shown in Figure 18, however, a large change in σ_R would affect wavelengths beyond 200 nm as well, and the data would have to be explained by a change in the variation of $\sigma_R(\lambda)$. Gas fluorescence or scattering by aerosols might be contributing to the scattered flux, but the added scattering occurs only below 210 nm, which limits its possible sources. The observations were apparently not affected by clouds (J. R. Herman, private communication, 1982). Nitric oxide fluorescence has been observed near 200 nm above the mesopause [e.g., Barth, 1964; Feldman and Takacs, 1974]. Barth et al. [1972] note that Rayleigh scattering should dominate NO fluorescence (in the gamma band) below about 70 km. Moreover, distinct NO bands would give more structure to the scattered flux observations, given the resolution of 2.2 nm. An interesting candidate could be fluorescence by molecular oxygen itself.

Absorption in the Schumann-Runge bands produces fine structure in the direct flux observations below about 195 nm (resolution of 0.21 nm), but this would be smoothed out in the less resolved scattered flux observations; diffuse flux data are not shown below 195 nm by Herman and Mentall [1982a]. In a different wavelength region (500 to 700 nm) the question of O_2 fluorescence was raised by MacAdam [1963] in relation to the spectral intensity distribution of direct and diffuse sunlight and the disappearance of absorption bands in the diffuse observations. In the case discussed here, we need to double the single-scattering albedo by adding a term $\sigma_s n_s$ to the numerator in $\tilde{\omega}_o$. At 40 km and for 200 nm, $\tilde{\omega}_o$ is equal to 0.08 (or 0.06 if the higher O_2 cross section is used). For O_2 fluorescence to provide the additional flux, this would imply a cross section for fluorescence at least 10-20% of the O_2 absorption cross section. Such a large effect has not been observed in the laboratory, although we are not aware of studies specifically designed for this purpose. The calculations of Frederick and Abrams [1982a,b] regarding NO and O_2 fluorescent emissions at somewhat longer wavelengths (beyond 250 nm) would seem to yield contributions to the scattered flux of less than 10%, although quenching rates of excited O_2 states are not well known. Frederick (private communication, 1983) notes that satellite BUV observations do not show significant discrepancies between observed and theoretical values of scattered flux. Further careful in situ observations should be performed, if we want to distinguish between possible measurement contamination and a real source of scattered flux near 200 nm in the stratosphere.

2.2 Diffuse Flux in a Spherical Shell Atmosphere: Effects on Photochemistry

In this section, we attempt to explicitly demonstrate the effect of sphericity in the atmosphere on the diffuse radiation field and, more importantly, on photochemistry. The NASA Report 1049 [Hudson and Reed, 1979] indicated that the assumption of a plane parallel atmosphere for the diffuse flux was one source of model uncertainty at large zenith angles. We will quantify this uncertainty to first-order for solar zenith angles close to but less than 90°, although we note at the onset that an exact and elegant method for treating multiple scattering in a spherical shell atmosphere has not yet been invented and will not be here. The equation of radiative transfer (22) needs to be modified to take into account a fourth coordinate, namely the angle between the radius vector and the solar direction, and this greatly increases the mathematical complexity. The Russian scientific literature seems to be proliferous in terms of various approaches to this problem. Reviews and references can be found in Sobolev [1975] or Nazaraliyev and Sushkevich [1975], as well as in the IAMAP Conference Report [Fouquart et al., 1980]. Monte Carlo studies are the most obvious (although by no means simple or fast) answer to complex problems such as this one; a good approximation and faster approach has been described by Whitney [1972].

The last term in equation (22), $(\tilde{\omega}_0/4)\, F\, e^{-\tau/\mu_0}\, p(\mu,\phi;-\mu_0,\phi_0)$, describes the contribution of single scattering to the diffuse intensity. A first-order approximation to the effects of sphericity can be introduced by modifying the slant optical depth τ/μ_0 to the appropriate value. Some

modelers have used this in their photochemical model, but we have not seen an explicit description of the associated effects. The modification of τ_s can be made using the Chapman function, but we use the geometric ray path calculation described in Chapter 1 and Appendix A. We first present results for a homogeneous and conservative ($\tilde{\omega}_o = 1$) atmosphere, in order to compare the diffuse intensities to the backward Monte Carlo calculations of Adams and Kattawar [1978]. The results at large zenith angle ($\theta_o = 84.26°$) are shown in Figures 19 and 20 for total normal optical depths τ_1 of 0.25 and 1.00, respectively, as a function of viewing angle θ at the top of the atmosphere and for two azimuthal directions ($\phi = 0$ and 180°). The plane parallel calculations are in excellent agreement. If sphericity is included, more direct radiation and therefore a higher single-scattered intensity will be present throughout the atmosphere. The slant optical depth for a homogeneous atmosphere of height z_h is easily evaluated analytically

$$\tau_s(z,\mu_o) = \tau(z)\ \left(\frac{R+z}{z_h}\right)\ -\mu_o + \left[\left(\frac{R+z_h}{R+z}\right)^2 + \mu_o^2 - 1\right]^{1/2} \qquad (37)$$

This correction to the single scattering term in the radiative transfer program leads to intensities very similar to the Monte Carlo results for $\theta \lesssim 75°$. At large viewing angles, sphericity can lead to large changes in the intensity. However, in terms of photochemical effects, the integral of the intensity over solid angle is the relevant quantity (see equation (14) in Chapter 1), and this diffuse flux is not very sensitive to the intensity changes at large θ. We also attempted to refine the diffuse radiation field calculation by using the source function

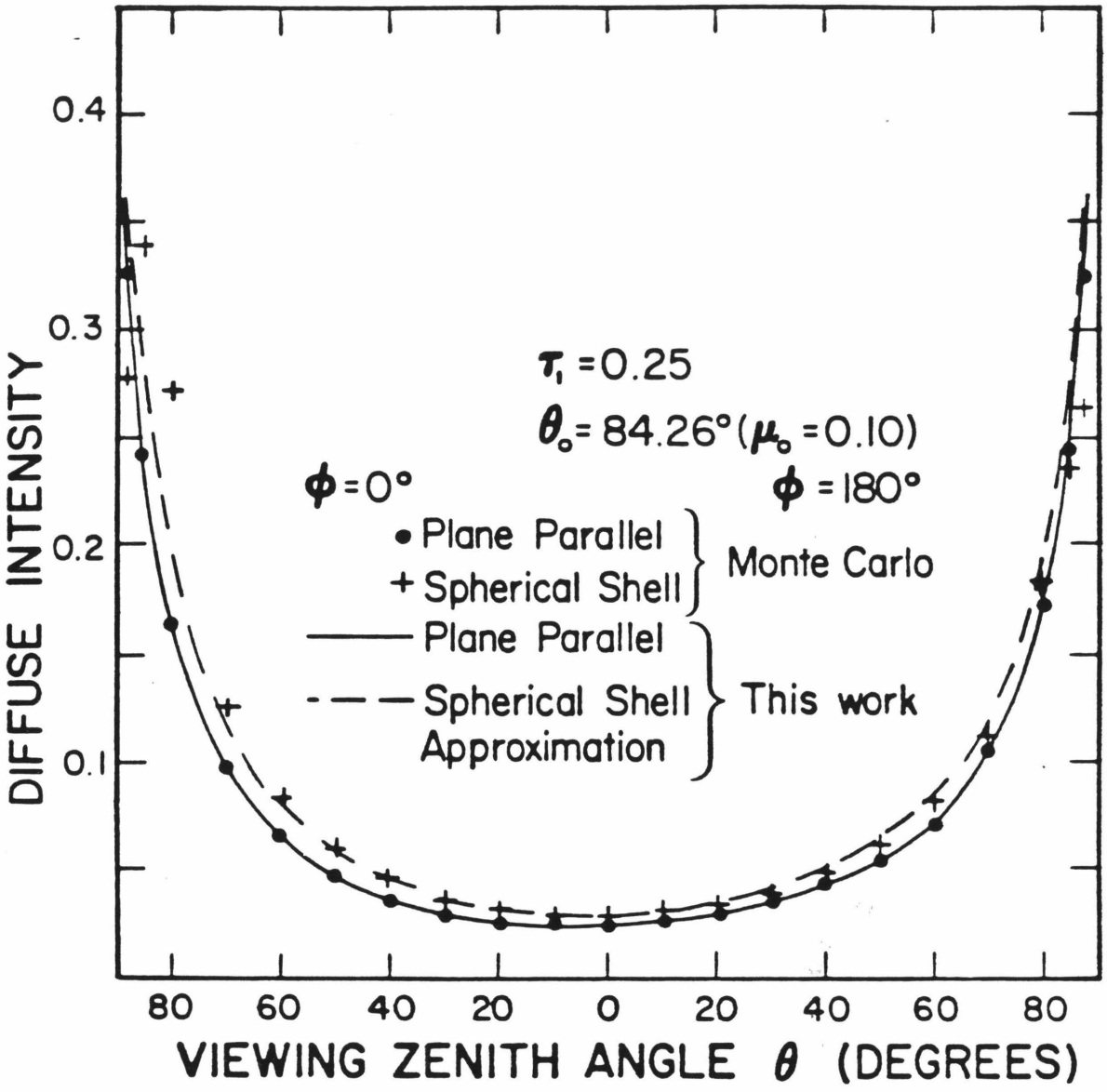

Figure 19. Intensities at the top of a 100 km thick (homogeneous and conservative) plane parallel or spherical shell model atmosphere of total normal optical depth $\tau_1 = 0.25$, for a solar zenith angle of 84.26°. The Monte Carlo results of Adams and Kattawar (1978) are shown. Our spherical shell approximation includes the first-order single scattering correction (see text).

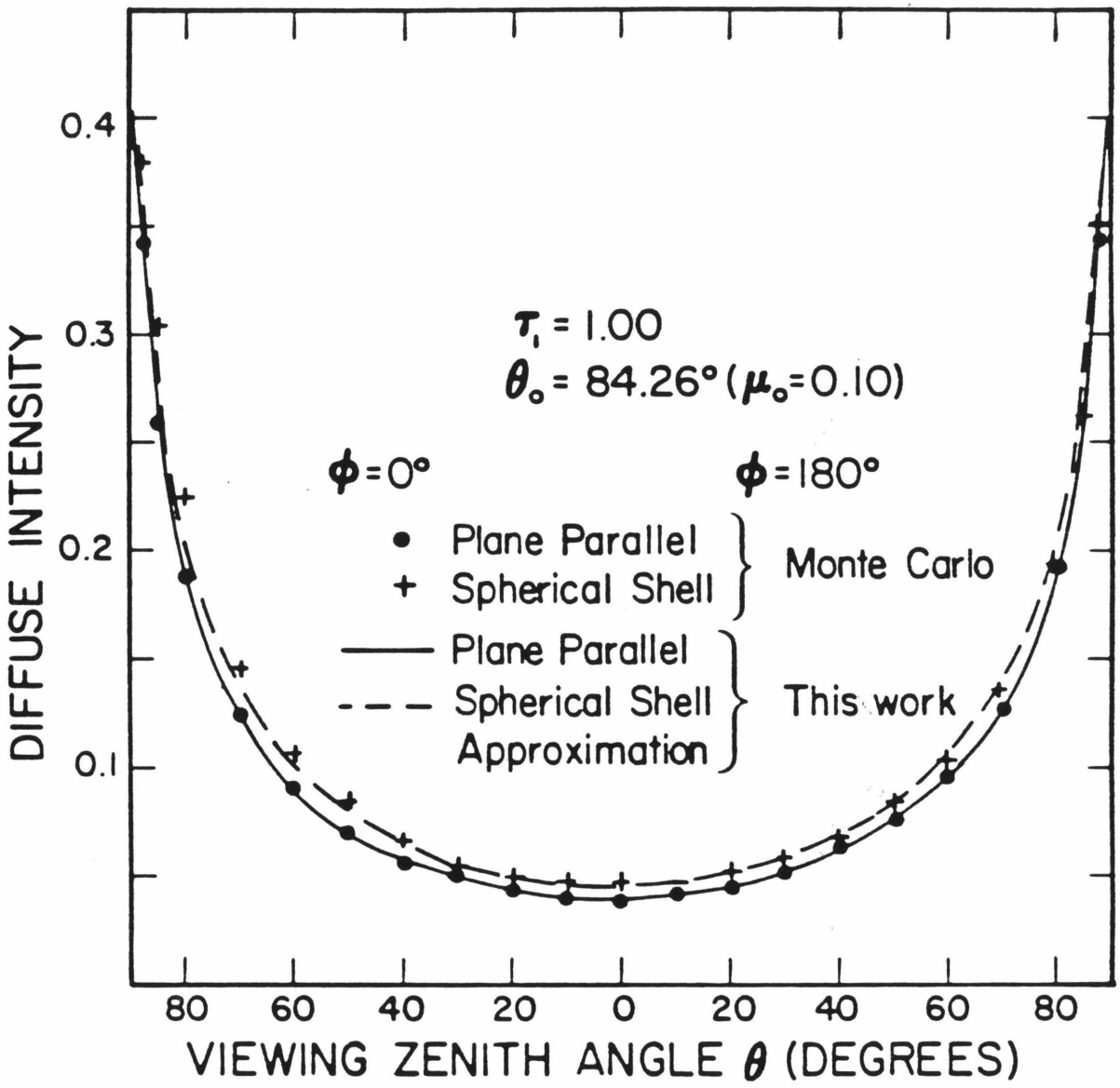

Figure 20. Same as Figure 19, but for τ_1 = 1.00 .

$$J(\tau,\pm\mu,\phi) = \frac{\tilde{\omega}_o}{4\pi} \int_0^{2\pi} \int_{-1}^{1} p(\pm\mu,\phi;\mu',\phi')\, I(\tau,\mu',\phi')\, d\mu'\, d\phi' + \frac{\tilde{\omega}_o}{4} F\, e^{-\tau_s(\mu_o)}\, p(\pm\mu,\phi;-\mu_o,\phi_o) \qquad (38)$$

where $I(\tau,\mu',\phi')$ and $\tau_s(\mu_o)$ are calculated as discussed above, and then recalculating the intensities from the formal solution to the radiative transfer equation [see e.g., Chandrasekhar, 1960]:

$$I(\tau,+\mu,\phi) = \int_{\tau}^{\tau_1} J(\tau',+\mu,\phi)\, e^{-(\tau_s' - \tau_s)}\, d\tau_s' \qquad (39a)$$

$$I(\tau,-\mu,\phi) = \int_{0}^{\tau} J(\tau',-\mu,\phi)\, e^{-(\tau_s - \tau_s')}\, d\tau_s' \qquad (39b)$$

where $\tau_s(\mu)$ is the slant optical depth in direction μ, and $I(\tau_1,+\mu,\phi)$ and $I(0,-\mu,\phi)$ are assumed equal to zero. This procedure was checked in the plane parallel case ($\tau_s = \tau/\mu$), where fluxes (and intensities) should not change from one iteration to the next (true to within one or two percent). Moreover, intensities can be calculated at any angle, rather than simply at the Gaussian quadrature points. For large solar zenith angles ($\theta_o > 85°$), we find that the above correction leads to diffuse fluxes very similar to the results obtained using only a correction to the single-scattered term. We have thus used the latter approximation for a real (inhomogeneous) atmosphere. The above test results were still an approximation to the problem of spherical shell atmospheres, since all points within the atmosphere are directly illuminated by the solar flux at a fixed angle. In reality, sphericity can affect the intensities even for $\theta_o = 0°$ [Adams and Kattawar, 1978]. However, the use of a sphericity

correction in the single-scattered term, coupled with the multiple scattering contribution for a plane parallel atmosphere, should give a reasonable estimate of the diffuse fluxes at large θ_0, as shown in Figures 19 and 20, even if the intensities at large θ are not well approximated. The intuitive comment that is often referred to in this respect is that photons that scatter many times have "lost track" of the geometry of the atmosphere, whereas the photons which are scattered only once "remember quite well" that the optical depth just traversed was smaller than in a plane parallel atmosphere. The above comments will not hold for twilight cases with θ_0 much larger than 90°, as shown for example by the Monte Carlo studies of twilight radiation--including refraction--by Blattner et al. [1974]. In a short report with few details about the spherical model, Anderson [1982] also concludes that the use of plane parallel geometry for multiple scattering and spherical geometry for single scattering leads to small errors in the fluxes for solar zenith angles less than 95°.

We now describe the effects of sphericity on the diffuse fluxes, photodissociation rates and species concentrations in the Earth's stratosphere. Only the first-order correction for single scattering is included. The importance of the diffuse flux relative to the total radiation field depends on the wavelength, but increases with solar zenith angle. At wavelengths where strong absorption occurs (below $\sim$300 nm), the fraction of diffuse flux is large but molecular photodissociation rates will be affected more (in terms of total flux) by the longer wavelengths. Ozone absorption is small in the Chappuis band (400 to 800 nm), but the small total opacity (Rayleigh + ozone) leads to

a large direct flux relative to the total flux. Species such as HNO_3 and HO_2NO_2, whose photodissociation occurs shortward of 330 nm, are most affected by the diffuse flux effect just longward of 300 nm, and in the lower stratosphere, as we will see. Figure 21 shows the ratio of fluxes calculated in the spherical shell approximation (SS) versus the plane parallel case (PP) for both diffuse and total fluxes at 312.5 nm and various altitudes. At 30 and 40 km, there are large changes in the diffuse flux near 90°, but the total flux changes very little since the diffuse radiation contributes only a small fraction to the total field. In the lower stratosphere, however, most of the radiation is diffuse at this particular wavelength and the total flux is also significantly affected by the inclusion of sphericity. This will affect the photodissociation rates sensitive to this wavelength. The effect on photodissociation rates and species concentrations is ultimately what we are really interested in for photochemical modeling. The most relevant changes in photodissociation rates (j^{SS}/j^{PP}) are plotted in Figure 22 as percent increases versus altitude for a solar zenith angle of 88.5° (diurnal model, 32°N Latitude, -11° Declination). As expected from the previous graph, the lower stratosphere is most affected and the wavelength-dependent diffuse flux effect, combined with the molecular photodissociation region, leads to the largest increases (about 30%) in $j(HNO_3)$ and $j(HO_2NO_2)$. Small changes also occur for $ClONO_2$, NO_2, NO_3 and O_3. We have included the effect of sphericity on the diffuse fluxes in a diurnal calculation (32° N latitude, -11° solar declination) , in order to investigate changes in species concentrations. The increased rates of photolysis near sunset or sunrise do not affect the "long-lived" (lifetime longer than an hour) species, since they cannot respond very fast. As

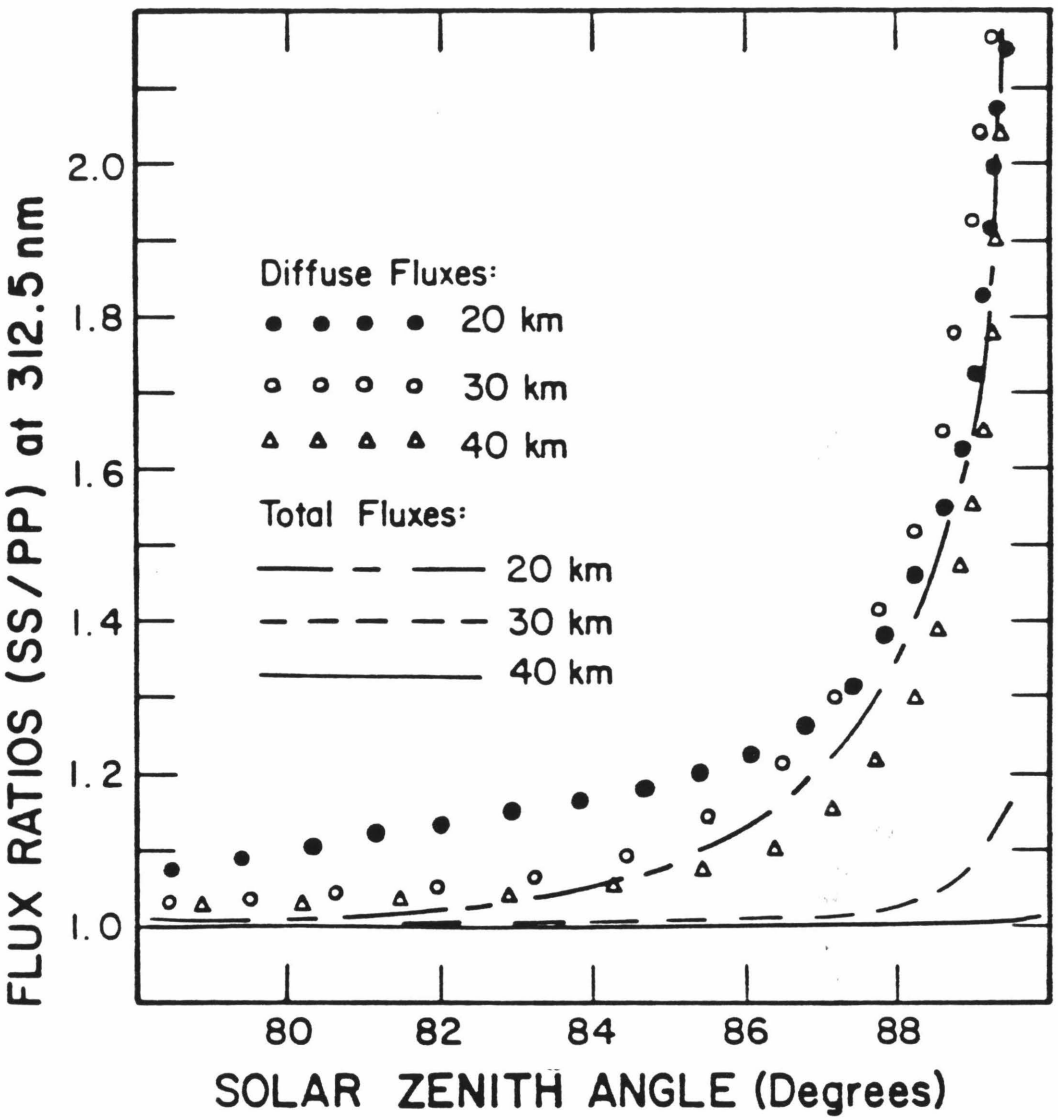

Figure 21. Ratios of fluxes (total and diffuse) from the (approximate) spherical shell (SS) to plane parallel (PP) cases in the Earth's stratosphere, as a function of solar zenith angle, for a wavelength of 312.5 nm. The effect of sphericity on the total flux is largest in the lower stratosphere, for large zenith angles.

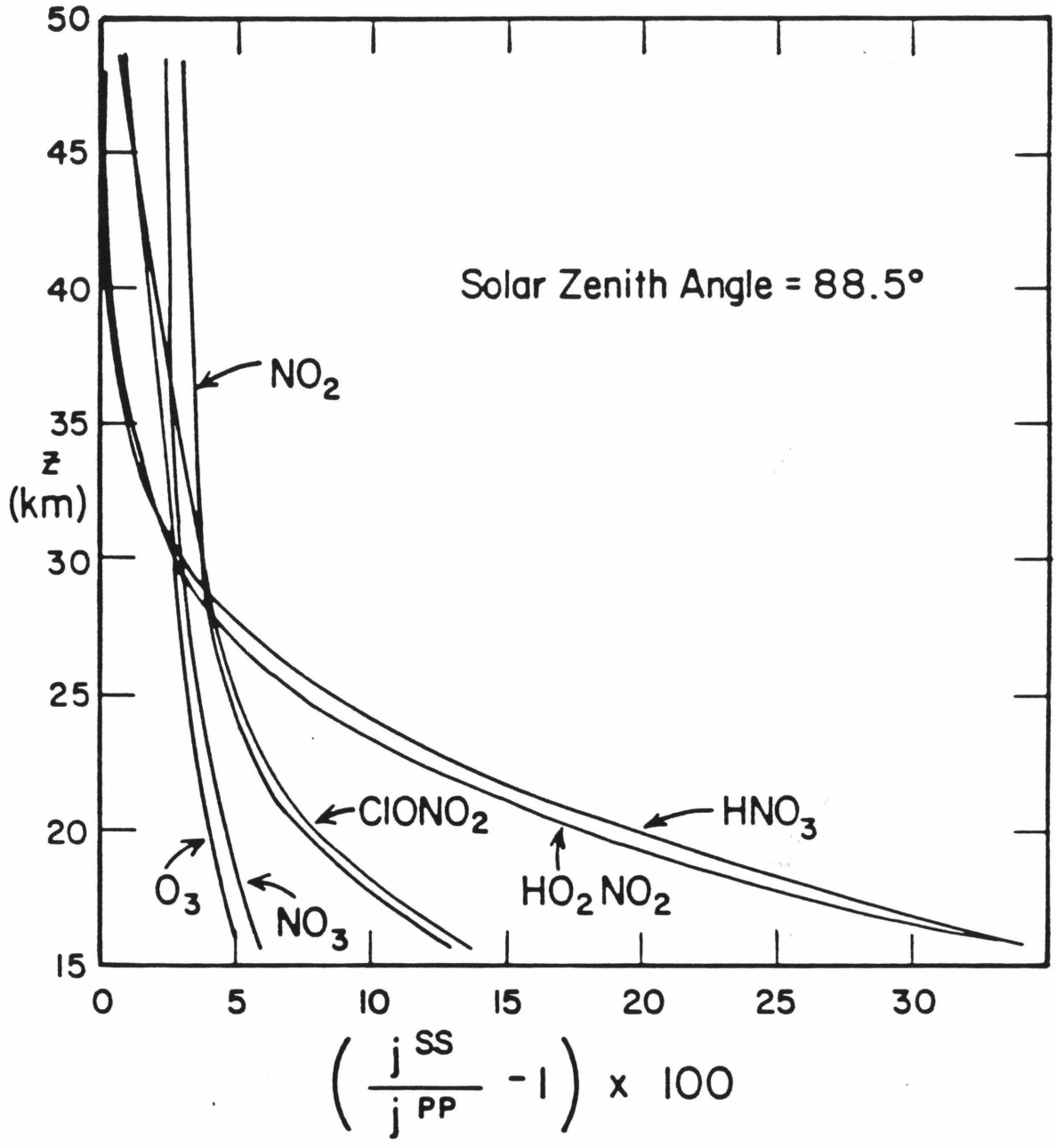

Figure 22. Percent increase in the photodissociation rate constants of certain stratospheric species due to the inclusion of sphericity in the single scattered intensities, for a solar zenith angle of 88.5°. The magnitude of the increase is largest in the lower stratosphere.

illustrated in Figure 23 for a height of 20 km, where the diffuse flux plays a large role, the short-lived radicals such as O, OH, ClO, NO, NO_2 and NO_3 display the effect of the above increases in photodissociation rates. $O(^1D)$ is also significantly affected (close to 30% in the lower stratosphere). The ozone photodissociation rate increase leads to more [O] and $[O(^1D]$. Moreover, [H], [OH] and $[HO_2]$ are all affected in a similar fashion by increased $j(HNO_3)$ and $j(HO_2NO_2)$ near 90° in the lower stratosphere. [NO] is increased due to $j(NO_2)$, $[NO_2]$ itself is decreased somewhat, while $[NO_3]$ decreases due to less $[NO_2]$ and a higher $j(NO_3)$. Chlorine nitrate photolysis leads to enhancement in the chlorine radicals (Cl,ClO,ClOO), although only [ClO] is plotted in the figure. [OH] shows the largest change, close to a 20% increase at the terminator. For most other radicals, less than 10% change occurs for zenith angles below 90°, and the effect diminishes at higher altitudes. An extrapolation to twilight effects would also indicate that the hydrogen radical (H, OH and HO_2) concentrations are underestimated in the standard model by possibly as much as 50% at 20 km. We should note, however, that other effects that are not included in photochemical models, such as refraction or aerosol absorption and scattering are sources of uncertainty, particularly at large zenith angles [Adams et al., 1974]. Such uncertainties preclude an exact determination of the chemical abundances of radicals near sunset and sunrise, especially during the twilight period. Moreover, observations of these radicals near the terminator contain intrinsic uncertainties as well. The above discussion concerning the diffuse flux near the terminator and its effects on the photochemistry, depending on the geometry used, is therefore more of a theoretical

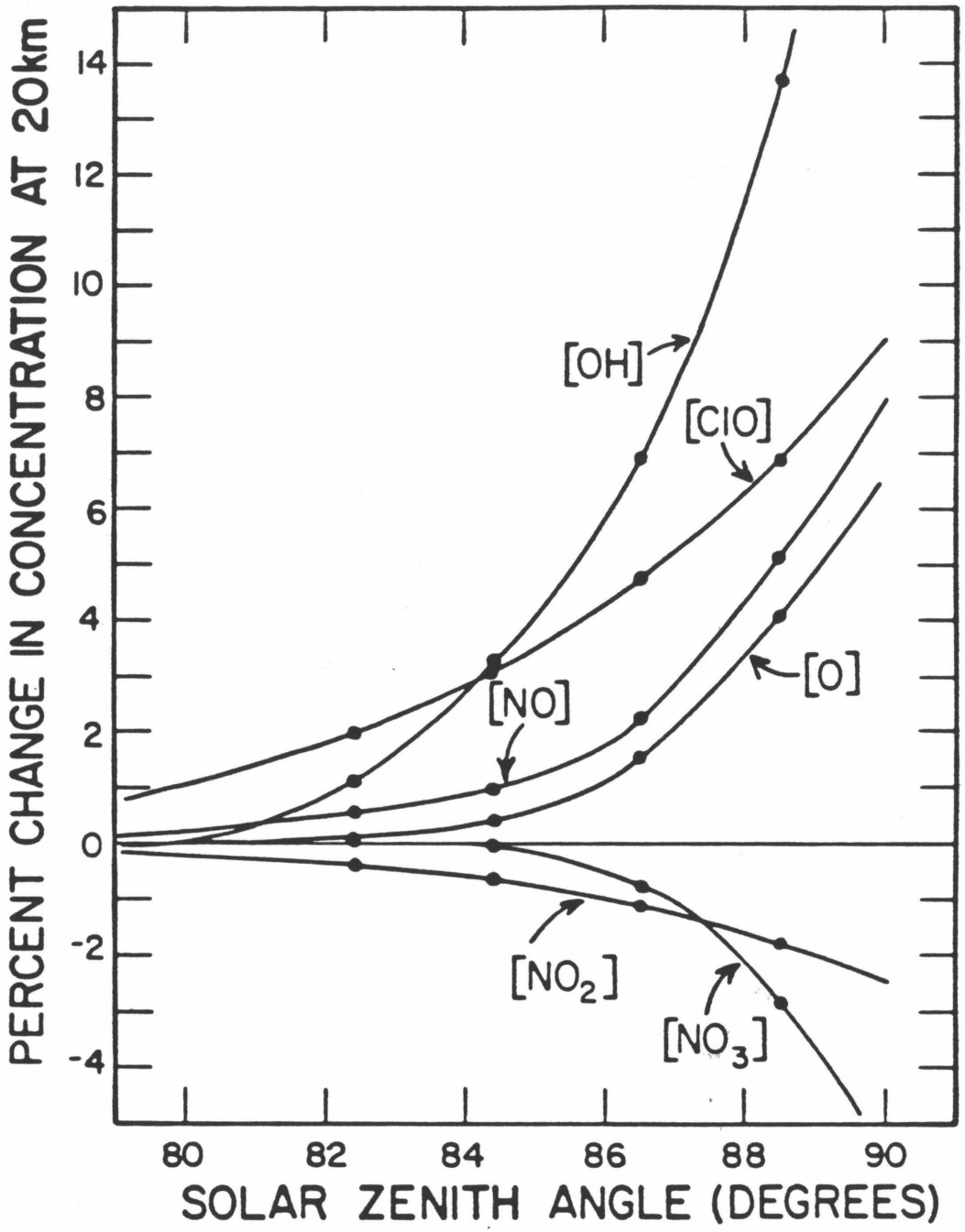

Figure 23. Effect of changes in the photodissociation rates (as shown in Figure 22 for 88.5°) on short-lived radical concentrations near the terminator, at an altitude of 20 km. HO_x radicals show the largest changes, but most variations are small compared to observational uncertainties (and other model uncertainties).

exercise than an observable effect. It is always useful, however, to be aware of the degree of uncertainty caused by various assumptions, and this was merely an attempt to show the model sensitivity to one particular assumption. A much more significant assumption is discussed in the next chapter.

References

Ackerman, M., Ultraviolet solar radiation related to mesospheric processes, in Mesospheric Models and Related Experiments, edited by G. Fiocco, Springer-Verlag, New York, 1971.

Adams, C. N., and G. W. Kattawar, Radiative transfer in spherical shell atmospheres I. Rayleigh scattering, Icarus, 35, 139, 1978.

Adams, C. N., G. N. Plass, and G. W. Kattawar, The influence of ozone and aerosols on the brightness and color of the twilight sky, J. Atm. Sci., 31, 1662, 1974.

Barth, C. A., Rocket measurement of the nitric oxide dayglow, J. Geophys. Res., 69, 3301, 1964.

Barth, C. A., D. W. Rusch, and A. I. Stewart, The UV nitric oxide experiment for Atmosphere Explorer, Radio Science, 8, 379, 1973.

Bass, A. M., and R. J. Paur, Ultraviolet absorption cross sections of O_3: The temperature dependence, Upper Atmosphere Programs Bulletin, No. 81-4, 9, 1981.

Blattner, W. G., H. G. Horak, D. G. Collins, and M. B. Wells, Monte Carlo studies of the sky radiation at twilight, Appl. Opt., 13, 534, 1974.

Chandrasekhar, S., Radiative Transfer, Dover Publications Inc., New York, 1960.

Feldman, P. D., and P. Z. Takacs, Nitric oxide gamma and delta band emission at twilight, Geophys. Res. Lett., 1, 169, 1974.

Fouquart, Y., W. M. Irvine, and J. Lenoble (Eds.), Standard Procedures to Compute Atmospheric Radiative Transfer in a Scattering Atmosphere, International Association of Meteorology and Atmospheric

Physics (IAMAP) Radiation Commission, Vol. II, Boulder Colorado, 1980.

Frederick, J. E., and R. B. Abrams, Model studies of nitric oxide fluorescence in the Earth's backscattered spectrum, Planet. Space Sci., 30, 137, 1982a.

Frederick, J. E., and R. B. Abrams, Dayglow emissions of the O_2 Herzberg bands and the Rayleigh backscattered spectrum of the Earth, Planet. Space Sci., 30, 575, 1982b.

Herman, J. R., and J. E. Mentall, The direct and scattered solar flux within the stratosphere, J. Geophys. Res., 87, 1319, 1982a.

Herman, J. R., and J. E. Mentall, O_2 absorption cross sections (187-225 nm) from stratospheric solar flux measurements, J. Geophys. Res., 87, 8967, 1982b.

Hudson, R. D., and S. H. Mahle, Photodissociation rates of molecular oxygen in the mesosphere and lower thermosphere, J. Geophys. Res., 77, 2902, 1972.

Hudson, R. D., and E. I. Reed (Eds.), The Stratosphere: Present and Future, NASA Reference Publication 1049, 1979.

Inn, E.C.Y., and Y. Tanaka, Ozone absorption coefficients in the visible ultraviolet regions, Adv. Chem. Ser., 21, 263, 1959.

Luther, F. M., and R. J. Gelinas, Effect of molecular multiple scattering and surface albedo on atmospheric photodissociation rates, J. Geophys. Res., 81, 1125, 1976.

MacAdam, D. L., Do oxygen and water vapor fluoresce?, J. Opt. Soc. Am., 53, 397, 1963.

Nazaraliyev, M. A., and T. A. Sushkevich, Calculation of the characteristics of the multiply scattered radiation field in a spherical

atmosphere, Izv. Atm. and Ocean. Phys., 11, 705, 1975.

Nicolet, M., Etude des réactions chimiques de l'ozone dans la stratosphère, Comité d'études sur les consequences des vols stratosphériques, Institut Royal Météorologique de Belgique, 1978.

Sobolev, V. V., Light scattering in planetary atmospheres, International Series of Monographs in Natural Philosophy, Vol. 76, Pergamon Press, 1975.

Whitney, C., Implications of a quadratic stream definition in radiative transfer theory, J. Atm. Sci., 29, 1520, 1972.

Chapter 3

MODEL SENSITIVITY TO O_2 ABSORPTION CROSS SECTIONS IN THE HERZBERG CONTINUUM

3.1 Photolysis of Stratospheric Gases in the 190-220 nm Spectral Region

In this section, we emphasize that photodissociation of certain species in the stratosphere is quite sensitive to the 190-220 nm spectral region, which coincides with the O_2 Herzberg continuum domain. Photochemical models, both 1-D and 2-D, have had difficulty producing a satisfactory simultaneous fit to the altitude distributions of all long-lived source species that diffuse upwards from the troposphere and undergo relatively simple chemistry in the stratosphere. In particular, it has been difficult to produce good simultaneous fits to N_2O, CH_4, CF_2Cl_2(FC12) and $CFCl_3$(FC11) profiles above 20 km. The calculated mixing ratios near 30 km for FC12 and FC11 are generally overestimated by a factor of about two and five or more, respectively, given a model that is in reasonable agreement with N_2O and CH_4. This general discrepancy holds for 1-D and 2-D models alike and seems to be fairly independent of latitude or season [see Hudson et al., 1982; Miller et al., 1981]. Possible solutions including either transport, unknown chlorofluorocarbon sinks or inaccurate solar radiation calculations in the Schumann-Runge bands have been suggested. We discuss in detail the most plausible solution, which involves the uncertainty in the photodissociation rate of some stratospheric molecules (such as N_2O, FC11 and FC12) due to uncertainties in molecular oxygen absorption cross sections near 200 nm.

Nicolet [1980, 1981] had reviewed the subject of absorption of solar radiation within the stratosphere, with some emphasis on molecular oxygen and ozone absorption; it certainly seems that the O_2 cross sections in the Herzberg continuum (200-242 nm) are uncertain by at least 25%. Moreover, the solar flux at the top of the atmosphere is not known to much better than 15% in this spectral region [see Hudson et al., 1982]. However, molecules that dissociate near 200 nm, where O_2 is the main opacity source, will be more sensitive to the O_2 cross sections $\sigma_\lambda(O_2)$ than to the solar flux, since $\sigma_\lambda(O_2)$ enters as an exponential factor in the photodissociation rate calculations. Indeed, $\Delta j_\lambda/j_\lambda = -\Delta\tau_\lambda = -\tau_\lambda(\Delta\tau_\lambda/\tau_\lambda)$, which implies that a small percentage change in total optical depth τ_λ can lead to a larger relative change in j_λ if τ_λ is larger than unity (below about 35 km in this case).

Figure 24 illustrates the importance of the 190-220 nm region for N_2O, HNO_3, CF_2Cl_2 and $CFCl_3$, for which j_λ peaks in the center of this spectral range; however, the total photolysis rate of HNO_3 also depends on the flux longward of 300 nm and actually peaks at $\sim$310 nm below about 20 km. Rates in Figure 24 were calculated with O_2 and O_3 profiles from the U. S. Standard Atmosphere 1976 and 24 hr diurnally-averaged transmission (see Chapter 1). The optical depths $\tau_\lambda(O_2)$ and $\tau_\lambda(O_3)$ in the 200-220 nm range are shown in Figure 25. O_2 and O_3 contribute roughly equally to the total opacity in this region, and it is clear that this model yields total τ_λ values of order 1 to 10 between 20 and 30 km. The O_2 cross sections above 207.5 nm follow the recommendation of the 1979 NASA Report [Hudson and Reed, 1979] and the O_3 values are from Ackerman [1971]. Below 207.5 nm, effective O_2 cross sections, depending on height

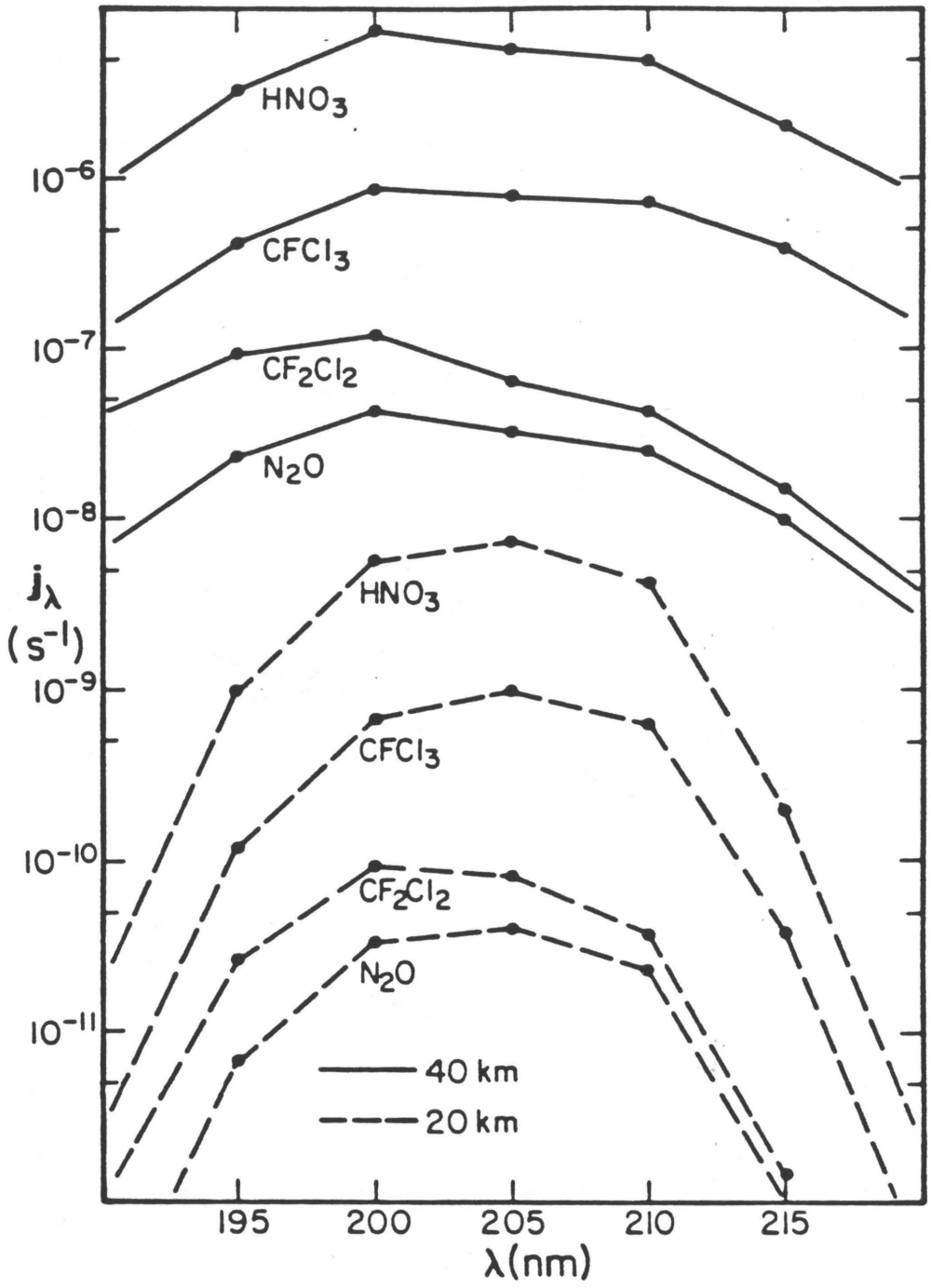

Figure 24. Diurnally-averaged photodissociation rate constants for HNO_3, $CFCl_3$, CF_2Cl_2, and N_2O at 40 and 20 km, in the O_2-O_3 spectral window near 200 nm. Model is for 45°N , and 23° solar declination (summer).

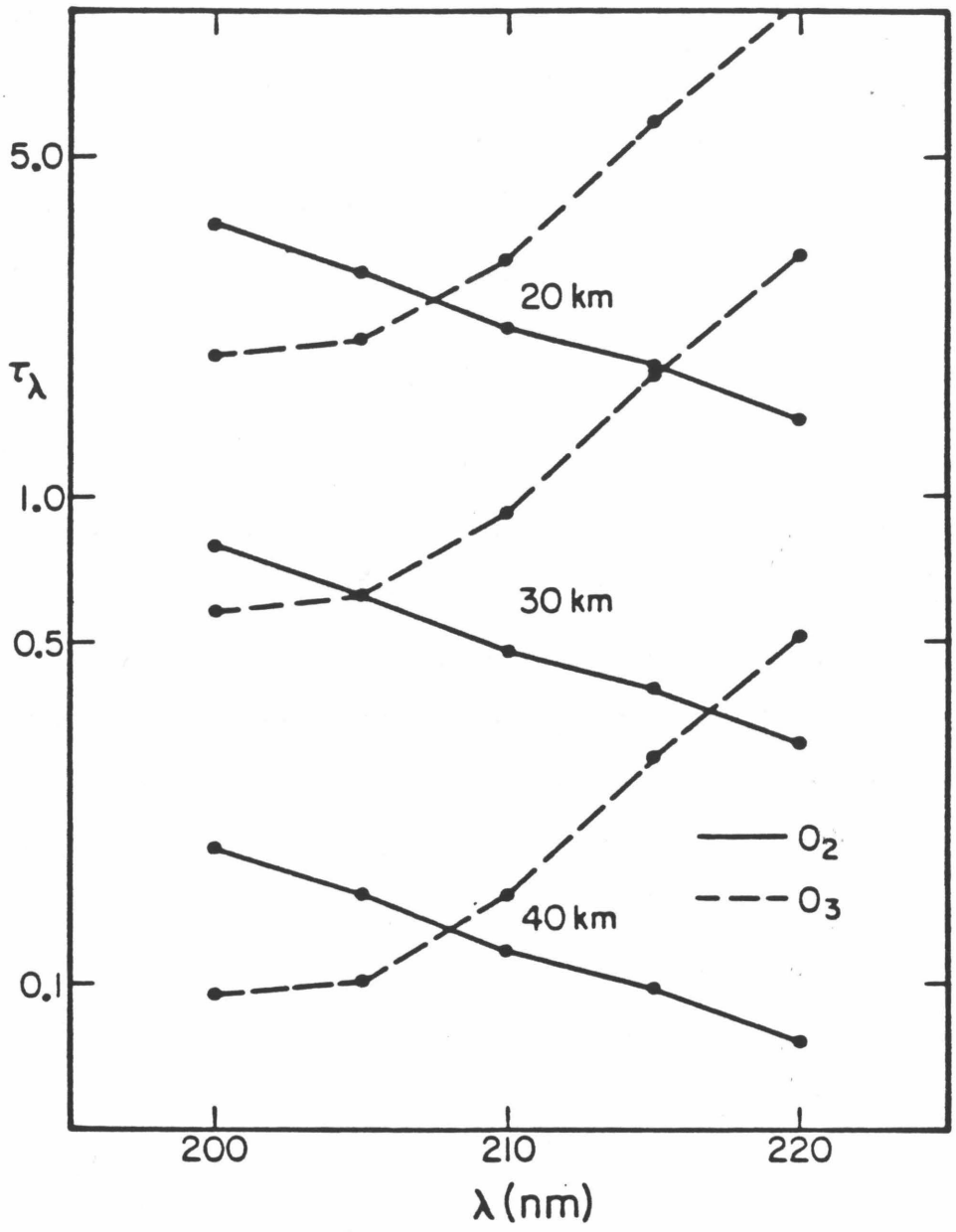

Figure 25. Normal optical depths for O_2 and O_3 at various altitudes; standard model O_2 cross sections are used (see text).

and zenith angle, are calculated according to the work of Allen and Frederick [1982]. Above 197.5 nm, the contribution from the bands should be about 5% or less, most of the absorption being due to the continuum [Hudson and Mahle, 1972]. Shardanand and Prasad Rao [1977] have obtained the latest (and smallest) measurements of O_2 cross sections in the Herzberg continuum and have described the problems associated with laboratory determinations of these very small cross sections.

If the older model cross sections (average values of 14.5, 11.5, 8.85, 7.43 and 5.75 in units of $10^{-24}cm^2$, for 200, 205, 210, 215 and 220 nm, respectively) are reduced by a factor of about 0.6, we find some fairly significant changes in relevant stratospheric profiles. Some of our preliminary sensitivity tests were presented by Y. Yung at the Chemical Manufacturers Association Meeting [Steed et al., 1982]. During that month, related work from the NASA/Goddard Space Flight Center became available to us, with quite timely and direct implications for the Herzberg continuum absorption of O_2. Frederick and Mentall [1982] discuss some of the direct solar flux measurements within the stratosphere (30-40 km) and conclude that the atmospheric transmission in the 200-210 nm range is larger than expected from laboratory data on O_2 and O_3 cross sections. Herman and Mentall [1982] give a more expanded analysis of the transmitted radiation from 190 to 320 nm, from which they derive some constraints on the absorption characteristics of O_2 and O_3. They find that the O_3 cross sections seem to agree within a few percent with the laboratory data, whereas the O_2 cross sections seem to have been overestimated by 30% or more by laboratory measurements, in agreement with

our own suggestion based on more indirect modeling tests of N_2O, HNO_3 and chlorofluorocarbon profiles.

3.2 Modeling of Stratospheric Species and Sensitivity to O_2 Cross Sections

Since Herman and Mentall [1982] have recently estimated that the O_2 cross sections in the Herzberg continuum region should be even lower (by $\sim$30%) than the lowest laboratory values, we adopt average cross sections in agreement with their results. We use reduced values of 5.6, 5.1 and 3.5 ($10^{-24}cm^2$) at 210, 215 and 220 nm, respectively, keeping in mind that these values have associated error bars of 10-30%. We note that these values were obtained prior to the final published results of Herman and Mentall [1982]. Their final results are slightly different and we use corresponding cross sections of 6.5, 5.8 and 4.6 (in units of $10^{-24}cm^2$) throughout the other chapters of this thesis, but the following discussion is not significantly altered by this revision. Below 207.5 nm we multiply the effective O_2 cross sections by a factor of 0.55, down to 196.1 nm (spectral interval 5 in Allen and Frederick, 1982). This produces effective average cross sections of about $8.0 \times 10^{-24}cm^2$ (200 nm) and $6.3 \times 10^{-24}cm^2$ (205 nm) at an altitude where the O_2 absorption effect is maximized.

The mid-latitude models presented below are compared to N_2O, CH_4, CF_2Cl_2, $CFCl_3$ and HNO_3 observations graphically summarized in Hudson et al. [1982]; the latter report describes in more detail the data base and the relevant references. Most of the observations were taken between 40°N and 50°N, during the summer, and the calculations refer to 45°N

latitude and summer solstice solar illumination. Two eddy-diffusion profiles are used ($K_1(z)$ and $K_2(z)$, see Chapter 1). Clearly, there is no "ideal" profile in this oversimplified representation of transport processes, but it will be seen that the slower K_2 model will result in better fits with observations near 45°N; indeed there is strong evidence that vertical transport is latitude-dependent and increases towards the tropics. In model A, we use the standard O_2 cross sections and transport profile K_2. Model B differs from A simply by the reduction (factor of 0.6) in O_2 cross sections described above and Model C is the same as case B, except that the K(z) profile is the faster K_1 model.

The N_2O profiles shown in Figure 26 illustrate the fact that both an increase in transport rates and an increase in O_2 cross sections can increase the mixing ratios above 20 km. Methane also shows an increase due to transport (from Model B to C), but is insensitive to the 200-220 nm spectral region and Models A and B yield similar profiles. Nevertheless, the N_2O and CH_4 observations do not provide the most sensitive test of these three models. FC11 and FC12 show larger reductions in mixing ratios in the middle and upper stratospheres, if Model B is used instead of A (see Figure 27): CF_2Cl_2 is reduced by factors of 0.62 and 0.41 at 30 and 40 km, respectively, whereas $CFCl_3$ is decreased by factors of 0.19 and 0.06 at these altitudes. A much better fit is obtained with Model B; use of the faster transport profile (Model C) increases the mixing ratios back to values similar to Model A. An additional improvement due to Model B is shown in Figure 28. Nitric acid (HNO_3) has always been in disagreement with observations above about 30 km. The increase in photolysis between models A and B is translated into a 50% decrease above 30 km,

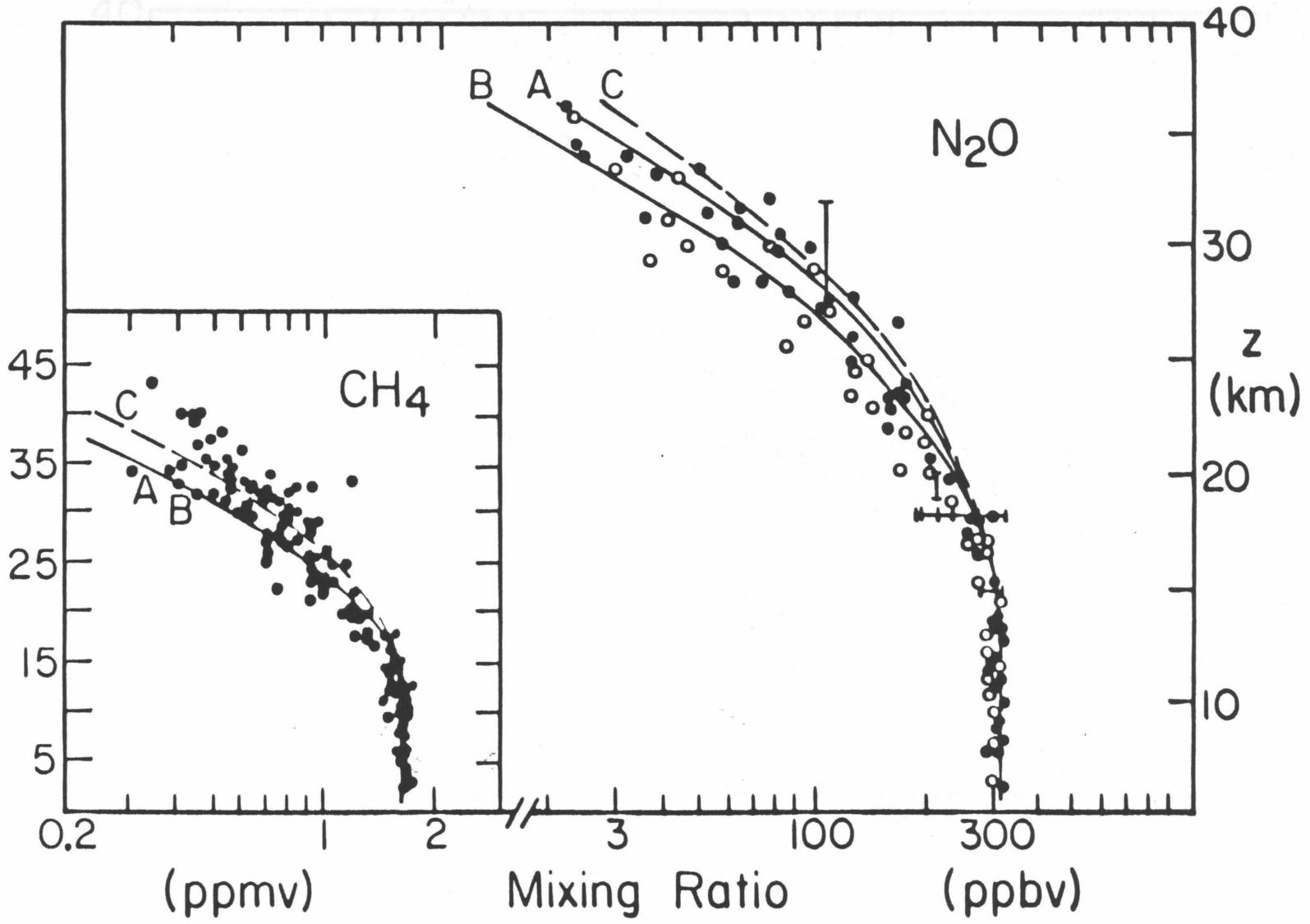

Figure 26. Model fits to N_2O and CH_4 data. N_2O observations are from 40 to 45°N, in the summer. CH_4 data are from 40 to 60°N, at various seasons (see Hudson et al., 1982).

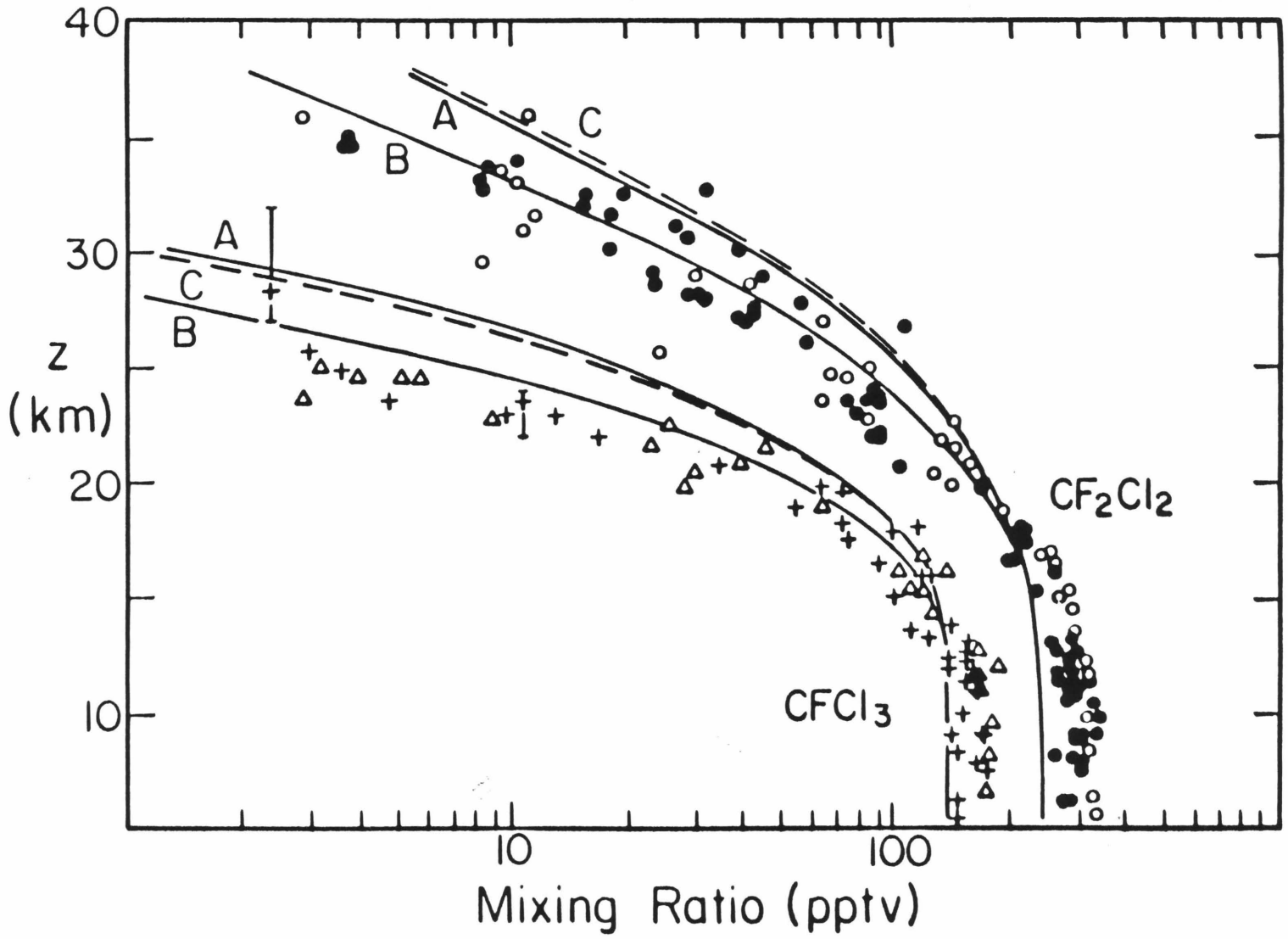

Figure 27. Sensitivity of CF_2Cl_2 and $CFCl_3$ to O_2 cross sections near 200 nm and transport. Observations are from 40-45°N, in the summer (see Hudson et al., 1982).

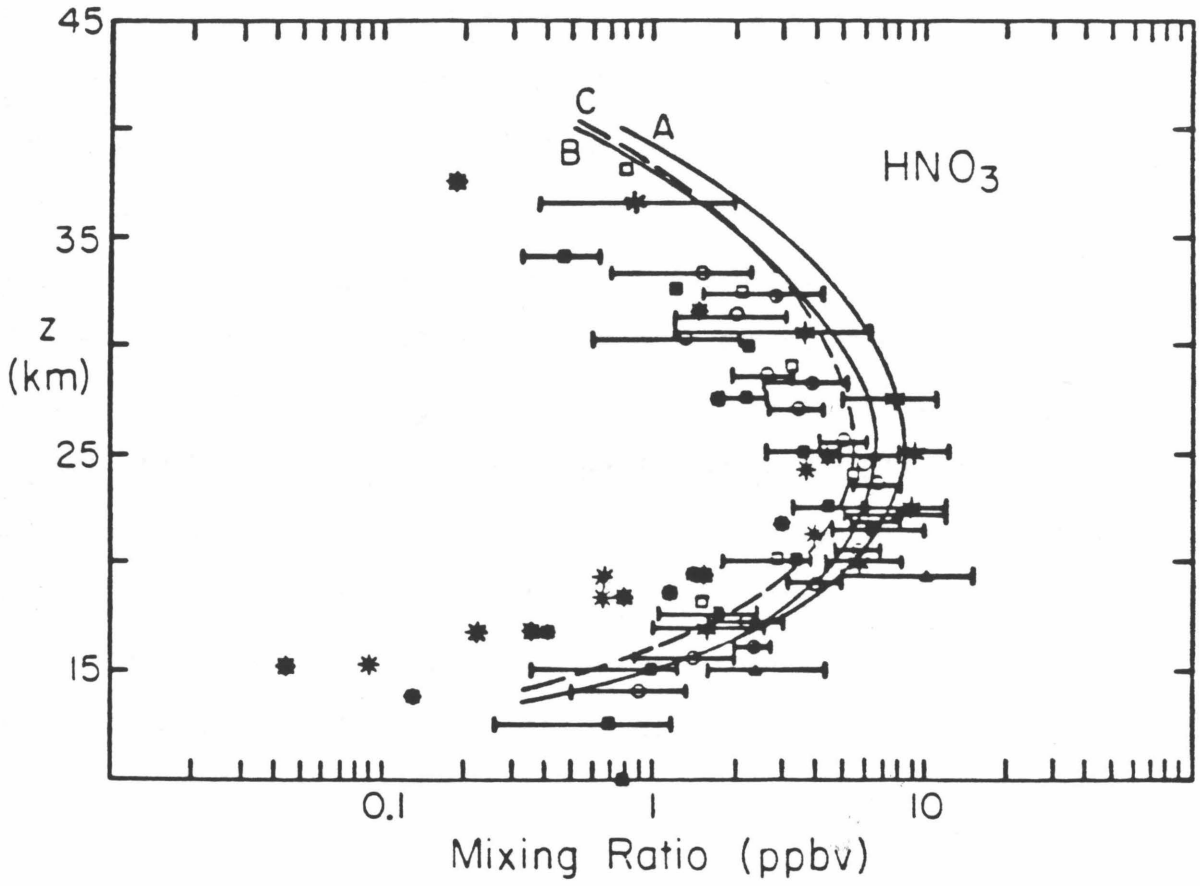

Figure 28. Same model conditions as for Figures 26 and 27 (45°N, summer), but for HNO_3 at mid-latitudes. Data are reproduced from Hudson et al.(1982); see references therein.

and much smaller changes in the lower stratosphere, where the total photolysis rate becomes insensitive to radiation in the O_2 Herzberg continuum. Moreover, as discussed in Chapter 1, the true diurnal average profile is in better agreement with observations. We emphasize that the significant lower stratospheric increase in flux near 200 nm in Model B (flux higher than in Model A by a factor of 2-5) cannot be caused by a 10-20% change in the solar flux at the top of the atmosphere, since the latter uncertainty is not amplified by an exponential factor, as in the case for $\sigma(O_2)$.

Other atmospheric gases are also affected--directly or indirectly--by a reduction in O_2 cross sections. The main direct effect is an increase in the photodissociation rates of other halocarbons in the middle and upper stratosphere, due to the larger fluxes in the 200-220 nm range. Large reductions in CCl_4 and $C_2H_3Cl_3$ are found, similar to the effect on $CFCl_3$ shown above (factor of 0.16 at 30 km). There are no published observations of CCl_4, and only tentative measurements (lower limit) of $C_2H_3Cl_3$ are presented by Fabian et al. [1981]; these authors find 1 pptv at 23 km, which is about an order of magnitude lower than in our model B. They also measured a few less abundant chlorofluorocarbons, and we compare our model to their observations of $C_2F_3Cl_3$(FC113) and $C_2F_4Cl_2$(FC114) in Figure 29. These species photodissociate very slowly and display much less of a decrease with height than the major halocarbons. Only the reduced cross section model (B) is shown in the figure. The $C_2F_4Cl_2$ profile varies little (< ±30%) from case B to A or C; $C_2F_3Cl_3$ is somewhat more sensitive (increase by up to a factor of two near 30 km if either model A or C is used). Given the uncertainties in both model and observed values,

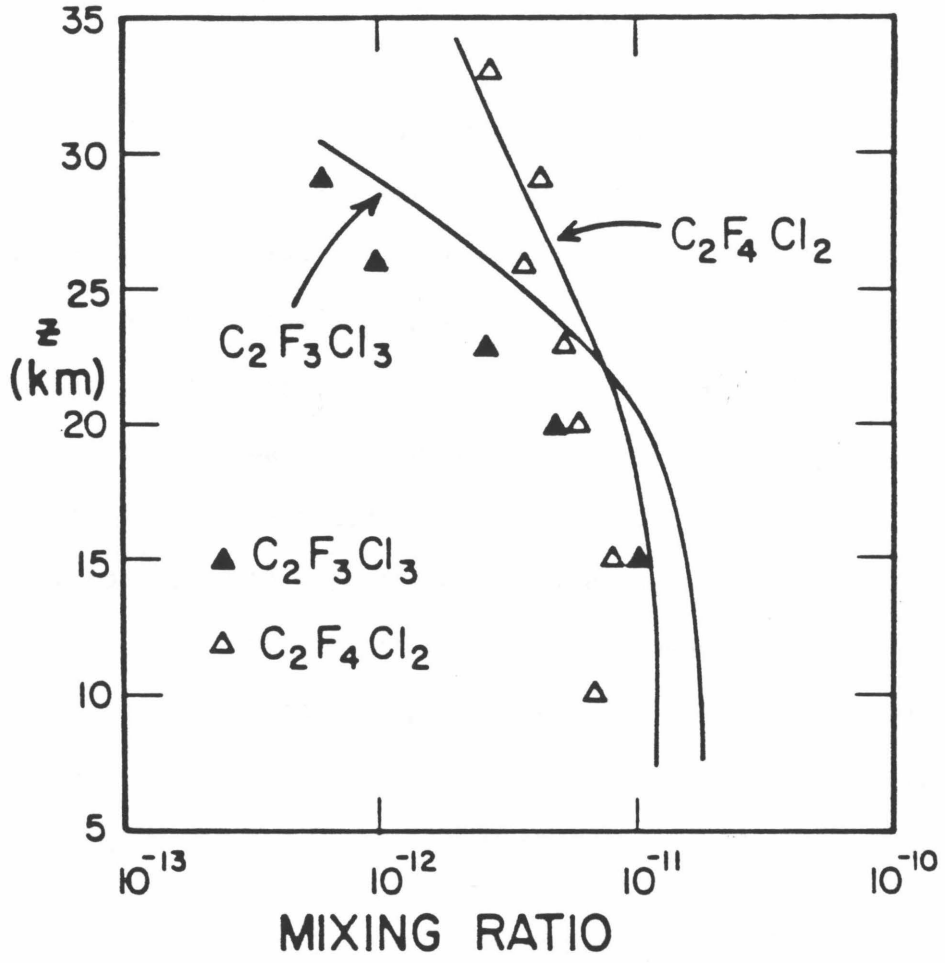

Figure 29. Preferred model (case B in text) results for $C_2F_3Cl_3$ and $C_2F_4Cl_2$, compared to measurements of Fabian et al. (1981).

FC113 and FC114 observations seem to be reasonably well reproduced. The large natural source of stratospheric chlorine, methyl chloride (CH_3Cl), is destroyed mainly by reaction with OH and is therefore not affected much by an increase in photolysis (22% decrease in concentration at 30 km). As seen in Figure 30, we find good agreement with the few observations of CH_3Cl presented in Hudson et al. [1982], regardless of the $\sigma(O_2)$ values, but a faster vertical diffusion (model C) worsens the model fit.

Another effect that could have some importance in determining the vertical distribution of source species with sharply decreasing concentrations in the stratosphere was recently discussed by Hunten [1983]. He argues that since air parcels spend some time above and some time below their mean vertical position, the dissociation rate at a given mean height will be biased towards the higher values (at higher z) due to the steep increase in j with altitude. This smearing effect will be most important for species with such a steep photodissociation gradient, like $CFCl_3$, CCl_4 or $C_2H_3Cl_3$, but its magnitude will depend on the value adopted for σ, the half-width at 1/e of the Gaussian type of altitude variation about the mean position. We have performed some model calculations including the reduced O_2 cross sections as well as this second-order effect of vertical motions, for various values of σ (0 to 8 km). Figure 31, also used in Hunten [1983], depicts the variation in the $CFCl_3$ vertical profile for a model with vertical eddy diffusion described by our faster $K_1(z)$ profile, similar to the composite profile of Massie and Hunten [1981]. The two sets of data shown in this figure illustrate the latitudinal dependence of the $CFCl_3$ concentration gradient in the stratosphere. The 40-45°N data were discussed above and the 25-40°N data were

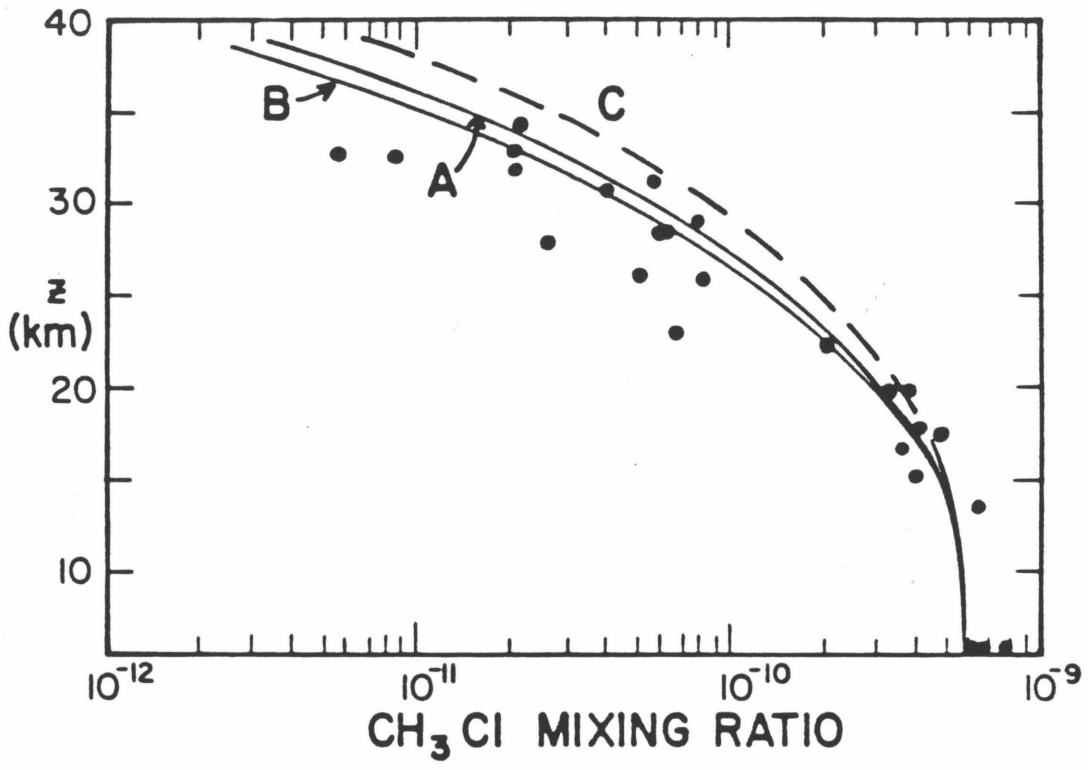

Figure 30. Same as Figure 27, but for CH_3Cl at mid-latitudes (data are taken from Hudson et al., 1982). Effect of O_2 cross section reduction (from case A to B) is small, since destruction of methyl chloride is mostly by OH, not photolysis.

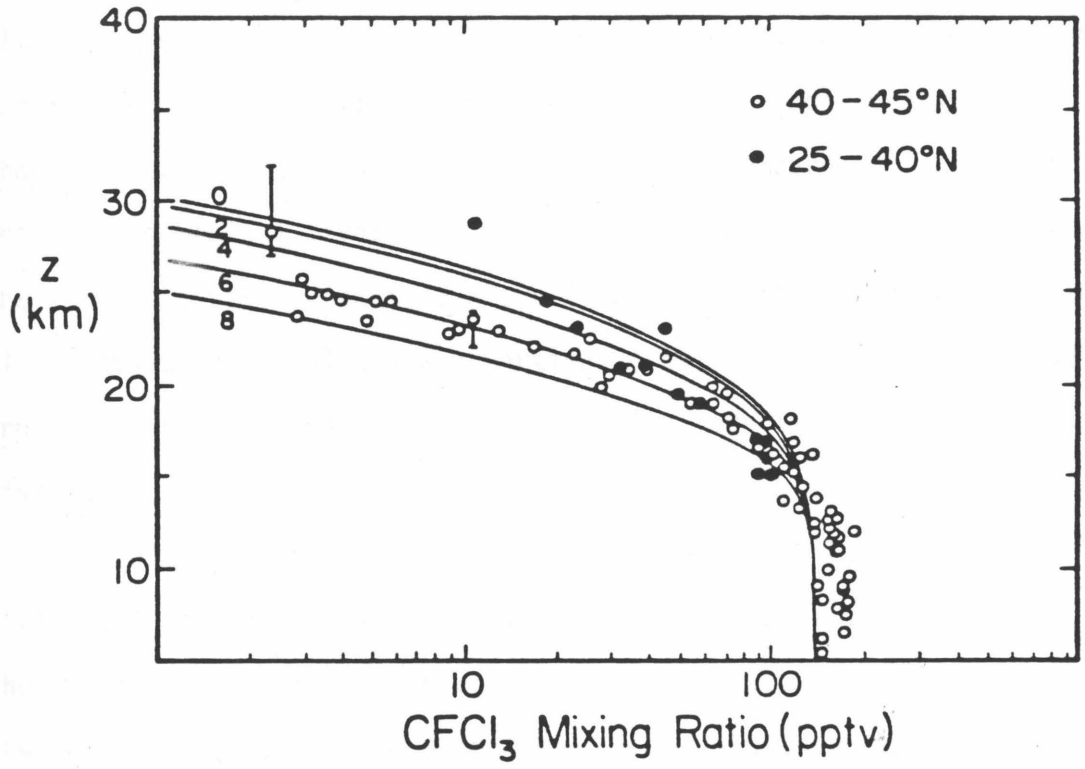

Figure 31. Effect of smoothing of the photodissociation rate constant over altitude on the $CFCl_3$ mixing ratio profile for values of σ between 0 and 8 km. See Hunten (1983) and text for definition of parameter σ. The 40-45°N data are as shown in Figure 27, and sources of the 25-40°N data are described in text.

obtained mostly near 32°N and are average values taken from Heidt et al. [1975], Williams et al. [1976], Krey et al. [1977] and Vedder et al. [1978]. The "$\sigma = 0$" case corresponds to model C in Figure 27. If σ is less than 2 or 3 km, the effect is not very significant, but the decrease in mixing ratio will become large if σ is larger than 4 km. It seems to us that an amplitude of several kilometers in vertical motion would be detectable by rigid balloons floating at constant pressure, although the question of time scale is another unknown parameter. In order to produce the effect described above, the oscillatory motion should occur on a time scale that is not long compared to the constituent's photochemical lifetime. We agree with Hunten that at least two of the three processes discussed above (vertical diffusion rate, O_2 absorption cross section values, and vertical oscillations of air parcels) are probably needed in order to fit the mid-latitude ($\sim 45°N$) $CFCl_3$ vertical distribution.

Above 30 km, the net effect of an increase in flux near 200 nm and a (larger) decrease in $\sigma(O_2)$ is a slight (up to 20%) decrease in O_2 photolysis rate. This leads to less ozone production and, along with the slight increase in ozone photolysis, to a 10-20% reduction in $[O_3]$ above 35 km. Our originally somewhat low $[O_3]$ values in the upper stratosphere thus become 20-40% smaller than the lower limits in the U. S. Standard Atmosphere 1976. We discuss this apparently significant discrepancy at more length in Chapter 5; Ko and Sze [1983] have also noted that current photochemical input data lead to low upper stratospheric ozone values. Below 30 km, the decrease in the large total opacity leads to a significant increase in flux between 200 and 220 nm,

with a net result of 30% larger O_3 concentrations at the 20-25 km level. This change near the $[O_3]$ peak leads to a 15% increase in total column ozone and brings our model into closer agreement with the U. S. Standard Atmosphere 1976. The 70% change in $\sigma(O_2)$ is more important than the 10-20% O_3 reduction above 30 km, which also leads to an increase in flux. Furthermore, the increase in O_3 below 30 km produces a decrease in flux in the lower stratosphere which counteracts the upper stratospheric O_3 reduction effect. To isolate the effect of a change in $\sigma(O_2)$, we have run a case identical to model B, but with the O_3 profile fixed as in the Model A case. We find that the largest part (80-90%) of the reductions in the trace species discussed above is due to the change in $\sigma(O_2)$, not to the subsequent change in the ozone vertical profile. Moreover, if we fix the O_3 profile as in the U. S. Standard Atmosphere 1976, we obtain chlorofluorocarbon concentrations close to the Model B values and actually smaller by up to 30% below 30 km. The Standard ozone concentrations are significantly higher than the model values above 35 km, but again, the chlorofluorocarbon profiles are more sensitive to the ozone profile in the lower stratosphere, where the Standard concentrations are somewhat (up to 25% lower than the Model B values. Uncertainties and variability in $[O_3]$ in the lower stratosphere can therefore also affect halocarbon and other species concentrations and accurate measurements of O_3 should be performed in conjunction with other observations whenever possible. In the upper stratosphere, we also find a reduction in NO_y species (NO, NO_2, NO_3, N_2O_5, HNO_2, HO_2NO_2) by 20-30%, due to the decrease in N_2O (and a small decrease in $O(^1D)$). In the 20-30 km region, the increase in $[O_3]$ and decrease in [NO] lead to a significant shift in $[HO_2]/[OH]$ and $[ClO]/(Cl]$, and ClO_x is enhanced due to increased halocarbon photolysis;

the above ratios are both almost linearly related to the $[O_3]/[NO]$ ratio there. [ClO] increases by a factor of 2.3 and $[HO_2]$ by 1.7 at 20 km; $[H_2O_2]$ is increased by a factor of 3 at 20 km, since it depends quadratically on $[HO_2]$. HCl, CO, and OH show little change ($\sim$10%) at all altitudes. The above changes will be reduced somewhat if the final $\sigma(O_2)$ values from Herman and Mentall [1982] are used. Moreover, lower stratospheric radical densities are not crucial in terms of ozone in this transport-dominated region and observations of OH, HO_2 and ClO are lacking, below 25 km.

A few further comments are indicated, regarding the reduction in $\sigma(O_2)$. The lower boundary condition for halocarbons in our model is a fixed concentration. The increased column destruction of these species, due to a decrease in $\sigma(O_2)$, leads to higher fluxes at the bottom in a steady-state calculation. It might be more realistic to use a model with fixed upward surface fluxes. However, the global emission rates of chlorofluorocarbons are probably not known to better than 40% and might be underestimated by such an amount, as pointed out by Rowland et al. [1982] and Crutzen and Gidel [1983], based on model analyses of lifetimes and abundances. If we fix the fluxes at the surface in our test of the effect of a reduction in $\sigma(O_2)$, we find that the concentrations of FCl1 and FCl2 are 45% and 25% higher (at any given altitude) than in the test with fixed surface concentrations. Equivalently, the surface fluxes are increased by similar respective amounts for these species, when fixed concentrations are used as a boundary condition. At 30 km, the reductions in FCl1 and FCl2 arising from the reduced $\sigma(O_2)$ values were a factor of 5.3 and 62%, respectively. A change in boundary

conditions (to fixed fluxes) would therefore dampen the above decreases somewhat, but for the most sensitive species such as FCl1, this effect is quite small compared to the $\sigma(O_2)$ effect itself. Various models will therefore lead to slightly different results, when a change in $\sigma(O_2)$ is considered, due to the choice of boundary conditions as well as the proposed reduction in $\sigma(O_2)$ versus wavelength, the model parametrization of the radiation field in the Schumann-Runge bands and the basic transport coefficients used. Subsequent studies by Ko and Sze [1983] and Brasseur et al. [1983] have led to results similar to ours. It is also worth pointing out that the resulting changes in the radiation field (decrease in upper stratosphere, increase in lower stratosphere) will lead to a modification of the eddy diffusion coefficients derived from N_2O or CH_4 data. This is a consequence of the steady-state assumption equating flux at a given height to the integrated column loss above that height, as done by Massie and Hunten [1981] for N_2O and CH_4. The direct or indirect changes in loss rates for these species, as a result of a reduction in $\sigma(O_2)$, will lead to a change in K(z) obtained from observations. This is illustrated in Figure 32 for our two model profiles K_1 and K_2. The effect is small for CH_4 loss rates (fluxes), since they are only indirectly affected by the radiation field. The changes in K(z) derived from N_2O observations could reach -50% in the upper stratosphere. However, the uncertainties or at least the spread in K(z) profiles derived by Massie and Hunten [1981] from N_2O and CH_4 data are of the order of a factor of two. Given the already existing uncertainties in the simplistic one-dimensional parametrization of transport processes, there is no urgent need to adjust the composite K(z) profile adopted by Massie and Hunten

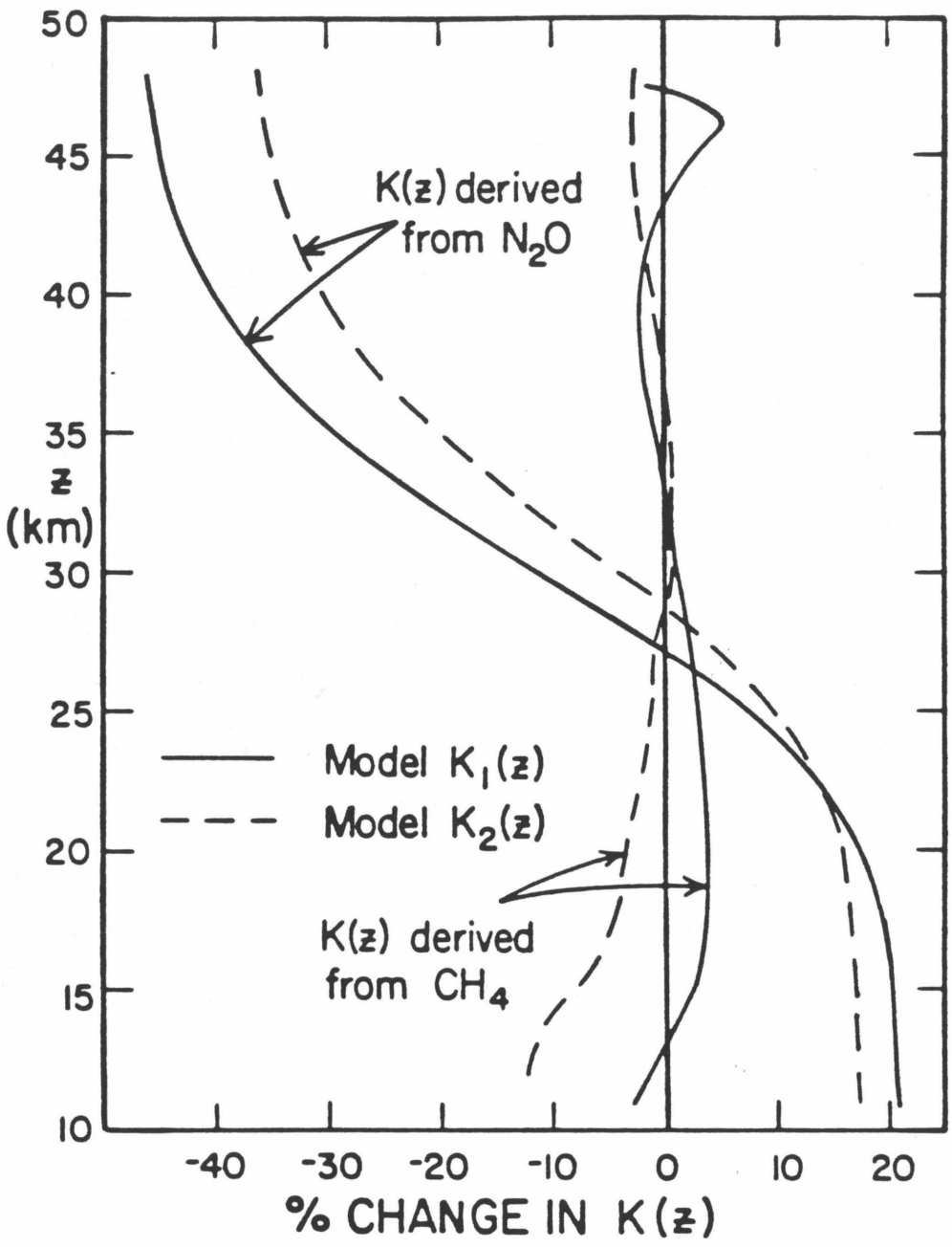

Figure 32. Assuming that our model eddy diffusion coefficients were derived from N_2O or CH_4 data, coupled with model loss rates for these species, we show the effect of a reduction in O_2 cross sections on the derived values of $K_1(z)$ and $K_2(z)$ in the stratosphere (due to the changes in loss rates versus height).

[1981], according to the effect due to reduced O_2 cross sections.

One should go beyond this one-dimensional sensitivity analysis and check the effects of O_2 cross section and transport uncertainties on the latitudinal distribution of halocarbons which are most sensitive to such effects (e.g., $CFCl_3$). Sze (private communication, 1983) has recently concluded that a more satisfying fit to the observed latitudinal dependence of CF_2Cl_2 and $CFCl_3$ can be obtained if the reduction in $\sigma(O_2)$ is included in the AER two-dimensional model. A better fit to halocarbon observations means that the reduced lifetimes of FC11 or FC12 due to the faster photolysis rates will be closer to reality. As pointed out by Ko and Sze [1983], this would tend to decrease steady-state ozone depletion estimates. We conclude by noting that it is interesting that over 17 years ago, Brewer and Wilson [1965] had measured the direct solar flux in the lower stratosphere and that these somewhat crude observations had already indicated that the O_2 cross sections were probably overestimated by at least 30% near 210 nm. The direct or indirect sensitivity of many stratospheric species to the radiation field in this spectral range has been demonstrated. These results should motivate further refinement of both laboratory and solar flux measurements related to these small, but important molecular oxygen cross sections.

References

Ackerman, M., Ultraviolet solar radiation related to mesospheric processes, in Mesospheric Models and Related Experiments, G. Fiocco, ed., 149, 1971.

Allen, M., and J. E. Frederick, Effective photodissociation cross sections for molecular oxygen and nitric oxide in the Schumann-Runge bands, J. Atm. Sci., 39, 2066, 1982.

Brasseur, G., A. De Rudder, and P. C. Simon, Implication for stratospheric composition of a reduced absorption cross section in the Herzberg continuum of molecular oxygen, Geophys. Res. Lett., 10, 20, 1983.

Brewer, A. W., and A. W. Wilson, Measurements of solar ultraviolet radiation in the stratosphere, Quart. J. Roy. Met. Soc., 91, 452, 1965.

Crutzen, P. J., and L. T. Gidel, A two-dimensional photochemical model of the atmosphere II: The tropospheric budgets of the anthropogenic chlorocarbons, CO, CH_4, CH_3Cl and the effect of various NO_x sources on tropospheric ozone, J. Geophys. Res., in press, 1983.

Fabian, P., R. Borchers, S. A. Penkett, and N.J.D. Prosser, Halocarbons in the stratosphere, Nature, 294, 733, 1981.

Frederick, J. E., and J. E. Mentall, Solar irradiance in the stratosphere: implications for the Herzberg continuum absorption of O_2, Geophys. Res. Lett., 9, 461, 1982.

Heidt, L. E., R. Lueb, W. Pollack, and D. H. Ehhalt, Stratospheric profiles of CCl_3F and CCl_2F_2, Geophys. Res. Lett., 2, 445, 1975.

Herman, J. R., and J. E. Mentall, O_2 absorption cross sections (187-225 nm) from stratospheric solar flux measurements, J. Geophys. Res., 87, 8967, 1982.

Hudson, R. D., and S. H. Mahle, Photodissociation rates of molecular oxygen in the mesosphere and lower thermosphere, J. Geophys. Res., 77, 2902 1972.

Hudson, R. D., and E. I. Reed, (eds.), The Stratosphere: Present and Future, NASA RP 1049, 58, 1979.

Hudson, R. D. (editor-in-chief), et al. (16 editors), The Stratosphere 1981 Theory and Measurements, WMO Global Ozone Research and Monitoring Project Report No. 11, 1982.

Hunten, D. M., A second-order effect of stratospheric vertical motions, Geophys. Res. Lett., 10, 333, 1983.

Ko, M.K.W., and N. D. Sze, Effect of recent rate data revisions on stratospheric modeling, Geophys. Res. Lett., 10, 341, 1983.

Krey, P. W., R. J. Lagomarsino, and L. E. Toonkel, Gaseous halogens in the atmosphere in 1975, J. Geophys. Res., 82, 1753, 1977.

Massie, S. T. and D. M. Hunten, Stratospheric eddy diffusion coefficients from tracer data, J. Geophys. Res., 86, 9859, 1981.

Miller, C., D. L. Filkin, A. J. Owens, J. M. Steed, and J. P. Jesson, A two-dimensional model of stratospheric chemistry and transport, J. Geophys. Res., 86, 12039, 1981.

Nicolet, M., Solar UV radiation and its absorption in the mesosphere and stratosphere, Pageoph., 118, 3, 1980.

Nicolet, M., The solar spectral irradiance and its action in the atmospheric photodissociation processes, Planet. Space Sci., 29, 951, 1981.

Rowland, F. S., S. C. Tyler, D. C. Montague, and Y. Makide, Dichlorodifluoromethane, CCl_2F_2, in the Earth's atmosphere, Geophys. Res. Lett., 9, 481, 1982.

Shardanand and A. D. Prasad Rao, Collision-induced absorption of O_2 in the Herzberg continuum, J. Quant Spectrosc. Radiat. Transfer, 17, 433, 1977.

Steed, J. M., A. Owens, and B. C. Lane (eds.), Proceedings of the Chemistry Task Force Workshop on Stratospheric Chemistry, NOAA Aeronomy Laboratory, Boulder, Colorado, 1982.

U. S. Standard Atmosphere 1976, U. S. Government Printing Office, Washington, D.C., 1976.

Vedder, J. R., B. J. Tyson, R. B. Brewer, C. A. Boitnott, and E.C.Y. Inn, Lower stratosphere measurements of variation with latitude of CF_2Cl_2, $CFCl_3$, CCl_4 and N_2O profiles in the northern hemisphere, Geophys. Res. Lett., 5, 33, 1978.

Williams, W. J., J. J. Kosters, A. Goldman, and D. G. Murcray, Measurements of stratospheric halocarbon distributions using infrared techniques, Geophys. Res. Lett., 3, 379, 1976.

Chapter 4

CHLORINE AND FLUORINE SPECIES

4.1 Vertical Distribution and Partitioning

Having discussed in the previous chapter some of the modeling uncertainties involved in terms of the chlorine and fluorine source species, and having adopted O_2 absorption cross sections that lead to a better fit of halocarbon observations, we now focus on the products themselves. Chlorine atoms are released by the various halocarbons via photolysis and attack by the OH or $O(^1D)$ radicals. One usually assumes that all the chlorine atoms are released at once (e.g., 2 atoms from CF_2Cl_2, 3 from $CFCl_3$, 4 from CCl_4, etc.). This is not strictly true, although we feel that it is probably a very good approximation, as discussed further below. Based on this assumption, the total chlorine production rates for each halocarbon as a function of altitude are shown in Figure 33 for 45°N latitude and 23° solar declination (model B of Chapter 3). The total Cl production rate peaks in the lower stratosphere. We have included the more minor species CHF_2Cl(FC22), $C_2F_3Cl_3$(FC113) and $C_2F_4Cl_2$(FC114) in our model calculations. These species are not very abundant at the ground, compared to FC11 or FC12 for example, but they contribute to the chlorine and fluorine release rates at higher altitudes than the major halocarbons [see also Wuebbles and Chang, 1981]; while they produce less than 10% of the total chlorine amount currently in the stratosphere, their relative importance will undoubtedly grow if their ground emission rates are not decreased or stabilized, as in the case of FC11 or FC12. The question of the number of chlorine atoms released in a given reaction could conceivably affect the model abundances of chlorine radicals in the lower stratosphere. In other words, we are not including possible intermediary

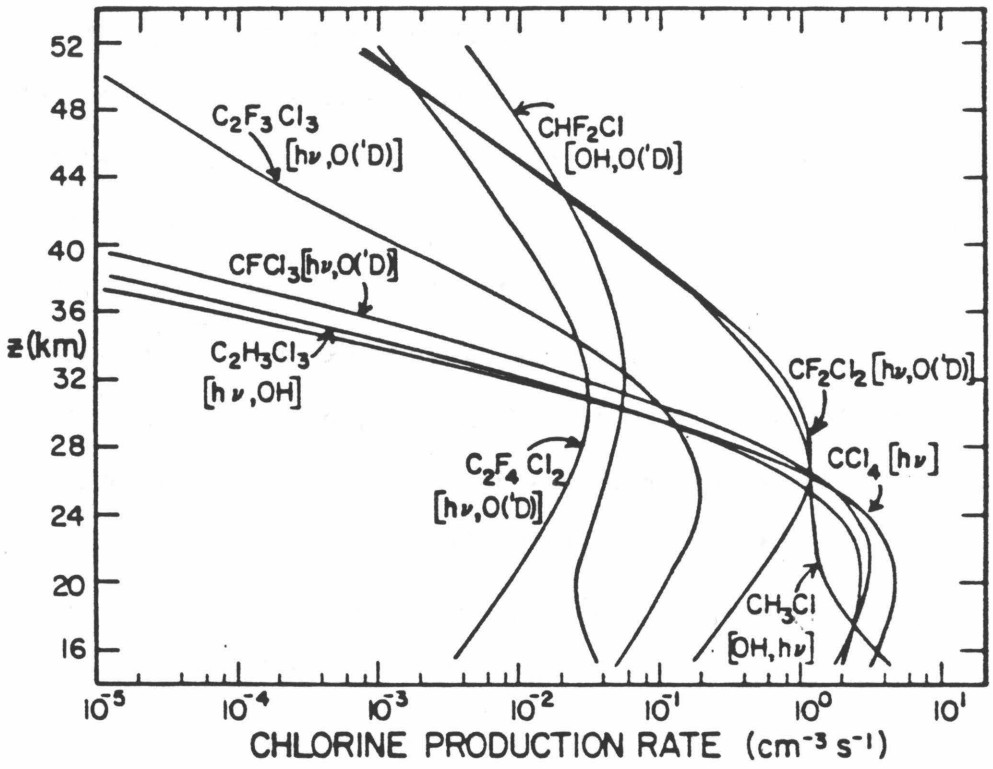

Figure 33. Chlorine production rates from halocarbon source species in the stratosphere. All chlorine atoms are assumed to be released during the primary decomposition (by hν, $O(^1D)$ or OH, as indicated) of each halocarbon. Model is for 45° N, summer.

products in our reaction set. Laboratory studies of the photolysis of CF_2Cl_2, $CFCl_3$ and CCl_4 in the presence of various gases, including O_2 and O_3, have been pursued in order to study the products and quantum yields in more detail [Marsh and Heicklen, 1965; Milstein and Rowland, 1974; Jayanta et al., 1975; Rebbert and Ausloos, 1975, 1976/77; Rebbert, 1978; Ralph and Wayne, 1981; Suong and Carr, 1982]. The exact mechanisms are not necessarily well known or directly measured, and the number of chlorine atoms released depends on the photon wavelength. Intermediary products that have been observed in the laboratory, and are believed to arise from the photolysis of CF_2Cl_2, $CFCl_3$ and CCl_4 and subsequent reactions, are COF_2, COFCl and $COCl_2$, respectively. These species are subject to photolysis in the atmosphere, with fairly well defined destruction rates (from laboratory data). Inclusion of these intermediary products in a photochemical model lead to a negligible decrease (a few percent) in active chlorine species (Cl, ClO). One could argue that other reactions occur in the atmosphere (not in the laboratory) before the above products are formed and that other complexes are produced. These products would have to be stable for about a year in the lower stratosphere in order to make a non-negligible effect on the current chemical scheme for chlorine products. There is, however, no observational evidence from in situ sampling and mass spectrometry analysis of atmospheric samples, that major intermediary products exist, although no thorough search has been undertaken. Given the above indirect evidence and the long lifetimes required, halocarbon intermediary products are not thought to play a significant role and the abundances of ClO or HCl are probably not affected (overestimated) by more than 10% by the

assumption concerning the number of chlorine atoms released by the source species.

Once the chlorine is produced in the stratosphere, it becomes partitioned into several constituents connected by various photochemical reactions. The main pathways are illustrated in Figure 34. Chlorine atoms form ClO by reaction with ozone and ClO is attacked by O and NO to yield Cl back again. This equilibrium is set up on a very short time scale (typically minutes) and represents the main chlorine catalytic cycle destroying odd oxygen (O, $O(^1D)$ and O_3) and reforming the O_2 bond. The large ozone abundance causes ClO to be the dominant radical throughout the stratosphere by a factor of about 1000 in the lower stratosphere and 10 close to 50 km. ClOO is of minor importance (less abundant than Cl) and is also in essentially instantaneous equilibrium with Cl. This system of radicals ($ClO_x = Cl + ClO \simeq ClO$) is tied to the major sink, HCl, as well as the more temporary reservoir species, $ClONO_2$ and HOCl. These gases reduce the effectiveness of the main ozone destruction cycle (from ClO_x) by tying up some of the chlorine atoms. Time scales for the exchange between ClO_x and $ClONO_2$ or HOCl are typically a few hours, but vary with altitude, and chlorine nitrate is the more abundant of these reservoir species, according to current photochemistry. The details of the diurnal behavior of these gases and observational constraints are discussed in section 4.2. HCl is the most abundant chlorine compound throughout the stratosphere, with a destruction lifetime (from $HCl + OH \rightarrow Cl + H_2O$) varying from a few months to a few days from the lower to upper stratosphere. Recombination of chlorine to HCl occurs mainly via $CH_4 + Cl$, although significant pathways in the upper stratosphere also

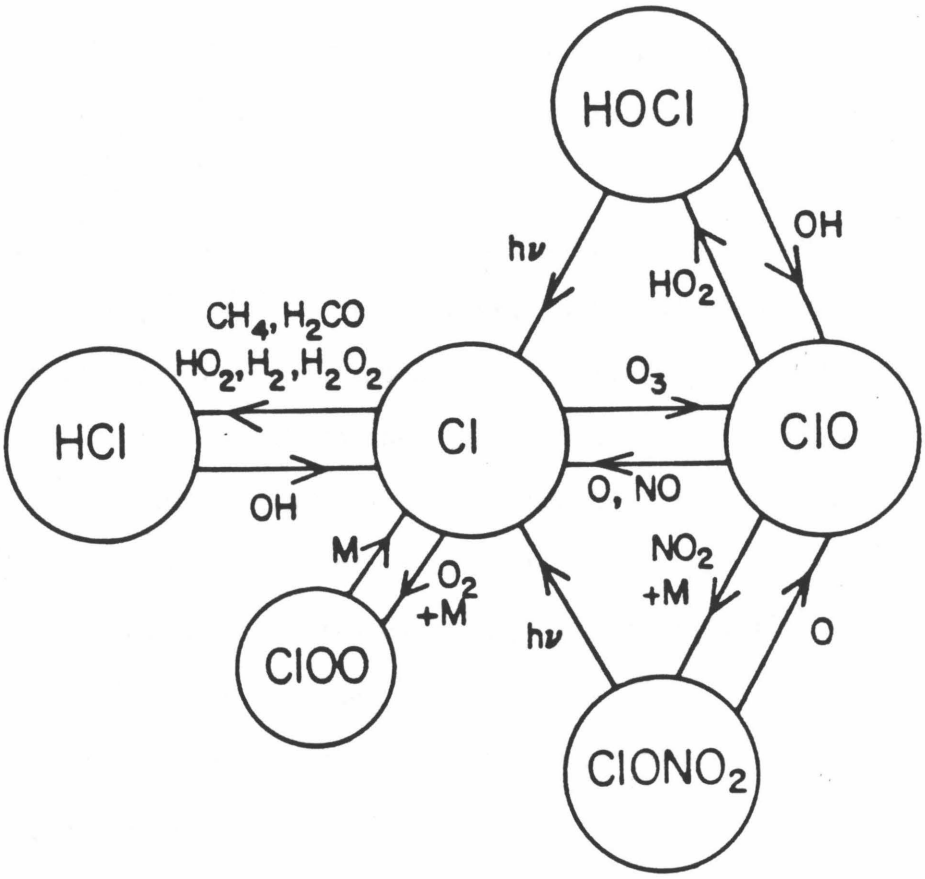

Figure 34. Schematic diagram of model stratospheric chlorine products and main photochemical pathways connecting them.

include Cl reaction with H_2CO, HO_2 and H_2. The total free chlorine ($Cl_x = Cl + ClO + ClONO_2 + HOCl + HCl$) lifetime in the stratosphere is very long, being governed by transport down into the troposphere on the time scale of a year or more. Rainout of HCl and surface deposition are the ultimate tropospheric sinks for chlorine species. This tropospheric sink leads to a downward flux of HCl and a decreasing mixing ratio towards lower altitudes; in the upper stratosphere and mesosphere, HCl becomes the only form of chlorine with a mixing ratio close to 2.6 ppbv for our mid-latitude models.

For the simple reason of detectability, observations have centered around ClO and HCl in the stratosphere, although unfortunately, there have not yet been any simultaneous measurements of both species. It is convenient to relate ClO to the stable (diurnally-invariant) constituent HCl, but even this ratio will be affected by transport due to the dependence on the recombination of Cl with CH_4, H_2CO, HO_2 and H_2. The latter species will all be affected by transport, directly (CH_4, H_2) or indirectly (H_2CO comes from CH_4 oxidation and HO_2 comes from H_2O). This will in turn produce a variable or uncertain rate of HCl production and if we do not have measurements of at least CH_4 in addition to ClO and HCl, the [ClO] / [HCl] model could be off by 50%; temperature will also affect reactions such as $Cl + CH_4$ or $Cl + H_2$. In general, we can write

$$\frac{[ClO]}{[HCl]} = \frac{[ClO]}{[Cl]} \times \frac{[Cl]}{[HCl]} \tag{40}$$

Referring to Figure 34 and the reaction set of Chapter 1, we have the radical equilibrium expression

$$\frac{[ClO]}{[Cl]} = \frac{k_{60}[O_3]}{k_{61}[O] + k_{62}[NO]} \tag{41}$$

and

$$\frac{[Cl]}{[HCl]} = \frac{k_{58}[OH]}{k_{59}[CH_4] + k_{85}[H_2CO] + k_{63}[HO_2] + k_{70}[H_2] + k_{102}[H_2O_2]} \tag{42}$$

For the lower stratosphere, where $k_{61}[O] \ll k_{62}[NO]$ and $k_{59}[CH_4]$ is the dominant term in the denominator of equation (42), we obtain the familiar expression

$$\frac{[ClO]}{[HCl]} = \frac{k_{60}k_{58}[O_3]}{k_{62}k_{59}[CH_4]} \frac{[OH]}{[NO]} \tag{43}$$

This is one example of the interdependence between HO_x, NO_x and ClO_x species. The source of OH and HO_2, rapidly equilibrated radicals similar to Cl and ClO, is from $H_2O + O(^1D)$, while $N_2O + O(^1D)$ produces NO (leading to NO_2) in the stratosphere. The photolysis of ozone below about 310 nm produces $O(^1D)$ radicals, which are rapidly quenched by O_2 and N_2. Our previous comment about transport also applies in terms of these source species, H_2O and N_2O (or total NO_y), which affect the ClO abundance in an indirect way. An ideal experimental test of the chemistry would involve a simultaneous measurement of all the constituents in (43), as well as temperature, in order to check the relationship's validity. Such measurements are difficult and not yet available, so that average observational data are the best means of comparison with models.

A large number of ClO measurements has been performed by the group

of J. Anderson [Anderson et al., 1980], from in situ balloon observations. The resonance fluorescence technique that is used actually measures the Cl atomic resonance scattering after conversion of ClO to Cl by NO addition to the flow sample. Additional summaries of these observations appear in Weinstock et al. [1981], and the recent stratospheric reports [Hudson et al., 1982; NRC, 1982]. The observations cover the period 1976-1979 and the mean of these data, excluding the anomalously high July 14, 1977 profile was compared in Weinstock et al. [1981] to a model by Logan et al. [1978]. The spread in the nine observational ClO profiles is quite large (factor of two to three from the mean), although the gradient versus height is well represented by the mean profile. As illustrated in Figure 35, the older models [such as Logan et al., 1978] did not give a satisfactory fit to the observed average ClO profile shape. Later revisions in the laboratory rate constant data for $OH + HNO_3$ and $OH + HO_2NO_2$ significantly improved the lower stratospheric ClO model fits. Increases in the above reaction rates lead to an increased loss of HO_x via the following cycles:

$$OH + NO_2 + M \rightarrow HNO_3 + M$$

$$\underline{OH + HNO_3 \rightarrow H_2O + NO_3}$$

$$\text{Net: } 2OH + NO_2 \rightarrow H_2O + NO_3$$

and

$$HO_2 + NO_2 + M \rightarrow HO_2NO_2 + M$$

$$\underline{OH + HO_2NO_2 \rightarrow H_2O + O_2 + NO_2}$$

$$\text{Net: } OH + HO_2 \rightarrow H_2O + O_2$$

The effects of such changes are nicely reviewed in Hudson et al. [1982]

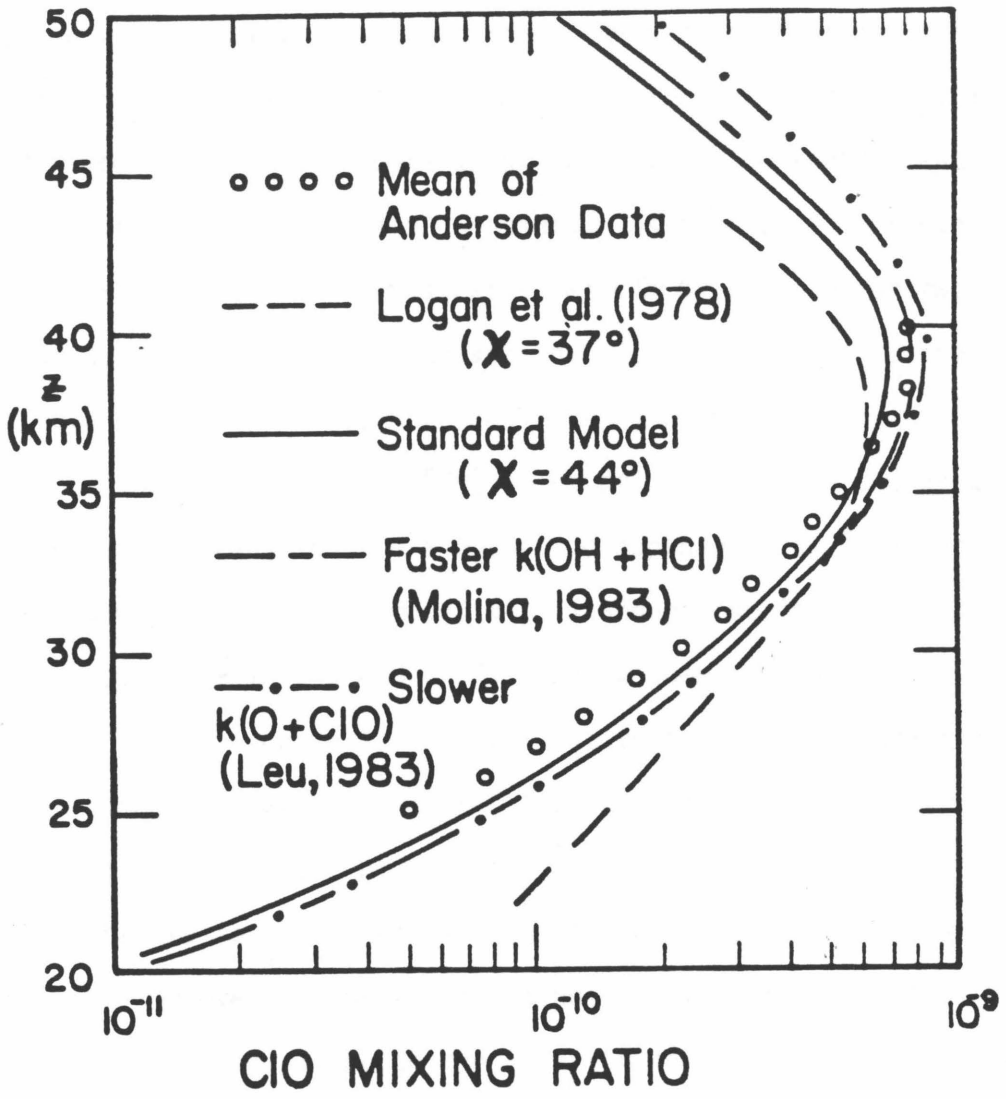

Figure 35. ClO model profiles compared to the mean of J. Anderson's daytime resonance fluorescence measurements (excluding the anomalously high July 14, 1977 data). Older chemistry, illustrated by old model of Logan et al. (1978), predicted a much slower decrease in lower stratospheric ClO than observations and current photochemistry indicate. More recent possible changes in rate constants would further modify the ClO abundance, as shown, particularly in upper stratosphere.

and partially discussed in Sze and Ko [1981] as well. The main loss of HO_x in the upper stratosphere is through the direct recombination $OH + HO_2 \rightarrow H_2O + O_2$. The above loss mechanisms (via HNO_3 and HO_2NO_2) and the direct recombination contribute about equally in the lower stratosphere, with current chemical rate constants. As discussed in Hudson et al. [1982], the decrease in lower stratospheric OH by a factor of two or more has led to an even greater decrease in ClO. This is due to the fact that less OH leads to less HNO_3 and more nitrogen tied up in NO and NO_2. Since [ClO] depends on [OH]/[NO] in equation (43), the decrease in [OH] and increase in [NO] lead to a quadratic dependence on [OH] for lower stratospheric [ClO]. Our model with standard chemistry now shows a much faster decrease in the ClO profile below about 30 km, as can be seen in Figure 35. The curve is for 32°N latitude, -11° solar declination, a model used further below to fit the February 1981 microwave observations of J. Waters and his group.

Further changes in the kinetics since the WMO Report [Hudson et al., 1982] have also improved the upper stratospheric ClO model profile. The latter report noted that, although the Anderson data did not exist above about 40 km, there did not seem to be much decrease, if any, in most of the profiles above 35 km, while models predicted a reasonably fast drop in mixing ratio above that height. Ozone steady-state depletion due to chlorine is most sensitive to the upper stratospheric ClO profile (via the O+ClO reaction). New careful studies of the $O + HO_2$ reaction converting HO_2 to OH [Keyser, 1982; Sridharan et al., 1982], and its associated temperature dependence have increased the adopted rate constant by about a factor of two at stratospheric temperatures. The

average recommendation from DeMore et al. [1982], used in our standard model, has increased OH by about 30% in the upper stratosphere near the ClO peak mixing ratio. This, coupled with a small decrease in CH_4 (by added OH), leads to a 40% increase in ClO_x near 40 km, since exchange between ClO_x and HCl is mainly governed by $Cl + CH_4$ and $OH + HCl$ [see also Ko and Sze, 1983]. This effect is largest in the upper stratosphere due to the atomic oxygen abundance increase with height, and therefore favorably modifies the ClO profile shape. Two additional changes in laboratory data have been suggested very recently, both of which also tend to increase the upper stratospheric ClO mixing ratio, as shown in Figure 35. Molina (private communication, 1983) finds a new value for k_{58} ($OH + HCl$ reaction) of $4.6 \times 10^{-12} \exp(-500/T) cm^3 s^{-1}$. The temperature dependence is not much different than in our standard expression for k_{58}, but the difference in A-factor leads to a 20% increase (nearly independent of T) in this rate constant. The resulting increase in ClO ranges from 10% near 30 km to over 20% at 50 km. The associated decrease in HCl is everywhere less than 10%. However, since several previous studies of k_{58} were in excellent ($\lesssim$ 10%) agreement, it is not clear that one should adopt a higher value for this rate constant. The recent measurement of k_{61} ($O + ClO \rightarrow Cl + O_2$) by Leu [1983] yields $4.8 \times 10^{-11} \exp(-96/T) cm^3 s^{-1}$. Our adopted (standard) value is about 40% higher, independent of temperature. Recent laboratory work on the $O + ClO$ reaction by J. Birks (private communication, 1983) and coworkers apparently confirm a reduction in k_{61} by at least this much. This decreases the [Cl]/[ClO] ratio above 35 km, where the $O + ClO$ reaction dominates the $NO + ClO$ pathway in the conversion of ClO to Cl. As shown in Figure 35, the increase in [ClO] is about 10%

near 40 km and increases to 35% at the stratopause; both diurnal average and diurnal sensitivity tests yield similar results. Since the O + ClO reaction is the rate-limiting step in the major chlorine catalytic cycle destroying ozone, we also expect changes in $[O_3]$ from a decrease in k_{61}. Small changes in our model ozone abundances occur, with a peak increase close to 5% at 40 km. Since the steady-state total ozone column depletion due to chlorofluorocarbon emissions should be roughly linear in k_{61}, we expect a decrease in depletion estimates by 30-40% [Leu, 1983, quotes a model decrease by Cicerone from -6.8% to -4.1%]. Recent estimates have become fairly small [see e.g., Ko and Sze, 1983] and this revision in k_{61} should lower most estimates to less than 5% total O_3 column depletion. One further note concerns the effect of a smaller OH abundance in the lower stratosphere on nitrogen compounds. Simultaneous observations of NO_2 and HNO_3 led to a significant discrepancy between observed and theoretical values for $[HNO_3]/(NO_2]$ [see Evans et al., 1976; Harries, 1978]. This ratio (during the daytime) can be written as:

$$\frac{[HNO_3]}{[NO_2]} = \frac{k_{45}[M]\,[OH]}{j_{HNO_3} + k_{46}[OH]} \tag{44}$$

Less [OH] now implies that $j_{HNO_3} >> k_{46}[OH]$ and that the above ratio is proportional to [OH]. As surmised by Evans et al. [1982], a decrease in [OH] can considerably improve the model fit. We compare our current mid-latitude model (same diurnal run as for ClO) to the observations in Figure 36, taken from Harries [1978]. The "old chemistry" model reported by the above author can be seen to predict a much larger ratio for $[HNO_3]/[NO_2]$ than our standard model. We make a distinction between noon

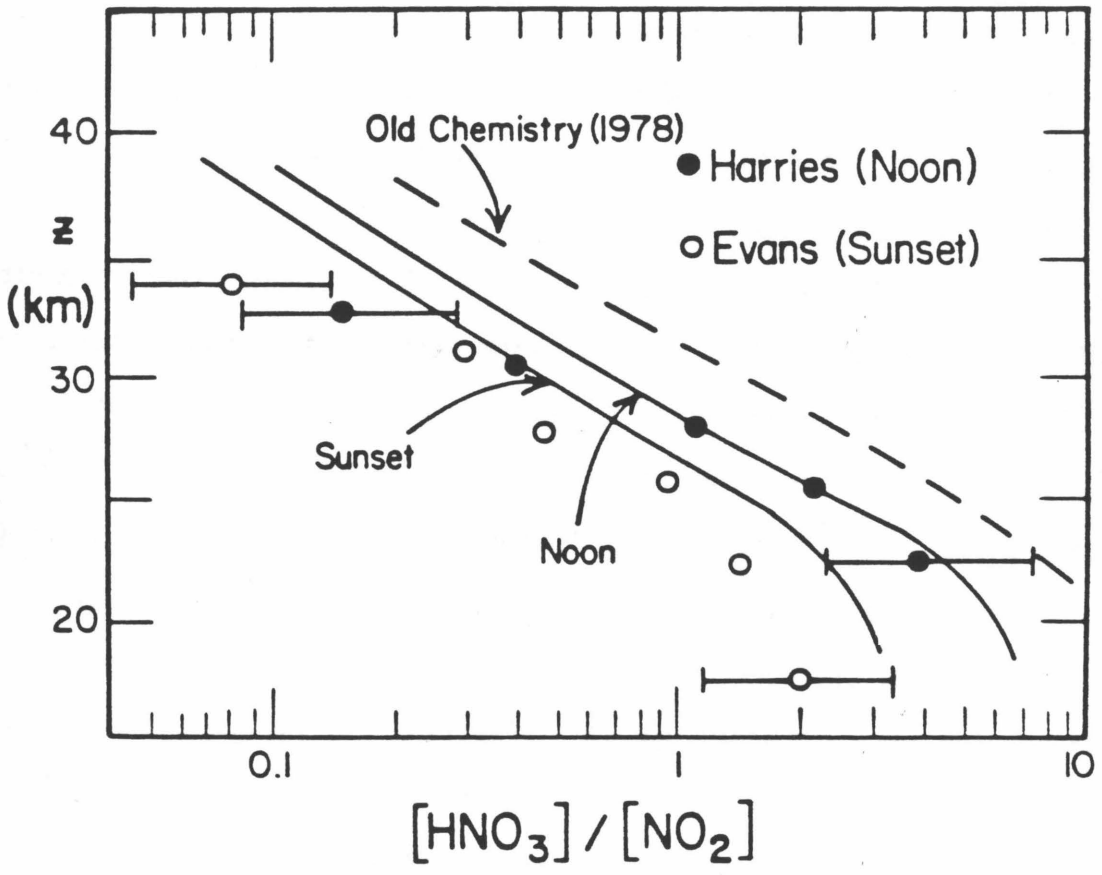

Figure 36. Improvement in the value of the ratio $[HNO_3]/[NO_2]$, according to changes in lower stratospheric HO_x concentrations. Model is for 32°N latitude, -11° solar declination. See text for data references.

and sunset profiles; the model fit is considerably improved with the current chemistry and reduced OH concentrations.

Other measurements of ClO in the stratosphere were made by Parrish et al. [1981], and Waters et al. [1981] by (respectively) ground-based and balloon-borne microwave spectral observations. Recent reanalysis of the ground-based data [Solomon et al., 1983] indicates good agreement with the mean of J. Anderson's in situ data (excluding the largest two values). New ground-based observations by Solomon et al. [1983] have recently been obtained from Hawaii and show a strong diurnal behavior, as discussed in the next section. The re-evaluated laser heterodyne radiometer measurements of ClO at sunset by Menzies [1983] are also discussed later since they pertain more directly to the diurnal changes in the ClO profile. The daytime (between noon and 4 p.m. local time) ClO data of Waters et al. [1981] are compared to our model for 2:00 p.m. in Figure 37. Good agreement between both the ClO and O_3 measurements and models is found, although the slope in the ClO profile between 30 and 23 km seems somewhat steeper than in the model (note the large uncertainty in the observation at 23 km). The H_2O_2 detection was only tentative, due to possible contamination of the line by other features and the low signal-to-noise ratio. Model results near 30 km predict significantly less H_2O_2 than one part per billion. As shown in Figure 37, the more recent determination of the formation rate constant and its temperature dependence [Kircher and Sander, 1983] lead to 0.1 - 0.2 ppbv. Refer to Chapter 1 for the standard (old) and new values for k_{51} ($HO_2 + HO_2 \rightarrow H_2O_2 + O_2$). A more definite detection of H_2O_2 is needed. We discuss OH and HO_2 observations in Chapter 5.

Figure 37. Simultaneous measurements of O_3, ClO, and (tentatively) H_2O_2 by Waters et al. (1981) on February 20, 1981. Model profiles for similar conditions of illumination (32°N latitude, -11° solar declination, 2 p.m.) are shown. The old (standard in this work) and new H_2O_2 model profiles refer to the value of the HO_2 + HO_2 reaction rate constant (see text).

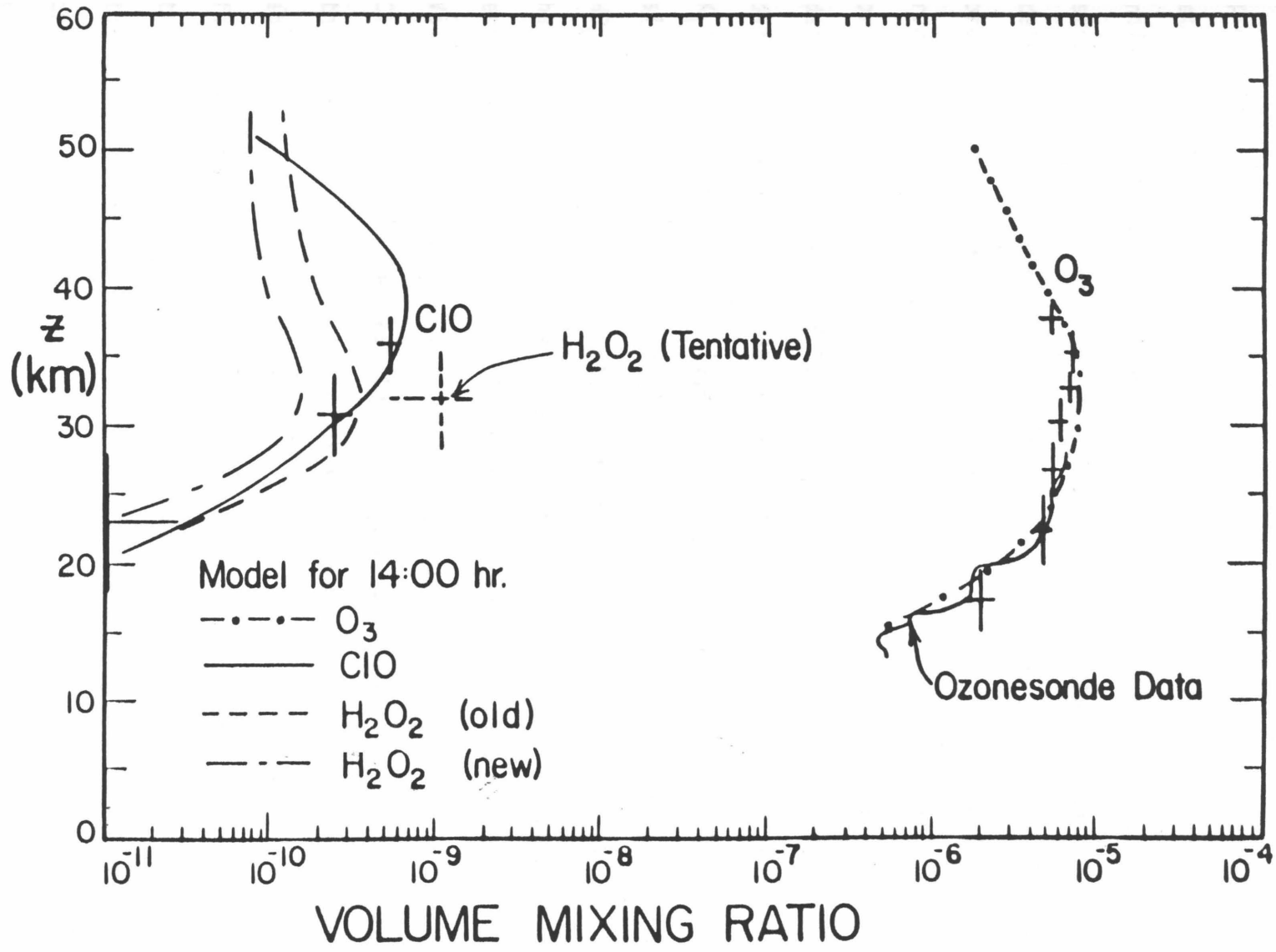
60
50
40
z
(km)
30
20
10
0
ClO
H_2O_2 (Tentative)
O_3
Model for 14:00 hr.
O_3
ClO
H_2O_2 (old)
H_2O_2 (new)
Ozonesonde Data
10^{-11}
10^{-10}
10^{-9}
10^{-8}
10^{-7}
10^{-6}
10^{-5}
10^{-4}
VOLUME MIXING RATIO

A further constraint on [Cl] and [ClO] in the stratosphere can be provided by observations of ethane (C_2H_6), as was indicated by Rudolph et al. [1981]. Their in situ measurements, however, implied that significantly less free chlorine (Cl, to be exact) was present in the lower stratosphere than predicted by models, since the ethane abundance--determined in large part by destruction by chlorine atoms--was over two orders of magnitude higher than theoretical values in the 25-30 km region. Possible uncertainties due to transport, the [Cl]/[ClO] ratio or rate constant values do not seem large enough to explain the C_2H_6 data. The sensitivity of C_2H_6 to various assumptions and the ethane data are shown in Figure 38 (model is for 45°N, summer). For the faster $K_1(z)$ eddy diffusion profile, we also show the effect of possible Cl sinks. Conversion of Cl to HCl could occur by hydrogen abstraction from HO_2NO_2 and $CH_3O_2NO_2$; the rate constants for these additional pathways have not been quantitatively measured in the laboratory, and we have used estimated probable upper limits (Simonaitis, private communication, 1983). Values of $2 \times 10^{-11} cm^3 s^{-1}$ for $Cl + HO_2NO_2$ and $1 \times 10^{-10} cm^3 s^{-1}$ for $Cl + CH_3O_2NO_2$ could increase the conversion rate to HCl by close to 50% in the lower stratosphere ($Cl + CH_4$ is still the dominant term), and lead to an increase in $[C_2H_6]$, as shown in Figure 38. The possible effect of faster upwards diffusion is nevertheless more important. A better fit to the data of Rudolph et al. [1981] would be obtained if [Cl] was lower than expected by a factor of 4 to 5 below 30 km. This significant discrepancy has no obvious solution and the possibility of measurement error (contamination) should be considered further. Indeed, more recent in situ measurements by the group of P. Fabian seem to be in much better

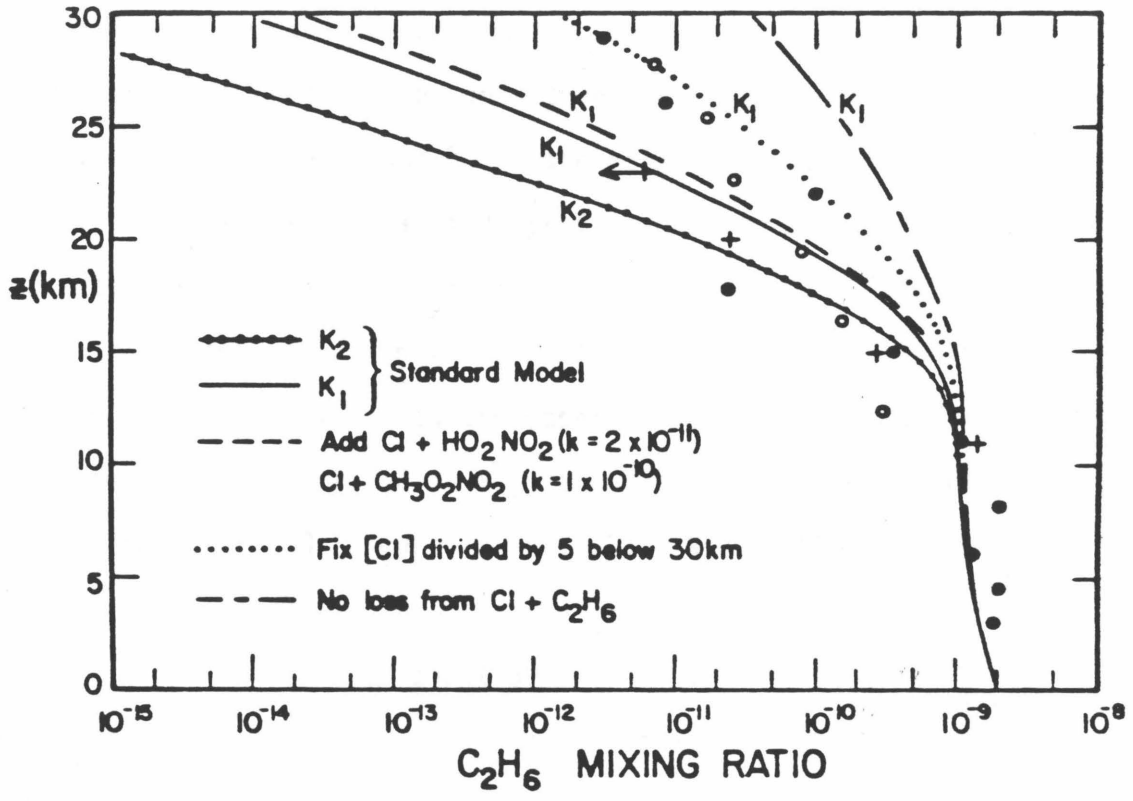

Figure 38. Ethane data and model tests below 30 km. The in situ sampling results of Rudolph et al. (1981) are shown by closed circles (16 June 1979) and open circles (28 June 1979). Crosses are results from a recent analysis (by S. Penkett) of C_2H_6 data collected by P. Fabian's group, and they compare more favorably with standard model results. Model sensitivity tests are described in text.

agreement with the theory (preliminary results provided by S. A. Penkett, private communication, 1982), as shown also in Figure 38. P. Fabian (private communication, 1983) believes that the much larger samples obtained by his group are less subject to contamination than the measurements of Rudolph et al. [1981], although the latter authors ruled out contamination as a significant source of error. The C_2H_6 discrepancy does not really exist, according to the later observations, but further investigations will have to confirm this contention.

The longer-lived chlorine constituent, HCl, has been measured mostly by near-infrared ground-based and balloon-borne absorption spectroscopy. The average mid-latitude profile and the associated spread in various observations has been presented in Hudson et al. [1982]. As also shown in the latter report, model profiles fall within the bounds of the observations and roughly follow the observed vertical mean profile. A similar result is illustrated in Figure 39 for model conditions as described above for ClO (Figures 35 and 37). Reasonable changes in K(z) and seasonal changes (in solar radiation) can modify this one-dimensional model profile by about 30%. The upper stratospheric HCl mixing ratio (near 50 km) is close to the total free chlorine (Cl_x) available in the stratosphere and should be increasing slowly with time due to anthropogenic sources. The slope of the HCl profile is somewhat different than the mean data and than most individual observations [see also summary of data in Zander, 1981, or NRC, 1982]. However, significant differences exist between the observations themselves, presumably related to the combined effects of transport and chemistry (direct and indirect effects on HCl). Lower stratospheric [HCl] seems somewhat high

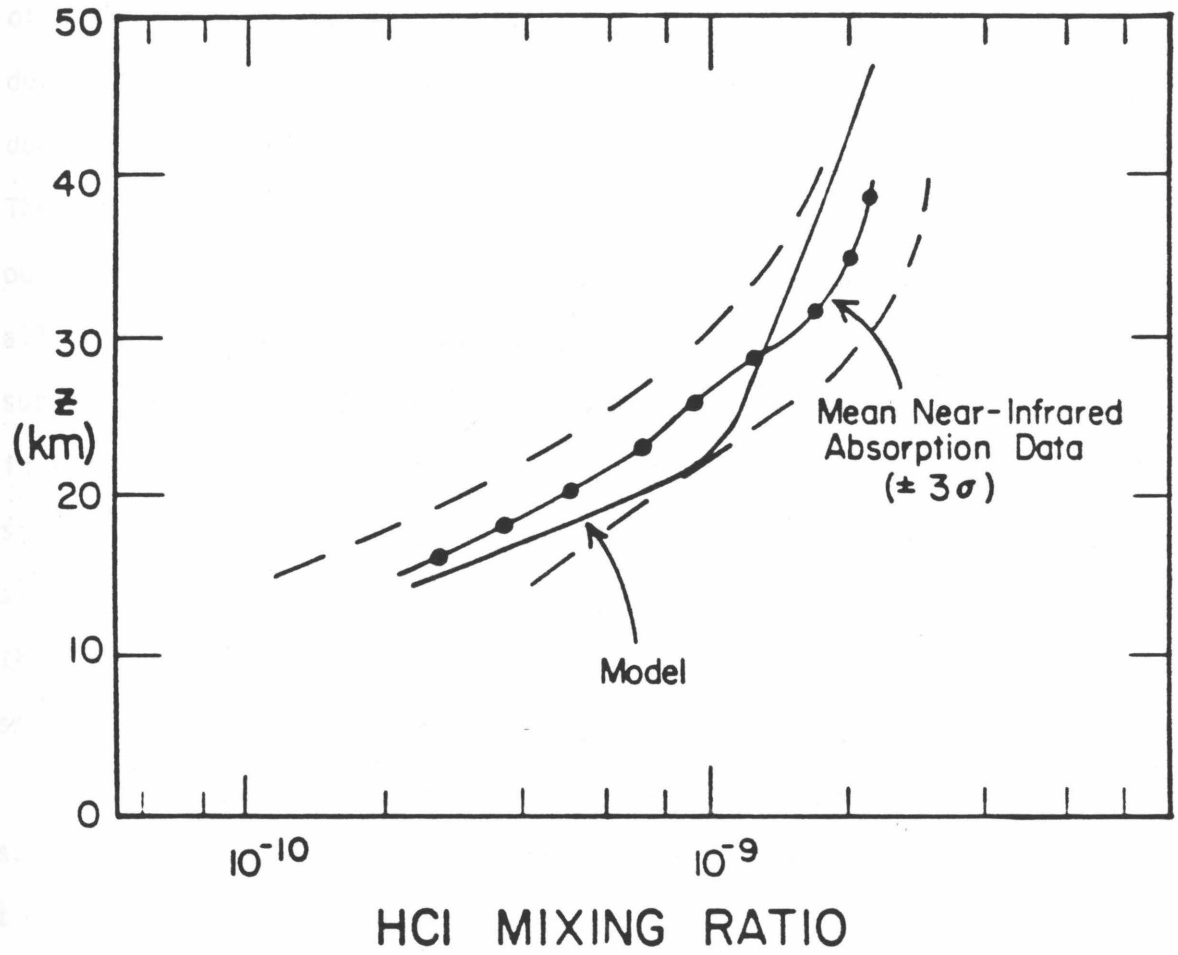

Figure 39. Mean of mid-latitude HCl infrared absorption data (see Hudson et al., 1982) and typical mid-latitude model profile (see text).

in most models, particularly at higher latitudes [e.g., 2-D model of Miller et al., 1981]. Aerosols might be contributing to a chlorine sink below ~25 km, although quantitative information on this subject is lacking. The reaction probability γ , per molecule-aerosol collision, is not well known [see e.g., Cadle et al., 1974]. Observations of the effects of heterogeneous chemistry could be performed by searching for changes during a major volcanic event such as El Chichon, although other changes due to a different temperature or radiation field could mask such effects. The ClO and HCl mid-latitude observations are in general agreement with our model, and the changes in the kinetics during the last few years have all helped improve the fit to the mean slope of the ClO profile. The subsequent increase in the relative amount of ClO above 35 km is also in agreement with the recent ground-based microwave observations of ClO spectral line shape and peak height [Solomon, et al., 1983]. These observations are most sensitive to the ClO abundance above about 30 km and the indirect evidence for the existence of the third major chlorine constituent ($ClONO_2$) in the stratosphere is discussed in section 4.2.

Fluorine products of chlorofluorocarbon destruction in the stratosphere are of lesser importance than chlorine products to ozone destruction. The radicals F and FO play similar roles as Cl and ClO in the chlorine system, although the catalytic ozone destruction is reduced by about 10^4 due to their much smaller abundance [Stolarski and Rundel, 1975]. HF is the sink for fluorine, as HCl is for chlorine, but the much greater stability (bond energy) of HF eliminates the channel releasing free fluorine by reaction with OH (as in the analog reaction OH + HCl). Only $O(^1D)$ is believed to attack HF, and although the kinetics of

fluorine chemistry are not as well quantified as for chlorine compounds, the HF molecule will undoubtedly be the major constituent, with little sensitivity to the rates related to F and FO exchange, or the $O(^1D) + HF$ reaction. A tropospheric sink (rainout and ground deposition of HF) is included in our model, as for HCl; the long photochemical lifetime (years) of stratospheric HF implies that transport will significantly affect its vertical distribution, leading to a roughly constant mixing ratio in the upper stratosphere, with a decrease towards the lower stratosphere and troposphere, where fluorine is effectively retained by the chlorofluorocarbon source species. We have included intermediary halocarbon products in our model (32°N latitude, equinox) of fluorine compounds. CF_2Cl_2 and CHF_2Cl are assumed to yield COF_2 as a stable intermediary, whereas $CFCl_3$ photolysis and subsequent oxidation yields COFCl. The main stratospheric fluorine compounds then become HF and COF_2, as illustrated in Figure 40. Models A and B refer to the uncertainty in the quantum yield for COF_2 photolysis. A quantum yield of 0.25 at 206 nm was measured by Molina and Molina [1982], as discussed in DeMore et al. [1982], but additional information at other wavelengths (from about 190 to 220 nm) is needed to determine the true value for $j_{COF_2}(z)$. Model A hence assumes a quantum yield $\phi_{COF_2}(\lambda) = 1$ for all λ, whereas model B uses $\phi_{COF_2}(\lambda) = 0.25$ for all λ. This leads to a factor of four difference in upper stratospheric $[COF_2]$ and produces a decrease of about 40% in [HF] between models A and B. COFCl photodissociates more rapidly and is less abundant than COF_2, as are CF_2Cl_2, CHF_2Cl and $CFCl_3$. Simultaneous observations of COF_2 and HF in the stratosphere could also differentiate between models A and B, since--

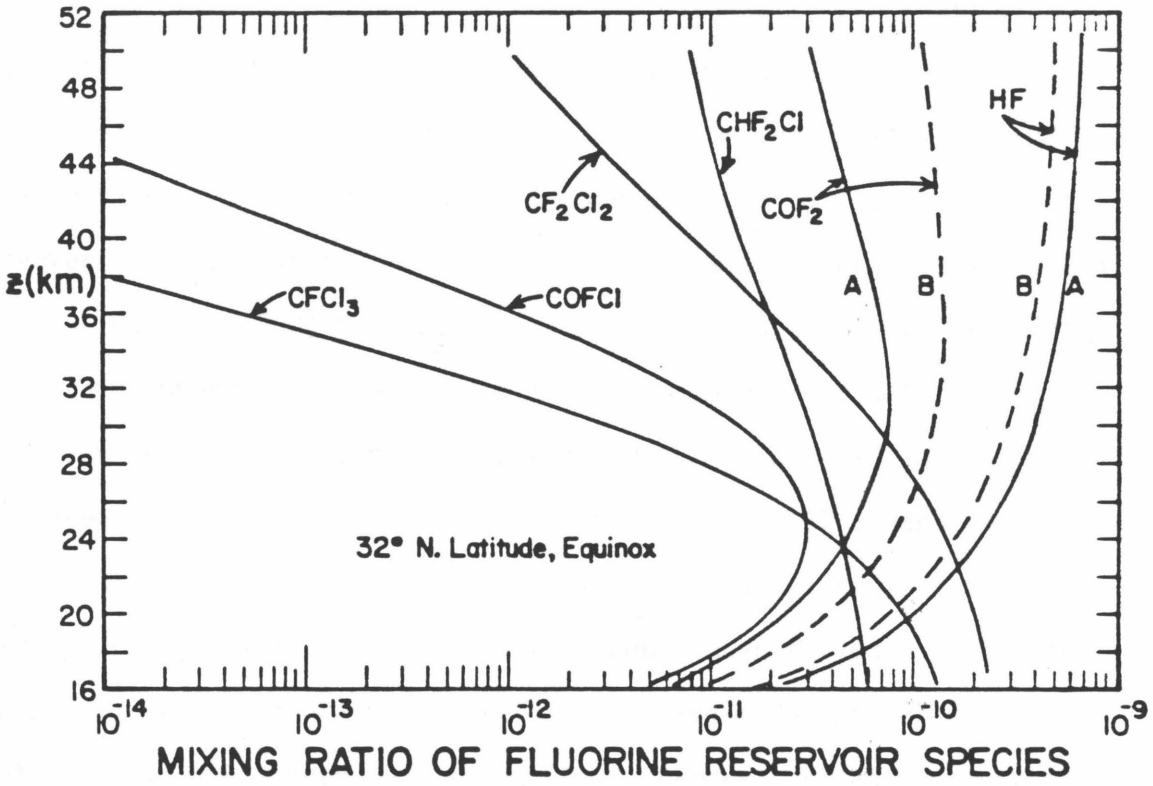

Figure 40. Model mixing ratio profiles for fluorine reservoir species. Cases A and B refer to the uncertainty in the quantum yield ϕ for COF_2 photolysis (ϕ = 1.0, and ϕ = 0.25, respectively).

depending on the altitude--the ratio $[COF_2]/[HF]$ differs by a factor of 2 to 5 between cases A and B. The actual profiles (at least their ratios) should lie within these upper and lower model bounds. The radicals F and FO are not shown in the figure because their mixing ratios are of order 10^{-16} or less in the stratosphere and they are not likely to be directly measured. The rates of COF_2 production from CHF_2Cl and CF_2Cl_2 are shown in Figure 41, along with the yield of F (and therefore HF) from COFCl and COF_2 (cases A and B).

Available HF observations [see summary in Hudson et al., 1982] are compared to model profiles in Figure 42. One has to be cautious, however, when comparing these various observations. Data sets 1 and 5 [Farmer et al., 1980; Mroz et al., 1977] are significantly lower than the other observations (excluding the 30 km point from data set 6). This can be at least partially understood. The infrared absorption measurements of Farmer et al. [1980], obtained in 1977, were from the southern hemisphere (30°S), and could--in part only--reflect the inter-hemispheric gradient in chlorofluorocarbon concentrations. Moreover, uncertainties in the data and profile retrievals do not rule out [HF] values about 50% higher than shown (C. B. Farmer, private communication, 1983). The data of Mroz et al. [1977] were obtained by in situ filter collection, which presumably samples COF_2 (and COFCl) as well as HF. However, HCl filter collections [Lazrus et al., 1977], which should yield an upper limit to [HCl], have also led to results lower than most remote sensing data; we are not convinced that the collection efficiency of filter techniques is well known for such in situ atmospheric sampling. Measurement 6 [Bangham et al., 1980] employs a technique

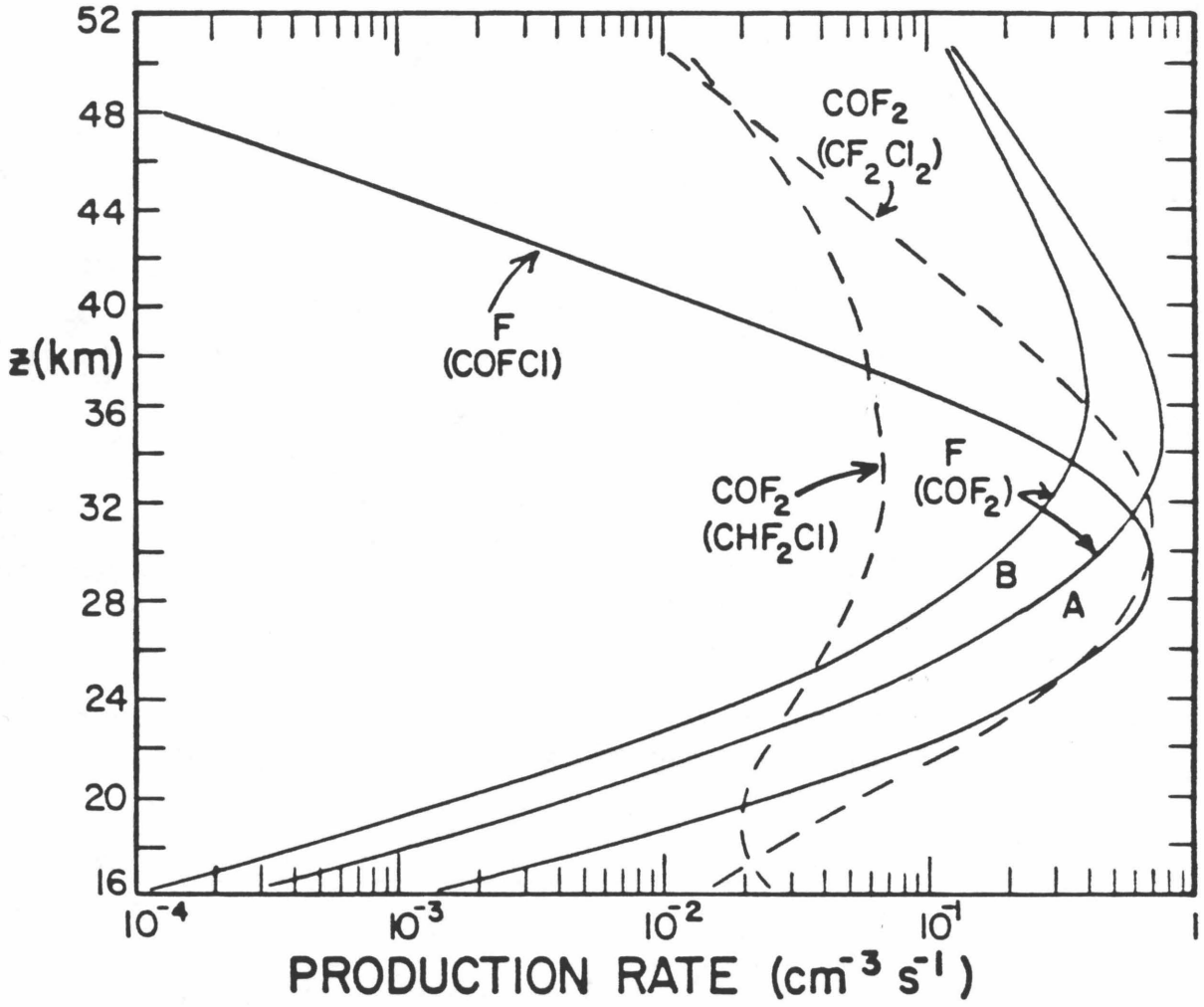

Figure 41. Production rates of F (from COF_2 and COFCl) and COF_2 (from CF_2Cl_2 and CHF_2Cl) in the stratosphere (same model as in Figure 40). Cases A and B refer to uncertainty in COF_2 photolysis rate (quantum yield value).

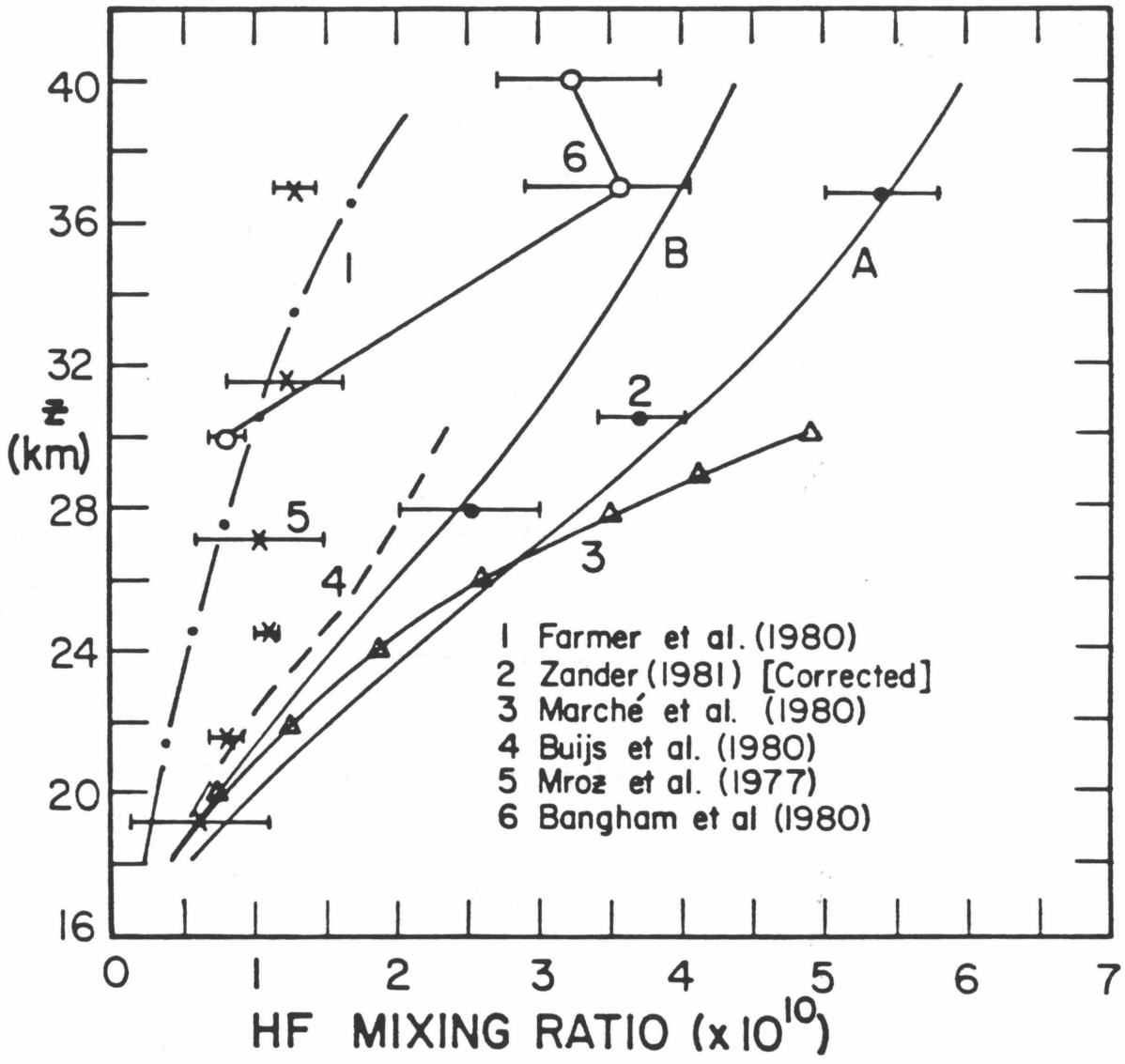

Figure 42. Comparison of available HF measurements with models (A and B) for 30°N latitude, equinox conditions. Column abundance results of Zander (1981) have been converted to mixing ratios (see text).

different from 2, 3 and 4. Infrared emission, rather than absorption, is used. Although model B is not inconsistent with the 37 and 40 km points, the observation at 30 km shows a sharper decrease than the model and other observations. If this is indeed real, transport processes not modeled here, rather than direct photochemistry would probably have to be invoked; intercomparisons between various measurement techniques are needed. Model B fits profiles 2, 3 and 4 within the uncertainties involved. All these data come from infrared absorption measurements. Profile 3 from Marché et al. [1980] cannot be very sensitive to the exact slope, since these were ground-based (column) measurements. The balloon-borne observations of Buijs et al. [1980] are also consistent with a model such as B; however, these data were obtained at 65°N latitude. The data of Zander [see Zander, 1981] represent three average column mixing ratios above 27.9, 30.5 and 36.8 km. We have converted these to mixing ratios at these altitudes in Figure 42, by assuming a model profile such as B. Since these data were taken, respectively, during 1976, 1978 and 1979, we should allow for an increase in the atmospheric fluorine content. A 10% increase per year is in good agreement with both the above data set and observed tropospheric increases in the source species (principally CF_2Cl_2). In summary, there are inconsistencies between various sets of data for HF, the major fluorine sink in the stratosphere, but given the measurement uncertainties, mean models and observations are not in violent disagreement. This also holds for published data concerning the ratio of [HF] to [HCl] (see Figure 43), if one omits the southern hemisphere data of Farmer et al. [1980]. Model B is in better agreement with [HF] and [HF]/[HCl]

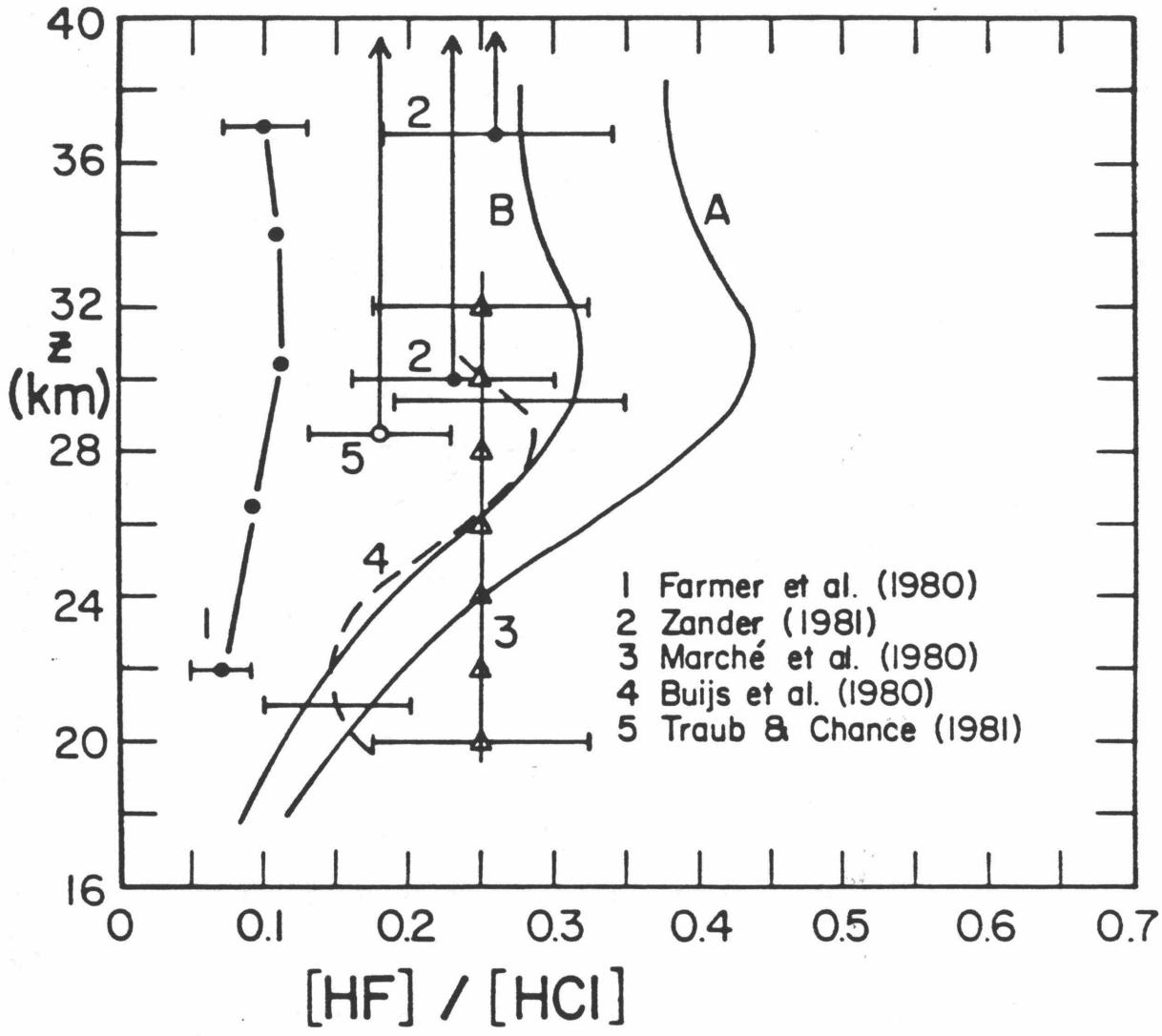

Figure 43. Stratospheric measurements of the [HF]/[HCl] ratio, compared to our model results (cases A and B, as before).

observations, which indicates that COF_2 might indeed photolyze with an effective quantum yield closer to 0.25 than to 1. This seems to be a more reasonable--although not experimentally verified--explanation of the observations than the use of a very low H_2O abundance (1 ppm instead of 4 or 5 ppm), as used by Sze [1978], which reduces the conversion rate of F to HF (reaction (138)). Decrease in lower stratospheric model [OH] in the past few years has also decreased the [HF]/[HCl] ratio by increasing [HCl], although most HCl observations are lower than the models in the lower stratosphere. If future laboratory data on the COF_2 photodissociation quantum yield point to an average value much larger than 0.25 (model A instead of B), other fluorine reservoir(s) might have to be searched for in order to reduce the model HF abundances. Laboratory and atmospheric data on COF_2 would therefore be useful. The relative increase in HF observed by Zander between 1976 and 1979 is consistent with tropospheric increases in the halocarbon source species.

4.2 Diurnal Variation of ClO

The previous section described measurements and models of the daytime ClO profile and the diurnally-invariant (in theory) HCl profile. The other major active compound is chlorine nitrate ($ClONO_2$), which builds up at night through the recombination reaction $ClO + NO_2 + M$ and photodissociates during the day to regenerate the chlorine radicals. Its abundance peaks in the lower stratosphere and decreases sharply in the upper stratosphere, due to the decrease in $[NO_2]$ and [M]. HOCl is a reservoir of secondary importance (according to current photochemistry) formed from the radicals ClO and HO_2, and destroyed mainly by photolysis

(see Figure 34). The resulting diurnal variation of the active chlorine species is illustrated for various altitudes in Figure 44 (32°N latitude, -11° solar declination). Observations of the ClO diurnal variation in the stratosphere can conceivably provide indirect evidence for the main "breathing cycle" between ClO and $ClONO_2$, even though chlorine nitrate is not measured directly. A possible $ClONO_2$ detection (by infrared absorption) near 30 km has been reported by Murcray et al. [1979], although this is a difficult measurement and at best represents an upper limit consistent with model values [Hudson et al., 1982]. To first order, the sum $[ClO] + [ClONO_2]$ will be constant during the diurnal cycle and their combined abundance depends on the partitioning with HCl. The effect of chlorine nitrate is to reduce the amount of free radicals (Cl and ClO) available to destroy ozone, although the largest $ClONO_2$ abundance occurs below the altitude ($\sim$ 40 km) of peak efficiency in the chlorine catalytic cycle. We note that we have used a rate of $ClONO_2$ formation in accord with the "fast" value for k_{64} (see Chapter 1) recommended in De More et al. [1982], and consistent with the absence of other isomers, as implied by the laboratory work of Margitan [1983]. We now discuss the implications of existing ClO abundance determinations that are relevant to diurnal variations and chlorine nitrate.

Measurements taken near sunset or sunrise have to be compared to the appropriate model profiles, since there is a strong variation in [ClO] at those times. This holds for the unpublished ground-based laser heterodyne radiometer observations of Rogers et al. [1982]. These measurements seemed to yield an upper limit for the ClO column amount that was significantly lower than model predictions, even near the

Figure 44. Model diurnal variation of active chlorine species at 24, 32, 40, and 48 km. Standard results for 32°N latitude, -11° solar declination are presented.

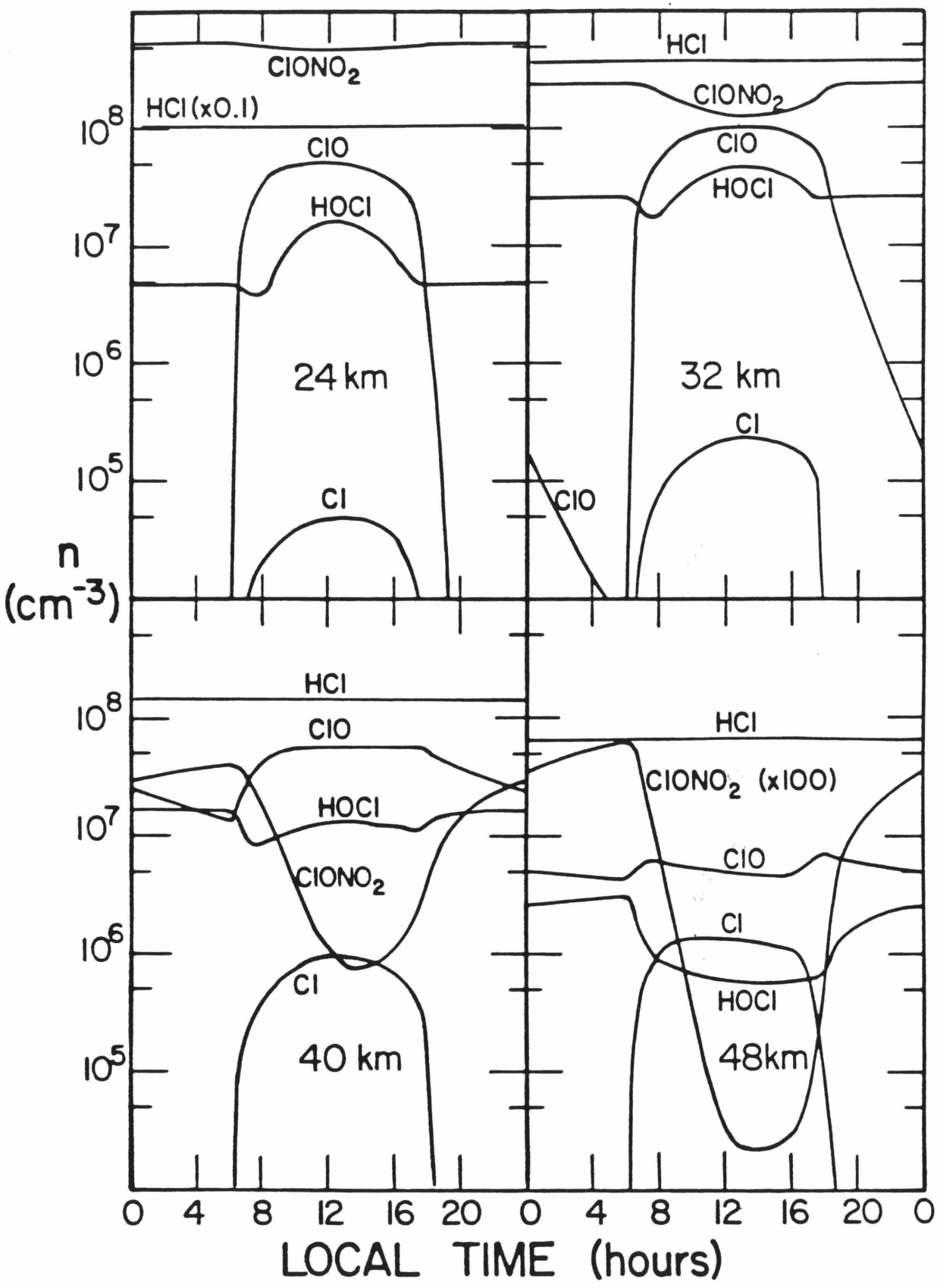
ClONO2
HCl(x0.1)
ClO
HOCl
24 km
Cl
HCl
ClONO2
ClO
HOCl
32 km
Cl
ClO
HCl
ClO
HOCl
ClONO2
40 km
Cl
HCl
ClONO2 (x100)
ClO
Cl
HOCl
48km
n
(cm-3)
10^8
10^7
10^6
10^5
0 4 8 12 16 20 0 4 8 12 16 20 0
LOCAL TIME (hours)

terminator; we feel that a positive detection is needed to validate this technique, particularly in light of the more recent millimeter ground-based observations of Solomon et al. [1983], which agree reasonably well with model results (see below). The balloon-borne measurements of ClO by Menzies [1979], also by laser heterodyne radiometer measurements of atmospheric transmission, did show a measurable absorption feature in the vibration-rotation band near 12 μm. The resulting profiles were significantly higher than model predictions, but new laboratory spectroscopic data have revealed that the ClO observations were referring to an incorrect line position. A re-evaluation of the observations [Menzies, 1983] in terms of another spectral line apparently due to ClO has led to a sunset ($\chi = 94°$) upper stratospheric profile, as shown in Figure 45. These November 1979 data are compared to our typical mid-latitude diurnal model (32°N latitude, -11° solar declination), plotted for solar zenith angles from noon to sunset. The observation at 36 km is an upper limit, which is not as satisfying as a definite detection, but agrees with the steep gradient versus height obtained at higher altitudes. This slope, rather than the absolute amount of ClO, constitutes the main difference between these results and model profiles. Other comparisons regarding the diurnal variation of ClO are now presented, prior to a discussion of model uncertainties.

Balloon-borne observations of part of the ClO diurnal variation have been performed by Waters et al. [1981]. These are microwave limb sounding measurements of the thermal emission from a ClO rotational transition near 204 GHz. The antenna beamwidth of 0.3° is mostly sensitive to an emission region about 4 km wide at the tangent altitude. The

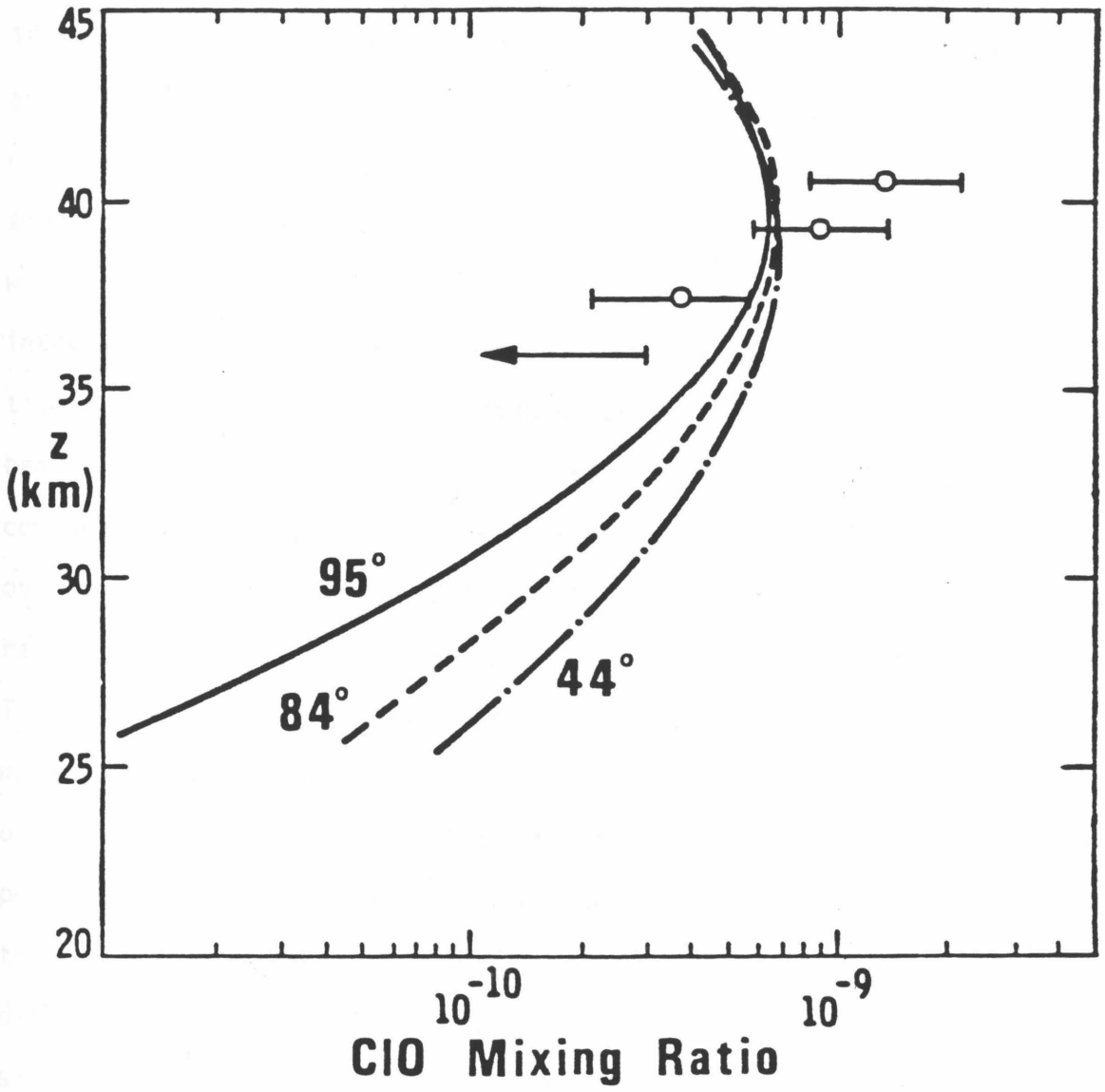

Figure 45. Re-evaluated November 1979 ClO data(Menzies, 1983) obtained during sunset by laser heterodyne radiometer measurements. Model ClO profiles are shown, for various solar zenith angles. At 95° (sunset), the model profile does not exhibit the sharp decrease observed between 40 and 35 km.

pointing uncertainty is believed to be ±1 km. The data shown in Figure 46 represent the observed brightness temperature as a function of local time, which corresponds to a normalized ClO amount between about 28 and 32 km. The measurements for 20 February 1981 [Waters et al., 1981] and 12 May 1981 (unpublished observations by the same group) were obtained above Palestine, Texas and are compared to model results for similar conditions of solar illumination (declination of -11° and +18°, respectively) and 32°N latitude. The model normalization chosen here is somewhat arbitrary and the separate curves shown for each flight were obtained by integrating (conservatively) over ±3 km around 29 and 31 km, respectively, to account for the pointing uncertainty as well as the antenna beamwidth. Absolute concentrations near 2 p.m. for the February flight compared favorably with our model, as shown previously in Figure 37. The observed relative decrease from noon to sunset also agrees with our model results, given the apparent scatter and uncertainties in the data points. The May observations from sunrise to noon show a slower increase than model predictions, even if one were to choose a noon value less than half of the noon February value. Note that both data sets are directly comparable in this figure and that the absolute ClO amount is less in May than in February, contrary to our model results. However, a multidimensional model is better suited for comparisons of seasonal variations, since meridional transport as well as solar radiation can (indirectly) alter the absolute abundance of ClO. These post-sunrise and pre-sunset microwave measurements should soon be repeated by the same group with an improved signal-to-noise ratio, in order to refine and (possibly) confirm the relative diurnal ClO variation presented here.

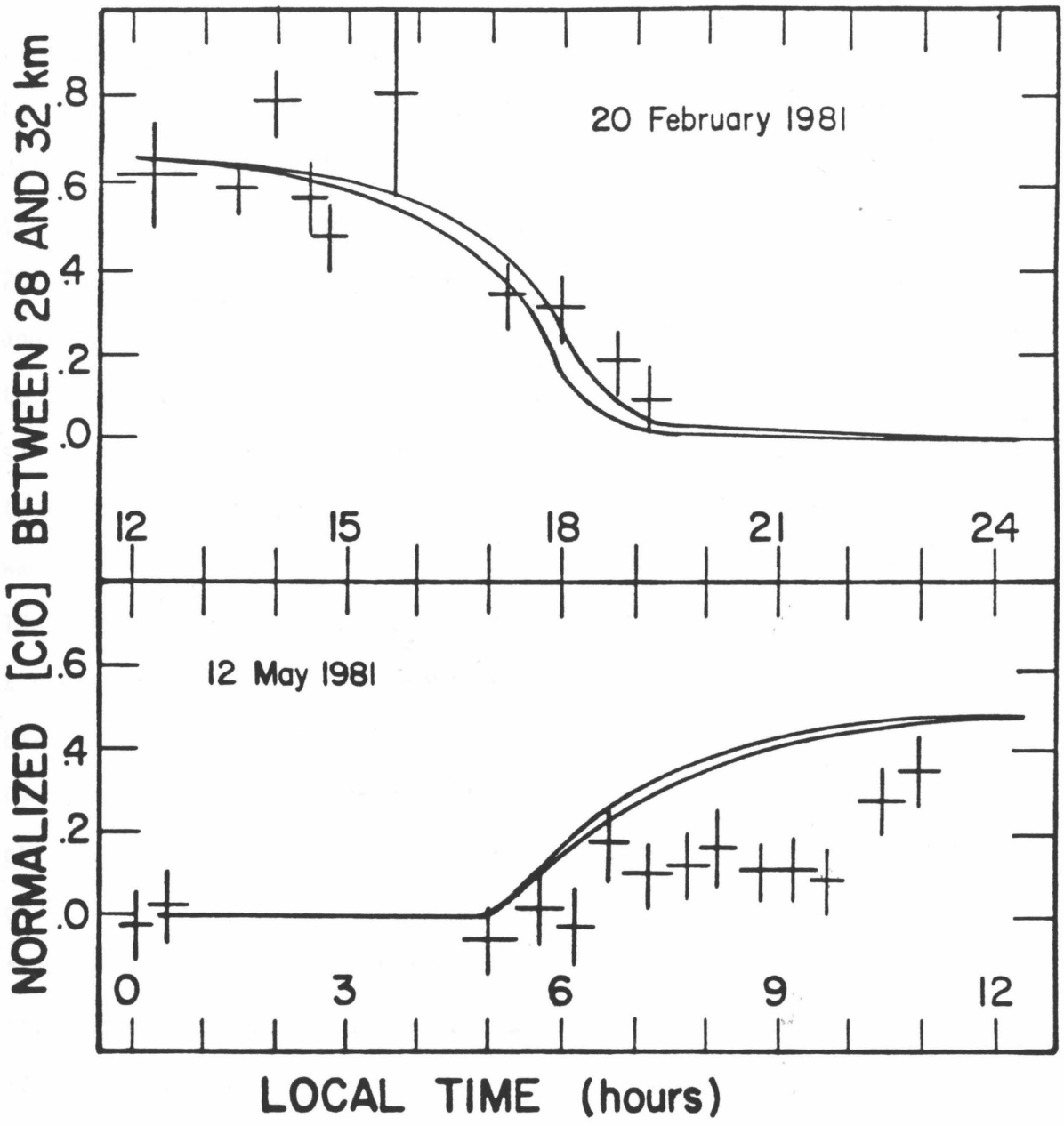

Figure 46. Comparison of balloon-borne microwave observations of ClO diurnal variation (J. Waters and coworkers, 1981) with normalized model results. Observed brightness temperature (ordinate) is proportional to the ClO abundance between about 28 and 32 km. Model curves for each flight correspond to the diurnal variation of the ClO abundance integrated over ±3 km around 29 and 31 km, and normalized to the noon value (see text).

Finally, ground-based measurements of the same nature as the above microwave observations have been made by Parrish et al. [1981] and recently again by the same group [Solomon et al., 1983]. The former data were taken at 42°N and the average of Anderson's in situ data (excluding the two large July values) is in good agreement with the 204 GHz emission line shape and intensity (ClO vertical distribution and column amount); a recent re-evaluation of the absolute amount leads to a 15% increase over the published values, bringing the average in situ and ground-based microwave observations in even better agreement (Solomon, private communication, 1983). The latest set of observations was taken from Mauna Kea, Hawaii (20°N latitude) during October 1-15, 1982, and December 9-16, 1982. The ClO rotational emission line at 278 GHz was observed fairly continuously during these periods, both at day and at night. The data are averaged over the several days of observation for October and December to obtain a signal-to-noise ratio of about 20 to 1. In order to compare absolute abundances and relative diurnal variations, the best approach is to use model ClO vertical profiles and compute the synthetic spectrum to fit the observed spectrum. Solomon et al. [1983] have performed such a study for various models, including our own.

We have used two models for 20°N latitude and -4° (October) or -23° (December) solar declination for comparison. The ClO emission line is underlined by a broad sloping baseline due to an ozone line wing. The column amounts deduced from such ground-based measurements are mostly sensitive to the ClO abundance above 30 to 32 km, which corresponds to a region within ±50 MHz from the line center. This is due to the pressure-

broadening effect in the wings of the line, and the fit is not affected much by the decreasing ClO concentration below 30 km. Our peak daytime December model ClO column amount of $1.1 \times 10^{14} cm^{-2}$ above 30 km provides very good agreement with the peak observed December intensity and ClO line shape (Solomon, private communication, 1983). Our October model yields a peak column abundance almost 20% higher than in December, whereas the observations imply less ClO (by about 20%) in October than in December. Again, seasonal variations are apparently not well predicted by a one-dimensional model and it remains to be seen how multi-dimensional models compare to these and future ClO observations. On the average, the agreement between our daytime model profiles and the observations of Solomon et al. [1983] can be considered reasonable, given the uncertainties of order ±20% in the data. Our model has about 2.6 ppbv of total free chlorine (mostly ClO and HCl in the upper stratosphere), and the 1982 amount should be at least this high, given the abundances of source halocarbons at the ground; total chlorine measurements [Berg et al., 1980] have also led to values between about 2.5 and 3.5 ppbv in the lower stratosphere. We now focus on the relative diurnal variation observed by Solomon et al. [1983]. Their data are presented in Figures 47 and 48 in terms of a relative integrated intensity within ±50 MHz of the line center, normalized to unity at noon. Two-hour averages for the whole set of October and December 1982 data are shown, respectively. Reasonable uncertainties of ±20% (Solomon, private communication, 1983) have been assigned to each observation. The model diurnal variations in the ClO column above 31, 33, 35, and 37 km, normalized to the noon values are shown for comparison. The main

Figure 47. Comparison of averaged ground-based microwave observations of ClO diurnal variation (Solomon et al., 1983) with our model results; both are normalized to noon value. Data correspond to column abundance above about 30 km, and model column abundances above various altitudes are shown.

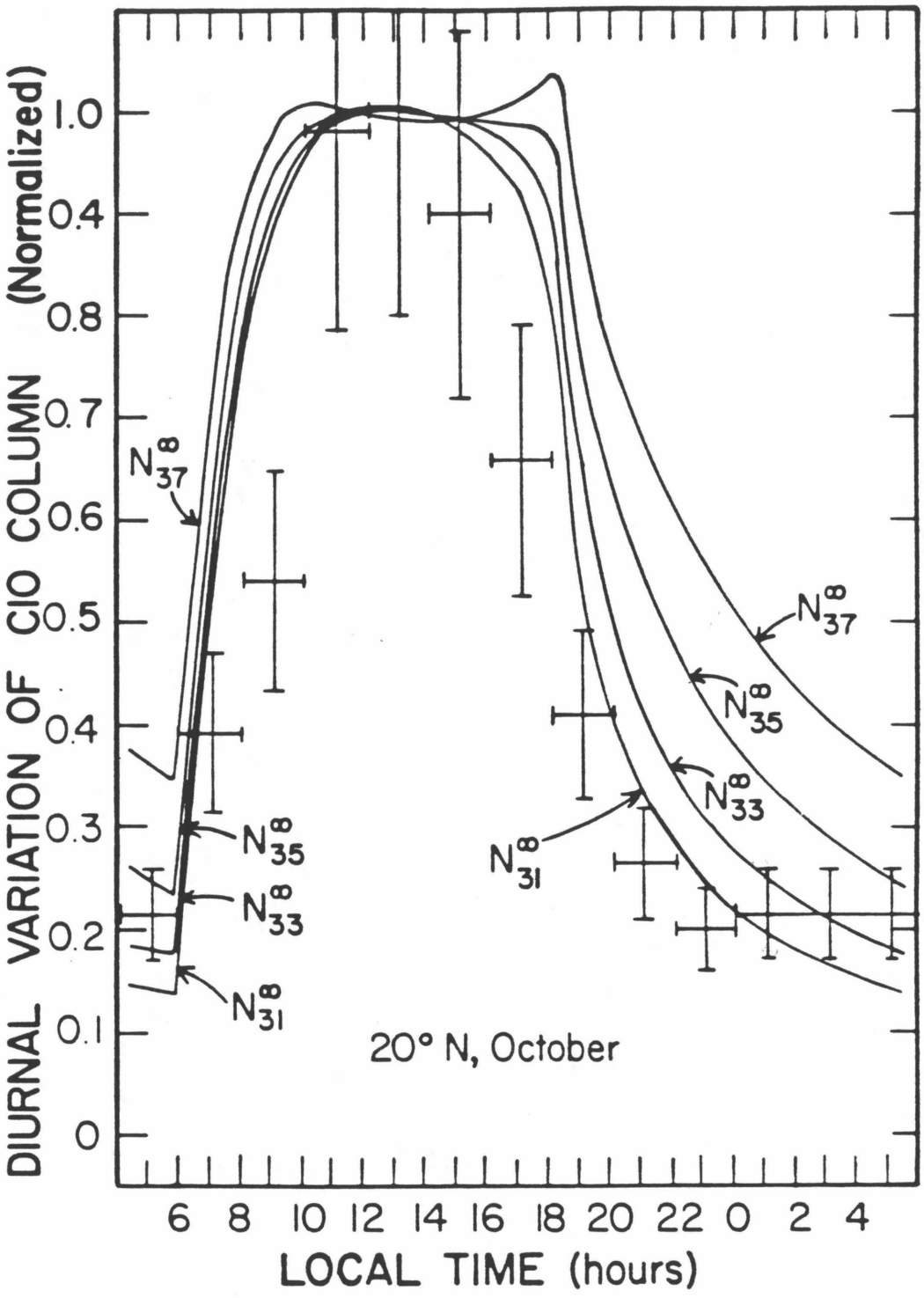
DIURNAL VARIATION OF ClO COLUMN (Normalized)
1.0
0.4
0.8
0.7
0.6
0.5
0.4
0.3
0.2
0.1
0
N_{37}^{8}
N_{35}^{8}
N_{33}^{8}
N_{31}^{8}
N_{37}^{8}
N_{35}^{8}
N_{33}^{8}
N_{31}^{8}
20° N, October
6 8 10 12 14 16 18 20 22 0 2 4
LOCAL TIME (hours)

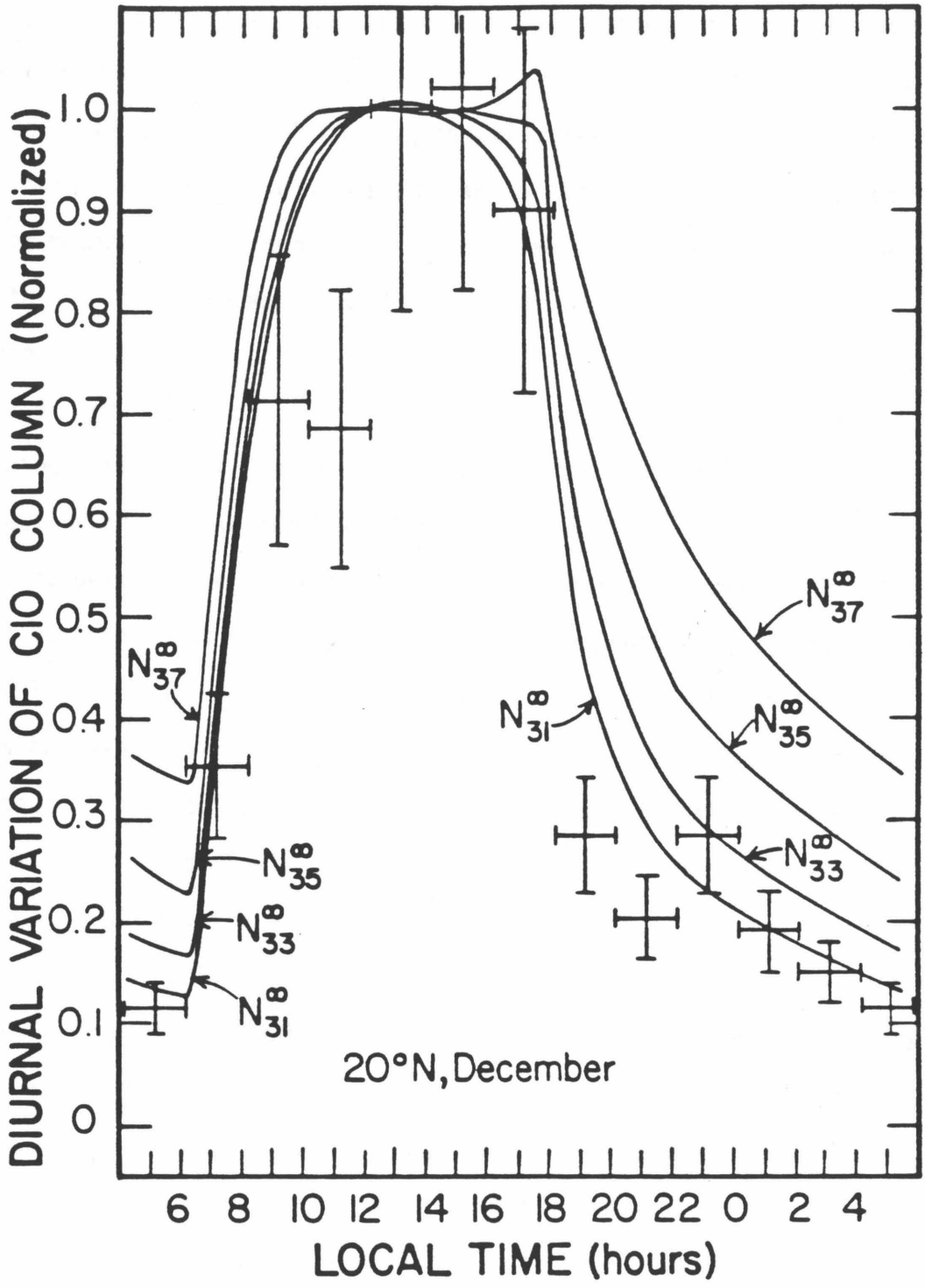

Figure 48. Same as Figure 47, except for December 1982 data.

difference between these model curves is the steepness of the decline near sunset and the ratio of N_{ClO}^{max} to N_{ClO}^{min}. A plot of this ratio as a function of height above which N_{ClO} is calculated is shown in Figure 49 for October (December values are similar to within 5%). The observed ratio of maximum to minimum intensities is about 7. This would correspond to the variation expected for a column abundance above 31 km, according to our model. This is also true for the comparisons shown in Figures 47 and 48, which to first-order show good agreement in the "breathing cycle" of ClO and--presumably--$ClONO_2$. The higher altitudes show less diurnal variation (see Figure 44), which is illustrated by the difference between the N_{31}^{∞} and N_{37}^{∞} curves. Figure 50 shows the model percent contributions to the total ClO column abundance as a function of time for various altitude ranges. During the day, most of the ClO resides between 30 and 40 km, while the 40-50 km range becomes dominant from about 10 p.m. to sunrise, due to the smaller diurnal variation at those heights. This should show up as a narrowing of the observed ClO emission line during the evening and night, in addition to the decrease in intensity. Such a behavior is at least qualitatively observed in the data of Solomon et al. [1983]. The main discrepancy between models and ground-based microwave observations versus local time seems to be the somewhat slower rise after sunset and possibly--although not as pronounced--the faster decrease in the afternoon. In particular, the October observations between 8:00 and 10:00 local time yield an intensity or column abundance a factor of about 0.55 lower than the 12:00 to 14:00 peak values. This contrasts with the model value of about 0.9 and would seem to qualitatively agree with the nearly constant ClO abundances near

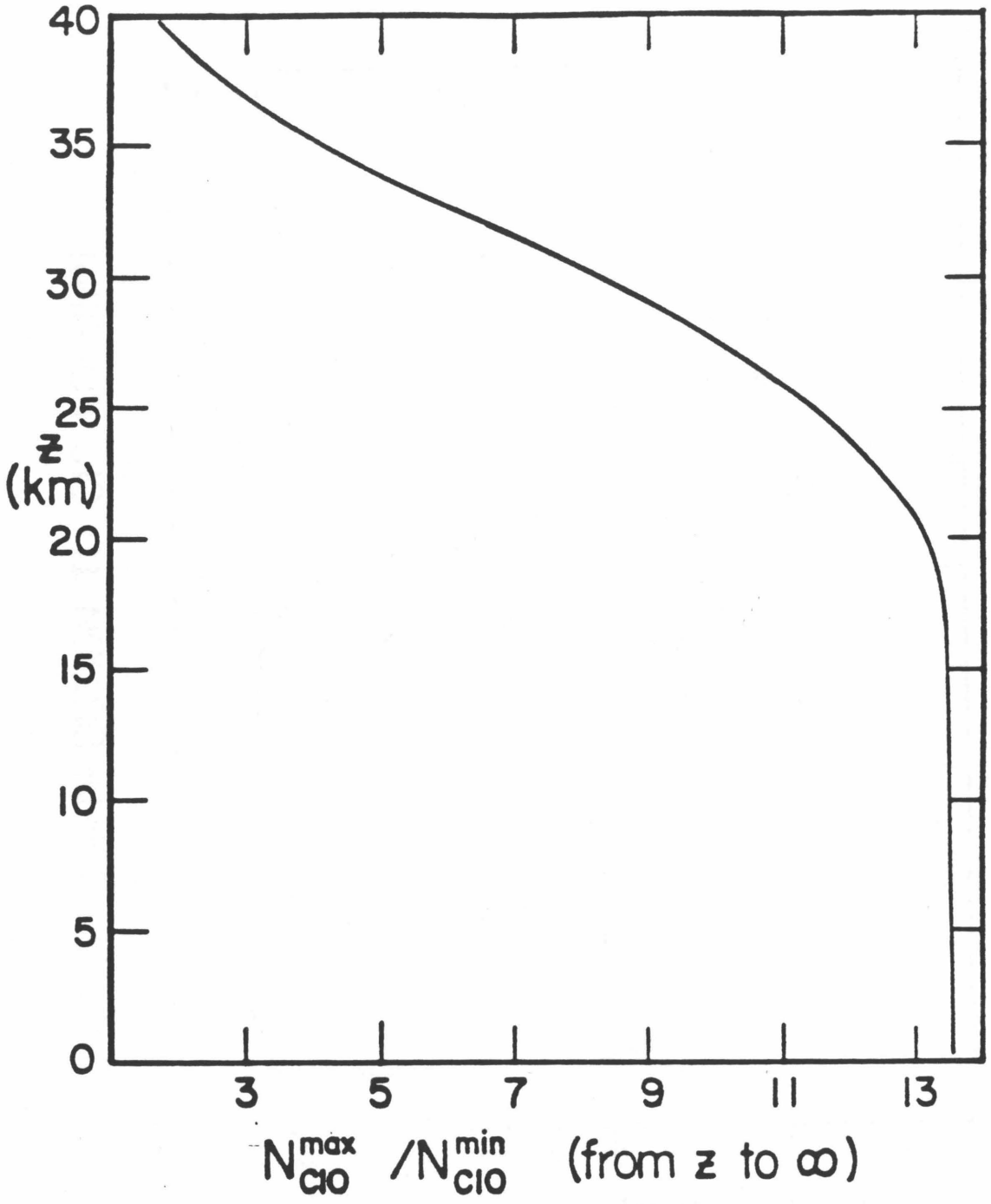

Figure 49. Ratio of maximum to minimum (day to night) ClO column abundance above height z (model for 20°N, October).

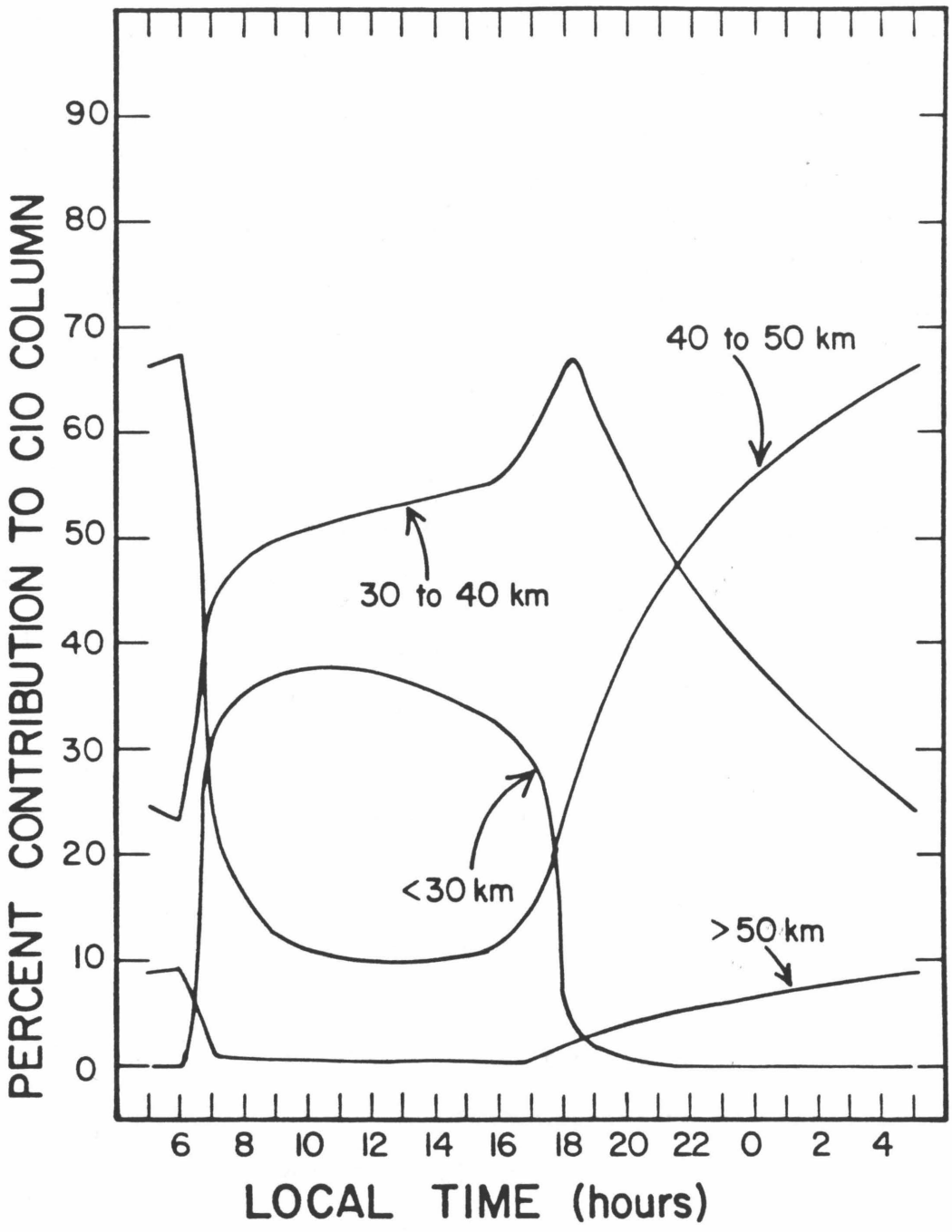

Figure 50. Model percent contribution from various altitude ranges to the total ClO column abundance variation as a function of time.

30 km observed between 7:00 and 10:00 by the balloon-borne Microwave Limb Sounder (Figure 46). However, the December ground-based data between near 9:00 yield values of $\sim$0.7, which persist into the 10:00 - 12:00 time bin. This difference between the data sets themselves also appears between 16:00 and 18:00 hours, when the October value of 0.65 is less in agreement with the model than the December value of 0.9. Within the observational uncertainties, the two sets of data might be considered consistent, although the relative change in intensity is better known than each individual average value. If the above differences between October and December are real, any model that can fit one set of data will probably not explain the other set. Further ground-based and balloon-borne observations will help define these apparent discrepancies between theory and measurements, as well as provide an intercomparison between experiments. A decrease in the average ClO amount available during the day can have an impact on the predicted catalytic destruction of ozone by chlorine radicals, which occurs mainly above 35 km, since the chlorine could be tied up in another "inert" reservoir reducing the efficiency of the catalytic cycle. Based on the observations, this effect should not be very large, unless it was due to some missing chemistry that also drastically altered the main Cl-ClO catalytic cycle in terms of the reactions destroying odd oxygen (e.g., by forming a "net-nothing" cycle instead). We do not wish to reopen the question of chlorine nitrate isomers, in light of the recent laboratory work of Margitan [1983]; moreover, the introduction of such rapidly photolyzing isomers would increase the amount of ClO and its rate of formation, and would not help resolve the possible discrepancies noted

above concerning the slope of the vertical profile near sunset or the time rate of change of the ClO column abundance above 30 km. One could also question other effects such as spatial inhomogeneities in the atmosphere (although the microwave observations represent averages over several days) or possible small changes in the ozone line wing which provides a baseline for the observed ClO emission line and might lead to larger changes in the latter line, but we have no firm basis for such mechanisms at the present time. It would be interesting to try to confirm the existence of discrepancies between these observations and models on a day-to-day basis, rather than for the averaged sets of data, although the signal-to-noise ratio will be lower for any given day.

Let us now consider the uncertainties in the current photochemical scheme, in relation to the column diurnal changes and the vertical gradient near the terminator. Herman [1979] has discussed some aspects of diurnal changes in stratospheric species concentrations. As he notes, the net variation as a function of time is often the difference between large production and loss terms. Rather than considering the terms that represent fast interactions between Cl and ClO in the expression for $\frac{d[ClO]}{dt}$, we find it more useful (and accurate enough) to group these short-lived radicals together and calculate:

$$\frac{d[ClO_x]}{dt} = \frac{d[Cl]}{dt} + \frac{d[ClO]}{dt} + \frac{d[ClOO]}{dt} \qquad (45)$$

Since [ClO] is typically much larger than [Cl] or [ClOO] in the stratosphere, $\frac{d[ClO]}{dt} \simeq \frac{d[ClO_x]}{dt}$. Furthermore, if we combine the individual

production and loss terms for each member of equation (45) and compute the net result, we find:

$$\frac{d[ClO]}{dt} = P(t) - L(t) = \Delta_{ClO} = \Delta_{ClONO_2} + \Delta_{HOCl} + \Delta_{HCl} \tag{46a}$$

where

$$\Delta_{ClONO_2} = J_{16} + K_{69} - K_{64}$$

$$= (j_{16} + k_{69}[O])[ClONO_2] - k_{64}[ClO][NO_2][M] \tag{46b}$$

$$\Delta_{HOCl} = J_{23} + K_{100} - K_{86}$$

$$= (j_{23} + k_{100}[OH])[HOCl] - k_{86}[ClO][HO_2] \tag{46c}$$

$$\Delta_{HCl} = K_{58} - K_{59} - K_{63} - K_{70} - K_{85}$$

$$= k_{58}[OH][HCl] - (k_{59}[CH_4] + k_{63}[HO_2] + k_{70}[H_2] + k_{85}[H_2CO])[Cl] \tag{46d}$$

The Δ expressions can be seen to represent production minus loss terms for $[ClO_x]$, or alternatively, loss minus production terms for $ClONO_2$, HOCl, and HCl, respectively. In other words, equation (46a) is equivalent--as it should be--to the condition $\frac{d}{dt}[ClO_x + ClONO_2 + HOCl + HCl] = 0$. Vertical transport can be neglected for the timescales considered here. If $\Delta(t)$ is the net photochemical production (or loss) of $[ClO_x]_t$, we can compute the estimate

$$[ClO]_t^e \simeq [ClO_x]_t^e = \Delta_{ClO}(t)\,\delta t + [ClO_x]_{t-1}^e \tag{47}$$

This should yield a good estimate of $[ClO]_t$, and in the upper stratosphere, where [Cl] becomes larger (up to 25% of [ClO]), we can use the following correction:

$$[ClO]_t^e = \frac{[ClO_x]_t^e}{1 + R_1(t)} \tag{48}$$

where

$$R_1(t) = \frac{[Cl]_t}{[ClO]_t} = \frac{k_{61}[O]_t + k_{62}[NO]_t + k_{103}[OH]_t}{k_{60}[O_3]_t}$$

The third term in the numerator of $R_1(t)$ is of minor importance. If we start with model values for $[ClO_x]_o$ before sunrise and compute $[ClO_x]_t^e$ at subsequent times, using the above expressions (and model values for $R_1(t)$ and $\Delta(t)$), we find excellent agreement with the model ClO diurnal behavior, as shown in Figure 51. The model solves each individual continuity equation and does not group species as we did in our estimate, but we expect similar answers. We have neglected a few small terms in our estimate and small errors tend to add up towards the end of the day. If we only include the $ClONO_2$ terms, and neglect Δ_{HOCl} and Δ_{HCl} in the estimates, we obtain somewhat different [ClO] values (dashed line in Figure 51). This is a way of illustrating the importance of the interactions between $[ClO_x]$ and $[ClONO_2]$, which provides the main diurnal variation in [ClO]. [HOCl] production and loss terms provide most of the remaining changes. If one considers the model diurnal variation for [HOCl] in Figure 44, it can be seen that in the lower and middle stratosphere, there is an increase in [HOCl] during the day, whereas photodissociation becomes more important in the upper stratosphere and leads to a decrease in daytime [HOCl]. This is consistent with the change between

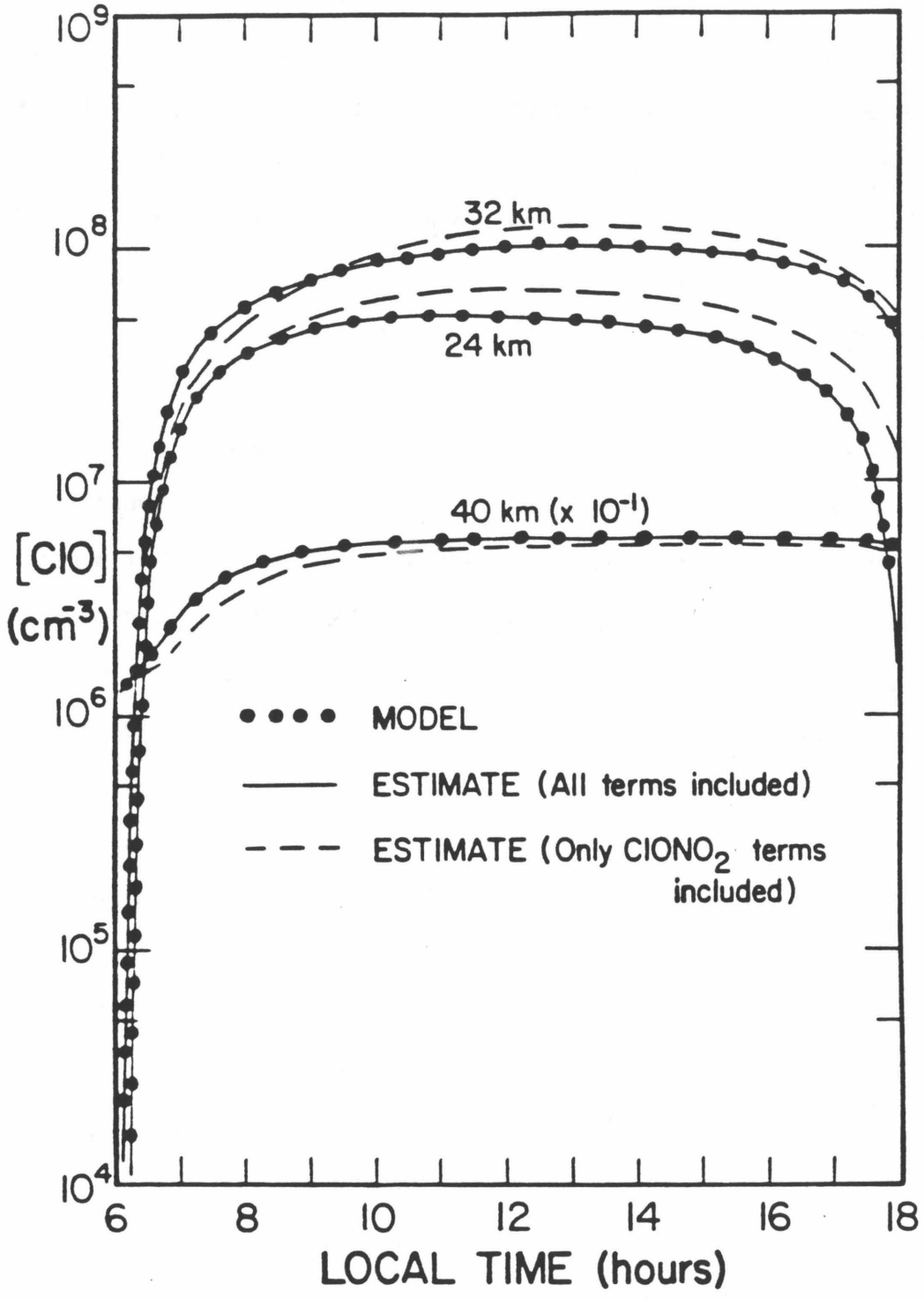

Figure 51. Daytime variation of ClO concentration at 24, 32, and 40 km (32°N, -11° solar declination). Numerical model is compared to estimates using photochemical production and loss rates for ClO_x (see text). Main coupling is with $ClONO_2$.

the dashed line (no HOCl effect on ClO) and the solid line (HOCl included) in Figure 51, where the lower stratospheric [ClO] decreases due to the increase in [HOCl], while the upper stratospheric [ClO] increases due to production by HOCl photolysis. The relative importance of HOCl increases in the lower regions of the stratosphere, where [ClO] concentrations are small. Figures 52 and 53 illustrate the relative contributions of the Δ (production minus loss) rates to $\Delta_{ClO} = \frac{[ClO]}{dt}$. At 32 km, most of the morning increase and afternoon decrease in [ClO] can be seen to arise from the Δ_{ClONO_2} term, with some enhancement or damping from Δ_{HOCl}. The same holds at 40 km, although the morning rise is not as strong and the subsequent small rate of change in [ClO], relative to the abundance at that height, results in a small diurnal variation (see also Figure 44). Furthermore, morning changes in ClO are mostly sensitive to the photodissociation rate (J_{16}) of $ClONO_2$, while afternoon and sunset variations are sensitive primarily to the conversion rate (K_{64}) of ClO to $ClONO_2$. Other terms play a smaller, but non-negligible role.

Uncertainties in the absorption cross sections for both $ClONO_2$ and HOCl are apparently less than 5-10% and the corresponding photodissociation rates in the stratosphere should be known to within 10-20%, if one considers the fact that the fluxes and atmospheric transmission in the 300-400 nm range are well determined, particularly above 30 km. The value for k_{64} is possibly somewhat more uncertain, but the four available studies [see DeMore et al., 1982] of this reaction show agreement within 20% of the mean, for the pressure and temperature ranges of interest here. The rate of formation of HOCl (K_{86}) involves a rate constant that could be uncertain by up to 50%, but the ClO

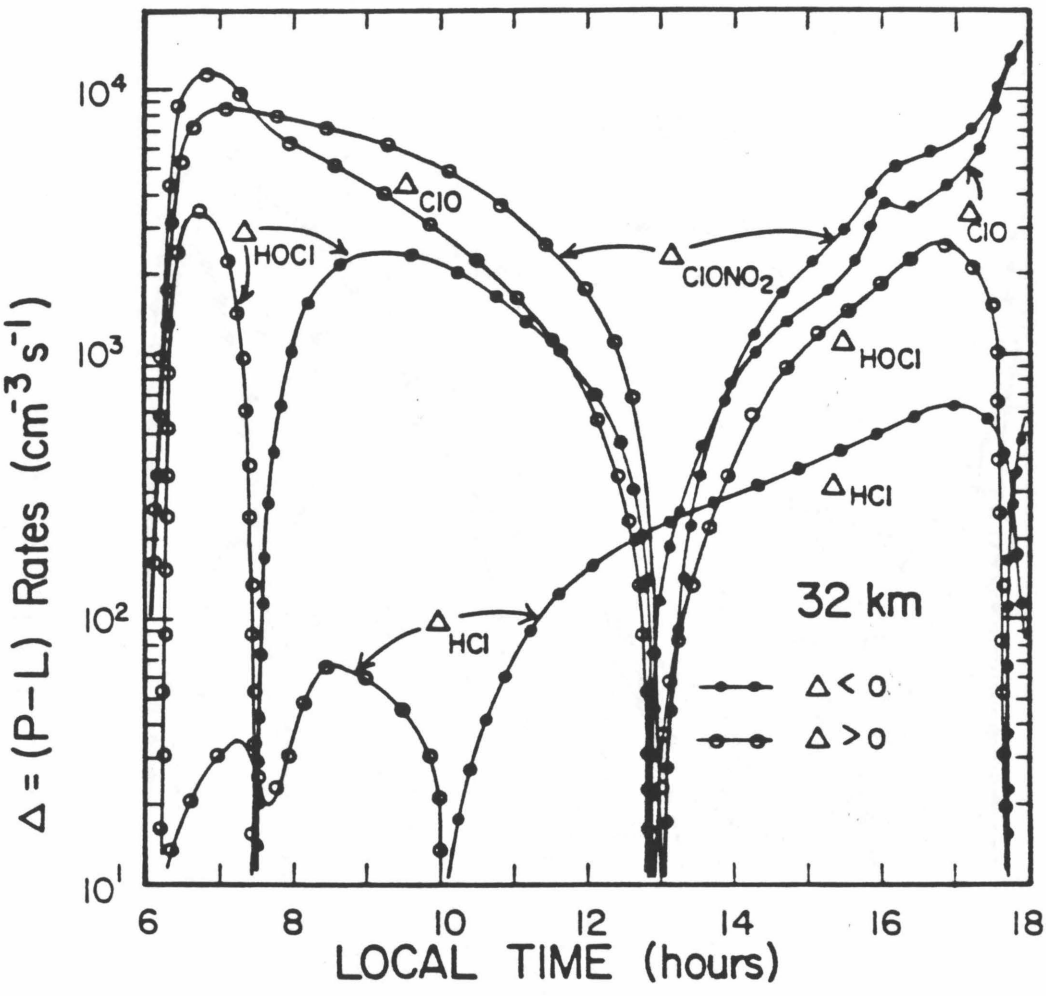

Figure 52. Contribution of the various Δ (production minus loss) rates relevant to diurnal changes in ClO at 32 km. Δ_{ClO} is the sum of Δ_{ClONO_2}, Δ_{HOCl}, and Δ_{HCl} (see equation (46)), and the first term is responsible for most of the diurnal variation in ClO concentration.

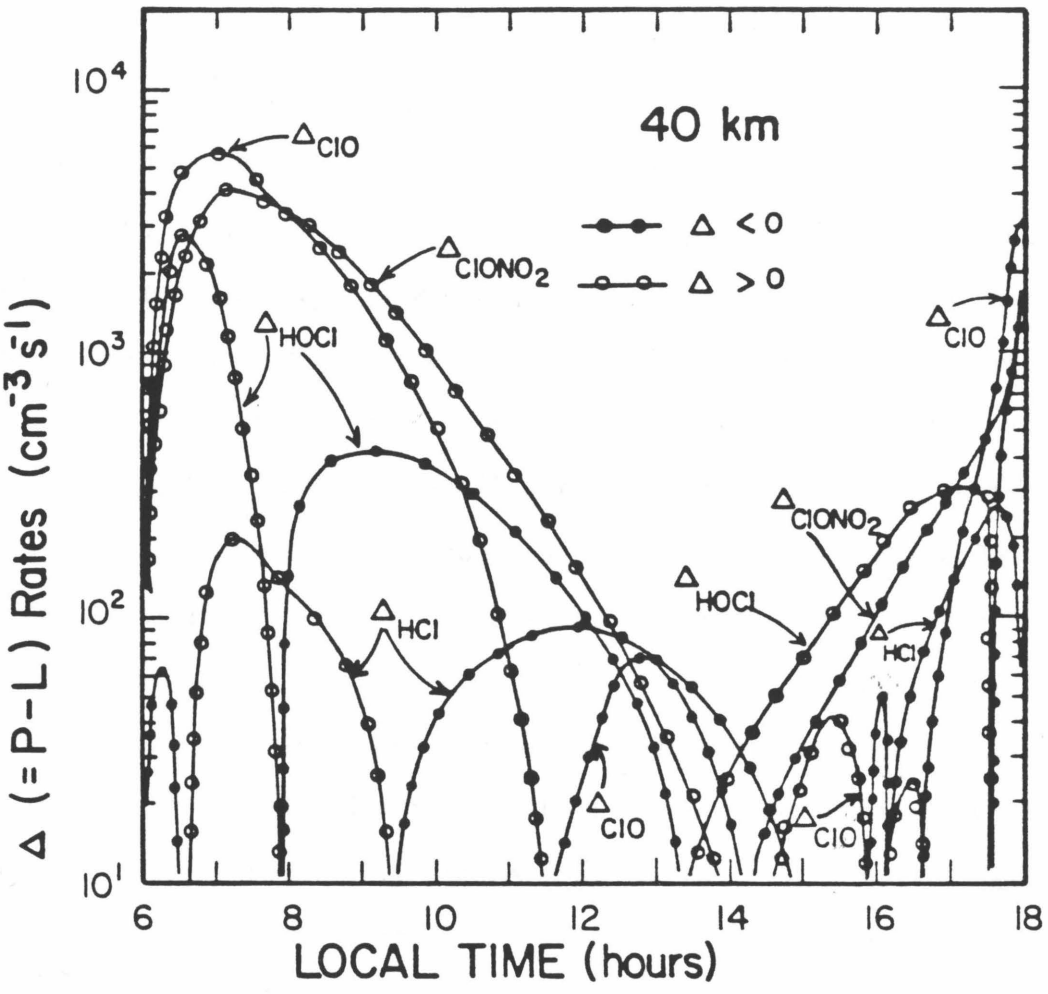

Figure 53. Same as Figure 52, except for 40 km, where diurnal variation of ClO is much smaller than in middle and lower stratosphere (see Figure 44).

sensitivity to such a change is less than the sensitivity to $ClONO_2$-related uncertainties. The OH + HOCl reaction rate has not been measured and is a rough estimate [DeMore et al., 1982], but since it is an order of magnitude less important than HOCl photodissociation in our current scheme, improvements in its rate constant would either increase the total destruction rate of HOCl or leave it essentially unchanged, which will not help improve upon the possible discrepancies between models and observations of the ClO diurnal variation. If we stretch the uncertainty in k_{64} by multiplying the current value by 1.50, we can indeed form more $ClONO_2$ and decrease the ClO abundance, although the increase in $ClONO_2$ partially compensates in the morning by releasing more ClO. The largest changes occur in the lower stratosphere, since the ratio $[ClO]/[ClONO_2]$ is smaller there. In terms of the sunset observations of Menzies [1983] above 35 km, we find less than a 20% change in the vertical gradient. The possible difference of more than 50% cannot be explained by the uncertainties in rate constants. The same holds for the apparently low ClO column abundances above 30 km obtained by Solomon et al. [1983] near 9 or 10 a.m. Missing chemical cycles and possibly missing relatively stable chlorine reservoirs might have to be invoked in order to account for such discrepancies, if real. The sensitivity to possible temperature changes (typically less than 10 K during the day at these altitudes) is not large enough either. In terms of NO_2, which recombines with ClO, we expect a smooth behavior during the day, and no sharp impulse that could possibly modify the ClO variation near 9 a.m. We stress again that differences exist between the October and December microwave data, that are as large as the

discrepancies between our model and these observations. If real, in general, such discrepancies could be significant in terms of our understanding of the chlorine-related photochemical cycles as well as the net ozone destruction, and further detailed observational work (some of which is already in progress) should help define--if not explain--the existence of potential problems. Direct observations of both $ClONO_2$ and HOCl would of course be very useful. To first order, at least, the diurnal variation of ClO can be explained by current theory.

References

Anderson, J. G., R. E. Shetter, H. J. Grassel, and J. J. Margitan, Stratospheric free chlorine measured by balloon-borne in situ resonance fluorescence, J. Geophys. Res., 85, 2869, 1980.

Bangham, M. J., A. Bonetti, R. H. Bradsell, B. Carli, J. G. Harries, F. Mencaraglia, D. G. Moss, J. Pollitt, E. Rossi, and N. R. Swann, New measurements of stratospheric composition using submillimeter and infrared emission spectroscopy, Unpublished manuscript, 1980.

Berg, W. W., P. J. Crutzen, F. E. Grabek, and S. N. Gitlin, First measurements of total chlorine and bromine in the lower stratosphere, Geophys. Res. Lett., 7, 937, 1980.

Buijs, H. L., G. L. Vail, G. Tremblay, and D.J.W. Kendall, Simultaneous measurements of the volume mixing ratio of HF and HCl in the stratosphere, Geophys. Res. Lett., 7, 205, 1980.

Cadle, R. D., P. Crutzen, and D. Ehhalt, Heterogeneous chemical reactions in the stratosphere, J. Geophys. Res., 80, 3381, 1975.

De More, W. B., R. T. Watson, D. M. Golden, R. F. Hampson, M. J. Kurylo, C. J. Howard, M. J. Molina, and A. R. Ravishankara, Chemical Kinetics and Photochemical Data for Use in Stratospheric Modeling, JPL Publication 82-57, Jet Propulsion Laboratory, Pasadena, California, 1982.

Evans, W.F.J., J. B. Kerr, D. I. Wardle, J. C. McConnell, B. A. Ridley, and H. I. Schiff, Intercomparison of NO, NO_2, and HNO_3 measurements with photochemical theory, Atmosphere, 14, 189, 1976.

Evans, W.F.J., C. T. McElroy, and J. B. Kerr, Simulation of the October 23, 1980 Stratoprobe flight, Geophys. Res. Lett., 9, 223, 1982.

Farmer, C. B., O. F. Raper, B. D. Robbins, R. A. Toth, and C. Muller, Simultaneous spectroscopic measurements of stratospheric species: O_3, CH_4, CO, CO_2, N_2O, HCl, and HF at northern and southern mid-latitudes, J. Geophys. Res., 85, 1621, 1980.

Harries, J. E., Ratio of HNO_3 to NO_2 concentrations in the daytime stratosphere, Nature, 274, 235, 1978.

Herman, J. R., The response of stratospheric constituents to a solar eclipse, sunrise, and sunset, J. Geophys. Res., 84, 3701, 1979.

Hudson, R. D. (editor-in-chief) et al. (16 editors), The Stratosphere 1981: Theory and Measurements, WMO Global Ozone Research and Monitoring Project Report No. 11, 1982.

Jayanta, R.K.M., R. Simonaitis, and J. Heicklen, The photolysis of chlorofluoromethanes in the presence of O_2 or O_3 at 213.9 nm and their reactions with $O(^1D)$, J. Phys. Chem., 4, 381, 1975.

Keyser, L. F., Kinetics of the reaction $O + HO_2 \rightarrow OH + O_2$ from 229 to 372 K, J. Phys. Chem., 86, 3439, 1982.

Kircher, C. C., and S. P. Sander, Kinetics and mechanism of HO_2 and DO_2 disproportionations, submitted to J. Phys. Chem., 1983.

Ko, M.K.W., and N. D. Sze, Effect of recent rate data revisions on stratospheric modeling, Geophys. Res. Lett., 10, 341, 1983.

Lazrus, A. L., B. W. Gandrud, J. Greenberg, J. Bonelli, E. Mroz, and W. A. Sedlacek, Mid-latitude seasonal measurements of stratospheric and chlorine vapor, Geophys. Res. Lett., 4, 587, 1977.

Leu, M. T., Kinetics of the reaction $O + ClO \rightarrow Cl + O_2$, submitted to J. Phys. Chem., 1983.

Logan, J. A., M. J. Prather, S. C. Wofsy, and M. B. McElroy, Atmospheric

chemistry: Response to human influence, Phil. Trans. Roy. Soc., 290, 187, 1978.

Marché, P., A. Barbe, C. Secroun, J. Corr, and P. Jouve, Mesures des acides fluorhydrique et chlorhydrique dans l'atmosphère par spectroscopie infrarouge à partir du sol, C. R. Acad. Sci. Paris, 290, 369 1980.

Margitan, J. J., Chlorine nitrate: The sole product of the $ClO + NO_2 + M$ recombination, J. Geophys. Res., 88, 5416, 1983.

Marsh, D., and J. Heicklen, Photolysis of fluorotrichloromethane, J. Phys. Chem., 69, 4410, 1965.

Menzies, R. T., Remote measurement of ClO in the stratosphere, Geophys. Res. Lett., 6, 151, 1979.

Menzies, R.T., A re-evaluation of laser heterodyne radiometer ClO measurements, Geophys. Res. Lett., in press, 1983.

Miller, C., D. L. Filkin, A. J. Owens, J. M. Steed, and J. P. Jesson, A two-dimensional model of stratospheric chemistry and transport, J. Geophys. Res., 86, 12039, 1981.

Milstein, R., and F. S. Rowland, Quantum yield for the photolysis of CF_2Cl_2 in O_2, J. Phys. Chem., 79, 669, 1975.

Molina, L. T., and J. M. Molina, Chemistry of fluorine in the stratosphere, 182nd American Chemical Society National Meeting, New York, 1982.

Mroz, E. J., A. J. Lazrus, and J. Bonelli, Direct measurements of stratospheric fluoride, Geophys. Res. Lett., 4, 149, 1977.

Murcray, D. G., A. Goldman, F. H. Murcray, F. J. Murcray, and W. J. Williams, Stratospheric distribution of $ClONO_2$, Geophys. Res. Lett., 6, 857, 1979.

NRC, Causes and effects of stratospheric ozone reduction: An update, National Academy Press, Washington, D.C., 1982.

Parrish, A., R. L. de Zafra, P. M. Solomon, J. W. Barrett, and E. R. Carlson, Chlorine oxide in the stratospheric ozone layer: Ground-based detection and measurement, Science, 211, 1158, 1981.

Ralph, D. G., and R. P. Wayne, Photochemistry of the ozone-holocarbon system, J. Photochem., 17, 405, 1981

Rebbert, R. E., Gas phase photolysis of CF_2Cl_2, $CFCl_3$ and CCl_4 in the presence of bromine at 213.9,163.3, 147.0 and 123.6 nm, J. Photochem., 8, 363, 1978.

Rebbert, R. E., and P.J. Ausloos, Photodecomposition of $CFCl_3$ and CF_2Cl_2, J. Photochem., 4, 419, 1975.

Rebbert, R. E., and P. J. Ausloos, Gas phase photodecomposition of carbon tetrachloride, J. Photochem., 6, 265, 1976/77.

Rogers, J. D., M. J. Mumma, T. Kostiuk, D. Deming, J. J. Hillman, and J. Faris, unpublished manuscript, 1982.

Rudolph, J., D. H. Ehhalt, and A. Tönnissen, Vertical profiles of ethane and propane in the stratosphere, J. Geophys. Res., 86, 7267, 1981.

Solomon, P. M., R. L. de Zafra, A. Parrish, and J. W. Barrett, manuscript in preparation, 1983.

Sridharan, U. C., L. X. Qiu, and F. Kaufman, Kinetics and product channels of the reactions of HO_2 with O and H atoms at 296 K, J. Phys. Chem., 86, 4569, 1982.

Stolarski, R. S., and R. D. Rundel, Fluorine chemistry in the stratosphere, Geophys. Res. Lett., 2, 443, 1975.

Suong, J. Y., and R. W. Carr, Jr., The photo-oxidation of 1,3-dichlorotetrafluoroacetone: Mechanism of the reaction of CF_2Cl with oxygen,

J. Photochem., 19, 295, 1982.

Sze, N. D., Stratospheric fluorine: A comparison between theory and measurements, Geophys. Res. Lett., 5, 781, 1978.

Sze, N. D., and M..W. Ko, The effects of the rate for $OH + HNO_3$ and HO_2NO_2 photolysis on the stratospheric chemistry, Atmos. Environ., 15, 1301, 1981.

Traub, W. A., and K. V. Chance, Stratospheric HF and HCl observations, Geophys. Res. Lett., 8, 1075, 1981.

Waters, J. W., J. C. Hardy, R. F. Jarnot, and H. M. Pickett, Chlorine monoxide radical, ozone and hydrogen peroxide: Stratospheric measurements by microwave limb sounding, Science, 214, 61, 1981.

Weinstock, E. M., M. J. Phillips, and J. G. Anderson, In situ observations of ClO in the stratosphere: A review of recent results, J. Geophys. Res., 86, 7273, 1981.

Wuebbles, D. J., and J. S. Chang, A study of the effectiveness of the Cl_x catalytic ozone loss mechanism, J. Geophys. Res., 86, 9869, 1981.

Zander, R., Recent observations of HF and HCl in the upper stratosphere, Geophys. Res. Lett., 8, 413, 1981.

Chapter 5

OZONE SPECIES AND DISCREPANCIES

5.1 Upper Stratospheric Ozone

Given the uncertainties in current photochemical data and observations of trace species in the stratosphere, we wish to bring attention to several discrepancies between updated models and observations of ozone, with potentially significant implications in terms of our understanding of present and future ozone concentrations. Although we cannot suggest definite solutions to these problems at this time, we present our way of thinking and test various hypotheses. The problems raised in the next two sections might turn out not to be real, given the limited observational evidence, but this section focuses on the better defined question of mid-latitude ozone abundances in the upper stratosphere, above about 35 km. We will see that a discrepancy of about 50% exists between measurements and theory. While this might not seem extremely significant, and comparisons of other constituents can show similar differences, we stress that ozone has been accurately measured by a wide variety of techniques and does not show much seasonal change (< 20%) at mid-latitudes, near 40 km. Even the lower limits of most observations are higher than our current model predictions and we believe that this systematic difference is real. Moreover, as we will show, the sensitivity of upper stratospheric ozone to various model input parameters or other species' concentrations is not very high, although $[O_3]$ depends on many photochemical processes and catalytic cycles in that altitude range.

5.1a Model comparison with observations

Theoretical and observational vertical profiles of ozone are compared in Figure 54. The U. S. Standard Atmosphere 1976 follows the observations summarized by Krueger and Minzner [1976], most of which are from optical (250-320 nm) ozone-sounding rocket measurements between 30 and 60°N latitude. The $\pm 1\sigma$ range of variability is indicated. The accuracy in individual determinations of $[O_3]$ is 15-20%, but the mean of these data and almost every single sounding [see also Krueger, 1973] yield upper stratospheric ozone abundances higher than our typical (32°N latitude, equinox) model. The same holds for the preliminary results reported in Hudson et al. [1982], concerning the International Ozone Rocket Intercomparison (IORI), which represents data obtained more recently by several types of sensors (optical, infrared and chemiluminescent). The standard deviation in this case relates to the intercomparison between various instruments flown nearly simultaneously, as opposed to the U. S. Standard Atmosphere 1976 estimate of ozone variability, which--to some extent--includes daily, seasonal, and yearly variations. The recent model results (30°N latitude, equinox) of Ko and Sze [1983] are also shown for comparison in Figure 54. In the upper stratospheric region, where disagreement between theory and data exists and where ozone should be in photochemical equilibrium, the two models agree to within a few percent. This should be the case, since both models are using similar photochemical data [mostly from DeMore et al., 1982] and reduced O_2 absorption cross sections [see model B of Ko and Sze, 1983]. We note that our model has been corrected for the small (< 10%) effects due to diurnal averaging (see Chapter 1), and represents true

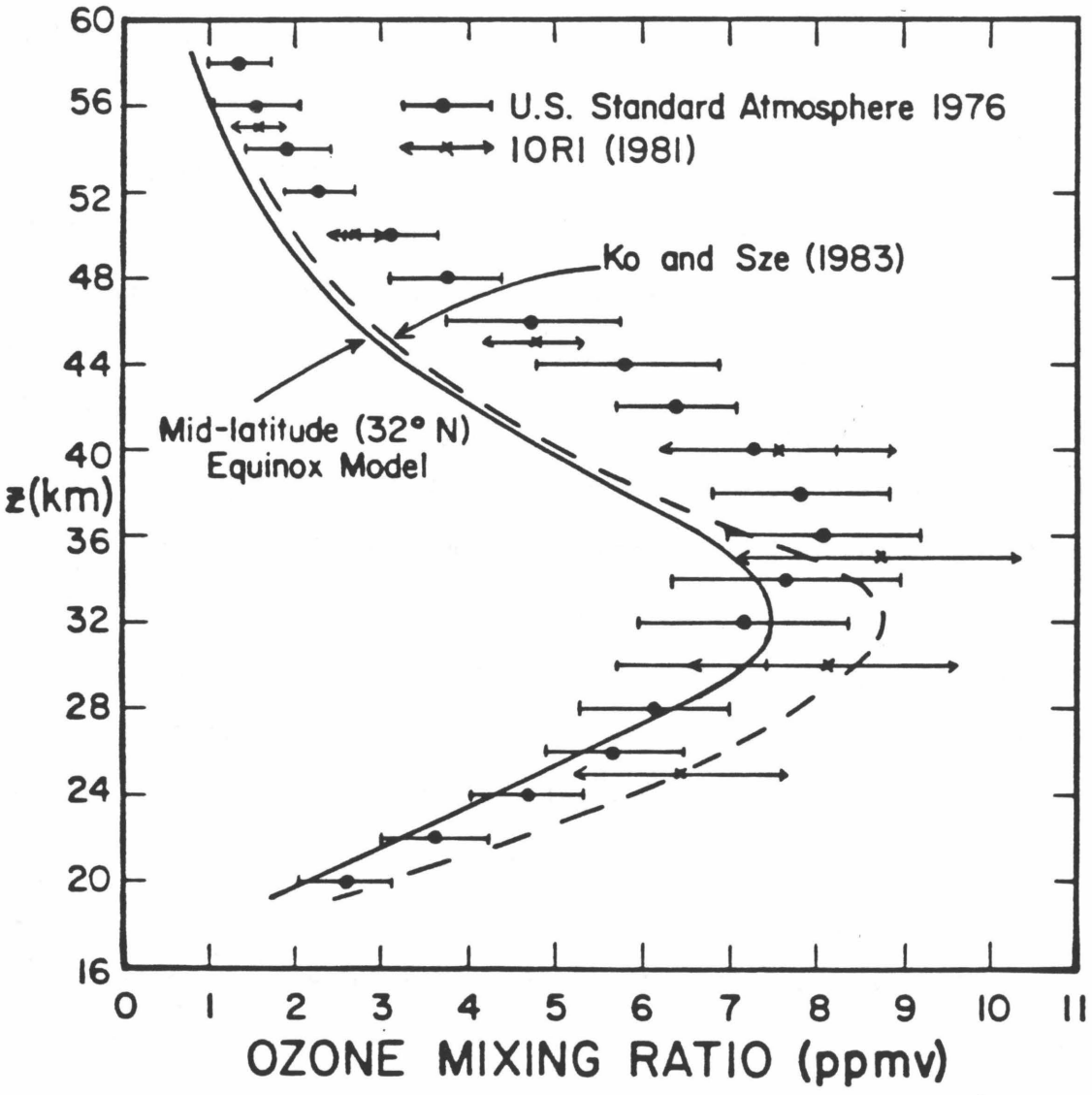

Figure 54. Theoretical and observed mid-latitude ozone vertical profiles. Note significant discrepancy between models and measurements in the 35-55 km range.

diurnal average values. Direct and indirect vertical transport effects and variations between the model atmospheres can cause differences between models below about 30 km (where Ko and Sze find somewhat more ozone than in our model). Another example of the systematic difference between our model and observations is illustrated in Figure 55. The data of interest in the 35-50 km region (5-1 mb) come from the Limb Infrared Monitor of the Stratosphere (LIMS) experiment on Nimbus 7 [Remsberg et al., 1983]. Figures 55a and 55b, taken from the above reference, also display the results of balloon-borne sensors flown at times and places close to the tangent point LIMS emission measurements. The LIMS experiment obtained many vertical ozone profiles over a 7 month period and the two profiles shown here should be typical of mid-latitudes and are in agreement with the data of Figure 54. The extent to which the ozone discrepancy reaches into the mesosphere is not clear. The lower limits of the data in Figure 54 are close to our model values, but the relative variability becomes larger in the mesosphere. Solomon et al. [1983] have found that their mesospheric model results are somewhat low, compared to Solar Mesosphere Explorer (SME) ozone observations. The analysis of Allen et al. [1983] shows that reasonable agreement can be found between models and observations in the mesosphere, although their results are also on the low side of measurements in the lower mesosphere. We have used the same model as in Figure 54 for comparison to the LIMS data, although the LIMS profiles refer to two slightly different latitudes and different seasons (October and May). Our model results in the upper stratosphere show little sensitivity to latitude and solar declination alone, but a comparison with average profiles is recommended. Observed upper stratospheric seasonal

Figure 55. a) Nimbus 7 LIMS ozone retrievals over Palestine, Texas, on October 31, 1978, along with similar results obtained from ECC and Dasibi measurements on balloon underflight (see Remsberg et al., 1983).

b) LIMS and ECC ozone data over Wallops Island, on May 1, 1979. In both cases, same model (32°N, equinox) is used to illustrate discrepancy in upper stratospheric ozone.

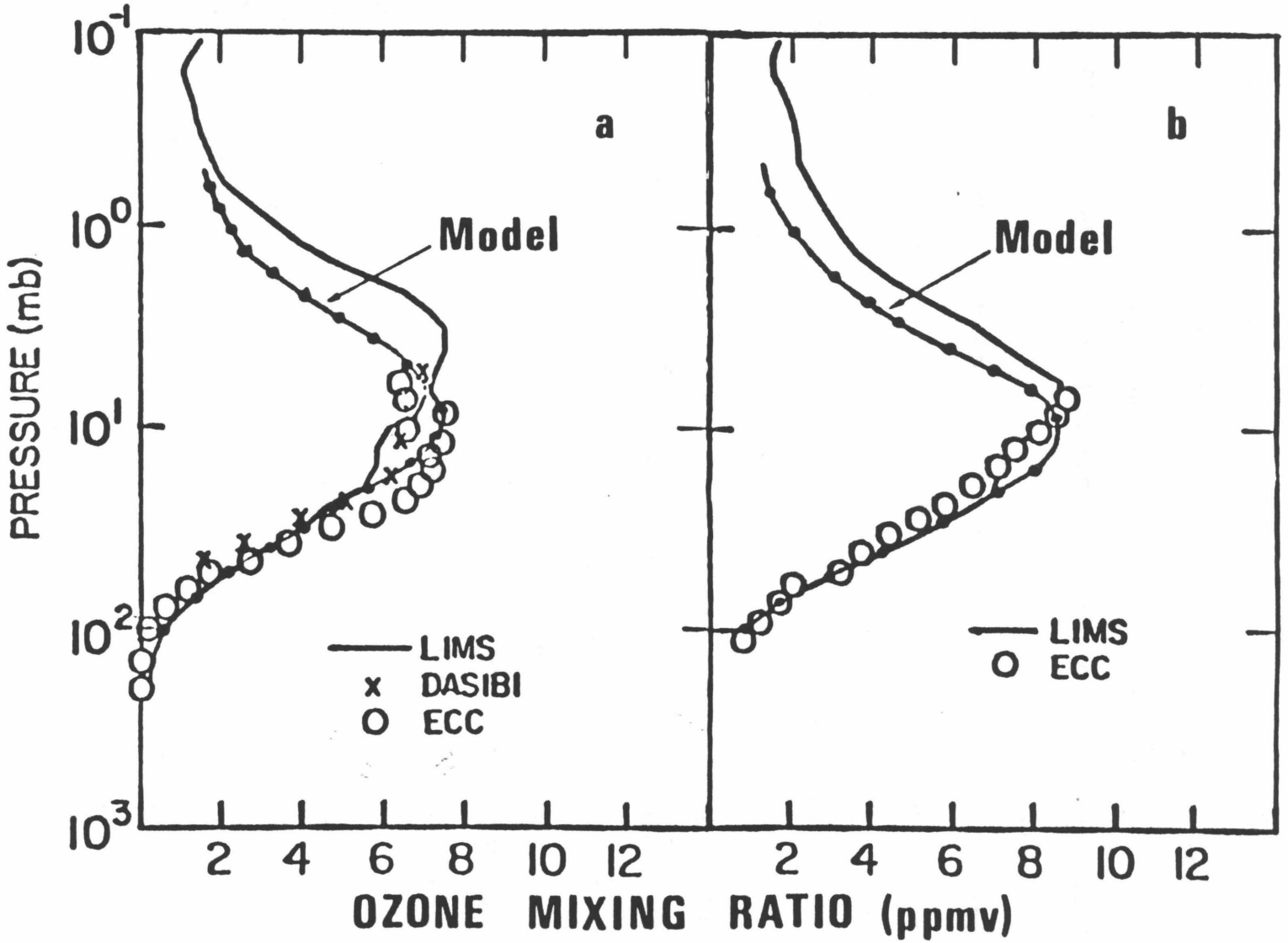
PRESSURE (mb)
10^{-1}
10^{0}
10^{1}
10^{2}
10^{3}
a
b
Model
Model
LIMS
x DASIBI
O ECC
LIMS
O ECC
2 4 6 8 10 12
2 4 6 8 10 12
OZONE MIXING RATIO (ppmv)

variations are generally less than 15-20% at mid-latitudes, as discussed by De Luisi et al. [1979], McPeters [1980], Prather [1981], and Frederick et al. [1983]. Ozone is quite sensitive to temperature [see also Krueger et al., 1980], as discussed further below, and the seasonal variations are reasonably well understood in terms of solar radiation and temperature changes. Other ozone observations generally fall within the limits shown in Figure 54. This holds, for example, for the early Ogo 4 BUV data [London et al., 1977], as well as for the recent SME satellite observations [Rusch et al., 1983], and the measurements from the satellite sensor SAGE (Stratospheric Aerosol and Gas Experiment) described by Reiter and McCormick [1982]. The balloon-borne measurements presented by Mauersberger et al. [1981] also show a similar trend, although they apply mostly to altitudes below 38 km. In summary, the mean observed ozone abundances in the upper stratosphere are in disagreement with model results, given the typical measurement uncertainties of less than 20%, the variety of techniques used, and the limited seasonal (and diurnal) variations.

There exists one experiment (see Anderson,1980) during which both ozone and atomic oxygen were measured simultaneously (Dasibi instrument and resonance fluorescence, respectively) from a balloon flight above Palestine, Texas (32°N latitude, 2 December 1977). The atomic oxygen observations (smoothed profile sampled every 2 km with ±25% uncertainties) are compared to our model in Figure 56. As shown also in Anderson [1980], there is good agreement between the slope and magnitude of the [O] measurements (mean data) and model results, although observed individual profiles (not shown here) show small scale structure as large as

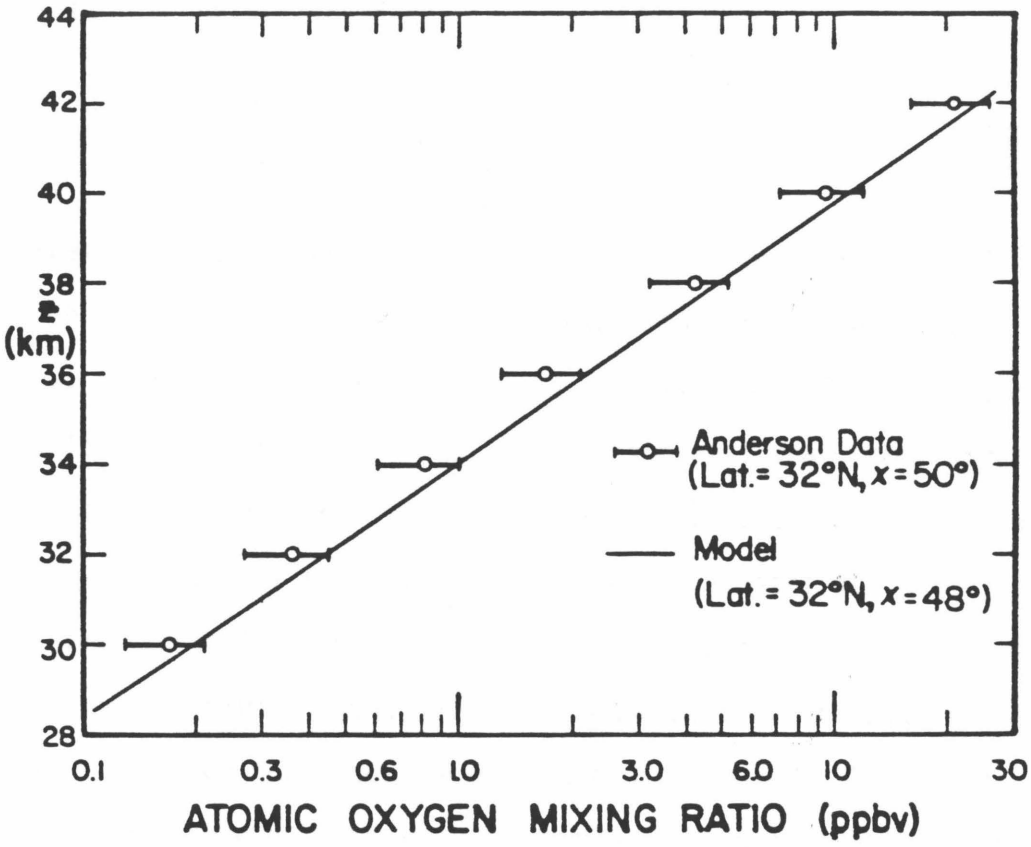

Figure 56. Atomic oxygen resonance fluorescence observations (2 December 1977, see Anderson, 1980) compared to our model for similar solar zenith angle. We show a smoothed version of the data between 30 and 42 km, sampled every 2 km.

a factor of two in some cases. The ozone observations carried out on December 2, 1977, in conjunction with the atomic oxygen data presented here, are displayed in Figure 57, along with our ozone model and other data shown previously. The similarity between Anderson's ozone data and our model profile is striking, which leads to excellent agreement [see also Anderson, 1980] between the only measurement of $[O]/[O_3]$ and the expected ratio in the stratosphere:

$$R_o = \frac{[O]}{[O_3]} = \frac{j_3 + j_4}{k_{31}[O_2][M]} \tag{49}$$

The fact that this particular ozone profile departs from the generally observed behavior above 35 km, in a way very similar to current photochemical theory, is puzzling and not explained at this time. A recent ozone intercomparison shown in Hudson et al. (1982) suggests that upper stratospheric ozone measurements obtained by Dasibi instruments are lower than other data by 30% or more (this might be related to losses at the cell's walls). Given the limited nature of the $[O]/[O_3]$ determination and the possibly systematic errors noted above, it could be that the real value of this ratio is lower than model predictions by as much as 50%. The apparent agreement between this measured ratio (Anderson, 1980) and theoretical results should thus be considered with caution. More evidence is needed in order to ascertain the value of this important quantity.

5.1b Model sensitivity and uncertainties

We now wish to address the possible model uncertainties that could help resolve the upper stratospheric ozone discrepancy. The various

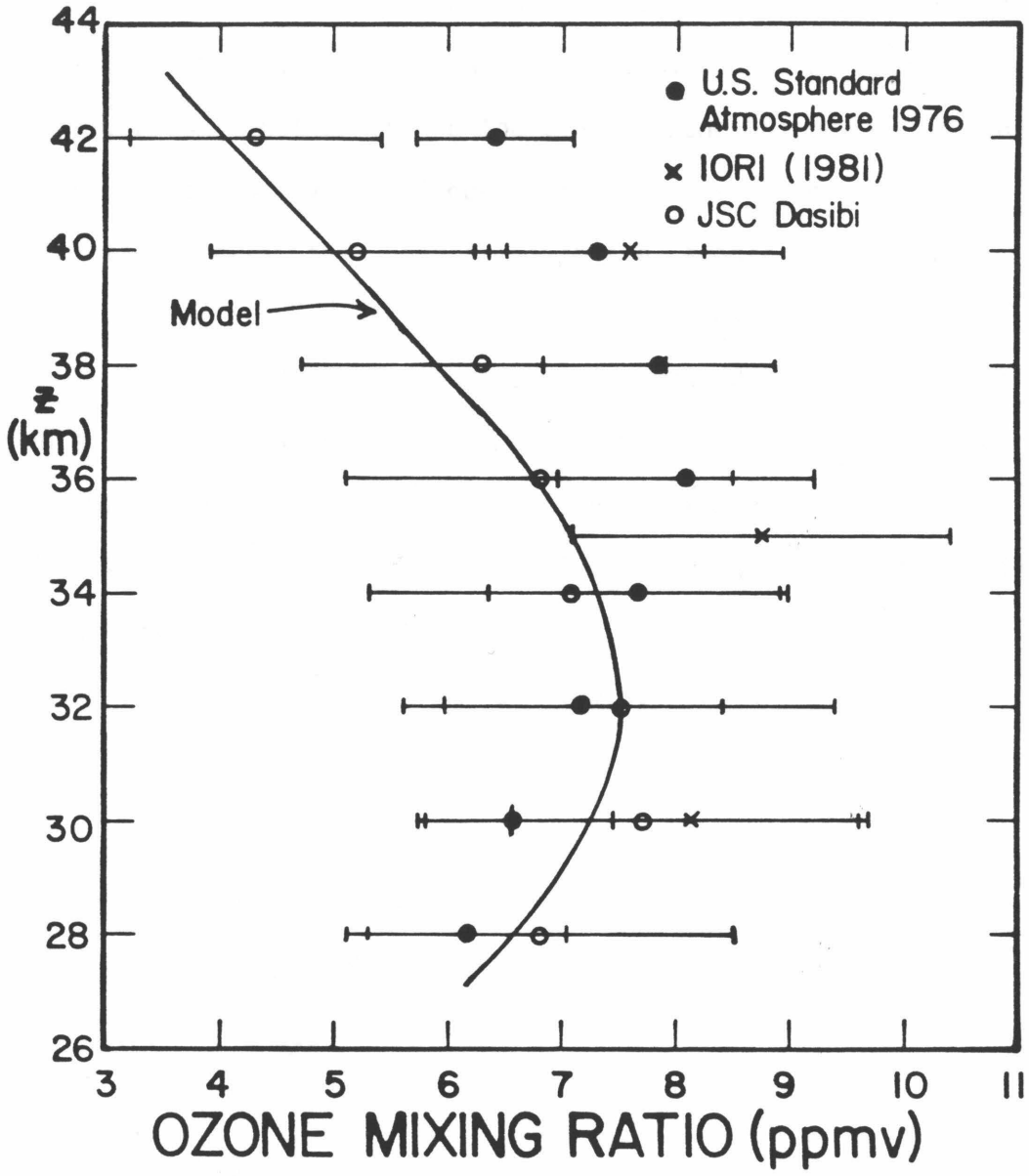

Figure 57. Same ozone model and data as in Figure 54, but over a more limited altitude range. Also shown are the results from the Johnston Space Center Dasibi instrument of D.E. Robbins and J.G. Carnes, obtained simultaneously with the atomic oxygen abundances shown in previous figure; these Dasibi ozone data agree with our model, but not with other measurements.

photochemical cycles affecting ozone have been extensively discussed elsewhere and some of the key references were alluded to in the Introduction. Clearly, pure oxygen chemistry cannot fully describe the ozone concentrations in the stratosphere [see also Nicolet, 1975; Johnston, 1975]. Solomon et al. [1980] further tested the global ozone balance by including nitrogen dioxide observational constraints. A complete description of ozone (particularly in the upper stratosphere) should include losses due to all four catalyzing radical groups (O_x, NO_x, ClO_x, and HO_x). Johnston and Podolske [1978] have considered in great detail the various production and loss mechanisms for odd oxygen and conclude that the net destruction of ozone in the stratosphere is dominated by six or seven chemical reactions which take part in catalytic cycles. Furthermore, in the upper stratospheric region of interest here, the main HO_x rate-limiting step is the $O + HO_2$ reaction, and the set of important odd oxygen destruction reactions becomes:

$$O + O_3 \xrightarrow{k_{32}} 2\,O_2 \tag{50a}$$

$$O + NO_2 \xrightarrow{k_{35}} NO + O_2 \tag{50b}$$

$$O + HO_2 \xrightarrow{k_{40}} OH + O_2 \tag{50c}$$

$$O + ClO \xrightarrow{k_{61}} Cl + O_2 \tag{50d}$$

with minor contributions from

$$O_3 + HO_2 \xrightarrow{k_{38}} OH + 2\,O_2 \tag{50e}$$

and

$$O_3 + H \xrightarrow{k_{41}} OH + O_2 \tag{50f}$$

The source of odd oxygen, which breaks the O_2 bond, is provided by

$$O_2 + h\nu \xrightarrow{j_1} 2\,O \tag{51}$$

with negligible contribution from the channel forming $O(^1D)$. In photochemical steady-state, the balance between those processes that produce or destroy (via catalytic cycles) two odd oxygen members can be written as:

$$P(O_x) = L(O_x) = L_{O_x} + L_{HO_x} + L_{NO_x} + L_{ClO_x} \tag{52a}$$

where

$$P(O_x) = 2j_1[O_2] = 2J_1 \tag{52b}$$

$$L_{O_x} = 2k_{32}[O][O_3] = 2K_{32} \tag{52c}$$

$$L_{HO_x} = 2\{k_{40}[O][HO_2] + k_{38}[O_3][HO_2] + k_{41}[O_3][H]\}$$
$$= 2\{K_{40} + K_{38} + K_{41}\} \tag{52d}$$

$$L_{NO_x} = 2k_{35}[O][NO_2] = 2K_{35} \tag{52e}$$

and

$$L_{ClO_x} = 2k_{61}[O][ClO] = 2K_{61} \tag{52f}$$

The importance of these various destruction rates is shown as a percentage of $P(O_x)$ in Table IV, for altitudes between 32 and 48 km, and 32°N latitude. These diurnal average results are similar to the results shown in Hudson et al. [1982], although the importance of the chlorine cycle is higher near 40 km and above, in our model. This is due to our higher ClO abundances at those altitudes, and a reduction in $k_{61}(O + ClO)$ --as

Table IV

Relative Importance* of Odd Oxygen Destruction Rates

z (km)	L_{O_x}	L_{HO_x}	L_{NO_x}	L_{ClO_x}
32	9	6	74	8
36	9	6	68	16
40	11	8	53	27
44	16	19	31	34
48	20	39	13	28

*Numbers represent percentages relative to $P(O_x)$

discussed in the previous chapter--would further enhance the relative effect of chlorine radicals in the upper stratosphere. The sum of the contributions in Table IV at any given altitude is very close to 100%. Although destruction by NO_x dominates below 40 km, all four loss processes are seen to play a non-negligible role in the 40-50 km range, where significant differences exist between observed and theoretical ozone profiles. If we include only the major HO_x loss term ($2K_{40}$) and make use of the instantaneous equilibrium relation (49) between [O] and $[O_3]$, we can replace relation (52) by a quadratic equation in $[O_3]$

$$k_{32}[O_3]^2 + (\Sigma \ell)\,[O_3] - J_1/R_o = 0 \qquad (53)$$

which can be solved for an estimated ozone concentration

$$[O_3]^e = \frac{(4k_{32}\, J_1/R_o + (\Sigma \ell)^2)^{1/2} - \Sigma \ell}{2k_{32}} \qquad (54)$$

with $$\Sigma \ell = \ell_{HO_x} + \ell_{NO_x} + \ell_{ClO_x}$$

$$= k_{40}[HO_2] + k_{35}[NO_2] + k_{61}[ClO]$$

and

$$R_o = (j_3 + j_4) / k_{31}[O_2][M], \quad \text{as before.}$$

If the reactions involving $HO_2 + O_3$ and $H + O_3$ were considered as well, the above equation for $\Sigma \ell$ would simply include two additional terms ($k_{38}[HO_2] + k_{41}[H]$) of smaller importance. An expression such as (54) can adequately represent ozone concentrations in the upper stratosphere, given the appropriate radical concentrations, as discussed below. However, the ozone sensitivity to various parameters is not immediately apparent

from this equation, since there is an implicit dependence on rate constants through the radical concentrations, and changes in one radical can indirectly affect the other terms. Also, the loss terms enter in a nonlinear fashion in equation (54) and $[O_3]$ itself affects the radical concentrations. An explicit equation for ozone in terms of long-lived species only is not readily inferred for the stratosphere, whereas the simpler mesospheric O_x-HO_x system lends itself more easily to such a relationship [Allen et al., 1983].

Since the odd oxygen photochemical lifetime is of order $[O_3]/2J_1$, ranging from a few hours near the stratopause to over a year in the lower stratosphere, ozone displays little diurnal variation below 50 km. The radical concentrations $[HO_2]$, $[NO_2]$, and [ClO] that enter in (54), however, do vary significantly during a 24 hour period. The diurnally-invariant ozone abundances will therefore be in equilibrium with time-averaged radical concentrations. Daytime averages, rather than 24 hour averages, provide a good ozone estimate ($[O_3]^e$), when compared to the model results (obtained by simultaneous solution of all continuity equations). The difference between the use of $\bar{n}$(24 hr) and $\bar{n}$(12 hr) for the radical abundances in (54) is illustrated in Figure 58. The latter method of evaluation is very close to our model results (32°N latitude, -11° declination). If we use $[\overline{HO_2}]$, $[\overline{NO_2}]$ and $[\overline{ClO}]$ 24 hour averages instead, the $[O_3]^e$ values are up to a factor of two smaller than expected. The explanation [see Kurzeja, 1977], lies in the fact that the ozone balance depends on average rates of the form $\overline{k[X][Y]}$ rather than on the separated $k[\bar{X}][\bar{Y}]$ product. In particular, the accurate rate expression (52) implies essentially no ozone loss at night, since the key [O] radical concentration disappears rapidly after sunset.

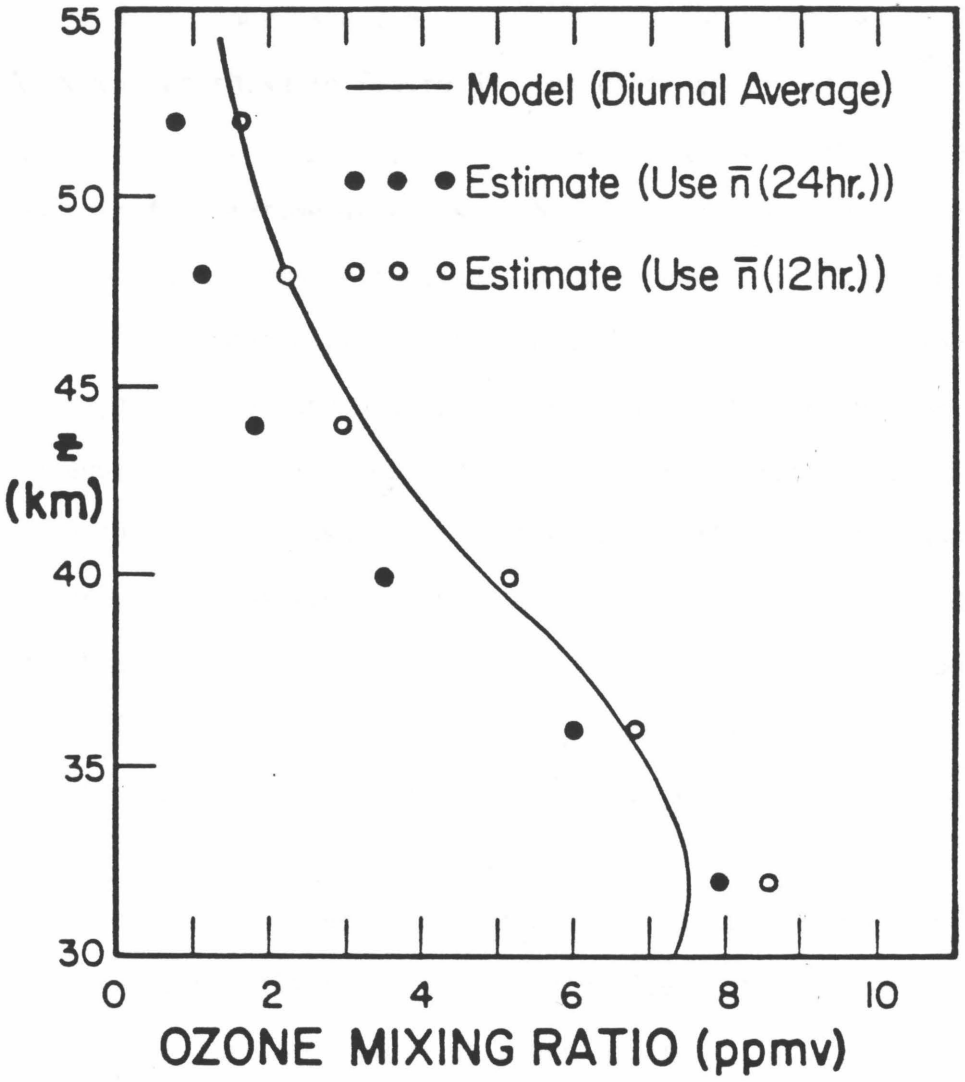

Figure 58. Diurnal average model ozone vertical profile compared to estimates using equation (54), with HO_2, NO_2, and ClO concentrations averaged over 24 hours ($\bar{n}$(24hr.)) or only over daytime hours ($\bar{n}$(12hr.)). Latter estimate yields better fit to model. Results are for 32°N latitude, -11° solar declination.

However, equation (54) depends explicitly only on average HO_2, NO_2 and ClO concentrations. While $[HO_2]$ and [ClO] show significant nighttime decreases, $[NO_2]$ increases at night due to the $NO + O_3$ reaction and the absence of NO_2 photolysis. This leads to the different diurnal (24 hour) and daytime ($\sim$ 12 hour) average radical abundances displayed in Figure 59. Moreover, as shown in Figure 60, the differences between $\overline{k[X][Y]}$ and $k[\bar{X}][\bar{Y}]$ are significantly larger for 24 hour averages (true diurnal average) than for daytime averages. These factors combine to explain the reliable ozone estimate obtained by using equation (54) with daytime average radical concentrations, since nighttime ozone destruction is negligible, regardless of the NO_2 abundance. Used with the appropriate (simultaneous) daytime-averaged observations of key radicals, equation (54) could therefore be used to test the ozone balance in the upper stratosphere. Alternatively, the rate equation (52) can be tested if [O] is observed as well (and R_o is not assumed known). A partial comparison was made by Anderson [1980], but the data necessary for a meaningful test of upper stratospheric ozone balance have not yet been satisfactorily measured.

Solutions to the ozone abundance problem could in principle involve one or more of the following (not entirely independent) answers: 1) The current photochemical laboratory data are sufficiently uncertain as to not preclude typical mid-latitude ozone profiles. 2) The radical concentrations affecting ozone, and the abundances of longer-lived species related to these radicals, are not in good agreement with average daytime observations (what role does transport really play?). 3) The model description is lacking a significant "ingredient." We note that any

Figure 59. Diurnal (24 hr.) and daytime average concentrations for O, HO_2, NO_2, and ClO (same model as in Figure 58), obtained by integration of diurnal run results. Note behavior of NO_2, which shows a nighttime increase in concentration, rather than the decrease seen in other radicals.

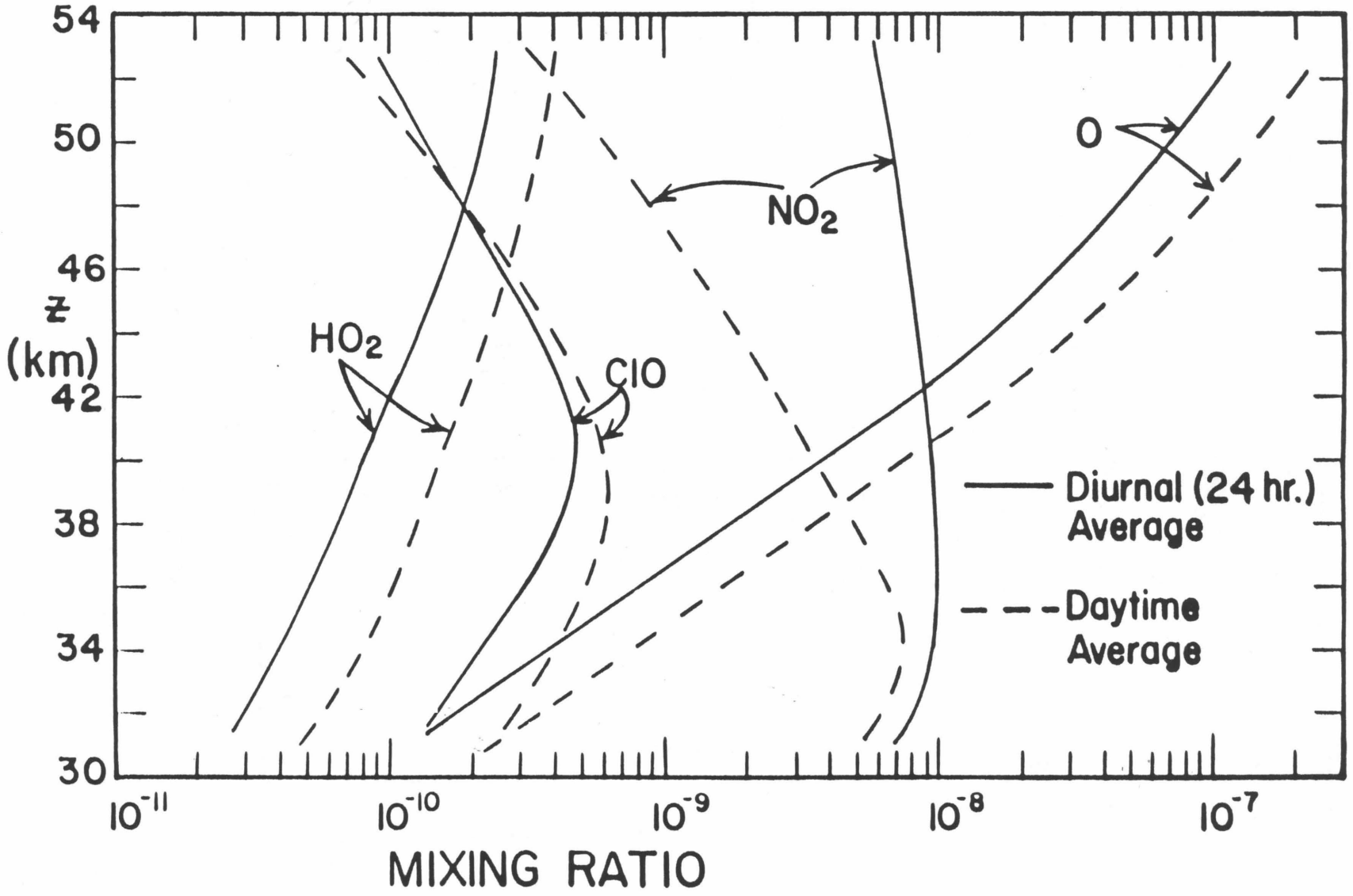
54
50
46
z
(km)
42
38
34
30
10^{-11}
10^{-10}
10^{-9}
10^{-8}
10^{-7}
MIXING RATIO
HO_2
ClO
NO_2
O
Diurnal (24 hr.) Average
Daytime Average

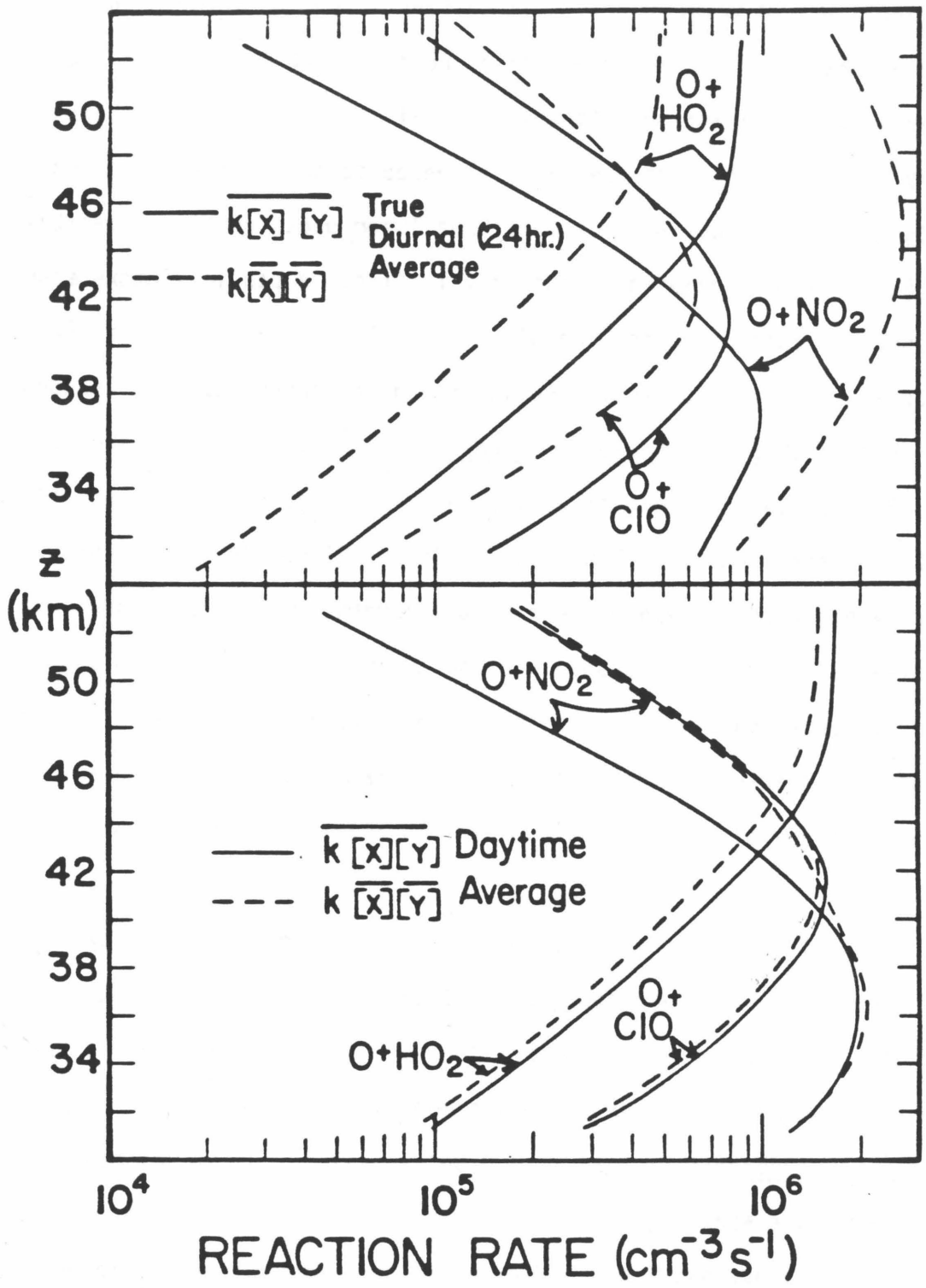

Figure 60. Differences between reaction rates $\overline{k[X][Y]}$ and $k\overline{[X]}\overline{[Y]}$ for odd oxygen loss terms above 30 km. Daytime-averaged values (bottom curves) lead to better agreement between above quantities.

postulated solution that significantly affects ozone in the right way should be regarded with caution if it produces a disagreement in other stratospheric gases, or if it significantly worsens the mesospheric ozone profile fit. As stressed earlier, equation (54) can only give an indication of the ozone model sensitivity to various terms. An approximate example of ozone sensitivity to the main terms ($\Sigma \ell$ and J_1/R_o) in (54) is shown in Figure 61. The enclosed area delineates the percent changes that are required in our current ozone model to fit the upper and lower bounds of the U. S. Standard Atmosphere 1976 data (see Figure 54). As expected, the ozone sensitivity is greater towards J_1/R_o than towards $\Sigma \ell$. Between 40 and 50 km, a significant enhancement in J_1/R_o would be required in order to match the observed mean, while a large reduction in the loss term $\Sigma \ell$ would be necessary. Such changes are quite large, given current uncertainties in laboratory data, but this approach is very approximate. We now describe the results of a more exact and detailed analysis of the $[O_3]$ sensitivity to various parameters.

We have performed sensitivity tests for our mid-latitude (32°N) equinox model. Diurnal average steady-state results are shown in Figure 62, in terms of the percent increase in ozone abundance arising from a change in input photochemical data; the upper and lower bounds required to fit the limits of the U. S. Standard Atmosphere 1976 are shown, as in the previous figure. We typically change a parameter by a factor of two (increase or decrease); diurnal average tests--although economical--are not exactly accurate, but these are mainly intended to give us a reasonable idea of the sensitivity to various model changes.

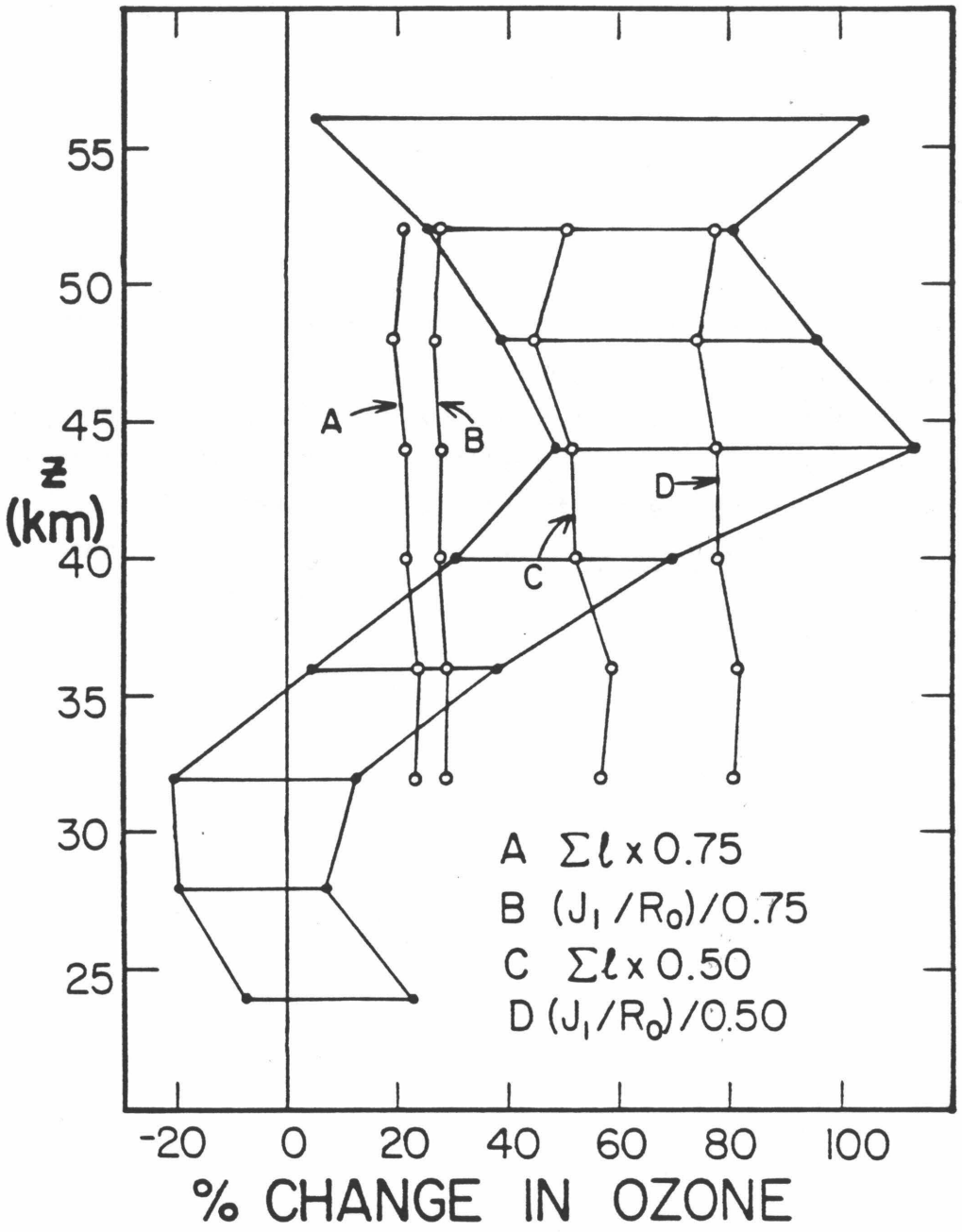

Figure 61. Approximate example of the ozone sensitivity to the two main terms ($\Sigma\ell$ and J_1/R_0) in our ozone abundance estimate (equation (54)). The enclosed area represents the percent increase needed in our model ozone concentrations to fit the bounds of the U.S. Standard Atmosphere 1976 data.

Figure 62. Model tests (steady-state diurnal average runs) of the ozone sensitivity to various photochemical parameters, classified according to O_x, HO_x, NO_x, and ClO_x terms. Labeled curves represent the effect on ozone concentrations of changes in model parameters, as indicated in the figure and discussed in the text. The percent ozone increases necessary to fit the upper and lower bounds of the U.S. Standard Atmosphere 1976 data are indicated by enclosed area , as in Figure 61.

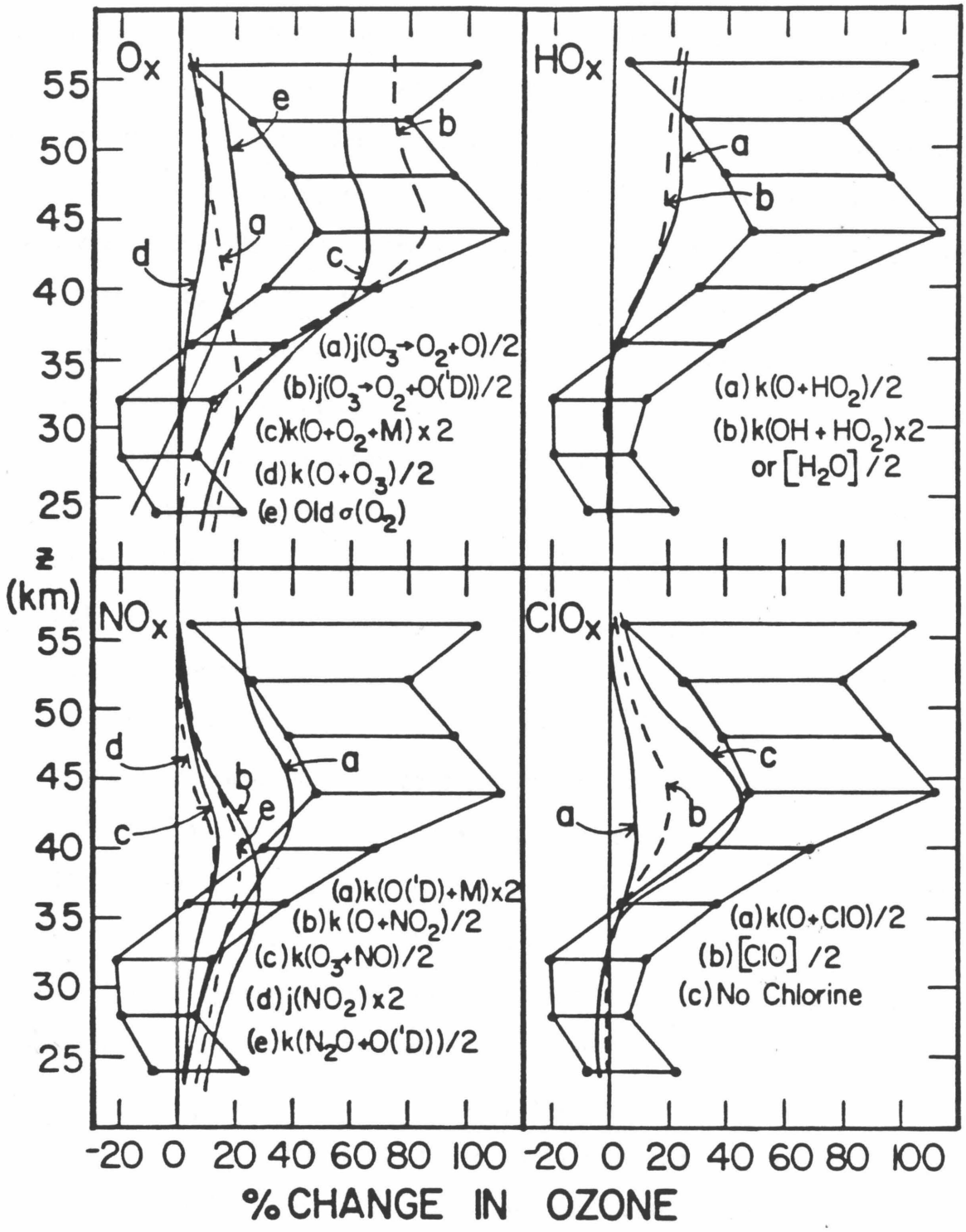
Ox
HOx
NOx
ClOx
z (km)
55
50
45
40
35
30
25
(a) j(O3→O2+O)/2
(b) j(O3→O2+O('D))/2
(c) k(O+O2+M) x 2
(d) k(O+O3)/2
(e) Old σ(O2)
(a) k(O+HO2)/2
(b) k(OH + HO2)x2
or [H2O] /2
(a) k(O('D)+M)x2
(b) k(O+NO2)/2
(c) k(O3+NO)/2
(d) j(NO2) x2
(e) k(N2O+O('D))/2
(a) k(O+ClO)/2
(b) [ClO] /2
(c) No Chlorine
-20 0 20 40 60 80 100
-20 0 20 40 60 80 100
% CHANGE IN OZONE

No single parameter shown in the figure is as uncertain as a factor of two, and we are merely showing how difficult it is to significantly change the ozone abundance, even with unrealistically high variations in input data. Halocarbon source concentrations were held fixed in these tests. We have separated the changes due to parameters related primarily to O_x, HO_x, NO_x, and ClO_x. In the O_x category, the rate constant $k_{31}(O + O_2 + M)$ affects ozone formation, and $[O_3]$ depends quite sensitively on its value, as can also be seen from equation (54). However, the change in k_{31} necessary to fit the mean ozone data is unrealistically high, given the agreement (within $\sim$20%) between various laboratory studies [DeMore et al., 1982, and references therein]; this would also imply undesirably high mesospheric ozone values [see also Allen et al., 1983]. A decrease in $k_{32}(O + O_3$ reaction) reduces the effectiveness of the direct loss channel for O_x, but even a large change will not significantly increase $[O_3]$, since the total destruction rate depends only to a small extent on L_{O_x} (see Table IV). The photodissociation rate of O_3 will obviously play a role in controlling the ozone abundance and Figure 62 illustrates the sensitivity to j_3 ($O_3 + h\nu \rightarrow O_2 + O$) and j_4 ($O_3 + h\nu \rightarrow O_2 + O(^1D)$). The difference in the effects of a decrease in j_3 or j_4 is due to two factors: j_4 is sensitive to wavelengths below 310 nm and dominates over j_3 above about 35 km, and a reduction in j_4 will also decrease the $O(^1D)$ concentration, which in turn reduces HO_x, NO_x and ClO_x abundances and the efficiency of these catalytic cycles. The combination of smaller j_4 and smaller O_x destruction results in large $[O_3]$ increases, while a change in j_3 is not significant for upper stratospheric ozone. Although model NO_x abundances might be somewhat high compared to

observations, as discussed further below, 30-40% changes in the various radicals, coupled with significant mesospheric increases in ozone, do not seem to provide a satisfactory answer to the upper stratospheric ozone discrepancy. More important, the O_3 absorption cross sections are known quite accurately from laboratory data (see also Chapter 3) and we feel that the photodissociation rate of ozone in the upper stratosphere is known to better than 15%. Finally, one could go back to the old absorption cross sections $\sigma(O_2)$, which is equivalent to the effect of a significant change in J_1. This effect alone, however, is not enough to eliminate the ozone discrepancy. We have already indicated (Chapter 3) our preference in terms of the effect of $\sigma(O_2)$ on the halocarbon vertical profiles (opposite to the effect on ozone), although further measurements are needed to confirm the results of Herman and Mentall [1982]. Figure 62 shows a few examples of the ozone sensitivity to the HO_x radicals. The production of HO_x occurs via $O(^1D)$ attack of H_2O, while the primary loss process at altitudes above 35 km is through the $OH + HO_2$ reaction, reforming water vapor. The ratio of [OH] to $[HO_2]$ depends to first order on four reactions [see, e.g., Hudson et al., 1982] and can be written as:

$$\frac{[OH]}{[HO_2]} = \frac{k_{40}[O] + k_{54}[NO]}{k_{39}[O] + k_{37}[O_3]} \qquad (55)$$

It is possible that our 6-7 ppmv amount of H_2O between 35 and 50 km is somewhat high; a decrease by a factor of two in $[H_2O]$ produces changes similar to the effect of a factor of two increase in $k_{47}(OH + HO_2]$, by reducing HO_x by 30-40%. The effect of a decrease in $k_{40}(O + HO_2)$, which appears in (55) and has recently been revised upwards by almost a factor

of two, is also shown in Figure 62 [see also Ko and Sze, 1983]. Similar changes in other rate constants affecting HO_x will produce changes of order 20% or less in $[O_3]$. Large changes in individual rate constants would be needed to satisfy the ozone observations, and since HO_x is the primary component affecting mesospheric O_x, one has to reconcile possibly large effects on stratospheric ozone with even larger changes in mesospheric ozone. Moreover, as we show later, necessary reductions in model HO_x by a factor of two or more (to significantly increase $[O_3]$) would not be consistent with currently existing observations of OH and HO_2. The $O(^1D)$ concentration--although very small--is a key variable affecting the HO_x, NO_x, and ClO_x stratospheric abundances. Since NO_x is the main ozone-destroying component in most of the stratosphere, we have shown the effect of a reduction in $[O(^1D)]$ (by about a factor of two) in the NO_x segment of Figure 62. This reduction is achieved by increasing the quenching rate of $O(^1D)$ by a factor of two; $O(^1D) + M$ refers to both $O(^1D) + N_2$ and $O(^1D) + O_2$ reactions (rate constants k_{24} and k_{25}). A significant (up to 40%) increase in ozone results, but the real uncertainty in the above rate constants appears to be less than 20% [DeMore et al., 1982]. The production of $O(^1D)$ through ozone photolysis should be even less uncertain than its destruction rate, and unless an unknown mechanism exists in the atmosphere to deplete the $O(^1D)$ abundances (assuming that the 30-40% resulting changes in HO_x, NO_x and ClO_x are acceptable), the ozone discrepancy cannot be explained by such uncertainties. In the upper stratosphere, NO and NO_2 are the main odd nitrogen species and we can write

$$[NO] + [NO_2] = [NO_x] \qquad (56)$$

with (to first order)

$$\frac{[NO_2]}{[NO]} = \frac{k_{34}[O_3]}{j_{10} + k_{35}[O]} \tag{57}$$

so that the ℓ_{NO_x} term in (54) can be expressed as

$$\ell_{NO_x} \doteq k_{35}[NO_2] = \frac{k_{35}[NO_x]}{1 + \{(j_{10} + k_{35}[O]) / k_{34}[O_3]\}} \tag{58}$$

The ozone sensitivity to the various parameters (k_{34}, k_{35} and j_{10}) in (58) is not very large in the upper stratosphere. In this case, large ozone changes above 40 km would have to be accompanied by larger changes in the 30-40 km. The same holds for the 30-40% reduction in NO_x caused by dividing $k_{29}(N_2O + O(^1D))$ by two. Finally, the effect of changes in chlorine radicals cannot by itself produce the necessary ozone increase, although the variation with altitude qualitatively matches the required changes, as illustrated in Figure 62. Even if no chlorine species are included in our model, the mean ozone data are still high compared to theoretical values.

The above analysis indicates that no single change in the relevant photochemical data can, given the current uncertainties of about 20% (up to 40% in a few cases), increase the ozone abundance by more than 20% (much less in most cases). One would need to change several rate constants to get the required effect. An example for four important reaction rate constants, changed by ±30% in a way to increase the ozone abundance, is shown in Figure 63. It turns out that the O + ClO reaction has recently been studied in more detail and that a 30-40% reduction is

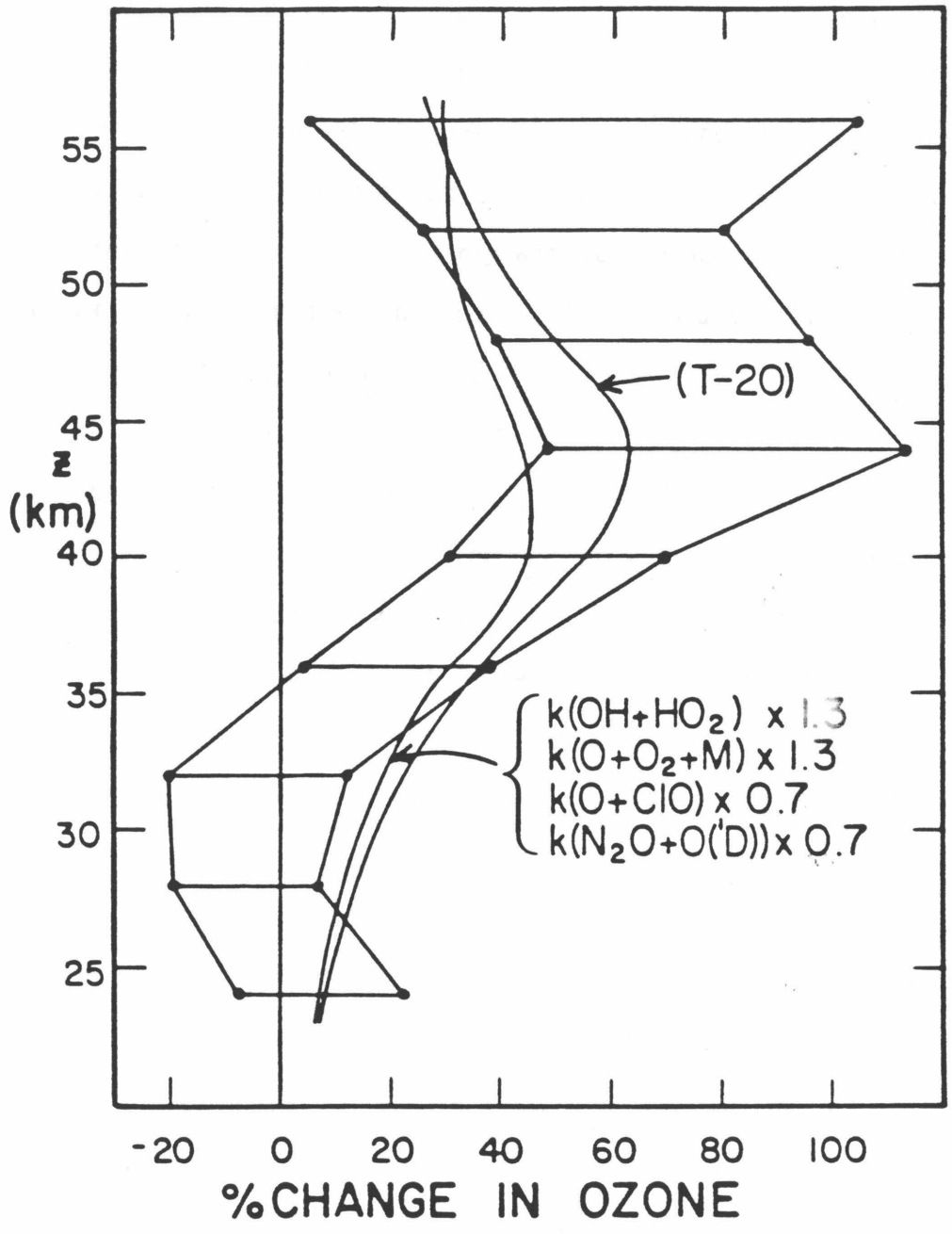

Figure 63. Ozone sensitivity to a combination of properly chosen (to increase $[O_3]$) ± 30% changes in four rate constants. Also shown is the effect of a 20 degree decrease in temperatures.

indicated (see Chapter 4). Taken alone, however, this change affects $[O_3]$ by 5% or less. We do not find it satisfactory to suggest that small (10-15%) changes in 8 to 12 reaction rate constants (or photodissociation rates) can explain the observed ozone concentrations. While such changes can undoubtedly exist, a random combination of increases and decreases would not significantly affect the ozone abundance, since a cancellation of effects would occur. Figure 63 also illustrates the large ozone sensitivity to temperature changes. This follows from the temperature dependences of the $O + O_2 + M$ and $O + O_3$ reactions, which both tend to increase ozone (primarily the latter reaction) if T decreases. However, a systematic 20-30 K difference between our model temperatures and the actual stratospheric values is not likely, given that model values are obtained from observations with uncertainties of less than 5 K, in general. The range in the observed ozone data can probably, in large part, be explained by temperature changes, but we do not have the freedom to vary T very much for mean mid-latitude model results.

Further clues can be sought by comparing key radical observations with our model results. We have previously presented the reasonably good agreement for the ClO vertical distribution and diurnal variation. A limited number of mid-latitude observations of HO_x and NO_x radicals in the upper stratosphere currently exist. Comparisons with models have been made by various groups [see, e.g., Hudson et al., 1982] and our model is in general agreement with other recent results. We briefly provide further model validation by comparing our typical mid-latitude results (32°N latitude, -11° solar declination) with observations of OH, HO_2, NO and NO_2. Anderson's balloon-borne molecular resonance

fluorescence measurements of OH [summarized in Anderson, 1980] above 30 km at 32°N are shown in Figure 64. The averages of the observed profiles for $\chi = 80°$ and $\chi = 41°$ are in good agreement with model results at similar zenith angles, given the observational uncertainties of about ±30%. Further evidence of the general validity of model OH values can be found in Figure 65, where average ground-based Pepsios spectrometer measurements [Burnett and Burnett, 1981, 1982] of OH absorption near 308 nm are plotted versus sec χ . The column abundances represent fits through average data taken during 1977-79 and during solar maximum in 1980; 1981 data (not shown here) are 3% lower than during 1980, on average. Our model results (solar maximum flux conditions), extrapolated above 60 km by an additional 20% for total column abundance, agree with both data sets to within 20% for sec $\chi \lesssim 3.5$ ($\chi \lesssim 73°$). In terms of the effects on ozone, the average daytime model OH column abundance appears to be within 15% of the average Pepsios results, and an extrapolation of Anderson's in situ data agrees with the latter results as well [see Hudson et al., 1982]. The sharp decrease in the observed N_{OH} at large zenith angles is somewhat puzzling, if it is real and not caused by some contamination of the absorption feature. A factor of two difference near 80° could imply a possible overestimate of $[O(^1D)]$ by a factor of four in the upper stratosphere and mesosphere. At noon, the model OH column above 45 km provides about half of the total column abundance, but its contribution is reduced to one-third for $\chi \simeq 80°$. The discrepancy at large χ thus seems to imply that a large part of this effect has to come from the uppermost stratosphere and mesosphere. The limited data of Anderson shown

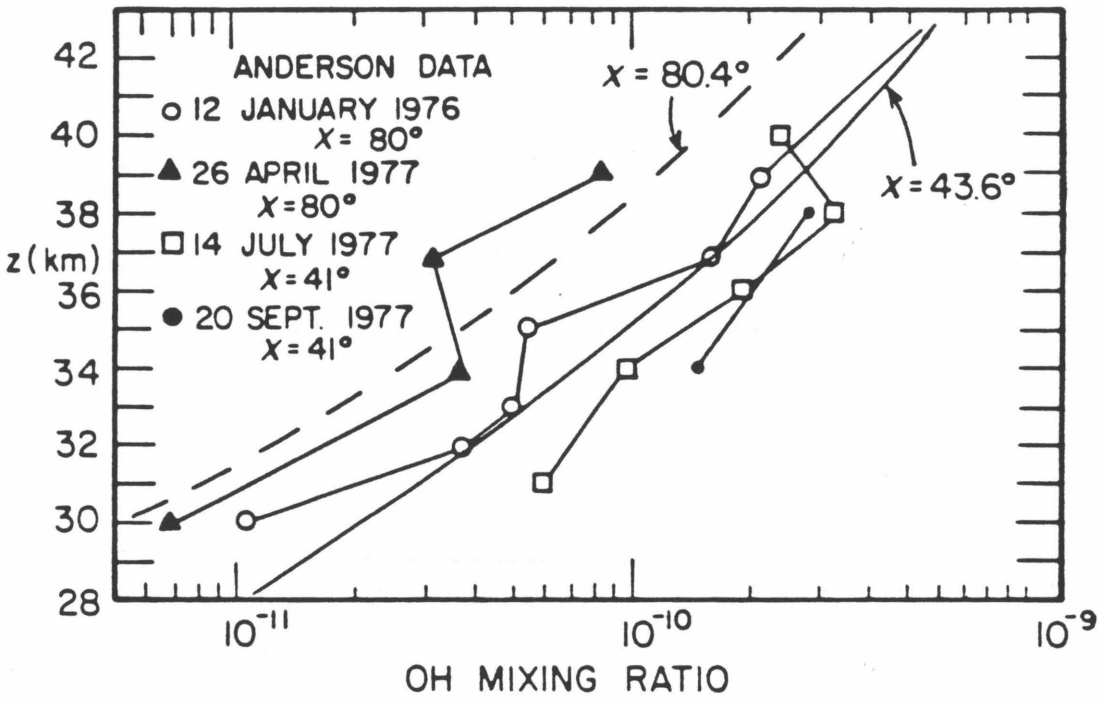

Figure 64. Resonance fluorescence measurements of OH (see Anderson, 1980) compared to model OH mixing ratio profiles for similar solar zenith angles (at 32°N).

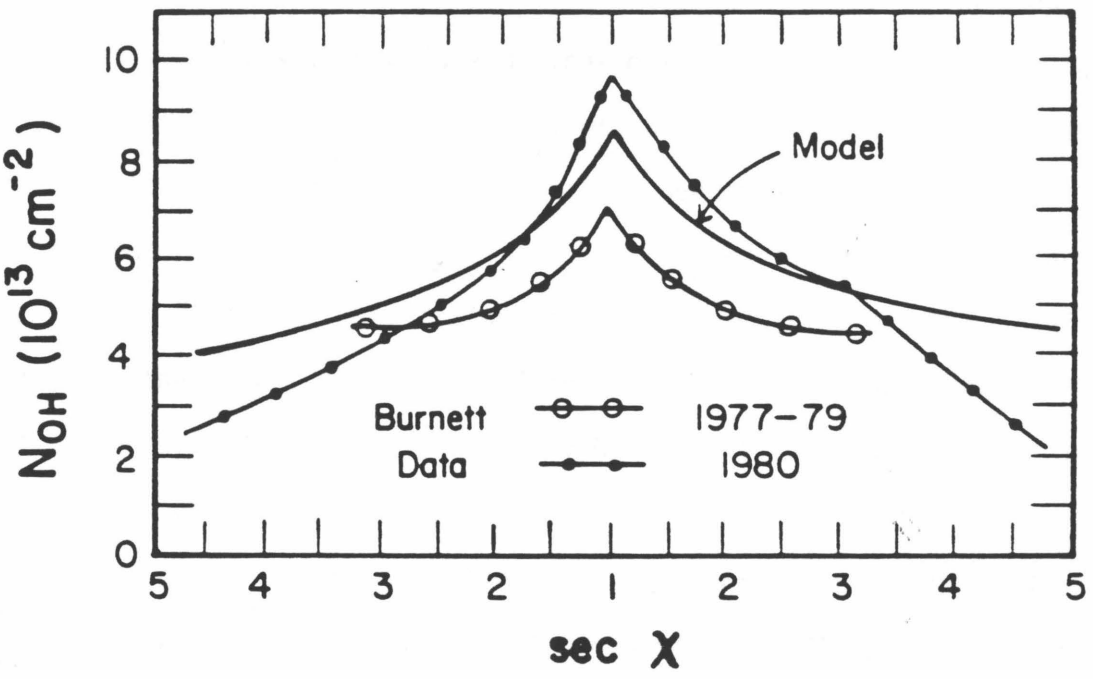

Figure 65. Total OH column abundance (N_{OH}) measurements by Burnett and Burnett (1981,1982), as a function of secχ for 1977-79 and 1980 averages. Our standard mid-latitude results (32°N latitude, -11° solar declination) are shown for comparison.

in the previous figure did not show a factor of two discrepancy with the model for $\chi = 80°$. One expects more sensitivity to $O(^1D)$ and the short wavelength solar flux producing this radical at the higher altitudes. There are other aspects of these ground-based observations that are not clearly understood, such as large sudden changes during the day and larger than expected variations as a function of season and solar cycle. Other observations of OH near 35 km by balloon-borne laser radar (LIDAR) through the afternoon and early evening [Heaps and Mc Gee, 1983] show large disagreement with models and other measurements discussed above; in view of this and the large uncertainties associated with these observations, we feel that further LIDAR data are needed for a more accurate test of this method and its repeatability. The HO_2 radical has been observed to a limited extent in the stratosphere. Our summary plot, Figure 66, is taken from the recent paper by de Zafra et al. [1983], who observed HO_2 from the ground (Mauna Kea, Hawaii, 20°N latitude) during four days in September-October 1982. Microwave emission lines were observed near 266 GHz by this group, whose ground-based ClO measurements were discussed in Chapter 4. The in situ cold trap measurement by Mihelcic et al. [1978] at 32 km has a large uncertainty, as shown in the figure. The somewhat indirect in situ observations of HO_2 (conversion via NO to OH followed by resonance fluorescence detection of OH) by Anderson et al. [1981] are also illustrated. The range and average profile of three 1977 measurements are indicated. Both of these data sets were taken below the altitude region of most interest to us, in terms of the ozone profile. Curves a, b, and c in Figure 66 are model results used by de Zafra et al. [1983] to compare with their ground-based data. The main difference from model b to

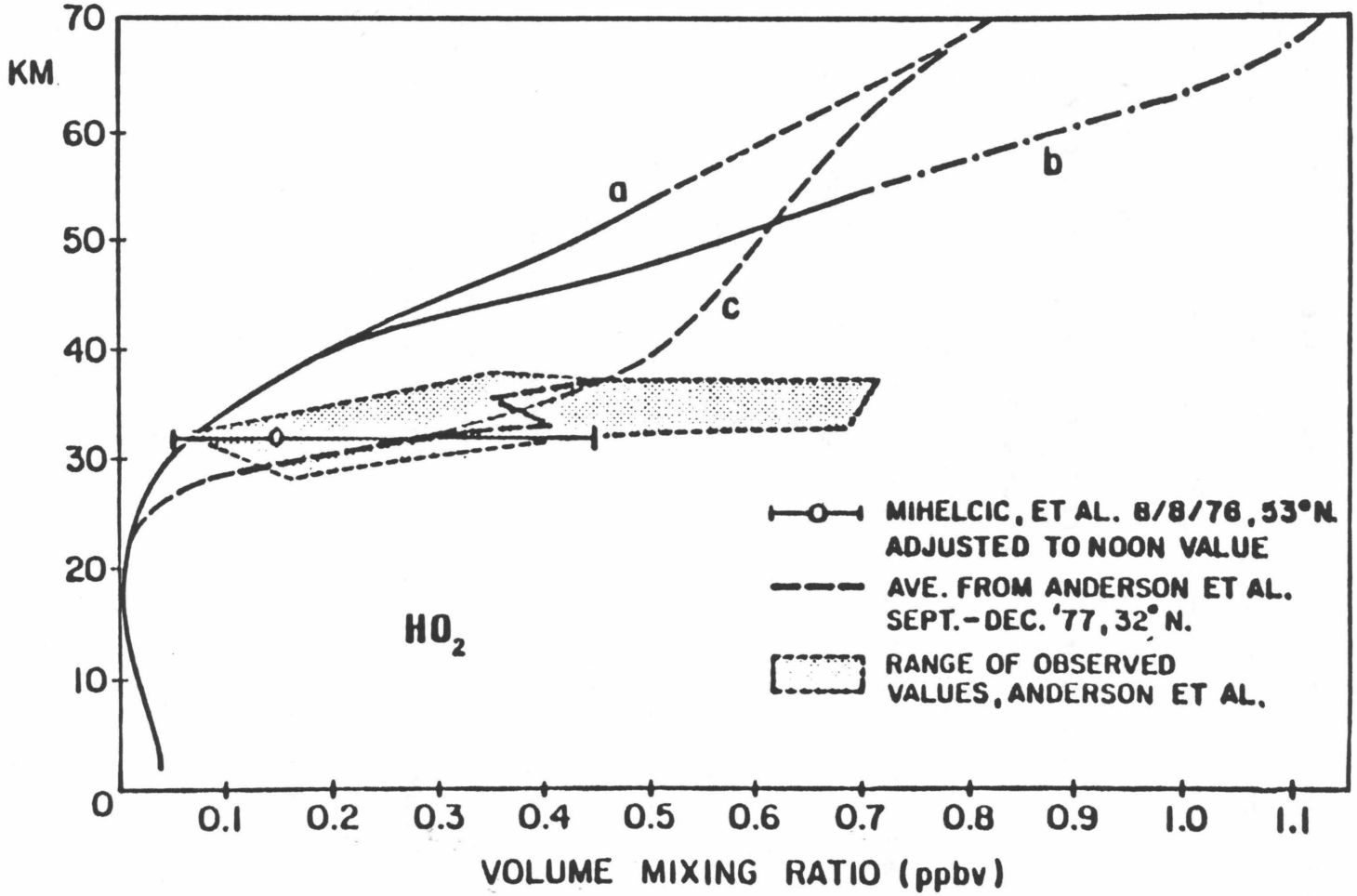

Figure 66. HO_2 data and models, as discussed by de Zafra et al.(1983), who measured HO_2 emission in the microwave (Fall of 1982). Their results agree best with model a, which is essentially the same as our model results. Model b uses slightly older photochemical data, and model c combines the mean of Anderson's data with model a.

model a is an increase in k_{40} ($O + HO_2 \rightarrow OH + O_2$) by almost a factor of two (as discussed previously), which shifts the value of the ratio $[OH]/[HO_2]$ ($\simeq k_{40}/k_{39}$ above 45 km) and decreases $[HO_2]$. Curve c is a rough fit through Anderson's data, combined with a smooth increase towards profile a. The average of four days of HO_2 measurements taken between 10 a.m. and 5 p.m. by de Zafra et al. [1983] agrees quite well with a synthetic line profile generated from model a. As shown by the above authors, model b leads to a higher peak line intensity than observed, whereas model c provides too much low altitude HO_2 (pressure-broadened in the wings of the emission line). Our model results for 20°N latitude (October), averaged between the appropriate times of observation, are essentially similar to model a. Although models b and c might be considered marginally acceptable, or one could argue that variations in H_2O could produce different HO_2 abundances such as cases a and b, it is reassuring that the most recent photochemical data (particularly the value for k_{40}) provides the best fit to the ground-based microwave data. These results show a systematic difference between Anderson's data and models which agree better with the ground-based data (cases c versus a). If anything, the higher HO_2 abundances measured by Anderson et al. [1981] would tend to reduce the ozone concentration, although this effect would be small for the altitudes covered by the in situ observations. The ground-based observations are not very sensitive to HO_2 below 35 km, or to the exact profile shape, but since most ($\sim$ 80%) of the HO_2 column amount resides below about 50 km for model a, with 40% in the 35-50 km region relevant to upper stratospheric ozone, we feel that there is good agreement between these observations and our model. Therefore, considering the model agreement with existing OH

and HO_2 observations, we are not free to argue for changes in the rate constants affecting HO_x radicals in order to increase the ozone amount. Such changes would undoubtedly worsen the agreement between models and observations by decreasing the HO_x abundance to unacceptably low levels.

A brief overview of NO_x radical observations also indicates generally good agreement with model results, given the uncertainties and apparent spread or variability in some of the data. Figure 67 displays some of the more recent NO_2 data, taken from the summary by Roscoe et al. [1981]. Model results for <Day> and <Night> indicate the variation during the 8-hour time periods centered around noon and midnight, respectively. There are few observations above 35 km. Daytime balloon-borne pressure modulated radiometer observations of NO_2 emission at 6.2 μm were obtained by Drummond and Jarnot [1978] and Roscoe et al. [1981]. The latter data represent an average daytime result similar to our average model profile. We note that these authors' simultaneously determined NO data (see Figure 70) are in fair agreement with our NO model profile from about 35 to 50 km (but drop off much faster below 30 km). The earlier measurements [Drummond and Jarnot, 1978] were made about one hour after sunrise, at a time when the NO_2 abundance starts dropping fairly fast. Nevertheless, the point near 50 km is still significantly higher than expected, although we note that measurements above the balloon float altitude represent average column results and might be more uncertain than indicated. A partial summary of sunset NO_2 data, taken from Hudson et al. [1982] (see Figure 68) shows an average vertical distribution similar to our model sunset results, although the model profile is somewhat on the high side below ∿30 km. Russell et al. [1983] have

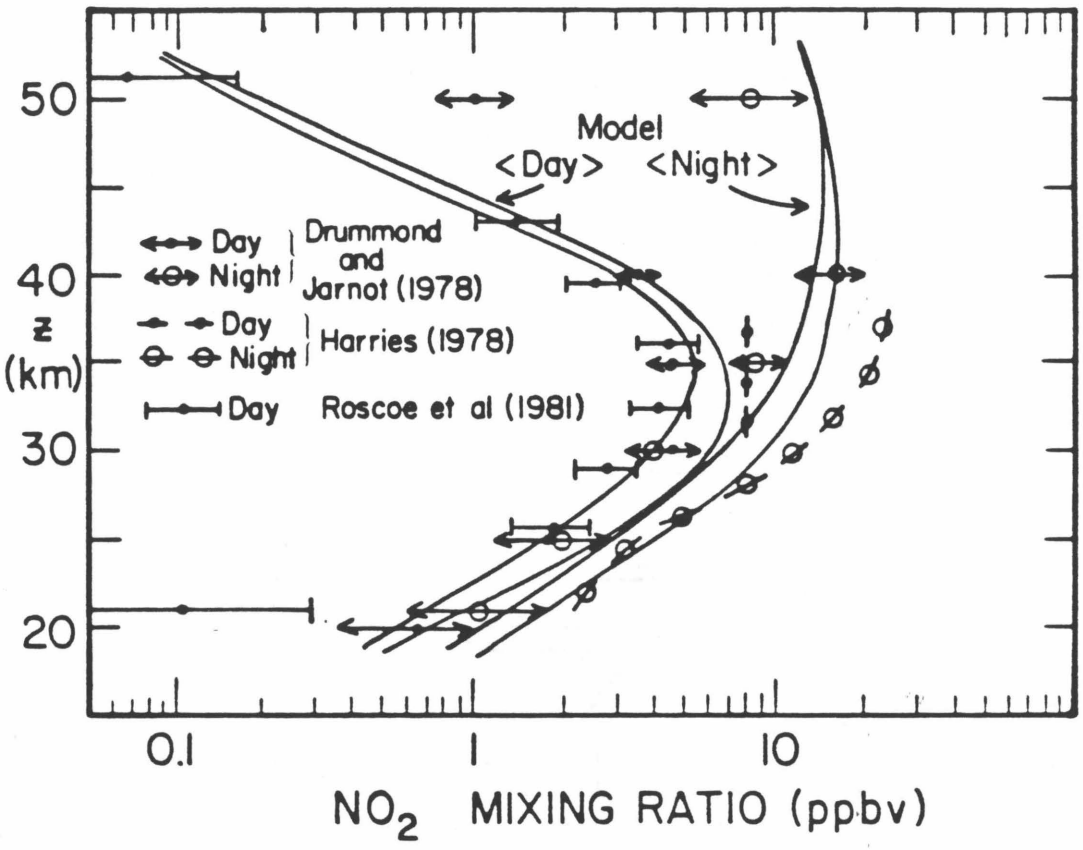

Figure 67. Day to night variation in NO_2 mixing ratio profile, as illustrated by mid-latitude observations and our standard model (same as in Figure 65) results for 8-hour periods centered around noon and midnight.

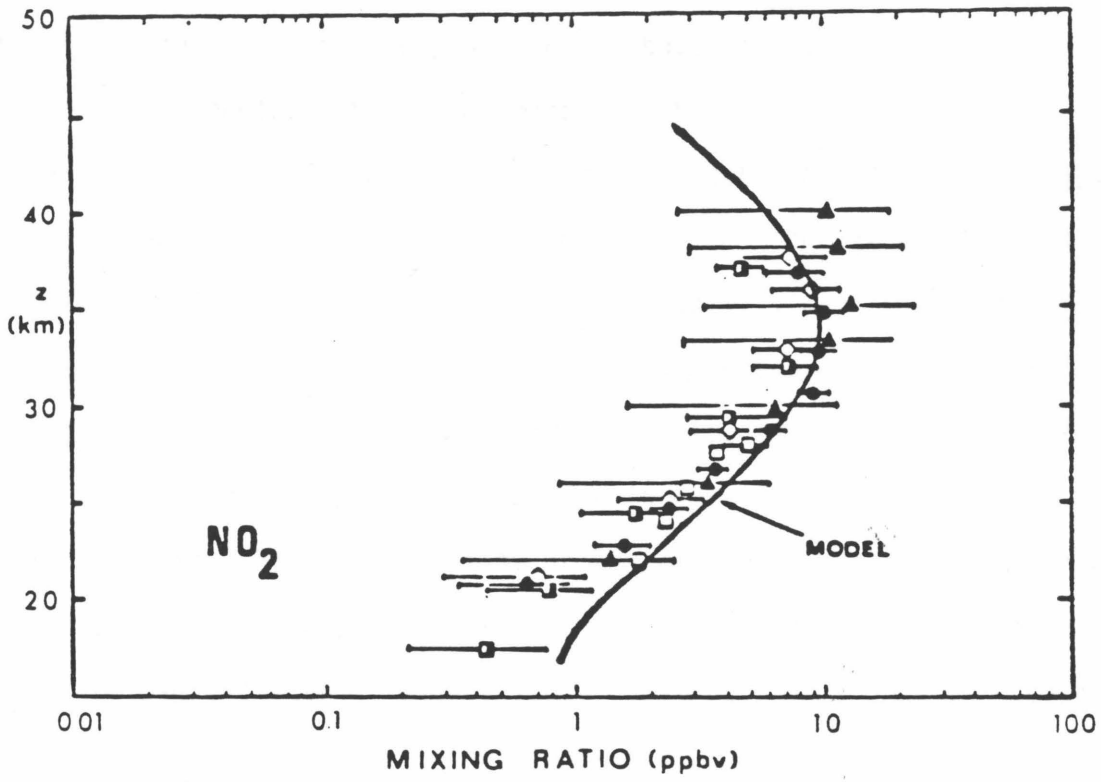

Figure 68. Summary of sunset NO_2 mid-latitude observations (see Hudson et al., 1982, for references) compared to our standard model profile at sunset.

compared and validated some of the LIMS NO_2 data below 40 km with other data sets. One such comparison with balloon-borne solar occultation measurements [see Russell et al., 1983] is reproduced in Figure 69. Within the observational uncertainties, these NO_2 day and night profiles at 32°N latitude agree with our model results for the appropriate times. Further analysis of the LIMS data, in terms of the simultaneously observed O_3, H_2O, and NO_2 profiles (plus HNO_3 as well), will be useful in assessing the relative importance of various catalytic cycles affecting ozone, although the O_3 and NO_2 data shown above should be typical of mid-latitudes. We conclude these comparisons with a summary [from Hudson et al., 1982] of various daytime NO mid-latitude data (Fig.70). There are relatively few measurements of NO above 35 km, and the range of values covers about a factor of five. Seasonal variability and transport effects on the long-lived NO_x ($\simeq NO + NO_2$) total abundance are at least a partial explanation for such differences [Horvath et al., 1983]. Transport effects that are not properly accounted for in our 1-D model could indirectly affect the concentrations of key radicals involved in the ozone destruction process. Overall, however, we do not find that there is a significant overestimate of mid-latitude model HO_x, NO_x, or ClO_x radical abundances which could resolve the upper stratospheric ozone problem, although the necessary accurate and simultaneous observations have not yet been satisfactorily performed.

Rather than attempting to find a way to reduce the photochemical destruction of ozone, can we enhance its production? The molecular oxygen photolysis rate, which is the source of odd oxygen, is somewhat uncertain due to the problems associated with the O_2 absorption cross

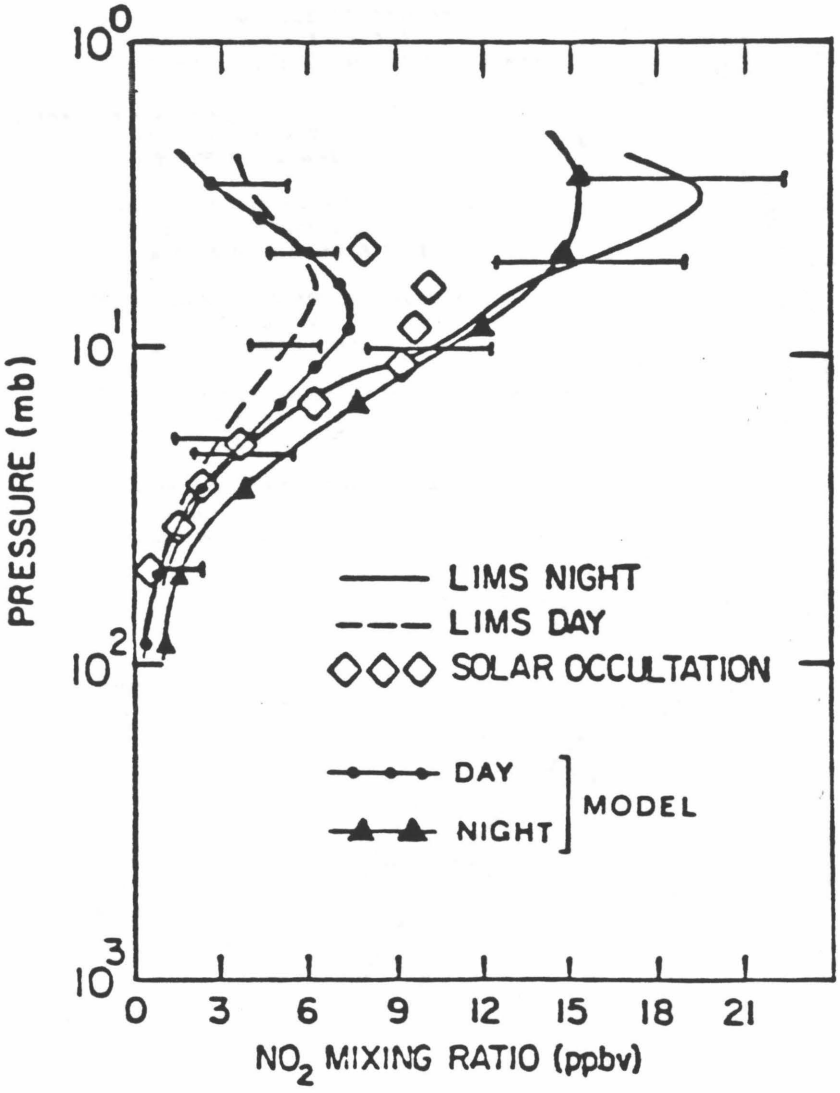

Figure 69. LIMS day and night NO_2 mid-latitude observations compared to balloon underflight solar occultation measurements (see Russell et al.,1983). Our model results are shown (32°N) for times corresponding to the LIMS data (about 1 and 10 pm).

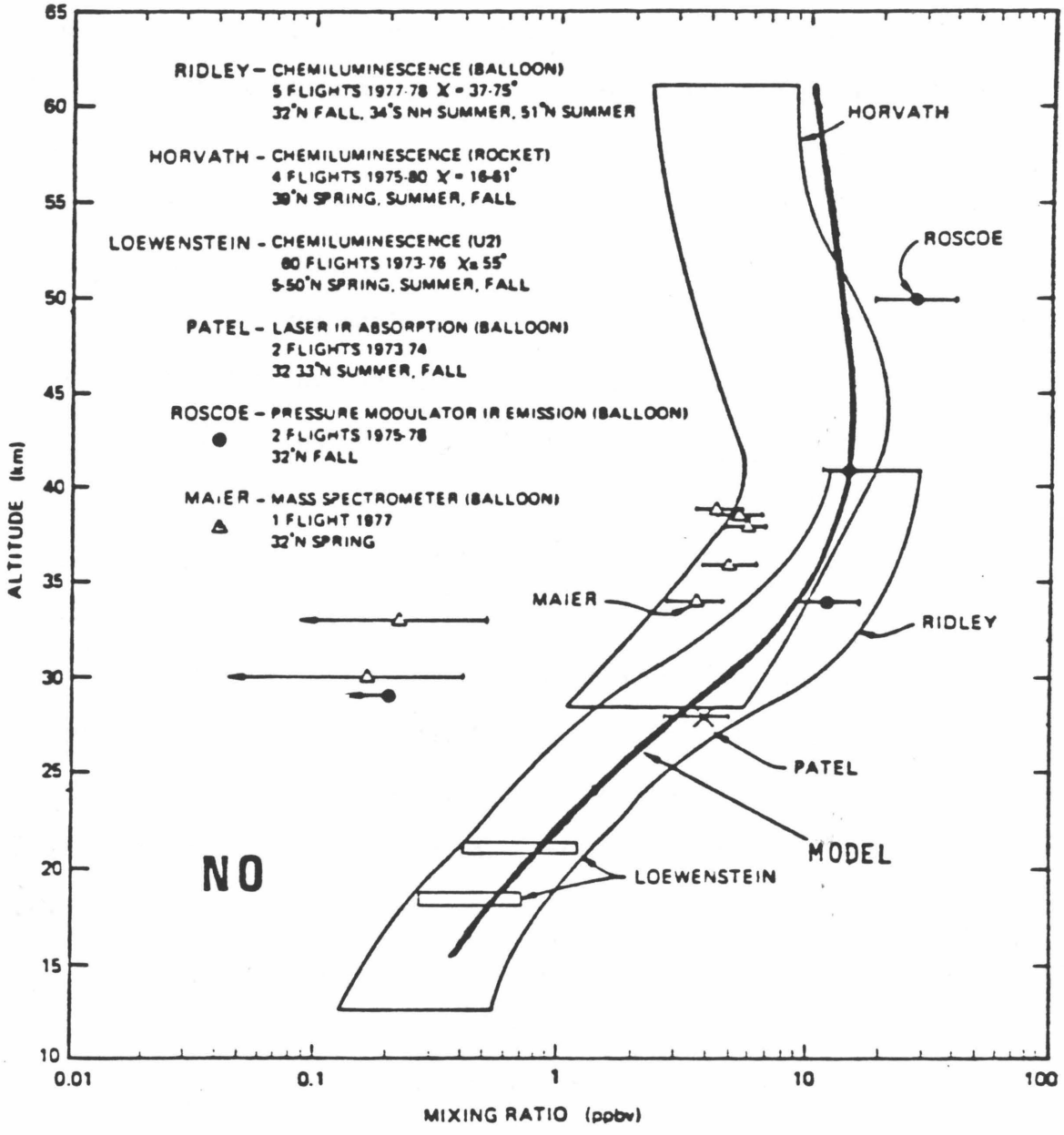

Figure 70. Summary of mid-latitude daytime NO observations (from Hudson et al., 1982) compared to mid-day model results. Note large spread in observations, due to measurement uncertainties as well as real variations in the NO abundance.

section measurements in the Herzberg continuum. Following the analysis in Chapter 3, we would argue that uncertainties in J_1 of up to 25% currently exist in the upper stratosphere (with much higher uncertainties, of opposite sign, in the lowermost stratosphere). However, recent evidence would indicate the need for a reduction in cross section, and a corresponding decrease in $[O_3]$, as discussed above. In terms of other possible sources of odd oxygen in the stratosphere, the evidence--and speculation--is limited. One possible mechanism involving an asymmetric $ClO.O_2$ complex was proposed by Prasad [1980] in relation to the lower-than-observed stratospheric ClO abundances predicted by earlier models. Briefly, the idea involves the possible decomposition of $ClO.O_2$ (formed by $ClO + O_2 + M$) into $OClO + O$, with subsequent photolysis of OClO into $ClO + O$. This process would hence break the O_2 bond and form odd oxygen. Only limited laboratory evidence exists regarding the above speculative scheme [see DeMore et al., 1982; Zellner and Handwerk, 1982]. Moreover, even if we assume somewhat unreasonable rate constants and $ClO.O_2$ abundances near 40 km in order to provide a significant odd oxygen source, we would find unrealistically high (much higher than [ClO]) $ClO.O_2$ concentrations near 30 km. This scheme, as it stands, is not really plausible in terms of a significant ozone source. Other possible sources of ozone could involve excited states of molecular oxygen (formed for example by the $O + O + M$ reaction), reacting with O_2 to form ozone. No quantitatively significant scheme has been found for the stratosphere, and such processes tend to be more effective in the mesosphere, where quenching is less (and photon energies are higher). Finally, heavy molecular oxygen ($^{18}O^{16}O$) photodissociation could provide a source of odd

oxygen in our atmosphere [Cicerone and McCrumb, 1980]. Although the $^{18}O^{16}O$ abundance is less than one percent of $[O_2]$, this heteronuclear molecule has twice as many lines in the Schumann-Runge bands, resulting in an increased photodissociation coefficient for the heavy molecule which absorbs more sunlight between the O_2 lines. The estimates by Cicerone and McCrumb [1980] are fairly rough and they erroneously assumed equal line strengths for both isotopes (D. Freeman, private communication, 1983), but even their upper limit implies only a few percent contribution to odd oxygen production near 40 km, with a more significant effect in the 60-70 km region. The transmission through the Schumann-Runge bands has been underestimated in the past, and further detailed investigations of the possibility of a significant ozone source by photolysis of heavy O_2 in this intricate spectral region would be worth while. Heavy ozone is interesting in itself and is discussed in section 5.3.

The last question that one should consider is the possible role of transport in the upper stratospheric ozone distribution. Our one-dimensional model does not include an explicit description of transport processes, particularly meridional and zonal motions, which are typically much more rapid than vertical processes. Clearly, we cannot adequately simulate the latitudinal behavior of ozone or other long-lived species in the lower stratosphere, where horizontal motions dominate the photochemistry. Indeed, the observed global distribution of total ozone does not show a peak during the summer at the equatorial regions of maximum photochemical production, but rather at high latitudes during winter and spring [Dütsch, 1974]. Mixing ratios show a peak at mid-latitudes during the spring. Meridional and vertical transport both play a role in the

redistribution of ozone in the lower stratosphere and such dynamical processes cannot be ignored in that region. Planetary scale waves (of low wave number) generated in the troposphere are thought to play a dominant role, notably during the winter, when they can propagate upwards into the stratosphere and interact with the mean flow. Such aspects of stratospheric dynamics are reviewed to some extent in Hudson and Reed [1979] and Hudson et al. [1982], along with pertinent observations of ozone. Backscatter ultraviolet observations from satellites [Heath et al., 1973; London et al., 1977; Frederick et al., 1977, 1980, 1983] have provided interesting global information on the ozone distribution and the influence of planetary waves. The question of importance for upper stratospheric ozone is the extent to which photochemical equilibrium is really valid. Observations (see references above) as well as models [e.g., Cunnold et al., 1980; Harwood and Pyle, 1980] definitely point to dynamical control in the lower stratosphere, below 25 to 30 km. It is also generally agreed that above about 45 km, photochemistry will dominate. The coupling between radiation, chemistry and dynamics (planetary waves) can lead to significant poleward and downward transport, according to the model of Hartmann and Garcia [1979], which yields a peak in horizontal transport near 45 km [see also Hartmann, 1981; Rood and Schoeberl, 1983]. Temperature-dependent reaction rates (for $O + O_3$, $O + O_2 + M$) lead to the coupling between photochemistry and temperature, which is in turn coupled to dynamical perturbations. Pyle and Rogers [1980] and Strobel [1981] have discussed these coupling effects in terms of the limitations of eddy diffusion parametrization in one or two dimensions [Reed and German, 1965]. Nevertheless, the observed

relationship between ozone and temperature perturbations in the upper stratosphere is generally an inverse relationship [Barnett et al., 1975; Ghazi et al., 1976; Gille et al., 1980; Nagatani and Miller, 1983] in accordance with photochemical control. A direct relationship has been observed in the lower stratosphere [Sreedharan and Mani, 1973; Gille et al., 1979]. Ghazi et al. [1976] note that even in the upper stratosphere (2 mb pressure), there are instances where warm temperatures are accompanied by high ozone concentrations, as observed near 60°N latitude in January, indicating the influence of dynamical processes, possibly of the type discussed by Hartmann and Garcia [1979]. Hartmann (private communication, 1983) indicates that a purely photochemical model could underestimate the mean ozone abundance by as much as 15% near 40 km, although such differences will tend to be more prominent at higher latitudes, where ozone gradients and planetary wave activity are larger. At mid-latitudes, we cannot expect much contribution from transport processes in terms of a significant (30-50%) increase in mean ozone abundances. Changes in the current photochemical data or missing photochemical processes must be involved. In the next section, we look for possible clues in the observed diurnal behavior of stratospheric ozone.

5.2 Diurnal Variations of Ozone in the Stratosphere

The expected daytime variations of ozone below 50 km are about 10% or less, due to the magnitude of the ozone abundance and its net daily production or loss rate. The absence of significant loss processes at night leads to a constant ozone nighttime concentration. If there are certain missing or inaccurate elements in our current photochemical

representation of ozone, perhaps we can also find some discrepancies between theoretical and observational variations of ozone during the day.

Few measurements of diurnal ozone variations have been made in the stratosphere, and the constraints on the accuracy required for a meaningful comparison with models are quite severe. Hilsenrath [1971] obtained daytime and nighttime ozone observations in the stratosphere and mesosphere at 38°N latitude, by means of a chemiluminescent parachutesonde released from a rocket. Given the 20% accuracy and 10% precision of these data, as well as the small daytime ozone changes in the stratosphere, we cannot find any significant discrepancy with model results. A more accurate and meaningful comparison can be made with the broadband photometer rocket measurements of Hartley band absorption by Lean [1982]. These carefully planned observations were performed from seven rockets (ascent and descent) with similar instruments sensitive to three separate wavelengths, flown during various times of day and night (by moonlight). One notes that the data were acquired on three different days over a period of two weeks. Averaged results with typical uncertainties (repeatability) of ±3% are shown in Figure 71, in terms of the percent change relative to nighttime data. Adjustments have been made by Lean [1982] for independently measured temperature and density changes from night to day. Ozone concentrations will be sensitive to such changes, as mentioned earlier, primarily via the $O + O_2 + M$ and $O + O_3$ reactions. The percent daytime changes in model ozone concentrations (32°N latitude, -11° solar declination) agree quite well, in general, with the rocket results (Figure 71). The observed morning change near 60 km is apparently uncertain by much more than 3% (Table 2 of Lean, 1982) and

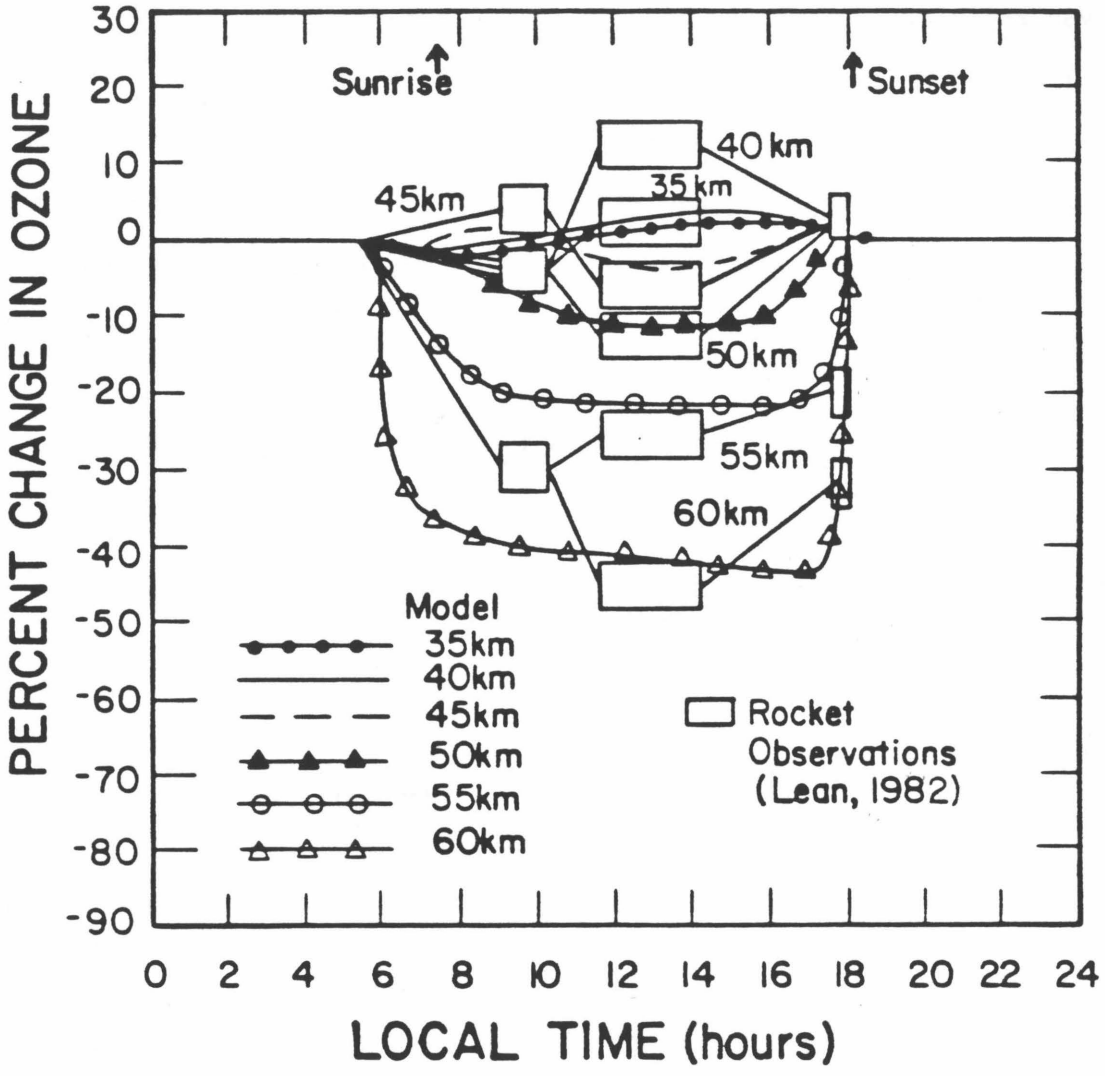

Figure 71. Percent daytime variation in ozone between 35 and 60 km. Rocket data of Lean (1982) were obtained at 38°N, over several days. Overall agreement with our model is good , although observed increase at 40 km is significantly larger than expected. See text for discussion of model and observational uncertainties.

should be considered compatible with model results. A possible discrepancy occurs at 40 km, where the observed afternoon increase is about 13%, whereas our model result is close to only 3%, in agreement with most current models. This difference might not seem large, but we find it difficult to explain, if real.

Daytime variations in various ozone production and loss rates have been briefly discussed by Herman [1979]. Our approach is to follow the changes in odd oxygen (ozone + atomic oxygen) concentrations by considering the terms $P(O_x)$ and $L(O_x)$ described in the previous section. The estimated ozone concentration $[O_3]^e_t$ at time t during the day can be obtained from:

$$[O_x]^e_t = [O_x]^e_{t-1} + (P(O_x) - L(O_x))\,\delta t \tag{59a}$$

with

$$[O_3]^e_t = [O_x]^e_t / (1 + R_o(t)) \tag{59b}$$

and

$$R_o(t) = \frac{j_3(t) + j_4(t)}{k_{31}[O_2][M]} \tag{59c}$$

where the time variation of $P(O_x)$ and $L(O_x)$ is used, and the starting value for $[O_x]^e$ is given by the model value before sunrise. Figure 72 illustrates the fact that the use of J_1 (production process) and K_{32}, K_{40}, K_{38}, K_{41}, K_{35} and K_{61} (loss processes), as described in equation (52), can also provide a good description of the ozone daytime variations in the upper stratosphere. Details of the daytime variations for the relevant production and loss rates are presented in Figures 73 and 74,

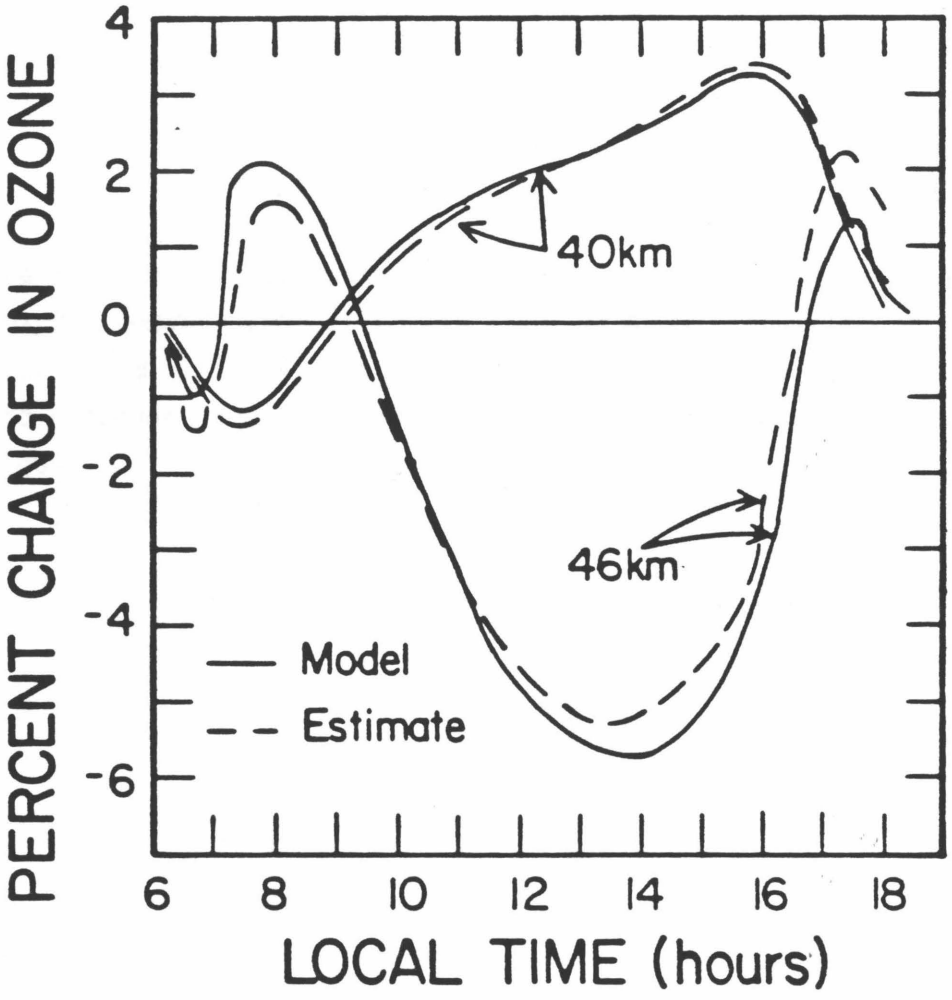

Figure 72. Daytime changes in ozone concentration at 40 and 46 km from our standard model , as well as estimates using the time variation of production and loss terms for odd oxygen; see equations (52) and (59).

Figure 73. Individual contributions from O_x, NO_x, ClO_x, and HO_x to the odd oxygen (ozone) production and loss rates as a function of time of day for 40 km altitude. Note that main loss term just after sunrise is due to nitrogen oxides. Changes in P-L cause daytime variations shown in Figure 72.

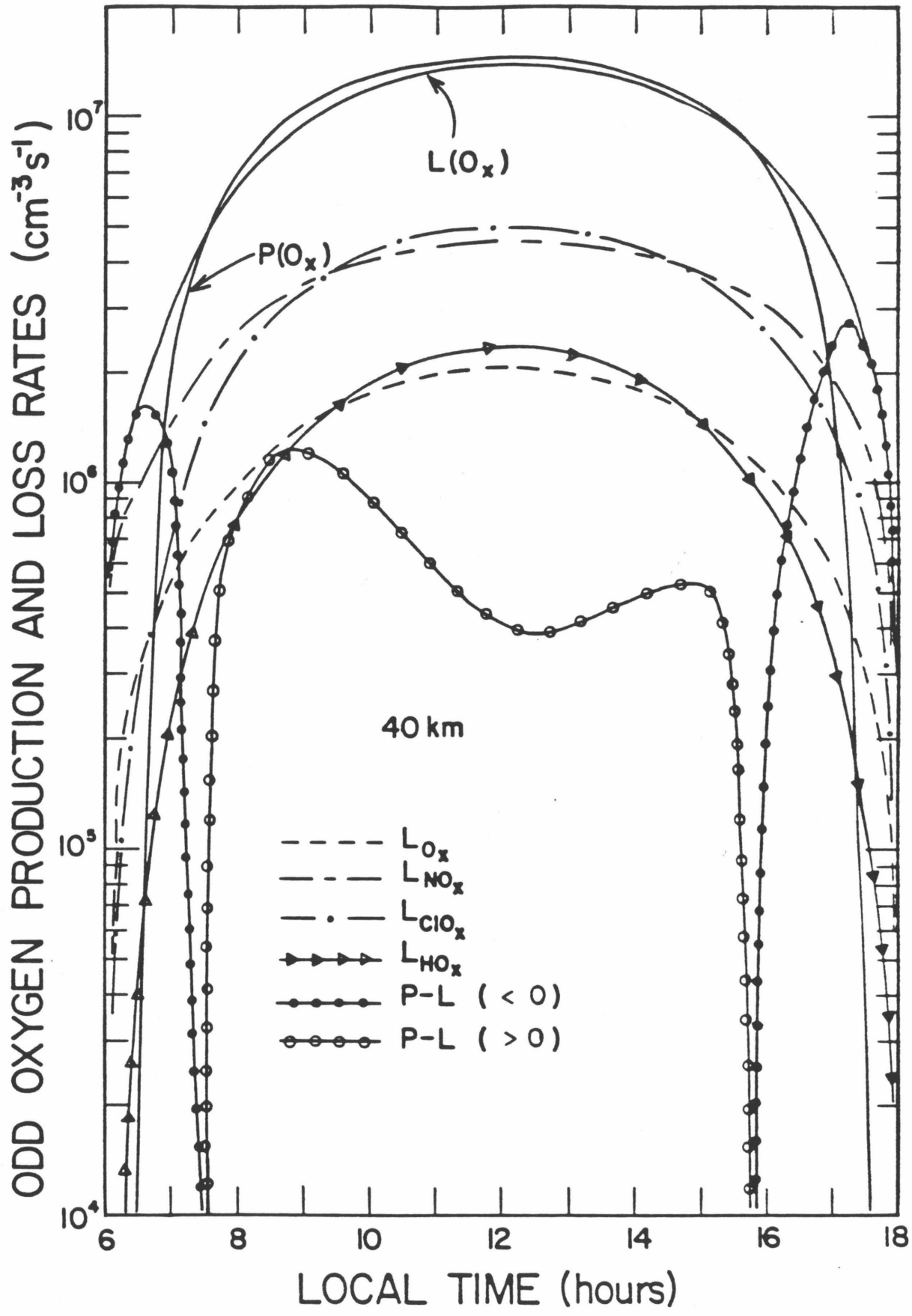
ODD OXYGEN PRODUCTION AND LOSS RATES (cm⁻³s⁻¹)
10⁷
10⁶
10⁵
10⁴
L(Ox)
P(Ox)
40 km
LOx
LNOx
LClOx
LHOx
P-L (< 0)
P-L (> 0)
6
8
10
12
14
16
18
LOCAL TIME (hours)

Figure 74. Same as Figure 73, except for 46 km altitude. Note increased loss term from HO_x (L_{HO_x}), which leads to decrease in mid-day ozone concentration (see variation in Figure 72).

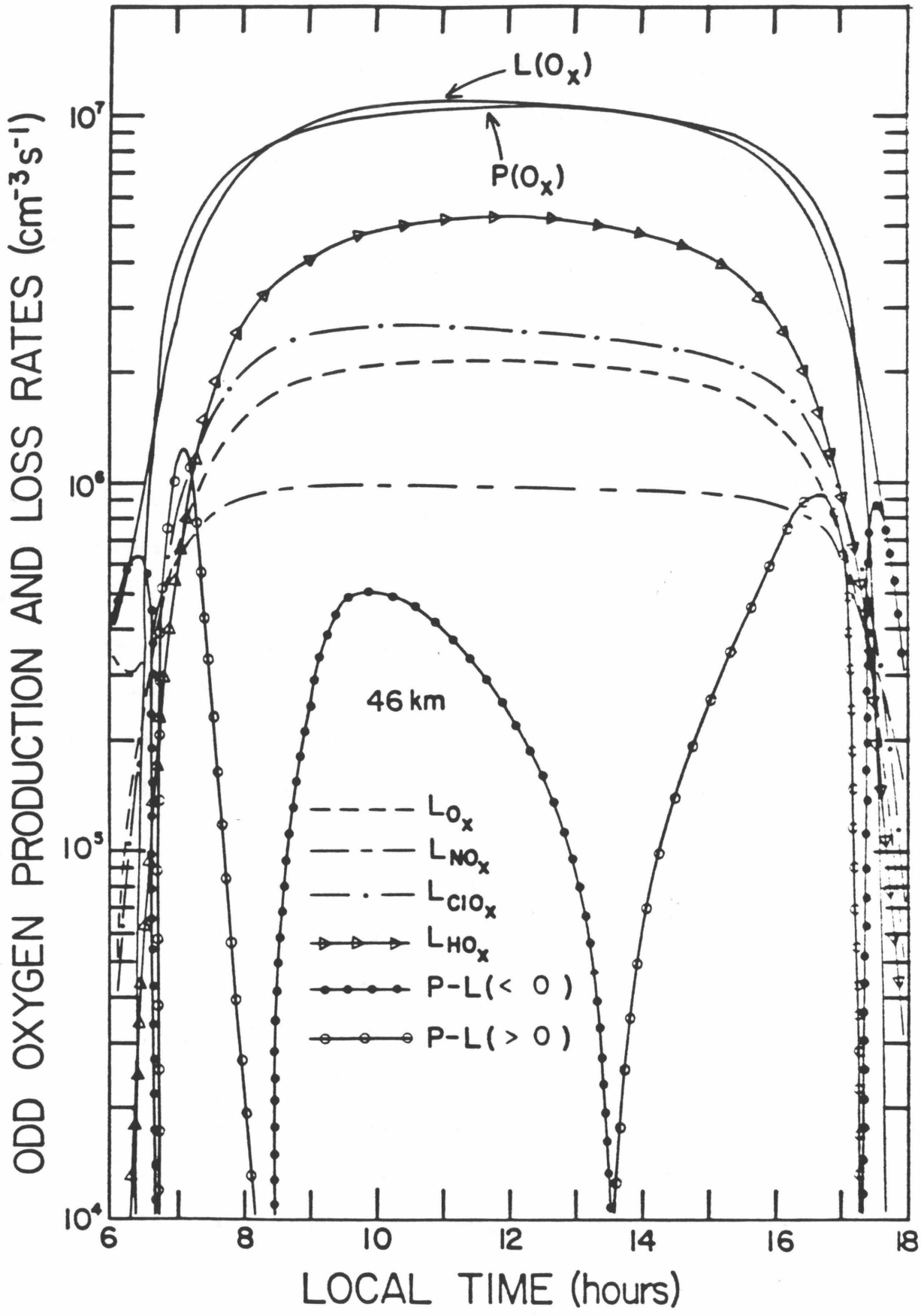
L(Ox)
P(Ox)
46 km
LOx
LNOx
LClOx
LHOx
P-L(< 0)
P-L(> 0)
ODD OXYGEN PRODUCTION AND LOSS RATES (cm-3s-1)
LOCAL TIME (hours)
10⁷
10⁶
10⁵
10⁴
6
8
10
12
14
16
18

for 40 and 46 km. The small differences between P and L cause the ozone variations as a function of time. Just after sunrise, for example, we see that the contribution from L_{NO_x} dominates the loss terms because NO_2, unlike HO_2 and ClO, does not disappear at night. The atomic oxygen concentration rises sharply after sunrise, due to ozone photolysis, while the total odd oxygen production rate is sensitive to shorter wavelengths and increases less rapidly. These effects combine to produce a negative value for P - L at sunrise and a small decrease in ozone. Small decreases in the stratospheric ozone abundance have been observed shortly after sunrise [see Aimedieu et al., 1981; Hudson et al., 1982], which could be taken as a measurement of the NO_x catalytic destruction of ozone. Although the observations tend to agree with our model in terms of a few percent decrease near 40 km, a quantitative comparison is difficult because of measurement uncertainties, and--maybe more important--other variations due to temperature and density changes. Moreover, a variable NO_2 concentration could affect the magnitude of the ozone decrease [see also Zucconi et al., 1981].

At 40 km, we see from Figures 73 and 74 that the terms L_{NO_x} and L_{ClO_x} dominate the daytime ozone loss processes, whereas at 46 km, HO_x becomes the major loss mechanism and the small net destruction causes a decrease in ozone. In the mesosphere, atomic oxygen becomes the major odd oxygen component and is converted into ozone at night, so that nighttime ozone densities are generally higher than during the day [for further details, see Allen et al., 1983]. In order to produce a 13% increase in ozone at 40 km, we would have to multiply the average value for (P - L) by a factor of four. This would require significant changes in the individual loss

terms from NO_x or ClO_x, even though (P - L) is generally small (< 10%), compared to P or L. We find, for example, that the new laboratory results which indicate a 30-40% decrease in k_{61} (O + ClO reaction) would change our daytime percent ozone increase at 40 km from 2-3% (current model) to 3-5% (new diurnal run test). We do not favor an increase in J_1 (production term), since this would affect other altitudes and would also increase the loss rates (via the atomic oxygen concentration increase), so that a change by more than 20% is probably needed. An increase in R_o (= $[O]/[O_3]$) could also change the ozone daytime variation. It is quite plausible that whatever change is needed in our current photochemical model to increase $[O_3]$ in the upper stratosphere will also increase the percent daytime increase below $\sim$40 km, since both effects are tied to the balance between $P(O_x)$ and $L(O_x)$. However, despite the careful data acquisition and analysis by Lean[1982], the measurements could be in error by an amount large enough to reconcile them with a daytime ozone increase of about 5% near 40 km. Indeed, measurements performed during different days could be prone to systematic changes, and although a correction was made for observed density and temperature changes, these variables themselves are subject to uncertainties. The corrections ranged from a few percent to 20 percent changes in $[O_3]$. The temperature correction $(\Delta[O_3]/O_3] = (-1364/T)(\Delta T/T))$ leads to an enhancement by a factor of five between percent temperature and ozone changes. Moreover, this expression is valid for a pure oxygen atmosphere only, and our model tests as well as observations by Barnett et al. [1975] indicate that a factor of about 900 (rather than 1364) would be more appropriate in the upper stratosphere. Also, the quoted nighttime measurement uncertainty at 40 km

[Table 2 of Lean, 1982] is ∿8%, larger than at all other altitudes. The ± 3% uncertainty that we used in Figure 71 is most certainly an underestimate and the discrepancy at 40 km should be considered with caution.

It is interesting--although possibly questionable as well--that an increase (from night to day) of close to 10% in O_3 near 30-35 km was seen by the LIMS instrument aboard Nimbus 7 [Remsberg et al., 1983]. This systematic diurnal increase in zonal mean ozone (at constant pressure), observed at more than one latitude (J. Russell, private communication, 1983), appears to be real. The large abundance of ozone near 30 km makes it very difficult to produce such an increase, and our model predicts a 1-2% change, at most. The observed increase near 40 km, however, is close to 5%, in much better agreement with model results, and significantly less than the 13% increase obtained by Lean [1982]. The LIMS data do not show any systematic temperature changes near 30 km that could be related to the ozone daytime increase.

In view of the limited and somewhat uncertain data discussed above, the magnitude of possible discrepancies between observed and theoretical diurnal ozone variations in the stratosphere is not clearly defined. Larger-than-expected increases would tend to substantiate the current discrepancy in the upper stratosphere ozone abundance, and further high precision observations are needed.

5.3 Heavy Oxygen and Ozone

The abundance and photochemistry of heavy ozone have recently become a topic of interest, primarily as a result of the controversial balloon-borne mass spectrometer data of Mauersberger [1981]. These results show a

significant enhancement in $^{50}O_3$, relative to $^{48}O_3$, at stratospheric altitudes from about 23 to 38 km. This effect disappears in the lower stratosphere and also seems to go to zero near 40 km; the peak enhancement of about 40% occurs near 32 km. Mauersberger [1981] refers to the work of Cicerone and McCrumb [1980], concerning the enhanced photodissociation of heavy O_2 in the Schumann-Runge bands as a possible source of heavy ozone in the stratosphere. However, the latter authors were comparing the light odd oxygen source (O_2 photolysis) to the additional source of light O_x due to heavy O_2 photolysis. They alluded to the likely dilution of isotopic effects in heavy ozone, due to the rapidity of the Chapman reactions. Since there has been some confusion concerning heavy ozone photochemistry and the expected ozone enhancement in the stratosphere, we describe below our understanding of the heavy odd oxygen system.

One should stress that a 40% fractionation in heavy ozone near 30 km is a very large effect. A preferential source near that height would be required, in order to provide a continuous effect that is not diluted by dynamics and mixing. Observed isotopic anomalies of a few percent in meteorites [see review by Clayton, 1978] are considered large; possible quantum mechanical effects have been discussed by Arrhenius et al. [1979]. Changes of that magnitude or less occur on the Earth as well, as in the case of ^{18}O variations in water sources [Epstein and Mayeda, 1953], where evaporation and distillation processes are thought to play a role. Fractionation has also been observed in laboratory experiments [e.g., Servigne et al., 1962], and a possible mass-independent effect has recently been discussed by Thiemans and Heidenreich [1983]. On the other

extreme, Clancy and Muhleman [1983] have detected an unexplainably large (factor of two) depletion of the ratio $[^{13}CO]/[^{12}CO]$ in the mesosphere of Venus, relative to the lower atmosphere and the Earth's ratio. We find no specific clues in any of the above studies, in terms of a large localized enhancement of heavy stratospheric ozone, relative to observed ground (laboratory) abundances.

For clarity in this section, we have not followed the reaction numbering scheme of Chapter 1. Furthermore, we use the simplified notation ^{e}O, $^{e}O_2$, and $^{e}O_3$ for ^{18}O, $^{18}O^{16}O$, and $^{18}O^{32}O_2$, respectively, where "e" stands for molecular weight eighteen (heavy component). Qualitatively, of course, the scheme would also hold for oxygen seventeen. For now, we do not distinguish between the two possible isomers of $^{e}O_3$, one with ^{e}O at the center ($O^{e}OO$) and one with ^{e}O at either end of the molecule (^{e}OOO). The photochemical reactions of interest are summarized below. For light odd oxygen, the Chapman reactions are

$$O_2 + h\nu \rightarrow O + O \qquad j_1$$

$$O_3 + h\nu \rightarrow O_2 + O \qquad j_2$$

$$O + O_2 + M \rightarrow O_3 + M \qquad k_1$$

$$O + O_3 \rightarrow O_2 + O_2 \qquad k_2$$

while the corresponding reactions for $^{e}O_x$ are

$$^{e}O_2 + h\nu \rightarrow {}^{e}O + O \qquad j_1^{e} = f_1 j_1 \quad (1 < f_1 \lesssim 100)$$

$$^{e}O_3 + h\nu \rightarrow {}^{e}O_2 + O \qquad j_{2a}^{e} = \frac{2}{3} j_2^{e} = \frac{2}{3} j_2$$

$$^{e}O_3 + h\nu \rightarrow O_2 + {}^{e}O \qquad j^{e}_{2b} = \frac{1}{3} j^{e}_{2} = \frac{1}{3} j_2$$

$$O + {}^{e}O_2 + M \rightarrow {}^{e}O_3 + M \qquad k^{e}_{1a} = k_1$$

$$^{e}O + O_2 + M \rightarrow {}^{e}O_3 + M \qquad k^{e}_{1b} = k_1$$

$$O + {}^{e}O_3 \rightarrow {}^{e}O_2 + O_2 \qquad k^{e}_{2a} = k_2$$

$$^{e}O + O_3 \rightarrow {}^{e}O_2 + O_2 \qquad k^{e}_{2b} = k_2$$

The most likely values of rate constants are indicated above, neglecting effects of a few percent that can be caused by the small mass difference between the elements of light O_x and heavy O_x. Mass-dependent effects (tied to the energy levels) have been quantitatively described by Urey [1947] and Bigeleisen and Mayer [1947] for isotopic exchange reactions. Based on simple symmetry arguments, the photodissociation of $^{e}O_3$ (total rate $j^{e}_{2}[^{e}O_3]$) will produce $^{e}O_2 + O$ twice as many times as it would $O_2 + {}^{e}O$, implying $j^{e}_{2a} = 2j^{e}_{2b}$. The value of f_1 has been estimated by Cicerone and McCrumb [1980] and could be as large as 100 in the mesosphere, dropping to 1 in the middle and lower stratosphere. In addition, isotopic exchange reactions between atomic and molecular oxygen should be rapid [e.g., Ogg and Sutphen, 1954] and this fast "scrambling" process has been examined in the laboratory [Jaffe and Klein, 1966]:

$$^{e}O + O_2 \rightarrow O + {}^{e}O_2 \qquad k_{E1} = 6.5 \times 10^{-12}\, e^{-555/T}$$

$$O + {}^{e}O_2 \rightarrow {}^{e}O + O_2 \qquad k_{E2} \simeq k_{E1}/2$$

From symmetry arguments, $k_{E1}/k_{E2} \simeq 2$, since the exchange between ^{e}O and O_2 always leads to $O + {}^{e}O_2$, whereas a "do nothing" channel exists for the

reverse reaction. As recently discussed by Kaye and Strobel (1983), k_{E1}/k_{E2} is probably slightly larger than 2 (2.16 at 298K), but this does not affect our analysis, since the expected variation (versus T or z) is less than 5%.

The ratio $[^eO_2]/[O_2]$ is equal to 0.409% [Nier, 1950] and should be constant in the Earth's stratosphere and mesosphere. The above exchange reactions lead to rapid equilibrium, given by

$$k_{E1}[^eO][O_2] = k_{E2}[O][^eO_2] \tag{60}$$

so that

$$[^eO]/[O] = \frac{k_{E2}}{k_{E1}} \frac{[^eO_2]}{[O_2]} = \frac{1}{2}(0.004) = 0.002 \tag{61}$$

The balance of production and loss terms for heavy ozone is written as

$$k^e_{1a}[O][^eO_2][M] + k^e_{1b}[^eO][O_2][M] = (j^e_{2a} + j^e_{2b})[^eO_3] + k^e_{2a}[O][^eO_3] \tag{62}$$

which can be combined with (61) to yield the expected heavy ozone mixing ratio:

$$\frac{[^eO_3]}{[O_3]} = \frac{\{k^e_{1a} + k^e_{1b}(k_{E2}/k_{E1})\}[O][O_2][M]}{(j^e_{2a} + j^e_{2b} + k^e_{2a}[O])\,[O_3]} \frac{[^eO_2]}{[O_2]} \tag{63}$$

Using $k^e_{1a} = k^e_{1b} = k_1$, $j^e_{2a} + j^e_{2b} = j_2$, $k_{E2}/k_{E1} = 0.5$, and $k^e_{2a} = k_2$, along with the fact that $k_2[O] < 0.01\ j_2$, and that $k_1[O][O_2][M] = j_2[O_3]$, we obtain

$$\frac{[^eO_3]}{[O_3]} = 1.5 \frac{[^eO_2]}{[O_2]} = 6.1 \times 10^{-3} \tag{64}$$

which is the ratio observed at the ground by Mauersberger [1981]. Our

result is not height-dependent. We note that if we consider the formation of isomers $^{e}000$ and $0^{e}00$ in the addition of atomic oxygen to either side of the oxygen molecule

$$P(^{e}000) = 0.5\ k^{e}_{1a}[O][^{e}O_2] + k^{e}_{1b}[^{e}O][O_2]$$

$$= k^{e}_{1a}[O][^{e}O_2] \qquad (65)$$

whereas

$$P(0^{e}00) = 0.5\ k^{e}_{1a}[O][^{e}O_2] = 0.5\ P(^{e}000) \qquad (66)$$

For equal photolysis rates of these isomers, we then expect $[^{e}000] = 2[0^{e}00]$ as a result of the preferential formation of the $^{e}000$ isomer. Although Mauersberger's mass spectrometer cannot distinguish between these two isomers, high resolution spectroscopic observations could.

The production and loss rates for heavy odd oxygen, as well as the modifications to the light odd oxygen system are summarized in Table V. Reactions involving HO_x, NO_x, or ClO_x are negligible in the destruction of heavy odd oxygen, given the magnitude of terms such as $k_{E1}[^{e}O][O_2]$ or even $j^{e}_{2a}[^{e}O_3]$. The main uncertainty in Table V centers around j^{e}_{1}, which has been estimated by Cicerone and McCrumb [1980]. In the production terms for ^{e}O, the fast isotopic exchange rate dominates by two orders of magnitude or more throughout the stratosphere, even if $j^{e}_{1} = 100\, j_1$ below about 40 km (a factor of ten larger than the upper limit of Cicerone and McCrumb, 1980). Terms such as $j^{e}_{2b}[^{e}O_3]$ or $k^{3}_{1a}[O][^{e}O_2][M]$ will also dominate over $j^{e}_{1}[^{e}O_2]$, at least in the stratosphere. Even if the Cicerone and McCrumb calculations significantly underestimated the magnitude of the

Table V. Production and Loss Rates for $^{e}O_x$ and O_x[†]

Species	Production Rate	Loss Rate
^{e}O	$k_{E2}[O][^{e}O_2]$ + $j^{e}_{2b}[^{e}O_3]$ + $j^{e}_{1}[^{e}O_2]$	$k_{E1}[^{e}O][O_2]$ + $k^{e}_{1b}[^{e}O][O_2][M]$ + $k^{e}_{2b}[^{e}O][O_3]$
$^{e}O_3$	$k^{e}_{1a}[O][^{e}O_2][M]$ + $k^{e}_{1b}[^{e}O][O_2][M]$	$(j^{e}_{2a} + j^{e}_{2b}[^{e}O_3]$ + $k^{e}_{2a}[O][^{e}O_3]$
$^{e}O_x$	$k_{E2}[O][^{e}O_2]$ + $k^{e}_{1a}[O][^{e}O_2][M]$ + $j^{e}_{1}[^{e}O_2]$	$k_{E1}[^{e}O][O_2]$ + $j^{e}_{2a}[^{e}O_3]$ + $k^{e}_{2a}[O][^{e}O_3]$ + $k^{e}_{2b}[^{e}O][O_3]$
O	$j^{e}_{1}[^{e}O_2] + j^{e}_{2a}[^{e}O_3]$	$k^{e}_{1a}[O][^{e}O_2][M]$ + $k^{e}_{2a}[O][^{e}O_3]$
O_3		$k^{e}_{2b}[^{e}O][O_3]$
O_x (see text)	$2j^{e}_{1}[^{e}O_2]$	$2k^{e}_{2a}[O][^{e}O_3]$ + $2k^{e}_{2b}[^{e}O][O_3]$

[†]For the O_x system, only additional production and loss terms due to heavy oxygen photochemistry are indicated.

heavy O_2 photolysis rate, we cannot arbitrarily set $j_1^e = 1000\, j_1$ or more, without affecting the average atmospheric transmission in the Schumann-Runge bands, in conflict with observations of direct solar flux. Heavy oxygen photodissociation will not affect heavy ozone, although it can still play a role in terms of light ozone production. We can rewrite equation (63) as:

$$\frac{[^eO_3]}{[O_3]} = \frac{(k_{1a}^e/k_1) + [(k_{1b}^e/k_1)(k_{E2}/k_{E1})]}{(j_2^e/j_2)} \frac{[^eO_2]}{[O_2]} \qquad (67)$$

In order to get a 40% enhancement over the factor of $1.5[^eO_2]/[O_2]$, significant departures from the expected values of (k_{1a}/k_1), (k_{1b}/k_1), (k_{E2}/k_{E1}), (j_2^e/j_2) or even $[^eO_2]/[O_2]$ would be required. Moreover, small mass-dependent effects would tend to favor the lighter isotope reaction over the heavier one. In terms of j_2^e, we do not have a situation similar to the intricate Schumann-Runge band region and photodissociation of heavy O_2. A large (40%) decrease in j_2^e/j_2 would be needed to enhance $^eO_3$ by 40%. It is hard to explain the <u>preferential</u> enhancement near 30 km. Temperature varies smoothly (by $\sim$10%) from 20 to 40 km, and temperature variations over a day are also small. Mauersberger's measurement was made at night and showed some temporal variation. We do not expect any nighttime change in $^eO_3$, since both production and loss mechanisms disappear at night. Further measurements and checks for possible contamination of any kind should be performed. Spectroscopic observations could also be attempted. A quantitative detection of heavy ozone in infrared spectra (O. Raper, private communication, 1983) does not appear feasible at this time, primarily because the exact line positions and parameters do not seem to be

known well enough. Microwave spectra from the ground [de Zafra et al., 1983] show the presence of heavy ozone in the atmosphere with the expected average abundance (P. Solomon, private communication, 1983), although this method is not accurate enough for the detection of a possible 40% enhancement near 30 km. Accurate balloon-borne observations could improve this situation. We have a little trouble believing that the existence of a phenomenon that can significantly and preferentially enhance heavy ozone near 30 km is more likely than the existence of a process that somehow contaminates the experiment itself, although it is certainly worth pursuing this question without ruling anything out. Kaye and Strobel [1983] have independently discussed the apparent difficulty associated with any significant heavy ozone enhancement in the stratosphere.

Heavy oxygen photochemistry provides a source of light odd oxygen, as shown in Table V. If we make use of the equilibrium between the secondary production and loss terms for $^{e}O_x$,

$$j^{e}_{2a}[^{e}O_3] = j^{e}_{1}[^{e}O_2] + k^{e}_{1a}[O][^{e}O_2][M] - k^{e}_{2a}[O][^{e}O_3] - k^{e}_{2b}[^{e}O][O_3] \ ,$$

in addition to the terms related to O and O_3, we obtain net production and loss terms for O_x, as shown in the table. The additional loss terms for O_x are small ($\lesssim$ 15%), compared to $2j^{e}_{1}[^{e}O_2]$, for reasonable values of j^{e}_{1} in the stratosphere and mesosphere. A net O_x source of 30% could result from heavy oxygen photolysis near 60 km, but Cicerone and McCrumb [1980] find less than a 5% increase in O_3 near 40 km. Although the calculations related to this additional source are approximate, we tend to agree with the upper limit results of the above authors. Even with low (continuum)

average absorption cross sections in the Schumann-Runge bands of O_2 (and hence higher fluxes), the contribution to O_x from $^eO_2$ photolysis will not be nearly as large as the 50% discrepancy in upper stratospheric O_3 would require.

References

Aimedieu, P., P. Rigaud, and J. Barat, The sunrise ozone depletion problem of the upper stratosphere, Geophys. Res. Lett., 8, 787, 1981.

Allen, M., J. I. Lunine, and Y. L. Yung, The vertical distribution of ozone in the mesosphere and lower thermosphere, submitted to J. Geophys. Res., 1983.

Anderson, J. G., Free radicals in the Earth's stratosphere: A review of recent results, Proceedings of the NATO Advanced Study Institute on Atmospheric Ozone: Its variation and Human Influences, Report No. FAA-EE-80-20, U. S. Dept. of Transportation, pp. 233-251, 1980.

Anderson, J. G., H. J. Grassl, R. E. Shetter, and J. J. Margitan, HO_2 in the stratosphere: Three in situ observations, Geophys. Res. Lett., 8, 289, 1981.

Arrhenius, G., J. L. McCrumb, and N. Friedman, Primordial condensation of meteorite components--Experimental evidence of the state of the source medium, Astrophys. Space Sci., 65, 297, 1979

Barnett, J. J., J. T. Houghton, and J. A. Pyle, The temperature dependence of the ozone concentration near the stratopause, Quart. J. Roy. Meteorol. Soc., 101, 245, 1975.

Bigeleisen, J., and M. G. Mayer, Calculation of equilibrium constants for isotopic exchange reactions, J. Chem. Phys., 15, 261, 1947.

Burnett, C. R., and E. B. Burnett, Spectroscopic measurements of the vertical column abundance of hydroxyl (OH) in the Earth's atmosphere, J. Geophys. Res., 86, 5185, 1981.

Burnett, C. R., and E. B. Burnett, Vertical column abundance of atmospheric OH at solar maximum from Fritz Peak, Colorado, Geophys. Res. Lett., 9, 708, 1982.

Cicerone, R. J., and J. L. McCrumb, Photodissociation of isotopically heavy heavy O_2 as a source of atmospheric O_3, Geophys. Res. Lett., 7, 251, 1980.

Clancy, R. T., and D. O. Muhleman, A measurement of the $^{12}CO/^{13}CO$ ratio in the mesosphere of Venus, submitted to Astrophys. J., 1983.

Clayton, R. N., Isotopic anomalies in the early solar system, Ann. Rev. Nucl. Part. Sci., 28, 501, 1978.

Cunnold, D. M., F. N. Alyea, and R. G. Prinn, Preliminary calculations concerning the maintenance of the zonal mean ozone distribution in the northern hemisphere, Pure Appl. Geophys., 118, 329, 1980.

DeLuisi, J. J., C. L. Mateer, and D. F. Heath, Comparison of seasonal variations of upper stratospheric ozone concentrations revealed by Umkehr and Nimbus 4 BUV observations, J. Geophys. Res. 84, 3728, 1979.

DeMore, W. B., R. T. Watson, D. M. Golden, R. F. Hampson, M. J. Kurylo, C. J. Howard, M. J. Molina, and A. R. Ravishankara, Chemical Kinetics and Photochemical Data for Use in Stratospheric Modeling, JPL Publication 82-57, Jet Propulsion Laboratory, Pasadena, California, 1982.

deZafra, R. L., A. Parrish, P. M. Solomon, and J. W. Barrett, A measurement of stratospheric HO_2 by ground-based mm-wave spectroscopy, submitted to J. Geophys. Res., 1983.

Drummond, J. R., and R. F. Jarnot, Infrared measurements of stratospheric composition II. Simultaneous NO and NO_2 measurements, Proc. Roy. Soc. London, A, 364, 237, 1978.

Dütsch, H. U., The ozone distribution in the atmosphere, Can. J. Chem., 52, 1491, 1974.

Epstein, S., and T. Mayeda, Variation of O^{18} content of waters from natural sources, Geochimica Cosmochim. Acta, 4, 213, 1953.

Frederick, J. E., B. W. Guenther, and D. F. Heath, Spatial variations in tropical ozone: The influence of meridional transport and planetary waves in the stratosphere, Beiträge zur Physik der Atmosphäre, 50, 496, 1977.

Frederick, J. E., R. B. Abrams, R. Dasgupta, and B. Guenther, An observed annual cycle in tropical upper stratospheric and mesospheric ozone, Geophys. Res. Lett., 7, 713, 1980.

Frederick, J. E., F. T. Huang, A. R. Douglass, and C. A. Reber, The distribution and annual cycle of ozone in the upper stratosphere, J. Geophys. Res., 88, 3819, 1983.

Gille, J. C., P. L. Bailey, and J. M. Russell, III, Temperature and composition measurements from the LRIR and LIMS experiments on Nimbus 6 and 7, Phil. Trans. Roy. Soc. London, A, 296, 205, 1980.

Ghazi, A., A. Ebel, and D. F. Heath, A study of satellite observations of ozone and stratospheric temperatures during 1970-1971, J. Geophys. Res., 81, 5365, 1976.

Hartmann, D. L., Some aspects of the coupling between radiation, chemistry, and dynamics in the stratosphere, J. Geophys. Res., 86, 9631, 1981.

Hartmann, D. L., and R. R. Garcia, A mechanistic model of ozone transport by planetary waves in the stratosphere, J. Atmos. Sci., 36, 350, 1979.

Harwood, R. S., and J. A. Pyle, The dynamical behavior of a two-dimensional model of the stratosphere, Quart. J. R. Met. Soc., 106, 395, 1980.

Heaps, W. S., and T. J. McGee, Balloon borne LIDAR measurements of stratospheric hydroxyl radical, J. Geophys. Res., 88, 5281, 1983.

Heath, D. F., C. L. Mateer, and A. J. Krueger, The Nimbus -4 backscatter

ultraviolet (BUV) atmospheric ozone experiment--Two years' operation, Pure Appl. Geophys., 106-108, 1238, 1973.

Herman, J. R., The response of stratospheric constituents to a solar eclipse, sunrise, and sunset, J. Geophys. Res., 84, 3701, 1979.

Herman, J. R., and J. E. Mentall, O_2 absorption cross sections (187-225 nm) from stratospheric solar flux measurements, J. Geophys. Res., 87, 8967, 1982.

Hilsenrath, E., Ozone measurements in the mesosphere and stratosphere during two significant geophysical events, J. Atmos. Sci., 28, 295, 1971.

Horvath, J. J., N. Orsini, A. R. Douglass, and J. E. Frederick, Nitric oxide in the upper stratosphere: measurements and geophysical interpretation, J. Geophys. Res., in press, 1983.

Hudson, R. D., and E. I. Reed (eds.), The Stratosphere: Present and Future, NASA RP 1049, 1979.

Hudson, R. D. (editor-in-chief), et al. (16 editors), The Stratosphere 1981: Theory and Measurements, WMO Global Ozone Research and Monitoring Project Report No. 11, 1982.

Jaffe, S., and F. S. Klein, Isotopic exchange reactions of atomic oxygen produced by the photolysis of NO_2 at 3660Å, Trans. Faraday Soc., 62, 3135, 1966.

Johnston, H. S., Global ozone balance in the natural stratosphere, Rev. Geophys. Space Phys., 13, 637, 1975.

Johnston, H. S., and J. Podolske, Interpretations of stratospheric photochemistry, Rev. Geophys. Space Phys., 16, 491, 1978.

Kaye, J. A., and D. F. Strobel, Enhancement of heavy ozone in the Earth's atmosphere?, J. Geophys. Res., in press, 1983.

Ko, M.K.W., and N. D. Sze, Effect of recent rate data revisions on stratospheric modeling, Geophys. Res. Lett., 10, 341, 1983.

Krueger, A. J., The mean ozone distribution from several series of rocket soundings to 52 km at latitudes from 58°S to 64°N, Pure Appl. Geophys., 106-108, 1272, 1973.

Krueger, A. J., and R. A. Minzner, A mid-latitude ozone model for the 1976 U. S. Standard Atmosphere, J. Geophys. Res., 81, 4477, 1976.

Krueger, A. J., B. Guenther, A. J. Fleig, D. F. Heath, E. Hilsenrath, R. McPeters, and C. Prabhakara, Satellite ozone measurements, Phil-Trans. R. Soc. London, A, 296, 191, 1980.

Kurzeja, R., Effects of diurnal variations and scattering on ozone in the stratosphere for present-day and predicted future chlorine concentrations, J. Atmos. Sci., 34, 1120, 1977.

Lean, J. L., Observation of the diurnal variation of atmospheric ozone, J. Geophys. Res., 87, 4973, 1982.

London, J., J. E. Frederick, and G. P. Anderson, Satellite observations of the global distribution of stratospheric ozone, J. Geophys. Res., 82, 2543, 1977.

Mauersberger, K., Measurement of heavy ozone in the stratosphere, Geophys. Res. Lett., 8, 935, 1981.

Mauersberger, K., R. Finstad, S. Anderson, and P. Robbins, A comparison of ozone measurements, Geophys. Res. Lett., 8, 361, 1981.

McPeters, R. D., The behavior of ozone near the stratopause from two years of BUV observations, J. Geophys. Res., 85, 4545, 1980.

Mihelcic, D., D. H. Ehhalt, G. F. Kulessa, J. Klomfass, M. Trainer, U. Schmidt, and H. Röhrs, Measurements of free radicals in the

atmosphere by matrix isolation and electron paramagnetic resonance, Pure Appl. Geophys., 116, 530, 1978.

Nagatani, R. M., and A. J. Miller, Stratospheric ozone changes and transports during the first year of SBUV observations November 1978 - October 1979, J. Geophys. Res., in press, 1983.

Nicolet, M., Stratospheric ozone: An introduction to its study, Rev. Geophys. Space Phys., 13, 593, 1975.

Nier, A. O., A redetermination of the relative abundances of the isotopes of carbon, nitrogen, oxygen, argon, and potassium, Phys. Rev., 77, 789, 1950.

Ogg, R. A., Jr., and W. T. Sutphen, Reactions of atomic oxygen with molecular oxygen, Disc. Faraday Soc., 17, 47, 1954.

Prasad, S. S., Possible existence and chemistry of $ClO.O_2$ in the stratosphere, Nature, 285, 152, 1980.

Prather, M. J., Ozone in the upper stratosphere and mesosphere, J. Geophys. Res., 86, 5325, 1981.

Pyle, J. A., and C. F. Rogers, Stratospheric transport by stationary planetary waves--the importance of chemical processes, Quart. J. R. Met. Soc., 106, 421, 1980.

Reed, R. J., and K. E. German, A contribution to the problem of stratospheric diffusion by large-scale mixing, Mon. Weather Rev., 93, 313, 1965.

Reiter, R., and M. P. McCormick, SAGE-European ozone-sonde comparison, Nature, 300, 337, 1982

Remsberg, E. E., J. M. Russell, III, J. C. Gille, L. L. Gordley, P. L. Bailey, W. G. Planet, and J. E. Harries, The validation of Nimbus

7 LIMS measurements of ozone, submitted to J. Geophys. Res., 1983.

Rood, R. B., and M. R. Schoeberl, A mechanistic model of Eulerian, Lagrangian mean, and Lagrangian ozone transport by steady planetary waves, J. Geophys. Res., 88, 5208, 1983.

Roscoe, H. K., J. R. Drummond, and R. F. Jarnot, Infrared measurements of stratospheric composition III. The daytime changes of NO and NO_2, Proc. Roy. Soc. London, A, 375, 507, 1981.

Rusch, D. W., G. H. Mount, C. A. Barth, G. J. Rottman, R. J. Thomas, G. E. Thomas, R. W. Sanders, G. M. Lawrence, and R. S. Eckman, Geophys. Res. Lett., 10, 241, 1983.

Russell, J. M., III, J. C. Gille, E. E. Remsberg, L. L. Gordley, P. L. Bailey, S. R. Drayson, H. Fischer, A. Girard, J. E. Harries, and W.F.J. Evans, Validation of nitrogen dioxide results measured by the Limb Infrared Monitor of the Stratosphere (LIMS) experiment on Nimbus 7, submitted to J. Geophys. Res., 1983.

Servigne, M., F. Mahieux, and P. Vernotte, An enrichment effect of oxygen in the isotope oxygen-18 obtained during an experiment with concentrated ozone, Nature, 193, 775, 1962.

Solomon, S., H. S. Johnston, M. Kowalczyk, and I. Wilson, Instantaneous global ozone balance including observed nitrogen dioxide, Pure Appl. Geophys., 118, 59, 1980.

Solomon, S., D. W. Rusch, R. J. Thomas, and R. S. Eckman, Comparison of mesospheric ozone abundances measured by the Solar Mesosphere Explorer and model calculations, Geophys. Res. Lett., 10, 249, 1983.

Sreedharan, C. R., and A. Mani, Ozone and temperature changes in the lower stratosphere, Pure Appl. Geophys., 106-108, 1576, 1973.

Strobel, D. F., Parametrization of linear wave chemical transport in planetary atmospheres by eddy diffusion, J. Geophys. Res., 86, 9806, 1981.

Thiemans, M. H., and J. E. Heidenreich III, The mass-independent fractionation of oxygen: A novel isotope effect and its possible cosmochemical implications, Science, 219, 1073, 1983.

Urey, H. C., The thermodynamic properties of isotopic substances, J. Chem. Soc., April, 562, 1947.

U. S. Standard Atmosphere 1976, U. S. Government Printing Office, Washington, D. C., 1976.

Zellner, R., and V. Handwerk, Kinetics of the reactions of ClO radicals with NO_2 and O_2, Paper presented at the International Symposium on Chemical Kinetics Related to Atmospheric Chemistry, Tsukuba, Ibaraki, Japan, June 6-10, 1982.

Zucconi, J. M., G. Moreels, and J. P. Parisot, Photolytic effects of solar radiation at stratospheric levels during sunrise and sunset, Can. J. Phys., 59, 1158, 1981.

CONCLUSIONS

We have discussed and tested our photochemical model, in relation to certain observations of minor and trace gases, as well as solar radiation measurements in the Earth's stratosphere. Progress has been made in the recent acquisition of atmospheric as well as laboratory data; the latter help reduce model uncertainties due to photochemical input data, while the former obviously are needed in order to test our current understanding of photochemistry. The present state of the atmosphere has to be better defined and understood, if we are to believe predictions of small (but possibly important) column ozone depletion rates.

We have shown that the vertical distribution of certain species, in particular the halocarbons, is quite sensitive to the assumed absorption cross sections of molecular oxygen in the Herzberg continuum. The direct solar flux measurements in the stratosphere [Herman and Mentall, 1982] should provide further incentive for a confirmation of the suggested reduction in O_2 cross sections. Similar measurements recently performed in the 28 to 39 km range [Anderson and Hall, 1983] also indicate that a reduction in these cross sections is in order. Our model results demonstrate that a much better fit to mid-latitude $CFCl_3$ observations arises, when reduced cross sections are used. Such factors will affect the lifetime of halocarbons in the stratosphere, and consequently, the ozone depletion estimates [Ko and Sze, 1983]. We also find that the current photochemical model provides a reasonably good fit to average ClO data, as well as OH, HO_2, and NO_x observations. In fact, older chemistry is generally not as acceptable, in terms of such observations (e.g., the

slope and magnitude of the ClO profile, OH and HO_2 ground-based data, $[HNO_3] / [NO_2]$ ratio). The model comparison to diurnal ClO observations indicates at least first order agreement in terms of a breathing cycle with $ClONO_2$.

However, certain discrepancies remain, or have recently surfaced. Low ClO abundances at certain times (morning in particular) are hardly explainable in terms of uncertainties in the current photochemical data and might suggest an unknown chlorine reservoir or some missing chemistry. Such effects could reduce the efficiency of the chlorine catalytic cycle. Simultaneous observations of ClO and HCl at various altitudes would represent a significant step in our attempt to close the gap between models and observations. The slope of the HCl profile is generally steeper than model predictions, and although individual profiles vary, a systematic difference appears to exist. In parallel with ClO and HCl observations, we have discussed the COF_2-HF system, whose modeling is uncertain primarily because of the uncertainty in the COF_2 photodissociation quantum yield. Simultaneous observations of these two compounds, as well as further laboratory studies of COF_2, would help reduce such uncertainties in the fluorine reservoir species, which are linked to the chlorine reservoirs through their common source. Observations of ethane in the stratosphere have proved controversial, and later data are in much better agreement with model results (P. Fabian, private communication, 1983). Before the modelers lose too much sleep over possibly large discrepancies in lower stratospheric chlorine, we should obtain accurate confirmation of unusually high ethane abundances. Caution toward observational contamination should also be used, when attempting to explain the amount of scattered

flux observed in the stratosphere at wavelengths near 200 nm (see Chapter 2).

The mean ozone abundance in the upper stratosphere is higher than in current photochemical models by about 50%. This is a systematic effect, apparent in virtually every observation, so that an underestimate of observational uncertainties does not seem to be a likely explanation. It is true that over five years ago, photochemical models were predicting too much ozone, so that certain changes have occurred in the photochemical data, as well as the inclusion of NO_x and ClO_x catalytic loss processes, in order to reduce the O_3 abundance by more than 50%. However, we currently have a more accurate and trusted laboratory data base, so that it is not as easy to argue for possible changes in rate constants or absorption cross sections. Further comparisons between various models should be performed. Our sensitivity analysis essentially rules out the possibility of one large necessary adjustment in the current photochemical scheme. A combination of six to ten smaller adjustments to certain key parameters, all changed in the right way to increase the ozone abundance, is not satisfying either. Moreover, we have to realize what such changes will do to mesospheric models and to radical concentrations which have been measured in the stratosphere and mesosphere, although one could argue that some of these data do not yet provide a good mean distribution and that variability certainly exists. We note that the $O(^1D)$ concentration is a key variable that could change the ozone concentration without affecting the radicals in a drastic way (given the observational coverage and uncertainties), since three major ozone destruction mechanisms (by HO_x, NO_x, and ClO_x) are simultaneously affected; however, uncertainties in the production and

loss mechanisms for $O(^1D)$ are not large enough. The atomic oxygen concentration (relative to ozone) is also an important variable, although changes in the stratosphere would probably lead to similar or larger changes in the mesosphere. The photodissociation rate of O_2 is the major term for O_x production, but given the uncertainties in absorption cross sections, we are faced with uncomfortable uncertainties in the value of this key rate (particularly in the lower stratosphere). We note that recent indications would tend to lower $\sigma(O_2)$, thus allowing more flux in the lower stratosphere and increasing the global production of ozone. This increase, however, should not manifest itself in the upper stratosphere, where transport processes should be of minor importance, and where a decrease in $\sigma(O_2)$ leads to a decrease in O_3 concentration. High-quality observations of the diurnal behavior of ozone in the stratosphere could suggest the existence of an ozone source; there are such indications in existing data, although the limited evidence should be considered with caution. Observations of a 40% enhancement in heavy ozone near 30 km [Mauersberger, 1981] provide another ozone discrepancy that we find very difficult to explain, given our presentation of the relevant photochemical reactions.

In terms of future research, more attention has to be paid towards quality of observation and the relevance to our gain in understanding. Harries [1982] notes, for example, that tests of certain photochemical equilibrium relations can be made meaningful only with highly accurate simultaneous observations. The detection of new species, such as HO_2NO_2, HOCl, $ClONO_2$, N_2O_5, or COF_2 would obviously increase the possibilities of comparing observations with models, which in that respect are ahead of the

observations. Simultaneous observations are still of primary importance and NASA is (rightly so) presently focusing more on joint balloon flights and intercomparisons between various measurement techniques. In other words, one more ClO profile is not nearly as important as a simultaneous detection of ClO and HCl, possibly by more than one or two instruments. Global satellite observations are also becoming more frequent, accurate and sophisticated. Comparisons of multi-dimensional models with latitudinal variations of stratospheric gases will also further our understanding of chemistry, dynamics, and their interaction. A recent example concerns the global NO_x observations and analysis [Noxon et al., 1983], coupled with two-dimensional model comparisons [Solomon et al., 1983]. Despite the encouraging results, there are indications that some missing factors still exist in relation to the NO_x reservoirs at high latitudes. Any changes that can affect the current state of the stratosphere will have some effect on ozone depletion estimates. Cicerone et al. [1983] stress the existence of nonlinear effects related to the chemistry (1-D model). The global interaction of dynamics and chemistry provides for even more nonlinearities and uncertainties.

The discovery--or at least the indication--of missing factors in current photochemical models is being facilitated by the continued efforts of laboratory kineticists, who help reduce model uncertainties, as well as the improvement in stratospheric observations and global coverage. The importance of excited states for certain species has not yet been analyzed in great detail. The photochemical modeler is often faced with the dilemma of suggesting a possible change that will help reduce a certain discrepancy in a constituent's abundance, while leaving other species

in reasonable agreement with observations. This challenge represents a kind of Rubik's cube, and while we seem to have mostly the right colors on each side, there are still some unmatched --and maybe missing-- spots.

References

Anderson, G. P., and L. A. Hall, Attenuation of solar irradiance in the stratosphere: Spectrometer measurements between 191 and 207 nm, J. Geophys. Res., in press, 1983.

Cicerone, R. J., S. Walters, and S. C. Liu, Nonlinear response of stratospheric ozone column to chlorine injections, J. Geophys. Res., 88, 3647, 1983.

Harries, J. E. Stratospheric composition measurements as tests of photochemical theory, J. Atm. Terr. Phys., 44, 591, 1982.

Herman, J. R., and J. E. Mentall, O_2 absorption cross sections (187-255 nm) from stratospheric solar flux measurements, J. Geophys. Res., 87, 8967, 1982.

Ko, M.K.W., and N. D. Sze, Effect of recent rate data revisions on stratospheric modeling, Geophys. Res. Lett., 10, 341, 1983.

Mauersberger, K., Measurement of heavy ozone in the stratosphere, Geophys. Res. Lett., 8, 935, 1981.

Noxon, J. F., W. R. Henderson, and R. B. Norton, Stratospheric NO_2:3, The effects of large-scale horizontal transport, J. Geophys. Res., 88, 5240, 1983.

Solomon, S., and R. R. Garcia, On the distribution of nitrogen dioxide in the high-latitude stratosphere, J. Geophys. Res., 88, 5229, 1983.

Appendix A

GEOMETRIC RAY PATH CALCULATION IN SPHERICAL SHELL ATMOSPHERE

Referring to Figure 4 in section 1.3, we wish to calculate the (non-refracted) path length $\overline{A_0T}$ in the plane A_0OS defined by the Sun, the Earth's center and point A_0 (latitude ϕ_0, local hour L(t), and solar declination δ determine χ_{a_0}, see equation (6)). We use the symmetry about the tangent point M to write:

$$\overline{A_0T} = 2\overline{A_0M} + \overline{C_0T} \tag{A1}$$

Let us define $\overline{OA_0} = h_{a_0} = R + z_{a_0}$

$\overline{OA_1} = h_{a_1} = R + z_{a_1}$

and $s_{a_1} = \overline{A_0A_1}$

and similar quantities for points $A_2, A_3, \cdots$ down to A_ℓ, the lowest level before the tangent point M. Simple trigonometry in triangle OA_0A_1 relates the following quantities:

$$h_{a_0}^2 = h_{a_1}^2 + s_{a_1}^2 - 2h_{a_1}s_{a_1}\cos\chi_{a_1} \tag{A2}$$

which can be solved for s_{a_1}

$$s_{a_1} = [h_{a_0}^2 - h_{a_1}^2\sin^2\chi_{a_1}]^{1/2} + h_{a_1}\cos\chi_{a_1} \tag{A3}$$

leading to the general equation (8) of Chapter 1. Moreover, let $\overline{OM} = h_m = R + z_m$, and consider triangles OMA_0 and OMA_1, for which:

$$h_m = h_{a_0}\cos(\chi_{a_0} - \pi/2) = h_{a_1}\cos(\chi_{a_1} - \pi/2) \tag{A4}$$

which leads to

$$\chi_{a_1} = \pi/2 + \arccos\{(h_{a_0}/h_{a_1})\cos(\chi_{a_0} - \pi/2)\} \tag{A5}$$

as described in section 1.3 (equation (7)) for any χ_{a_i} along the ray path.

Starting at A_o, we can use (A5) and (A3) to calculate the incremental path lengths in each layer down to A_ℓ. This integration is stopped when z becomes less than $z_m = (R + z_{a_0})\cos(\chi_{a_0} - \pi/2) - R$. The tangent layer contribution (often quite large) is given by $\overline{A_\ell M} = s_m$

$$s_m = [(R + z_{a_\ell})^2 - (R + z_m)^2]^{1/2} \tag{A6}$$

The average density between z_m and z_{a_ℓ} is obtained by simple linear interpolation between the two levels that define the tangent layer. In case the model's lowest altitude level is above portions of the ray path, the path length through these layers can still be obtained accurately as in (A6). The average number density below the lowest level is extrapolated by assuming an exponentially varying profile with scale height defined by the lowest two levels available. This could be done more accurately (in particular for ozone) by storing model profiles. The ray path length calculation for $\chi < \pi/2$ proceeds in a manner very similar to the above procedures. From C_o to T (top level), and with angles χ_{C_o}, χ_{C_1}, $\cdots$ up to χ_{C_t} defined by:

$$\chi_{C_i} = (\pi/2) - \arccos\{(h_{C_o}/h_{C_i})\cos(\chi_{C_o} - \pi/2)\} \tag{A7}$$

as in (A5) except for a sign change, we find the incremental path lengths

$$s_{C_i} = [h_{C_i}^2 - h_{C_{i-1}}^2 \sin^2\chi_{C_{i-1}}]^{1/2} - h_{C_{i-1}} \cos \chi_{C_{i-1}} \qquad \text{(A8)}$$

This is equivalent to an incremental path length symmetrically located with respect to the tangent point, as it should be, if one replaces $\chi_{C_{i-1}}$ by $(\pi - \chi_{C_{i-1}})$ to get a general expression similar to (A3) or (8), using the identities $\sin(\pi - \chi) = \sin \chi$ and $\cos(\pi - \chi) = -\cos \chi$. Finally, the contribution above the top level T is added by multiplying the normal column density $N(z_t) = n(z_t)\, H(z_t)$ for each absorbing species by the appropriate Chapman correction factor.

Appendix B

CHAPMAN FUNCTION $Ch(X,\chi)$

Referring to Figure B_1, we note that the zenith angle χ along a ray path increases as the ray gets deeper into the Earth's atmosphere. The slant optical depth τ_s cannot simply be related to the normal opacity τ by a $\sec\chi$ factor if χ is larger than about 75°; below 75°, χ varies by less than 2° from the surface to 100 km altitude. The Chapman function formulation assumes that the density along the ray path varies as

$$n(h') = n(h) \exp\{-(h' - h)/H\} \tag{B1}$$

where $h = R + z$, $h' = R + z'$, and H is a constant scale height. Then,

$$\tau_s = \int_{\text{along ray path}} \sigma n \, ds$$

or

$$\tau_s = \int_h^\infty \sigma(h')\, n(h')\, \sec\chi'\, dh' \tag{B2}$$

Noting that $h'\sin\chi' = h\sin\chi$ and $dh' = -h\sin\chi\cos\chi'/\sin^2\chi'$, we rewrite (B2) as:

$$\tau_s = \sigma\, n(h)\, h \int_0^\chi \exp\{(h - h')/H\}\, (\sin\chi/\sin^2\chi')\, d\chi' \tag{B3}$$

which is customarily written as

$$\tau_s = \sigma\, n(h)\, H\, Ch(X,\chi) = \tau\, Ch(X,\chi) \tag{B4}$$

where $X = (R + z)/H = h/H$

and the Chapman function replacing $\sec\chi$ (plane parallel atmosphere) is:

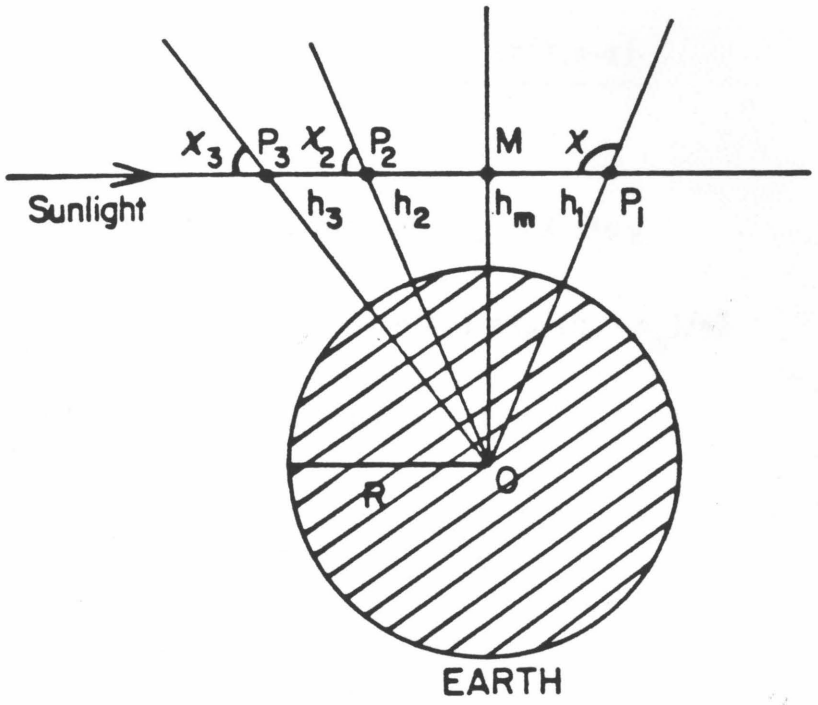

Figure B_1. Schematic representation of geometric ray path through the Earth's atmosphere, and changing solar zenith angle along the path.

$$Ch(X,\chi) = X \sin\chi \int_0^{\chi} \exp\{X(1 - \sin\chi/\sin\chi')\} \operatorname{cosec}^2\chi' \, d\chi' \qquad (B5)$$

for $\chi < \pi/2$.

For zenith angles larger than 90°, we make use of the fact that $\tau_s(P_1) = 2\tau_s(M) - \tau_s(P_2)$ in Figure B_1, and therefore $Ch(X,\chi) = \tau_s(P_1)/\tau(P_1)$ can be written as:

$$Ch(X,\chi) = \frac{2\tau(M)\ Ch(X_M,\pi/2) - \tau(P_2)\ Ch(X,\pi-\chi)}{\sigma\, n(h_1)\, H} \qquad (B6)$$

Now $\tau(P_2) = \tau(P_1) = \sigma\ n(h_1)\, H$; $X_M = X \sin\chi$

and $\tau(M) = \sigma\ n(h_m)\, H = \sigma H n(h_1) \exp\{(h_1 - h_m)/H\}$

or $\tau(M) = \tau(P_1) \exp\{X(1 - \sin\chi)\}$

so that (B6) becomes:

$$Ch(X,\chi) = 2 \exp\{X(1 - \sin\chi)\}\ Ch(X\sin\chi,\pi/2) - Ch(X,\pi - \chi) \qquad (B7)$$

for $\chi > \pi/2$.

Equations (B5) and (B7) correspond to (10) and (11) in section 1.3.